UNIVERSITY OF SOUTHAMPTON
BIOENGINEERING SCIENCES RESEARCH GROUP
School of Engineering Sciences

Probabilistic Finite Element Analysis of the Uncemented Total Hip Replacement

by

Carolina Dopico González

Thesis for the degree of Doctor of Philosophy

March 2009

ABSTRACT

There are many interacting factors affecting the performance of a total hip replacement (THR), such as prosthesis design and material properties, applied loads, surgical approach, femur size and quality, interface conditions etc. All these factors are subject to variation and therefore uncertainties have to be taken into account when designing and analysing the performance of these systems. To address this problem, probabilistic design methods have been developed.

A computational probabilistic tool to analyse the performance of an uncemented THR has been developed. Monte Carlo Simulation (MCS) was applied to various models with increasing complexity. In the pilot models, MCS was applied to a simplified finite element model (FE) of an uncemented total hip replacement (UTHR). The implant and bone stiffness, load magnitude and geometry, and implant version angle were included as random variables and a reliable strain based performance indicator was adopted. The sensitivity results highlighted the bone stiffness, implant version and load magnitude as the most sensitive parameters. The FE model was developed further to include the main muscle forces, and to consider fully bonded and frictional interface conditions. Three proximal femurs and two implants (one with a short and another with a long stem) were analysed. Different boundary conditions were compared, and convergence was improved when the distal portion of the implant was constrained and a frictional interface was employed. This was particularly true when looking at the maximum nodal micromotion. The micromotion results compared well with previous studies, confirming the reliability and accuracy of the probabilistic finite element model (PFEM). Results were often influenced by the bone, suggesting that variability in bone features should be included in any probabilistic analysis of the implanted construct.

This study achieved the aim of developing a probabilistic finite element tool for the analysis of finite element models of uncemented hip replacements and forms a good basis for probabilistic models of constructs subject to implant position related variability.

Acknowledgements

First of all, I would like to thank my parents (Lola and Juan Antonio), my aunty (Mari Carmen), my brother (Luis) and my sister in law (Trini) for being there to encourage me and make me see how proud they are of my achievements. It makes a big difference to the way I perceive them, it makes them much more important.

Secondly, I would like to thank all of those friends that helped me from many different perspectives: Those who gave me the courage to take the big decision and leave my life in Spain to start a new one in Southampton; thanks to my "malagueñas" y "malagueños" (including the adopted ones) Belén, Virginia, Carmen, Rocío, Antonio, Celia, Elena, Marimar, and Javi, and thanks to my "granaínas" (adopted, as most of us who fell in love with this wonderful city) Reyes, Flori, Marisa, Esther y Cristina. Those who I met in Southampton and made my life really joyful at all times: Luigi, Mounir, Mareen, Mika, Aurelien, Suzie, Erin, Tristen, Alberto, Francesca, Mónica, Celine, María Jesús, Mari Carmen v.1, Mari Carmen v.2, Remi, Ranjit, Marco, Joe, Bene, Claudio, Verónica, Mariano, Patricio, Pilar, Ioanis, Maria, Cristóbal, Yuh Tat, Daisy, Conrado, Iratxe, Matt, Katrin, Manuel, Sophie, Sara, Alessandro, Becky, Hatice, Catherine, Pramod, Loujaine, Lucy, Suk, Elena, Ian, Adam...

Thanks to Andrew and Martin for their great supervision and patience. Thanks to the University of Southampton for giving me the best opportunity of my life, for allowing me to develop my career and to acquire all this knowledge. You have made me think that it is worthwhile fighting for your dreams.

I greatly acknowledge the assistance of DePuy (Johnson & Johnson) and the Shool of Engineering Sciences at the University of Southampton for their financial support to this project.

And last, but not least, I would like to thank my boyfriend, Manu, for his confidence, support, patience and for coming all the way from his beloved Granada to stay with me... that says everything, doesn't it?

Contents

List of Figures

List of Tables

Nomenclature

AMV/AMV+	Advanced Mean Value
BB/BBM	Box-Behnken Matrix design
BPER	Bone percentage of volume exceeding a limit strain
BMD	Bone Mineral Density
BMI	Body mass index
BW	Body Weight
CCD	Central Composite Design
CDF	Cumulative Distribution Function
COV	Coefficient of Variation
CT	Computed tomography
DIST	Distal portion constraint
DOE	Design of Experiment
DOF	Degree of Freedom
DS	Direct Sampling
FE	Finite Element
FEA	Finite Element Analysis
FEM	Finite Element Model/Modelling
FKN	Normal penalty stiffness
FKT	Tangent penalty stiffness
FORM	First Order Reliability Methods
G	Geometry
GS	Grey scale
HA	Hydroxyapatite
HU	Hounsfield numbers
KN	Kilo Newtons
LHS	Latin Hypercube Sampling
LVDT	Linear Variable Differential Transducer
MAXSTR	Maximum nodal von-Mises elastic strain
MCS/MCST	Monte Carlo Simulation Techniques
MP	Material Properties
MV	Mean Value
Microm	Maximum nodal micromotion
MPa	Mega Pascal

MPP	Most Probable Point
MV	Mean Value
NJR	National Joint Registry
PDF	Probability Distribution Function
pf	Probability of Failure (as POF)
PFEM	Probabilistic Finite Element Model
PRNG	Pseudo random number generator
POF	Probability of Failure
REF.POS.	Reference position
RS/RSM	Response Surface Methods
RV	Random Variable
SD	Standard Deviation
SED	Strain Energy Density
SORM	Second Order Reliability Methods
THR/THA	Total Hip Replacement/Arthroplasty
TNH	Truncated Normal distribution with high standard deviation
TNL	Truncated Normal distribution with high standard deviation
UN	Uniform distribution
5NOD	5 distal nodes constraint
ρ	Bone ash density
E	Young's modulus
μm	Micrometer
g/cm^3	Grams by cubic centimeter

Chapter 1

Introduction

1.1 Total hip Replacement: Overview

The hip joint is essential to everyday activities and even mild joint disorders can greatly limit an individual's quality of life. Arthritis, trauma, deformity, tumours or bone necrosis may limit normal joint function to such an extent that corrective measures like surgery, medication, or physiotherapy, may need to be considered.

Total hip replacement (THR) is a common routine and highly successful operation performed hundreds of thousands of times each year worldwide to help restore joint function. In THR the physiological articulating surfaces of the hip joint are replaced with a mechanical substitute composed of a femoral and acetabular component. The femoral component consists of an articulating surface, a ball, and a method of support, either a stem or other features to engage with the reshaped femur, while the acetabular component consists of the opposing articulating surface, a cup, and a support structure (Figure 1.1). There are two main different groups of THR, based on the use or not of bone cement, i.e., cemented and cementless hip replacements. Both groups have undergone many improvements, but especially the uncemented THR, which are now producing very good results, in contrast to early uncemented designs.

Just as the biological joint can require replacement, the resulting replaced joint is also subject to complications such that a revision operation may be necessary.

Figure 1.1: Total Hip Replacement components [1]

Failure of THR can occur via a number of mechanisms, for example, stem or cement fracture, loosening, infection, wear, osteolysis, instability, femur fracture or a combination of these mechanisms and not necessarily in this sequence.

The importance of analysing the performance of the implants for THR lies in the fact that many of these surgeries are carried out every year all over the world, as can be seen in the Table 1.1, from the Canadian Joint Replacement Registry [20]. A set of approximate total hip and knee replacement primary and revision rates for selected countries is shown. It can be seen that Norway had the highest crude rate for primary and revision (135 and 21 per 100,000, respectively) hip replacements, and the United States the lowest crude rate for primary hip replacements (54 per 100,000).

These rates also have had an upwards trend, as shown in the Table 1.2, from the same Canadian Registry, which shows the changes in crude rates (per 100,000 population) over a period of one to four years. Crude rates for hip replacements have increased in these countries.

From the National Joint Report of England and Wales [21] (Table 1.3), for the period 2005-2006, it is known that there were 132,191 operations recorded on the NJR database between 1 April 2005 and 31 March 2006, representing an increase of 25,289 (24%) operations recorded over the previous 12 months.

Finite Element Analysis (FEA) is a common method of stress analysis used to examine complex structures and design parameters without expensive prototyping; this method is particularly suitable for the analysis of hip implants, as it can eliminate the need for in vivo testing if the implant is shown to have a negative effect. Fundamentally, FEA involves the discretisation of a complex continuum into elements wherein basic solid mechanics equations can be applied. It is the collection of the individual element's stress and strain components that approximates the stress-strain result for the whole structure.

Country	Crude rate per 100,000		Year	Reference
	Primary	Revisions		
Australia	93	18	Fiscal 2002	Australian Orthopaedic Association. National Joint Replacement Registry. Annual Report. Adelaide: AOA; 2004
New Zealand	124	19	2003	New Zealand National Joint Register
Norway	135	21	2002	Norwegian Arthroplasty Register, Annual Report June 2004
Canada	64	6	Fiscal 2002	Canadian Institute for Health Information
United States	54	11	2000	American Academy of Orthopaedic Surgeons Source: National Center for Health Statistics; Centers for Disease Control and Prevention, 2002, National Hospital Discharge Survey

Table 1.1: International Comparison of Crude Rates (per 100,000 population) of Primary Total Hip Replacements, Canadian Joint Replacement Registry [20]

It is also worth noting the large amount of uncertainty that is inherent in THR constructs, which will affect the performance of the implanted hip. These uncertainties are due to the surgical intervention process (insertion method, patient geometry, implant selection, etc.), or external factors (temperature, surgeon's skill, patient collaboration in the recovery, etc.), although every parameter's influence is different. However, most FEA research to date has focused on specific cases or a set of discrete conditions, rather than involving the random aspects. It is a fact that, for example, despite preclinical studies and patient planning, there is non uniformity in the final decision of the surgeon. In an effort to analyse these

Country	Primary Hip Replacements					Primary Knee Replacements				
	CJRR 2004 report		Latest statistic		% increase	CJRR 2004 report		Latest Statistics		% increase
	Year	Crude rate	Year	Crude rate		Year	Crude rate	Year	Crude rate	
Australia	Fiscal 1999	74	Fiscal 2002	93	25.7%	Fiscal 1999	81	Fiscal 2002	108	33.3%
Canada	Fiscal 2001	57	Fiscal 2002	64	12%	Fiscal 2001	74	Fiscal 2002	79	6.8%
New Zealand	Fiscal 2000	119	Fiscal 2003	124	4.2%	2000	75	2003	72	-4.0%
Norway	2000	124	2003	135	8.9%	2000	35	2003	50	42.9%
Sweden						Fiscal 1996	63	2003	81.5	29.4%

Table 1.2: International Comparisons, Changes Over Time for Primary Hip and Knee Replacements. Canadian Joint Replacement Registry [20]

Provider	Number of operations					
	2004			2005		
	Hip	Knee	Total	Hip	Knee	Total
NHS Hospital	30,990	29,592	60,582	38,189	39,044	77,233
Independent hospital	16,203	13,333	29,536	20,096	18,923	39,019
NHS treatment centre	1,118	1,186	2,304	1,930	2,250	4,180
Independent treatment centre	676	787	1,463	1,666	1,938	3,604
Total	48,987	44,898	93,885	61,881	62,155	124,036

Table 1.3: Distribution of hip and knee joint replacement operations by type of provider organization for 2004 and 2005. England and Wales NJR [21]

factors, probabilistic methods have been increasingly adopted in the bioengineering field. These types of analysis attempt to estimate the probability of failure as well as identify the parameters that most contribute to it thereby providing a more holistic description of the performance of the implant.

1.2 Purpose

The aim of this work was to present the development of a computational tool for the application of probabilistic methods to uncemented hip replacement. In order to create this complete probabilistic tool, different stages were followed, starting with simple assumptions and progressively adding different variables and model conditions to make it most realistic. In all cases, Monte Carlo method was applied, and the analyses differed mainly on the considered random input

variables, some sampling methods and the performance indicator.

In the so called pilot studies, the priority was the creation of a module that enabled the computation of probabilistic design loops in a Finite Element Model of a bone-implant construct. The process was designed to be automatic so that it was as efficient as possible. This initial model was setup with a real proximal femur and a real implant. Simplifications were adopted in the finite element (FE) model, such as fully bonded interface condition between bone and implant, application of hip contact force without muscle forces, both bone and implant materials were assumed to be homogeneous, isotropic and continuous. Two output parameters were successively used for the probability analyses, the maximum strain found in all the set of elements of the bone, and the percentage of bone volume exceeding von-Mises elastic strain limits. At the end of the pilot studies, bone-implant version angle was included and a robust performance indicator was found.

In the main studies, the model was modified to make it more realistic and representative of in service conditions. Combination of several bones and implants, comparison of different constraints, addition of models with bone-implant frictional interface, application of material properties to the bones from CT-scans, or application of some representative muscle forces were some of the main considerations in a model that included 6 degrees of freedom of bone-implant relative position among the random input variables.

1.3 Layout of the Thesis

This probabilistic study was divided into two stages, initially looking at simplified finite element models (pilot studies), then extending to more realistic models of proximal sections of uncemented total hip replacements (UTHR).

The following outlines the structure of the thesis and content of each chapter.

Chapter 2 reviews background material on hip anatomy, hip replacement, hip replacement failure mechanisms, evolution of hip replacement techniques, cemented and uncemented fixation, hydroxyapatite coated uncemented stems, variability factors, computational methods in implant design focussing on

Finite Element modelling, and a description of Statistical Methods in Bioengineering. A review on the probabilistic studies performed in bioengineering to date is also presented.

Chapter 3 describes the aims and objectives of the present work, the materials and methods relating to the deterministic and probabilistic models and the computational tools used within the different studies.

Chapter 4 describes the pilot studies on Probabilistic Analysis of an Uncemented Hip Replacement using (i) four random variables (RVs), (ii) the same RVs plus the bone-implant anteversion angle, and (iii) the previous RVs with a refined performance indicator. The objectives of the pilot studies were to (i) enable the automation of a probabilistic finite element model (PFEM) of the UTHR applying Monte Carlo simulation techniques (MCST), and (ii) to analyse several options in the probabilistic definitions, such as suitability of latin hypercube sampling (LHS) method and the selection of the performance indicator.

Chapter 5 describes the main studies on Probabilistic Analysis of an Uncemented Hip Replacement including variability in 6 bone-implant position related parameters, together with the load magnitude and its 3-D geometry. 3 models of proximal bones and 2 implants are combined in multiple parametric studies that benchmark the usefulness, reliability and accuracy of the PFE tool sought in this project. The objectives of the main studies were (i) to construct a more realistic PFEM of the UTHR considering variability in several bone-implant position related parameters, about what no probabilistic study has been performed to date; and (ii) to perform different parametric studies to benchmark the reliability and accuracy of the PFE tool.

Chapter 6 presents the general conclusions and proposed further work of this project.

Chapter 2

Literature Review

2.1 Hip Replacement

In this section the main features of the anatomy of the hip and the main disorders that lead to the need for a Total Hip Replacement are described. The main steps in the surgical procedure and major failure mechanisms after a THR are also discussed.

2.1.1 Hip anatomy and indications for surgery

The hip is one of the major load bearing joints of the human body. When it is healthy, it lets the person conduct typical daily activities, such as walking, sitting, bending and turning, without pain. To keep it moving smoothly, a complex network of bones, cartilages, muscles, ligaments, and tendons must all work in coordination.

The hip is a very stable ball-and-socket joint: A ball (femoral head) at the top of the thighbone (femur) fits into a rounded socket or cup-like cavity (acetabulum) in the pelvis. Bands of tissues called ligaments form a capsule connecting the ball to the socket and holding the bones in place. A layer of smooth tissue called cartilage cushions the surface of the bones, helping the ball to rotate easily in the socket. Fluid-filled sacs (bursae) cushion the area where muscles or tendons

glide across bone. The capsule surrounding the joint also has a lining (synovium) that secretes a clear liquid called synovial fluid. This fluid lubricates the joint, further reducing friction and making movement easier (Figure 2.1).

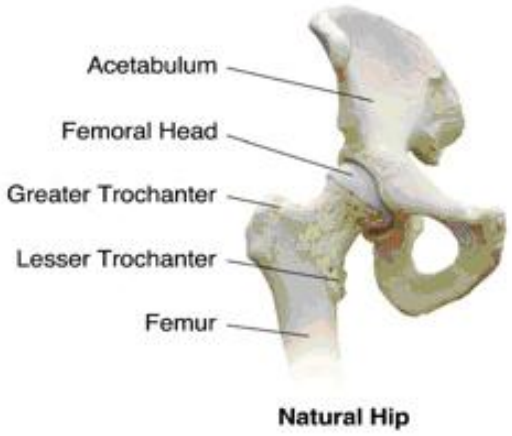

Figure 2.1: Components of the natural hip [2]

There is a very extensive literature on the description of the different aspects related to the hip and its functionality [27, 3]. In this section, descriptions are summarised to make the reader familiarised with the terminology and parameters adopted within research studies and the present work.

When either computer or experimental simulations are performed, the description of the directions and angles are related to a set of views. This can be seen in Figure 2.2, where femur's views are presented together with the most important landmarks.

It is also very common among professionals to refer to sections of the body in terms of anatomical planes (see Figure 2.3).

The meaning of some anatomical terms describing the relationship between regions is shown in Table 2.1

One of the most common human activities simulated in lower limb models is gait. Figure 2.4 shows the phases of the human gait, to which most of the authors refer when asigning loads or extracting results.

The hip replacement is one of the most successful and cost effective interventions in medicine. Currently, about 50,000 hip replacements are performed in United Kingdom annually, with a total of over 300,000 worldwide, and it

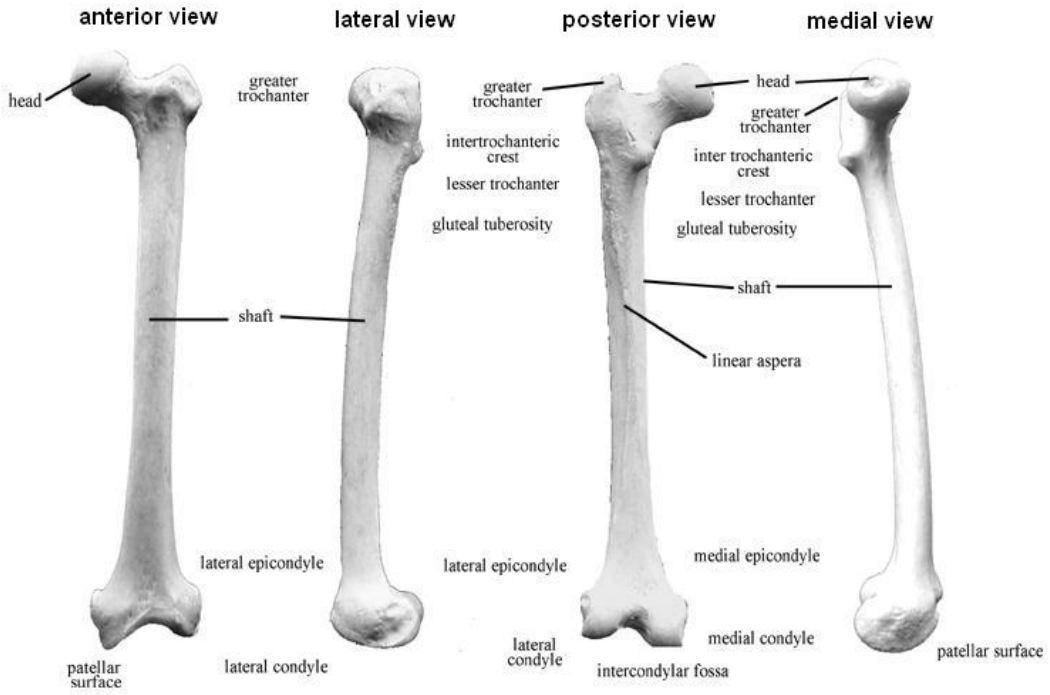

Figure 2.2: Views and landmarks of the femur [3]

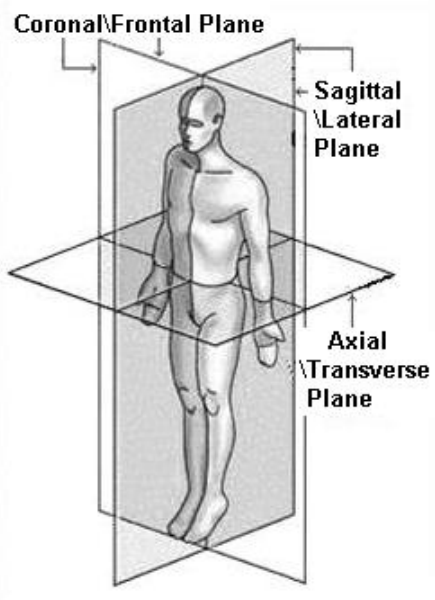

Figure 2.3: Body planes [4]

Term	Definition
Medial	Toward the midline of the body
Lateral	Away from the midline of the body
Proximal	Toward a reference point (extremity)
Distal	Away from a reference point (extremity)
Inferior	Lower or below
Superior	Upper or above
Anterior	Toward the front of the body
Posterior	Toward the back of the body

Table 2.1: Anatomical terminology [4]

is, in general, extremely effective in pain relief and improved physical function in, typically, patients aged 60 years or more who are suffering from osteoarthritis and rheumatoid arthritis. Osteoarthritis is associated with advancing age

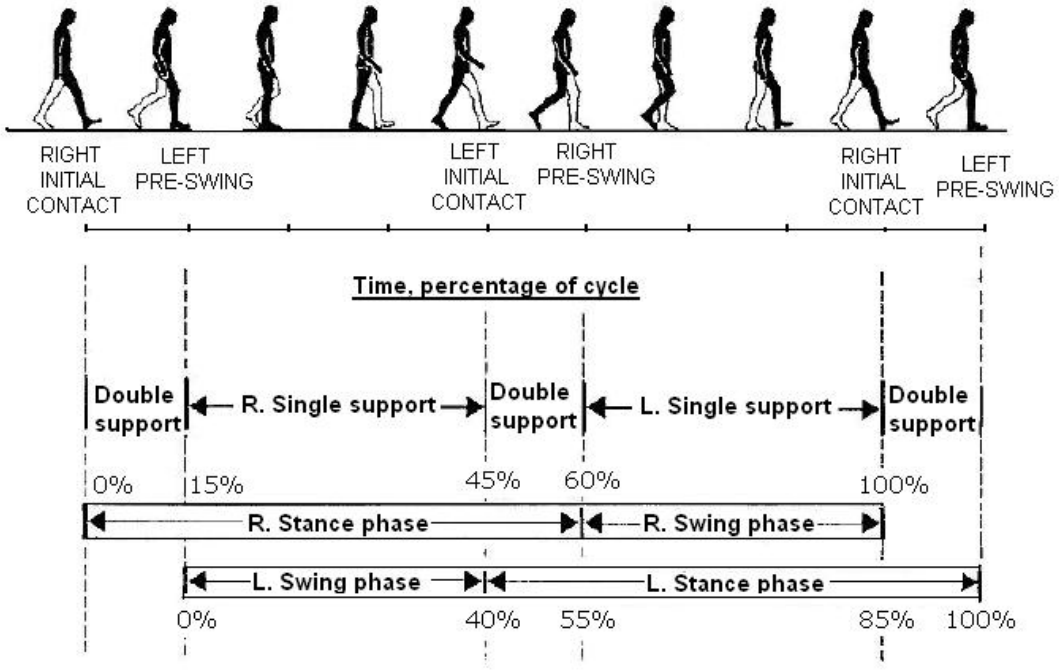

Figure 2.4: Phases of the human gait [5]

while rheumatoid arthritis is more likely to occur in young adults. Other diseases treated by the procedure include avascular necrosis, congenital dislocation, Paget's disease, ankylosing spondylitis and traumatic arthritis.

The main indications for hip replacement surgery are pain and functional limitations due to capsular contractions and joint deformity that cause a decreased range of motion of the hip. Pain relief is the main goal of hip replacement, especially for older patients with arthritic hips. Where joint deformity is severe, for example in patients with inflammatory arthritis, surgery may be indicated even in the absence of pain. While most hip replacements are performed in patients between 60 and 80 years of age, greater or lesser age is not an absolute contraindication to surgery.

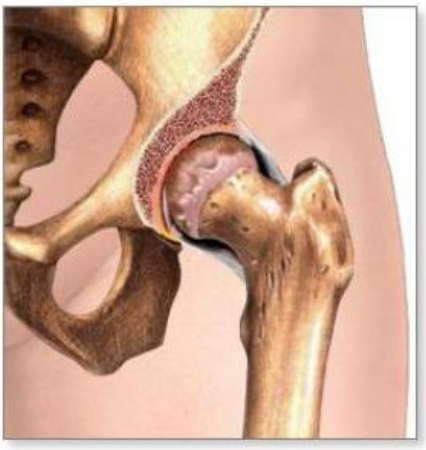

Figure 2.5: Example of a diseased hip joint [2]

2.1.2 THR: Procedure & Options

A traditional total hip prosthesis consists of three parts: a plastic cup that replaces the hip socket (acetabulum); a metal ball, that replaces the femoral head; and a metal stem that is attached within the shaft of the femur to provide stability to the prosthesis (Figure 1.1).

The surgery is performed using general or spinal anaesthesia. A well positioned

incision is made down the side of the hip joint. Deeper tissues (muscles and tendons) are either spread or incised and prepared for later repair. The hip capsule (a thick covering directly on top of the ball and socket joint), is then opened. The ball is gently levered out of the socket and is removed using a saw (Figure 2.6).

At this point, the damaged cartilage on the socket is removed using a scraping tool called a reamer, and the socket is shaped to form a hemisphere. The acetabular component is now inserted, with or without bone cement. Sometimes, in uncemented procedures, additional screws are used to hold the component firmly to the bone.

Next, the inside of the thigh bone (femur) is prepared using motorized and hand-held tools to shape it to accept a stem, at one end of which is the new artificial femoral head. Once the stem is inserted, leg and joint stability are verified, and the final components are inserted.

The tissues are cleaned with sterile saline solution, any deep tissues that were incised are now repaired, and the skin is closed. A surgical drain may be used to allow the escape of fluids that build up in the wound during healing, at the surgeon's discretion.

The description above is for a traditional hip replacement, using an incision that varies between 12.5 and 20 cm long proportional to the size of the patient. In contrast, 'minimally-invasive' hip replacement is a new surgical approach. The same approaches are used as in traditional hip replacement surgery but the incision is much shorter (usually 10 cm or less in length). In general, specially designed retractors and customised instruments are used to expose the hip joint, to prepare the socket and to insert the prosthesis. Some dissection of the muscle is necessary but to a lesser extent than in the traditional approach.

Selection of the type of implant, in terms of its materials, is another issue to consider. For the selection of the bearing surface between ball and socket there are several possibilities: polyethylene, ceramic and the metal-on-metal bearings.

Another issue to decide about the implant is the method of fixation in the bone. In cemented hip replacements, an acrylic bone cement is used to hold the implant in place. Alternatively with uncemented stems, the hip is implanted without

cement. These devices may have a porous metal coating or a chemical coating to which bone will attach and secure the implant. In Figure 2.7 a cemented Charnley implant and a cementless AML are shown.

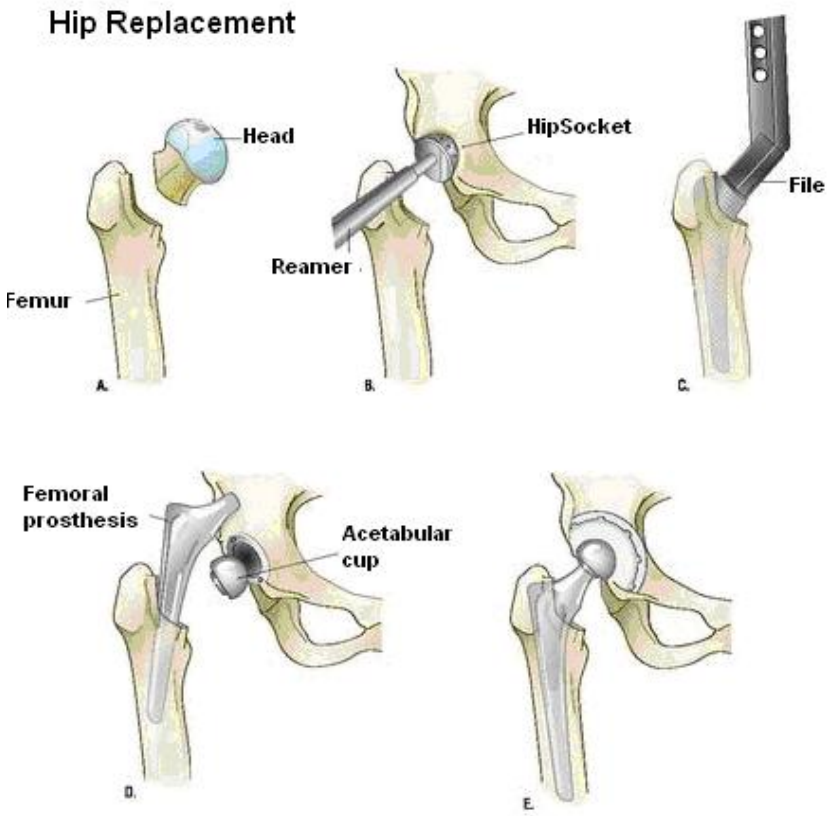

Figure 2.6: Process of the Total Hip Arthroplasty (THA/THR) [6]

2.1.3 Failure after THR

After a hip replacement, even with the most modern designs, failures occur, and such situations require removing the original components and insertion of new components (known as revision operations) which are significant undertakings. These secondary operations are often less successful than the primary surgery, and as such are hoped to be avoided.

The main complications of hip arthroplasty (replacement) are wear of the

Figure 2.7: A cemented Charnley implant (left) and a cementless AML implant (right)[7]

polyethylene liner, loosening of the joint components, infection of the joint, migration of the implant, fatigue failure and accumulated damage, most often of the cement mantle, dislocation and deep vein thrombosis. This chapter summarizes the most common failure mechanisms related to the femoral stem.

Dislocation is a painful condition in which the prosthetic femoral head, or the 'ball' on the proximal end of the femur or thigh bone no longer articulates, or 'comes out of joint', with the socket in the acetabular cup of the pelvis. Such a situation may be due to the loosening of the surrounding structures of the hip after arthroplasty, such as the muscles, hip joint capsule and ligaments. In addition, smaller head-neck ratios reduces the angle of motion allowed before the neck impinges on the acetabulum, and exceeding this angle can lead to dislocation. At 5 years postoperatively, the dislocation rate in Charnley THRs was found to be as high as 5% [28] in a single health region in England.

Aseptic loosening [29] occurs when any form of loosening which is not accountable to infection takes place, leading to loss of component fixation, resulting in the necessity of removal. This may happen if the bone does not grow into the component sufficiently or if wear particles from the bearing surface access the prosthesis-bone interface and produce weak pockets of bone around the prosthesis (osteolysis). Another cause may be the stress shielding of the cortical bone, since a stiffer material (the implant) is bearing a large part of the load, and consequently there is a reduction in the load transferred to the bone that leads to a thinning of the femoral cortex around the prosthesis. Stress bypass is a related phenomenon associated with a poor fixation in the proximal regions of the stem

and good fixation at the distal tip, due to surface-contour shape factors, leading to a transfer of the load down to the distal tip, hence the proximal femur is under-stressed and becomes subject to bone-resorption. Aseptic loosening is cited as the reason for failure in more than 65% of all failed THRs [30].

Infections [29] may be categorised as early (less than 12 weeks), generally acquired from intra-operative contamination; delayed (12 weeks to 1 year) and late (more than 1 year) generally acquired from distant sources such as the skin, ulcers, the urinary tract or dental caries. In these cases the implant forms an environment that antibiotics have trouble penetrating, allowing infections to spread rapidly.

Migration is permanent relative displacement between the implant and the host bone. All un-cemented implants display some migration in their first year. The cyclic loading of the bone can eventually lead to crack growth and propagation within the femur [31]; micro-cracking of the trabeculae [32] removes a portion of the implant support allowing it to sink down within the bone, and it is particularly notable in regions with high stress such as that around the tip of the femoral implant [33]. The effect of migration will be detailed in Section 2.6.1.1.

Fatigue failure and accumulated damage [30] are caused by repetitive loading, leading to the gradual build up of mechanical damage in materials and interfaces. In un-cemented implants, the lack of the weak cement link makes it less likely to suffer loosening from accumulated damage.

Deep Vein Thrombosis [30] are blood clots in the larger veins of the leg after THR, and may lead to re-admission for treatment. Treatment is through blood thinning medication, compression stockings to aid circulation and early mobilization.
The failure mechanisms described above have been linked to a number of risk factors:

- bone does not grow into the component sufficiently or the bearing surface wears out [29]
- the implant as a stiffer material bears a large part of the load producing stress shielding [29]
- surface-contour shape factors produce stress bypass effects [29]

- skin, ulcers, the urinary tract or dental caries may be a source of implant infection [29]
- migration [30, 31, 32]
- accumulated damage, especially in the cement layer [29]
- blood clots [29]

These factors may be related to interface conditions, implant material and shape, patient's condition, use of bone cement or the type of surgical intervention, all of them subject to a large amount of variability that makes the prediction of the performance of the construct difficult. Some studies describe the effects of specific techniques, implants and fixation techniques on hip replacement performance, and they will be discussed in the following sections.

2.2 Cemented vs cementless

One of the main questions when approaching a total hip replacement is about the use of cemented or uncemented implants, both in the acetabular cup and in the stem. There are some studies that have analysed the advantages of each method. Laupacis *et al.* [34] compared the fixation of a Mallory-Head total hip prosthesis with and without cement, and they found that the group that had the cemented prostheses required more revisions of the femoral component than did the cementless group. In a review performed by GECO FUTURA hip group [35] the disadvantages of cement were analysed, such as cardio-respiratory incidents during its use, which represents a risk which is greater than in the absence of cementing, or the complications with the removal of the cement in a revision surgery, that can leave necrotic bone of mediocre quality, or the formation of the fibrous membrane between the implant and the bone, that lets the migration of the debris liberated by the prosthesis along its whole length. They also noted the high price of uncemented implants, due to the high cost of the components when revision is needed, and also because of the manufacturing process regarding the hydroxyapatite coating. In a review performed by Faulkner *et al.* [22] for the NHS R & D HTA Programme, the effectiveness of hip prosthesis from the results

of clinical studies were analysed. From one comparative radiographic study they observed that cemented acetabular components performed better than porous-coated designs but that porous-coated stems performed better than cemented models. Also, from other radiographic studies of cemented versus HA-coated designs, it was suggested that HA-coated models have better early fixation and less migration than cemented models [22].

In the present work, attention will be focus on the uncemented stem characteristics.

There have been several generations of hip prosthesis. The first total hip prosthesis to be taken up was that designed by John Charnley in the early 1960s at Wrightington Hospital, near Wigan, in the industrial region around Manchester. For all the more modern (and more expensive) variants, the Charnley hip remains in common use today. In the 1970s, high failure ratios of the early cemented THRs were found, characterised by bone loss (osteolysis) and mechanical loosening of prosthesis. In the belief that cement reaction was the cause of these failures, the investigation for alternative solutions led to the concept of cement-free fixation. Methods of cementation have themselves evolved and are typically classified into the three generations with the characteristics noted in Table 2.2 [22].

Various cement-free methods have been developed which can be summarized broadly as:

Press-fit methods, in which fixation is sought by closeness of fit between prosthesis and bone, often assisted mechanically by techniques such as threading and augmentation by screws, nails or pegs, and 'macro-interlock' design features such as ribbed stems designed to improve fixation by wedging.

Porous-coating, in which an inert microporous coating in the form of mesh or beads is manufactured on the surface of the prosthesis with the aim of encouraging ingrowth of bone into the prosthesis surface.

Hydroxyapatite (HA-) coated, which is similar to porous coating in concept but the surfaces adjacent to bone are coated with HA, a form of calcium phosphate ceramic considered to be biologically active and capable of direct chemical bonding to bone.

Prosthesis Type	1960s	1970s	1980s	1990s
Cemented				
1^{st} **generation** Finger packing	1960s			
2^{nd} **generation** Intramedullary femoral plug, cement gun, superalloys for stems		mid-1970s		
3^{rd} **generation** (some still regarded as experimental) Pressurisation, porosity reduction, precoating, rough surface, centrisation			mid-to late 1980s	
Ceramic (head/cups)		late 1970s		
Uncoated press-fit cementless		late 1970s		
Porous-coated cementless			early 1980s	
Hybrid (cemented stem/uncemented cup)			early 1980s	
HA-coated			late 1980	
Fully modular			late 1980	early 1990

Table 2.2: Major developments in THR technology [22]

In the most common form of **hybrid** fixation, a cemented stem is combined with an uncemented cup, which retains the relatively good performance of cemented stems but substitutes possibly superior cement-free cups; this allows immediate weight-bearing.

In the **fully modular** type of prosthesis, the problem of achieving close anatomical fit is undertaken by making available a range of sizes of separate subcomponents of the total prosthesis, comprising the acetabular cup, the femoral stem, and the separate sleeve and head of the femoral component. Manufacturers are developing increasing modularity, and an increase in modular connections in a prosthesis leads to increased production costs and potential increase in wear.

Ceramic heads and cups (among other combinations of materials) have been developed in an attempt to diminish wear and thus reduce the production of

damaging particles at the bearing surfaces of the prosthesis.

2.3 Uncemented THR: clinical experience

In the 1970's and early 1980's bone cement was suspected to play a major role in bone resorption and aseptic loosening of prostheses. This led to the introduction of prostheses for cementless use [36]. The cementless technique relies on biological fixation provided by initial press fit insertion or screw fixation followed by bone ingrowth into a textured or porous implant surface [37]. Later calcium phosphate (Ca-P) coatings like hydroxyapatite were introduced for the purpose of enhancing the bone implant ingrowth [38, 39].

The belief that the cement itself caused the loosening of the prostheses explained their popularity, and surgeons used these prostheses in great numbers without any knowledge of their clinical results (Hip and Knee Replacement in Norway, 1987-2000 [39]).

It took only a short time (3-5 years) before some registers, such as the Swedish Knee and Hip registers [40], [41] and the Finnish Implant register [42], indicated that inferior results were obtained with un-cemented implants compared to cemented implants. This difference was largest in younger patients [43]. 398 femoral designs were actually used [44], and many of these have turned out to be catastrophes. An example of these studies with bad results of un-cemented implants was carried out by Duparc and Massin [45], who studied the results of 203 THR using a smooth, cementless femoral component. Thirty-two hips were revised due to mid-thigh pain, and the femoral implant was found to be loose in all. In the conclusion they suggested that the implantation of this stem should be restricted to patients in whom cement fixation is contra-indicated. Another example was a review by Havelin *et al.* [46] based on the Norwegian Arthroplasty Register [46], eight different designs were compared: Bio-Fit, the Corail, the Femora, the Harris/Galante, the LMT, the PM-Prosthesis, the Profile and the Zweimüller. At 4.5 years, the estimated probability of revision for aseptic loosening for all implants was 4.5%, for the Bio-Fit stem the probability was 18.6% and for the Femora stem it was 13.6%. The PM-Prosthesis and the Harris-Galante stem prosthesis needed revision in 5.6% and 3.6% cases, respectively. The clockwise threaded

stem of the Femora implant needed revision in 20% of right hips, but in only 4% of left hips. The short-term results of the four best cemented femoral components (Corail, LMT, Profile and Zweimüller) were similar to those for cemented stems, with revision for loosening in less than 1% at 4.5 years. In conclusion, the overall results of the un-cemented THR on Norway have been shown to be inferior to those for cemented THR [43].

After evidence of the poor performance of early uncemented components emerged, new designs of cementless prosthesis started to show better results. Shramm *et al.* [47], reviewed the results of the tapered femoral component designed by Spotorno [48] in 2000, and showed that the results obtained with CLS stem (press-fit design) during its 15 years of use seemed to demonstrate the hypothesis that an un-cemented stem can reach the requirements in both quality of results and survival curve. The cementless femoral prosthesis had a low revision rate (6%), most were associated with proximal femoral osteolysis. They observed minimal or no stress-shielding, and osteointegration and adaptive bone remodelling appeared to protect the proxima femur from distal endosteal osteolysis. The same good results for press-fit designs were obtained by Archibeck *et al.* [49], who assessed the results of an eight to eleven years follow-up study of second-generation cementless femoral components, whose main characteristics were the modification in the design to increase the initial press-fit and stability of the femoral component, to provide more reliable ingrowth and to limit distal osteolysis by incorporating proximal ingrowth surfaces. They studied seventy-eight circumferential proxima porous-coated hips (Anatomic Hip) for a mean of ten years follow up. They found that no femoral component was revised for any reason, and none were loose radiographically at the time of the last follow up. In conclusion, this second-generation cementless femoral component gave excellent clinical and radiographic results with a 100% survival rate at ten years improving ingrowth and preventing distal osteolysis.

At the same time, the new generation of un-cemented hydroxyapatite (HA) coated implants was showing very good results, such as was demonstrated by Epinette *et al.* [8], who assessed four uncemented HA coated femoral and acetabular implants (see Figure 2.8), with a follow-up of ten years or more: the Corail, the PRA, the Omnifit and the ABG hip prostheses. They found that at ten years after surgery, 95.9% of patients had good, very good and excellent func-

tional results acquired in the first post operative months. The 2.15% of loosening seen in the survivors during the 10 year follow up period were all cases in which early primary stability led to micromotion and lack of osteointegration. They concluded that the hydroxyapatite coating gave security as long as the primary stability was assured.

Another group of implants with similar results in terms of bone ingrowth fixation and mechanical stability is represented by the porous-coated implants. In 2003, Young-Hoo Kim *et al.* [9], looked at the results in young patients who had been followed for a minimum of eight years after treatment. There were a total of 118 hips in the study. They used a cementless Profile femoral component (porous-coated) in all hips. There was no aseptic loosening. One hip was revised because of recurrent dislocation. 12% of the hips had osteolysis in the calcar femorale. In conclusion, the mechanical fixation of the anatomic fit cementless Profile stem was excellent in this study.

In the same year, Bojescul *et al.* [50] studied the outcomes of a prospective series of primary cementless total hip arthroplasties after a minimum of fifteen years of follow-up. The porous-coated anatomic total hip prosthesis (PCA) without cement implanted between 1983 and 1986 was analysed. They found that only 7% of the entire cohort and 6% of the living cohort had undergone revision for loosening of the femoral component or osteolysis. They concluded that the porous-coated anatomic femoral component proved to be durable at a minimum of fifteen years postoperatively.

Garcia-Cimbrelo *et al.* [51] studied the performance of the Zweymüler Alloclassic total hip arthroplasty system. They looked at 124 implants, with a mean duration of follow-up of 11.3 years. Standard radiographs were made for all patients immediately after the operation, at six and twelve months, and annually thereafter for at least ten years. Multivariate analysis was performed to assess the influence of various factors on survival of the implant. They concluded that this prosthesis, particularly its femoral stem, demonstrated good results and durable fixation at a minimum of ten years of follow-up.

Sinha *et al.* [52] looked at eighty-eight implanted Harris-Galante Multilock femoral stems (porous-coated) with a minimum of five years of clinical and radiographic follow-up. 99% of the stems were biologically stable, with 95% having

osseous ingrowth and 3% having stable fibrous fixation. 38% had minimal proximal osteolysis, and no hip had diaphyseal osteolysis. 82% had some degree of stress-shielding in the proximal metaphysis, but only two hips had cortical resorption. None of these patients required additional surgery, and all reported a satisfactory outcome. To conclude, the level of patient function and satisfaction were good, the rates of loosening and revision were very low, and distal osteolysis did not occur. Osseous fixation occurred reliably. Proximal stress-shielding was seen but did not seem to be clinically important.

It has been shown how, after discovering that the uncemented implants were producing very bad results, new versions or modifications were produced that have offered excellent improvements, but still the failure incidence remains higher than that of cemented implants. There is therefore a need to identify what are the factors that predispose to revision surgery for cementless implants. The following section will focus in the findings related to hydroxyapatite coated femoral stems.

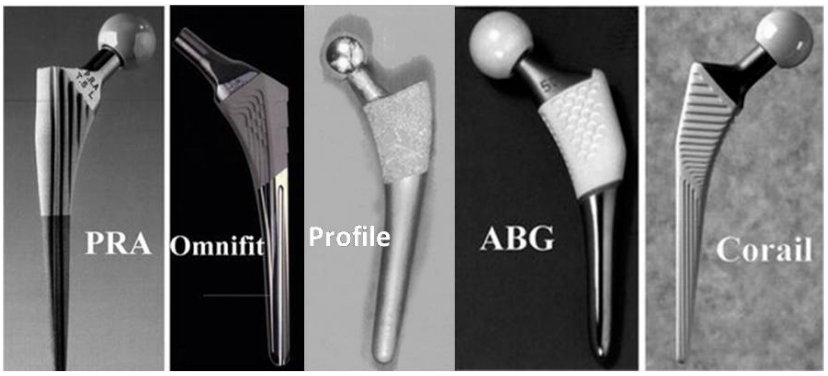

Figure 2.8: Different kinds of un-cemented hip stems [8, 9]

2.4 Hydroxyapatite coated femoral stems in THR

Hydroxyapatite (HA, Ca10[PO4]6[OH]2) is chemically similar to the mineral component of bones and hard tissues in mammals. This material is classed as bioactive, indicating that it will support bone ingrowth and osseointegration when used in orthopaedics [53].

The main property that makes HA suitable for prosthetic applications is its

ability to integrate in bony structures and support bone ingrowth, without breaking down or dissolving (i.e. it is osteoconductive), and the fact that it is thermally unstable compound, decomposing at temperature from about 800-1200°C depending on its stoichiometry [53].

HA coatings are mainly applied to metallic implants (most commonly titanium/titanium alloys and stainless steel) to change their surface properties. In this way the body perceives a hydroxyapatite-type material. Without the coating the body would see an unfamiliar body and work in such a way as to isolate it from surrounding tissues. To date, the only commercially accepted method of applying hydroxyapatite coatings to metallic implants is plasma spraying [53].

From 15 years of clinical experience with HA-coated hip prosthesis [53] there have been very positive outcomes:

In 1992, Kroon and Freeman [54] studied two groups of femoral prosthesis: Ti6Al4V ridged press-fit stems, and 26 with similar stems coated with hydroxyapatite on the proximal half. They measured the stability of the prosthesis radiologically. To estimate the vertical migration they calculated the distance between the tip of the greater trochanter and an adjacent point on the prosthesis, and they subtracted this value at six and twelve months from that observed immediately after operation to determine the migration. They found that HA-coated prosthesis migrated no more than 1 mm at six months or one year, and consequently they migrated significantly less than the Ti6Al4V press-fit stems both at six months and at one year.

In 1996, D'Antonio *et al.* [55] studied the remodelling of bone with proximally HA coated femoral stems in 224 total hip arthroplasties with a minimum follow-up of 71 months. The radiographic findings of progressive new-bone formation throughout the zones adjacent to the middle and distal portions of the stem were evidence of early, extensive proximal fixation of the implant. Remodelling of the femur began early, was predictable, and progressed throughout the follow-up period. They concluded that a circumferential coating of hydroxyapatite may effectively minimize migration of wear debris along the femoral stem.

In 1998, Capello *et al.* [56] investigated how hydroxyapatite coatings help bone ingrowth and ongrowth, and found that HA does enhance these two actions with no increased incidence of osteolysis for up to 10 years.

In 2000, Coathup *et al.* [57] analysed bone remodelling around hydroxyapatite-coated, porous-coated and grit-blasted hip replacements retrieved at post-mortem. They investigated the bone-implant interface around one design of proximally coated femoral stem. They estimated ingrowth and attachment of bone to the surface of the prosthesis and also the amount of hydroxyapatite coating was quantified. There was significantly more ingrowth and attachment of bone to the porous HA surface than to the plain porous surface. Bone grew more evenly over the surface of the HA coating whereas on the porous surface, bone ingrowth and attachment occurred more on the distal and medial parts of the coated surface. No significant differences in the volume of HA were found with the course of time. This better ingrowth and attachment for HA coatings may have an implication in reducing stress shielding and limiting osteolysis induced by wear particles.

Also in 2000, McNally *et al.* [58] conducted a similar investigation for HA coatings using the JRI Furlong femoral component, for a mean follow-up of ten years. They found the same satisfactory prosthesis-bone interface.

In 2001, D'Antonio *et al.* [59] continued his investigation with a 10-to 13-Year follow-up study of HA-coated titanium alloys stems, and showed an excellent lasting fixation of this stem, performed in a young, active, high risk population and in the hands of several surgeons.

In summary, all the studies developed so far show a satisfactory bone ingrowth and ongrowth, or in other words, a good long term fixation between bone and implant.

2.5 Variables in THR

One of the main aims of the present work focuses on the analysis of the performance of the THR as a function of different variables. It is evident that many different post operative failure mechanisms exist, and some can be related to abnormal stresses and strains generated by poor component design, deficiencies in component fixation or innaccurate implantation. Traditionally, experimental investigations into the performance of hip replacements have been limited to analysing one situation (e.g. one alignment and one bone). The results of these investigations can really only act as a qualitative indicator as the biological envi-

ronment can not be adequately simulated in the laboratory. Add to this the huge number of experiments that would be required to simulate all possible scenarios (combinations of alignment, geometries, bone quality etc.) and experimental investigations soon become unfeasible. While computational models may produce results in a much shorter time, most investigations to date again describe only one situation and many computational models are required to fully describe the effect of variations in only a single parameter. The present research attempts to address this shortcoming by developing computational tools that can account for variations in several parameters simultaneously and efficiently.

Listed below are some examples of variables that may affect the performance of a THR:

Surgical Approach: The surgical procedure has a direct effect on the soft tissues that are dissected during the intervention. There are traditionally two different surgical approaches: the posterolateral and anterolateral approaches [60]. The posterolateral approach has the highest associated incidence of dislocation, and this is believed to be due to straightening of the spine and flexing of the pelvis in the side-lying position used during this approach on the operating table. This may lead to an inappropriately positioned socket. The rate of dislocation with this approach and others decreases with the experience of the surgeon. The muscles that are usually affected by these surgical approaches are: for the posterior approach, gluteus maximus (extension), minimus and medius and tensor fasciae (abduction), and piriformis and quadratus femoris (lateral rotation); in the anterior approach: gluteus minimus, medius and tensor fasciae latae (abduction) and vastus lateralis (extension) [61]. However, the degree of muscle damage is different for each surgical approach, and this has been related to inadequate restoration of soft tissue tension. Restoring the appropriate degree of soft tissue tension (tightness) is one of the most important factors in preventing failures following a total hip replacement. 75% of patients with dislocation have poor soft tissue tension due to a variety of reasons. Previous hip surgery and/or revision arthroplasty surgery may predispose to problems with soft tissue tension and have been associated with increased incidences of dislocation. Detachment of the insertion of the abductor muscles into the greater trochanter of the femur or trochanteric nonunion following an approach using a trochanteric osteotomy leads to inadequate soft tissue tension.

Prosthetic component design and orientation: Proper component orientation is the most important factor in preventing future failures through dislocation. The prosthetic stem position depends upon the surgical approach. A malpositioned component may be protected from dislocation after the early postoperative period due to soft-tissue and capsular healing. Failures can also result from problems with component design and/or selection. If the components are not properly selected, the prosthetic femoral neck may lever against bony prominences around the pelvis. This 'impingement' must be avoided as the prosthesis can lever out of the acetabulum in certain positions: extension/external rotation and flexion/internal rotation.

Patient features: such as cooperation, since patient's noncompliance with total hip precautions (proper body positioning) increases the likelihood that dislocation will occur. Another factor is the femur geometry and quality. It is a fact that every femur has different dimensions, and bone properties can vary between patients, and even within the same bone.

2.5.1 Influence of Bone Geometry and Quality

Patient specific features may play an important role in the performance of a THR. The loading is directly related to the proportions of height and weight, usually represented by the body mass index (BMI). It seems obvious to think that for two persons with exactly the same femur, if one of them is heavier than the other, then the consequent higher loading of the bone may lead to higher stresses and deformations in a simple model where just the hip contact force were included. If muscle forces were the same in both individuals, then the increase in internal stress and strains would be more predictable, but the reality is that muscle strength varies also substantially between individuals. Muscle strength depends on life style and genetic factors. If variability in bone geometry is added, then the load is transmited to the bone in different directions, hence producing different stresses and deformations. Variability in bone geometry is large among the world's population. If variability of bone quality is considered, then each particular internal point of the bone has particular material properties. This aspect also changes for the same individual along his or her life, since the bone is a living material. Thus, an individual's femur at a particular moment of his

or her life is unique, and it is not appropriate to extrapolate the results obtained for a particular simulation of one implanted femur to the whole population of femurs.

Some authors have looked at the influence of geometric parameters of the bone on the incidence of bone degeneration. Among all the geometrical measures of the bone, anteversion has been considered a possible factor that enhances joint degeneration [62, 63, 64]. In a study by Heller *et al.* [65], the influence of femoral anteversion on proximal femoral loading was assessed validating musculo-eskeletal models of the lower limb of four real patients with the individual gate cycles. The anteversion angles of each patient were varied, simulating a decrease to -5° and an increase to +30°. All the boundary conditions were then recalculated and compared to the initial values.The results indicated that increased anteversion by more than 20° may lead to a considerable increase in femoral loading. If this anteversion is adopted in a hip stem, these results suggested that larger values may lead to increased proximal femoral bending moments and therefore influence bone remodelling and long-term performance of implants.

Femur and implant anteversions, and in general bone and implant geometries, may play a determinant role in the performance of the THR, and hence their variability should be considered in these analyses. Generalizing the outcomes of particular simulations to the entire population of THRs should be avoided until the effect of this variability is quantified. The next section focuses on literature on the influence of implant positioning and geometry.

As will be detailed later, it has been seen that the variability of bone material properties induces uncertainty in the response of the construct [66, 67, 68, 69, 70, 71]. One recently common procedure is to asign the properties of the elements of a meshed bone by relating them to the intensity of the corresponding pixels of its CT-scans. These CT scans are used to obtain a 3D reconstruction of the femur using and interpolating the contour of the slices. The bone density at each point of the bone volume is correlated with the gray scale (GS) (also called 'ash density') of the corresponding pixel, using a linear relationship between the Hounsfield (HU) numbers and the bone ash density [72, 73] (Equation 2.1).

$$\rho = a + b * GS \tag{2.1}$$

An exponential relationship between the Young's modulus and the bone ash density [74, 75, 76] is considered (Equation 2.2).

$$E = c + d * (\rho)^e \tag{2.2}$$

To obtain the values of the Young's modulus of the elements it is necessary to average or integrate the values of the corresponding points in the mapped 3D model. This may be performed in different ways. One common application is presented by the freeware program Bonemat V2 [77, 78], which calculates the HU value of an element by integrating the HU field over the element's volume. There is also the possibility to transform the HU field into a Young's modulus continuum field and then perform the numerical integration over the element's volume. This process was presented in BoneMat V3 [79], to analyse the influence of the mapping strategy in the accuracy of the predicted stresses and strains, compared with the experimental ones. It was found that the second approach improved the predictions of these outputs.

Another source of inaccuracy regards the calibration of the CT-scanner that determines the intensity of the pixels, and the values of the parameters in the relationships between pixel intensity-bone density-Young's modulus are specific to the patient and the user can choose them. Some of the most common relationships adopted in previous studies were analysed by Schileo *et al.* [80], and they found that the selection of the density-elasticity relationship greatly influenced the accuracy of numerical predictions. This means that comparisons may be performed in a population of bones when the same CT-scans calibration and density-Young's modulus relationship were used. In a more recent study [81], it was found that a correction of the densitometric calibration of the CT scans , i.e. the relationship between the HU values and the ash density, should be used when evaluating bone mineral density from clinical CT scans, to avoid the under or overestimation of the tissues. Also a constant relationship between ash density/aparent bone density equal to 0.6 can be assumed in the human femoral bone. The correction of the calibration and densities relashionships signifficantly affected the overall accuracy of the strains obtained by the FE simulations, hence special attention should be paid to these calculations.

2.5.2 Influence of Implant Material, Design and Positioning

Despite the great success of THR, large variability between different implant designs remains a major problem. Ahnfelt *et al.* [40] showed how different types of THR procedures may have considerably different survival rates. Influence of implant material on the performance of the THR has been reported by many researchers. Sarmiento and Gruen [82] compared the radiographic analyses of low-modulus titanium-alloy femoral components whose geometry was similar to the high-modulus Charnley prostheses, in a two to six-year follow-up study. They found that incidence of loosening, calcar resorption and cortical hypertrophy was lower in the titanium-alloy implants than in the Charnley implants.

Weinans *et al.* [83] also found that implant material and fixation method (cemented vs uncemented) had a great effect on the bone remodelling in the femur around the implant. They analysed cobalt-chrome and titanium alloy materials for both cemented and uncemented FE models, and an additional hypothetical uncemented implant (also called 'iso-elastic') with stiffness close to that of cortical bone. Cemented stems caused lower bone resorption and interface stresses than uncemented stems made from the same materials. A law for predicting bone remodelling around the implant was proposed and implemented, based on strain-energy stimulus. Interface stresses and bone remodelling were then investigated for fully bonded cases. Very little bone resorption was found around the iso-elastic stem, but the proximal interface stresses increased drastically relative to the other uncemented stems. Once more, this highlighted the effect of implant material on the performance of the THR, now using a different output indicator.

Component position and geometry are important factors in the performance of the femoral component that are under the direct control of the surgeon. It has been demonstrated how the relative position between the cup and the head influences the risk of dislocation [84]. Interface contact stress levels have been found to be lower under the proximal neck with a full length implant stem, compared to those of a similar implant with short stem [85].

As has been seen in Section 2.3, implants may have a large variety of surface finishes. However, it has been seen that these features do not have a great effect on

the cortical strain distributions of the bone or the stability of the implant [86, 87]. Gillies *et al.* [86] evaluated the influence of implant design parameters on the cortical strain distribution for a cementless titanium femoral stem in experimental simulations on 6 cadaveric femurs. An intact femur and 5 implanted femurs with different design features were used. The first implant was the geometrical design and subsequent implants featured distal flutes, a distal coronal slot, proximal steps and a proximal porous bead layer coating of the steps. There were no apparent differences observed between any of the design parameters. In all cases, proximal anterior strain distributions were greater than in the intact case. There were no statistical differences in the principal cortical bone strain distributions regardless of the prosthesis design. Biegler *et al.* [87] analysed the effect of two designs of hip prostheses with smooth and porous coated surfaces, in one-legged stance and stair climbing configurations. The amount of contact and the relative motion between bone and implant were calculated. Both micromotion and amount of contact at the bone-prosthesis interface were more dependent on load type than on implant geometry or surface coating type. These studies suggest that implant surface finishes may not have a significant effect on the performance of the THR compared to other parameters.

The effect of implant geometry has been analysed more often. Decking *et al.* [88] looked at the effect that 3 different hip stems had on the in vitro strains in the proximal femur. A conventional straight, an anatomic stem designed to encourage a proximal force transmission and a stemless femoral neck prosthesis were evaluated. The straight and anatomic stems led to a decrease in the longitudinal strains in the proximal femur, while the femoral neck implant mainly led to an increase of measured strains on the lateral side of the greater trochanter. The medial strains were closer to the physiological values in the stemless prosthesis than those of the two full-stem prosthesis. This may induce a remodelling process that better retains bone stock in the inferior base of the neck. In summary, an effect of the implant geometry on the strain distribution of the implanted femur was evident for this set of implants.

The most commonly analysed variable in implant positioning is the anteversion angle. This has been examined in several studies, such as that carried out by Nishii *et al.* [11], who found out that the cup anteversion is one of the important factors for risk of dislocation, and that intentionally placing it at low anteversion

to compensate for high femoral neck anteversion may predispose the hip to post-operative dislocation. Also the sum of the cup and the stem anteversion turned out to be quite low among the dislocated hips. Speirs *et al.* [89] looked at changes in the stress and strains in the femur, using a short-stemmed implant, comparing the femoral loading after THR for three different situations: the intact hip centre, implant placed in increased anteversion and implant with an offset, for walking and stair climbing. They found that small changes in stem placement would likely have little influence on the internal loading of the femur after bone ingrowth has been achieved, however a reduction in strain energy density and therefore stress shielding was seen, which may have consequences for longer-term remodelling. Similar work was developed by Aamodt *et al.* [90], who compared the changes in the pattern of the principal strains in the proximal femur after insertion of eight uncemented anatomical stems and eight customised stems in human cadaver femurs. Both stems induced significant stress shielding in the proximal part of the metaphysis, but the deviation from the physiological strains was most pronounced after insertion of the anatomical stems, which also induced more stress concentration on the anterior aspect of the femur than did the customised stems. They also increased the hoop strains in the proximo-medial femur.

Values of implant version angle can be found in the literature. It is currently recommended that reaming of the femoral medullary canal should proceed at approximately 15° of anteversion in relation to the axis of the flexed tibia [10]. Figure 2.9 shows the femoral anteversion angle without the implant (a), and with two different implant positions (b).

If the same anteversion angle is reproduced in every case, variations of the entry point to the medullary canal (e.g. P1, P2) will result in significant deviations (V1, V2) from the normal version (V) of the femoral head [91]. A prospective clinical study using computed tomography showed that an average preoperative femoral anteversion angle of $14.1 \pm 6.9°$ was reproduced to a mean of $10.8 \pm 6.2°$ [92]. The same anteversion angle was measured in a study by Nishii *et al.* [11] in an assessment of the influence of component position on dislocation, in 191 THAs without cement. They obtained values of $29.6 \pm 10.3°$ of stem anteversion, measured between a line drawn along the stem neck and between the posterior portions of the femoral condyles (Figure 2.10).

Taking the same reference lines, Kuen Tak Suh *et al.* [12] , measured the

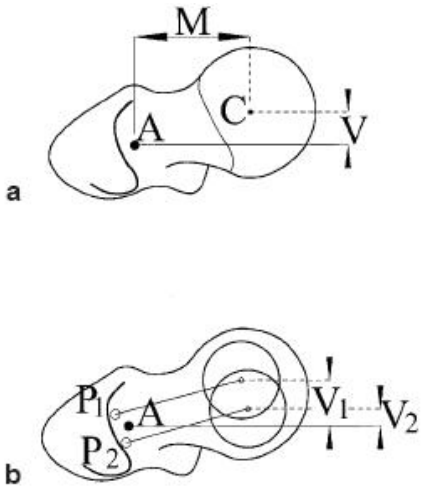

Figure 2.9: a) Medial offset (M) and version (anterior offset, V) of the femoral head as measured from the centre of the femoral head (C) and the intramedullary axis of the femur (A). b) A source of variation of the version (anterior offset) of the femoral head [10]

femoral stem anteversion in 33 patients with unilateral cementless THA, obtaining values of $17.8 \pm 6.3°$ (Figure 2.11).

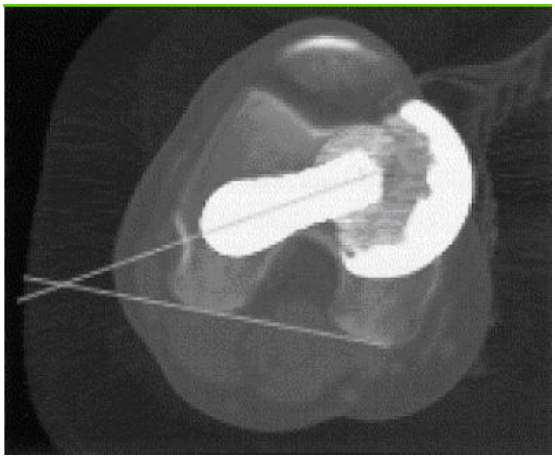

Figure 2.10: Calculation of the stem neck anteversion on a CT image of the femoral condyles [11]

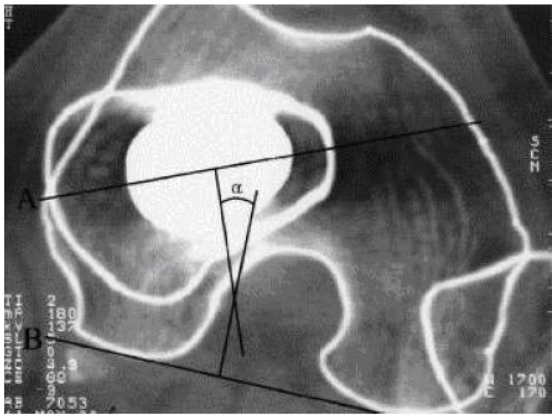

Figure 2.11: Femoral stem anteversion (a) on the lesion side was defined as the angle between the stem axis (A) and the posterior condylar axis [12]

In a study carried out by Mazoochian *et al.* [93], the accuracy of stem implantation in THR was assessed using a computer-aided system. The femoral stem anteversion angle was measured from 10 patients with cementless hip implants, obtaining values with a mean and standard deviation of $14.3 \pm 6.5°$.

All the above studies suggest that implant surface finish may not have a great effect on the performance of the THR. However, they suggest the importance of considering material and the geometric factors involving the femoral stem, such as dimensions, shape and relative position with the bone, in the performance of a THR.

2.6 Computational methods in bioengineering

Computational methods are based on mathematical models, and they have the advantage of analysing the physics of a system without the experimental simulation in a laboratory, therefore, they are quicker, since it is possible to simulate many scenarios in a very short time, and cheaper since only computers are needed to perform the simulations. Many recent studies address the analysis and simulation of bone remodelling around the implant, and the introduction of soft tissue behaviour in the implanted bone is being investigated. The use of integrated methods is being extended, which better simulate these complicated behaviours, i.e., Finite Element (FE) Modelling. Computational modelling is a very useful tool for predicting the behaviour of selected implant/bone scenarios. This has been demonstrated in many studies, and relevant examples are discussed below.

2.6.1 Finite Element Modelling of the Hip Replacement

The Finite Element Method was first applied to orthopaedic biomechanics in 1972 to evaluate stresses in human bones [94]. Since then the method, thanks to the increase in computing power, has improved and been applied with increasing frequency to the analysis of bone, prostheses, and tissue.

2.6.1.1 Factors to consider in FE Analyses of the uncemented THR

When approaching the deterministic design of the uncemented THR, a number of factors may be considered. The selection of these factors depends on the required accuracy of the results. Factors such as material properties of both the bone and the implant, the definition of the interface conditions, the refinement of the mesh, the hip contact load to apply, the inclusion of muscle forces or the constraints of the model are some of the parameters that define the design of the FE model. Numerous studies have looked at the influence of these parameters in the performance of the simulated THR, and these are discussed below.

Material properties.

It is necessary to choose the material model that best approximates the material under consideration. The implant may be modelled with sufficient accuracy as a linear, homogenous and isotropic material, with the corresponding Young's modulus and Poisson coefficient of the material. However, the assignment of material properties to bone is complicated. In some studies several simplifications about the material properties of the bone and the conditions at the interface between bone and implant have been made [95, 96, 97]. Homogeneous materials properties for cancellous bone have commonly been assumed. However, bones are highly non-linear, heterogeneous and anisotropic. Additionally, bone is a living material that reacts and adapts to changes in external and internal conditions. This makes the assignment of bone material properties a complicated task if relative accuracy is required. As discussed in Section 2.5, a common procedure is to assign material properties to a meshed model relating the intensity of the greyscale of the pixels in the CT scans to the Young's modulus of the element by using the Equations 2.1 and 2.2.

Mesh-Related Factors

When setting up the Finite Element model, the selection of type of element and its size does not follow any specific criteria, it is just known that the coarser the mesh is, the lower the resulting running time, but there is inherent loss of accuracy compared to a finer mesh. Although tetrahedral elements are usually used since high quality meshes are much easier to generate automatically, some researchers have used hexahedral meshes [95, 98].

Stolk *et al.* [98] assessed the sensitivity of different failure criteria of the cemented THR to mesh density. They performed a convergence study to a FE model of a proximal femur implanted with an Exeter hip prosthesis, using a mesh of hexahedral elements. They simulated both bonded and debonded implant-cement interfaces ($\mu = 0.25$). The load case represented the stance phase of gait, with 3 abductor forces acting on the greater trochanter, and a hip joint reaction force. Maximal cement and interface stresses and the fraction of cement volume loaded at tensile stresses above 10 MPa were compared. The results showed that the bonded case was not sensitive to mesh density. However, the unbonded cases showed that maximal cement and interface stresses were very sensitive to mesh density. Hence, this failure criteria would lead to a high level of uncertainty. The cement volume fraction loaded at lowerbound levels of tensile stresses appeared to be less sensitive to mesh density. This suggests that failure criteria or output parameters based on fraction of volume suffering stresses or strains above a limit might be a more robust indicator for performance analysis of FE models.

As an attempt to assess the difference in considering different types of elements, Ramos and Simões [97] performed a study to compare tetrahedral and hexahedral finite element meshes of simplified and realistic proximal intact femur geometries. Convergence tests with hexahedral (8- and 20-node bricks) and tetrahedral (4- and 10-node tetrahedrons) elements were performed by comparing the surface von-Mises stresses and principal strains at a selected point of the femur. The numerical surface strains were also compared with experimental ones to determine the accuracy of the finite element models. They compared the results with the theoretical von-Mises stress distribution and the theoretical equivalent displacement distribution of the simplified femur. They concluded, for the simplified femur, that tetrahedral linear element allowed results close to theoretical ones, but hexahedral quadratic elements seemed to be more stable and less influenced to the degree of refinement (number of degrees of freedom) of the mesh.

Modelling the Bone-Implant Interface

Elements across an interface are not always connected to each other and therefore are not inherently coupled via the stiffness matrix. A method of modelling interface characteristics is therefore necessary to achieve load transfer across an interface. A major concern in uncemented total joint replacement is the formation of a fibrous interface between the bone and the implant that can eventually

lead to loosening of the prosthesis, leading to pain and eventually implant failure. The biological factors causing the growth of the fibrous interface are not completely clarified [99]. Some studies pointed out the role of wear particles on bone osteolysis [100, 101]. Aspenberg and Hebertsson [102] suggested that the mechanical environment of the bone cells is more important for the fibrous tissue formation process than the presence of particles. Mechanical variables that have been suggested to be important in the process of formation of the fibrous tissue include the hydrostatic compression [103, 104], the fluid pressure [105, 106] and the fluid flow velocity [107, 108].

There are different approaches to the modelling of the interface between prosthesis and bone. In some cases researchers adopted a series of bone-implant contact pair parameters and specific material properties that accounted for varying behaviour of the real interface [99, 100]. Usually in these studies only two or three hypothetical stages of tissue development are modelled. Other researchers tried to develop laws for modelling the dynamic behaviour of the tissues surrounding the implant and tried to setup these changes after a number of load cycles [109, 110, 111, 112]. The present study approaches the model with fully bonded and friction contact interface between bone and implant.

Finite Element software present a set of multiple parameters to define this non linear behaviour at the contact surfaces between two bodies. Parameters have to be selected depending on the materials of the components, but some other parameters do not have a physical meaning and thus they can not be measured experimentally. One important parameter is the contact element type, which can be node-to-node, node-to-surface and surface-to-surface [18]. For the conditions present in bone-implant contact, where large sliding is involved, either node-to-surface or surface-to-surface are more accurate [113, 114] (Figure 2.12). Other parameters such as contact stiffness, convergence tolerance, contact algorithm, etc. are chosen based on engineering judgement. A study performed by Bernakiewicz *et al.* [115] analysed the sensitivity of the finite element results to some of these parameters. They found that contact stiffness and convergence tolerance played an important role on the accuracy of the results and therefore these values should be specified in any contact analysis study.

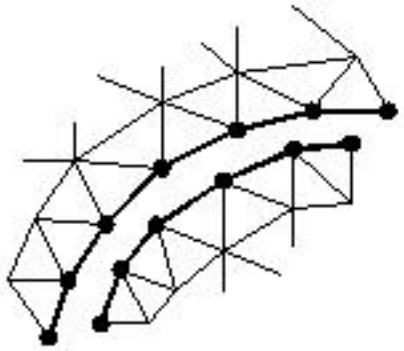

Figure 2.12: Surface-to-surface contact elements [13]

Selecting the hip contact force, muscle loads and constraints

It is usual in THR simulation to apply the hip contact force at some point close to the centre of the femoral head. Typical values of the hip contact load magnitude and angles are those corresponding to the peak loads during activities such as downstairs walking, stair climbing or normal walking [23]. Bergmann *et al.* [23] were able to measure the resultant hip joint contact force and its orientation for a variety of activities, determining that during walking the hip experiences its greatest load just after the heel strikes the ground, with a secondary smaller peak just before the toe leaves the ground. Table 2.3 shows the peak contact forces obtained by Bergmann *et al.* [23] during various activities, from 4 patients.

Task	**Patient 1**	**Patient 2**	**Patient 3**	**Patient 4**
Slow Walk	239	255	244	
Normal Walk	248	211	242	285
Fast Walk	279	218	275	
Up stairs	265	227	272	(314)
Down Stairs	263	226	316	
Standing	181	207	182	220
Sitting	176	153	149	(199)
Standing on 2-1-2 legs	253	223	(369)	
Knee Bend	177	117	147	

Table 2.3: Peak contact forces (% BW) during various activities [23]

There is little agreement on which muscle forces should be included in THR simulations, both experimental and computational. However, some studies have demonstrated their influence on the stresses and/or strains of the loaded bone

[116, 117, 118, 119]. Figure 2.13 shows some of the most important hip muscles.

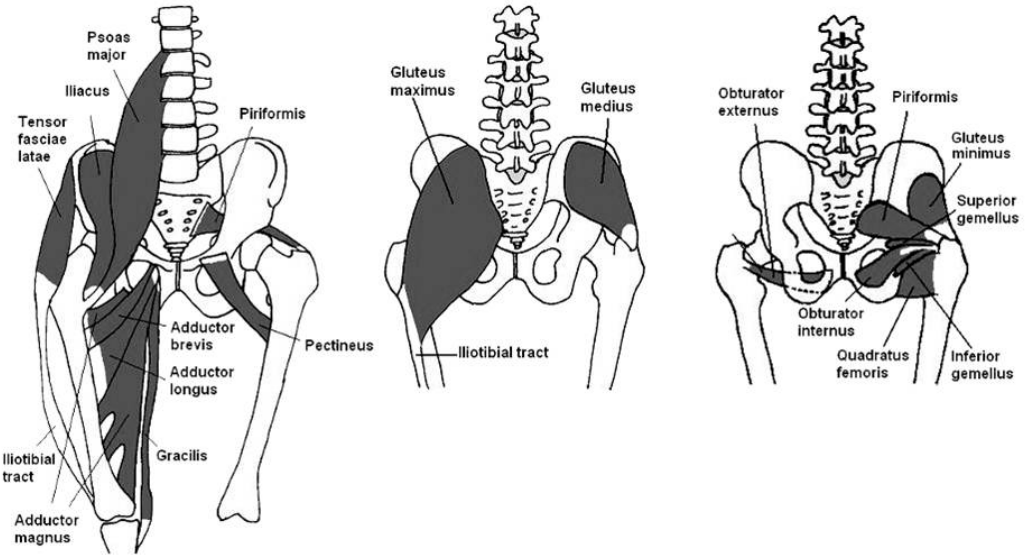

Figure 2.13: Muscles of the hip [14, 15, 16]

In a study performed by Duda *et al.* [117] a 3D model of the femur was built, accounting for all the thigh muscle forces, body weight and contact force at the hip, patello-femoral and knee joints. The internal loads were reduced by up to 50% compared to the case in which no muscle action was considered. The same was demonstrated by Cristofolini *et al.* [116], who experimentally simulated the action of the 10 most important thigh muscles, the three vasti, the three gluteal, rectus femoris, adductor longus and magnus, biceps femoris, using a custom made jig that simulated the hip contact force and muscles forces. The muscles forces were applied attaching nylon straps on the surface of the femur, and pulling them with the required tension by a screw device through a steel wire clamped to them. They looked at the effect of adding each muscle group in the femur on the axial and hoop strains. All the muscle forces had a large influence, particularly the three glutei, which were the principal muscles in determining the vertical strains, mainly in the medio-lateral aspects. On the posterior aspects, the most significant differences were produced by the biceps femoris.

Duda *et al.* [118] developed a FE model of a femur and analysed the stresses and strains with all thigh muscle and joint contact forces for four phases of a gait

cycle. This was compared to a reduced load case with only a few major muscles included. They found that, when including all thigh muscles, the surface strains were similar to those in *in vivo* recordings [120, 121], whereas the simplified load regimes produced differences in strain as high as 26%. The difference was reduced to 5% if the adductors were added to a loading regime consisting of hip contact, abductors and ilio-tibial band.

Among all the muscles acting in the femur, the ones that had the highest influence, according to the studies mentioned above, are the abductor muscles. This was confirmed by Stolk *et al.* [119], who wanted to find the minimum number of muscle forces that was necessary to include in pre-clinical tests in a FE model of a cementless THR, ensuring a good prediction of bone adaptation and mechanical failure. They simulated loads occurring during heel-strike, mid-stance and push-off phases of the gait. The stress and strain distributions were compared between the hip contact only case and those gradually including the abductors, the illiotibial tract and the adductors and vastii. Again, the abductors had the greatest effect, neutralising lateral bending at heel-strike and increasing medial bending at mid-stance and push-off. The addition of the other muscles produced relatively small effects during all gate phases. The authors concluded that a model including the hip joint contact force and the abductor muscle forces was sufficient to adequately reproduce in vivo loading of cemented THR in pre-clinical tests. This suggests that inclusion of muscle forces is essential in order to get reliable results, but that simplified models that include only the abductor forces may be sufficient.

The selection of constraints of the model still remains an important factor that has not been analysed carefully. In any FE analysis, constrained rigid body motion is an essential prerequisite, and the selection of these constraints has direct consequences on the resulting deformations, a fact rarely considered. Constraint selection differs greatly between studies, although a common criteria is to constrain at least 6 degrees of freedom (DOFs) at nodes in the mid-diaphysis [97, 67, 122] or to constrain nodes on the distal condyles [123, 124]. The first option is far from being a physiologic-like constraint, but the second may simulate passive soft tissue structures at the knee. As an attempt to assess the effect of modelling different boundary conditions in the performance of the femur, Speirs *et al.* [89] built a FE model of a femur, with loads applied in 5 different cases: di-

aphyseally constrained with hip contact and abductor forces, the same plus vasti forces, the first case with a complete set of muscle forces, distally constrained with all muscle forces and physiological constraints with all muscle forces. They found the latter to represent most accurately the physiological deflections of the femoral head. In particular the mid-diaphysis constrained models generally produced the lowest strain levels on the medial and lateral cortical surfaces while the distally constrained produced the highest strains, compared to those from the physiological case.

Thus, the selection of the constraints has an important effect that has been commonly neglected. More comparative studies should be performed to analyse the sensitivity of the output to the constraints, or convergence studies should be performed in each particular case to evaluate the best constraints to adopt.

Performance indicator

The FE models are assessed by post-processing the state of the model after the simulation has been performed. It is necessary to look at parameters that are representative of the behaviour of the construct, which are called performance indicators. These are desired to be robust enough so that comparisons and validations can be made reliably. Some of the most common performance indicators in bioengineering are stress and strains-based parameters or micromotion in frictional interface cases.

The strength of the bone, considered as the limit stress that leads to failure, has been considered in most reliability analyses since it is the variable that is assessed in fatigue tests and in the design of any construct. However bone does not behave in the same way as non-living materials, since it adapts to produce uniform functional apparent strains in both cortical and trabecular bone in response to habitual loads [125], i.e., bone is a 'living' material that adapts to the external conditions. In fact, variability in these strength limits has been included in many studies.

Crabtree *et al.* [126] measured the compressive stress, defined as the stress in the femoral neck at its weakest cross section arising from a standardized fall (a fall to the side with impact onto the greater trochanter [127]), in European men and women, using the following means and standard deviations: 132.8 (6.13) MPa in women, and 104.1(6.29) MPa in men. However, Cheng *et al.* [128]

found opposite results between women and men. They assessed the femoral strength by mechanical testing, using a loading configuration designed to simulate a fall on the greater trochanter. Maximum recorded loads in the femur were 3.98(1.60) kN for all the subjects, 3.14(1.24) kN corresponding to females, and 4.63(1.55) kN corresponding to males. To assess how these material properties (Young's modulus, strength, etc.) and yield strain of the bone relate to the apparent density (g/cm^3), Kopperdahl and Keaveny [17] developed experiments with human and bovine bone specimens. They found that both the yield stress and Young's modulus were strongly correlated to density, whereas tensile yield strains were approximately constant at 0.78% strain across the entire range of densities. This is demonstrated in the Figures 2.14 and 2.15.

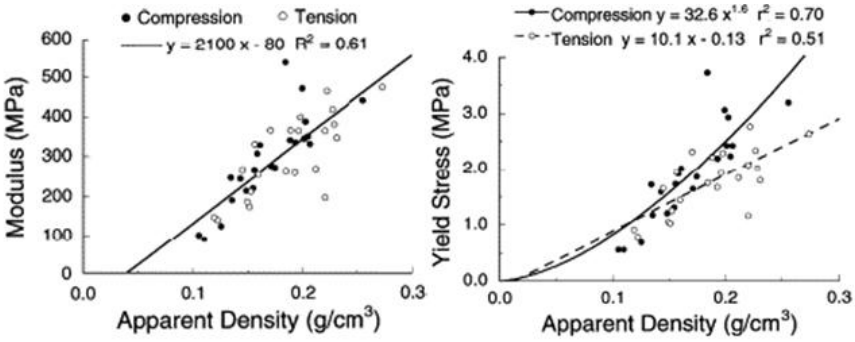

Figure 2.14: Compressive and tensile elastic moduli for the human vertebral specimens (left), and compressive and tensile yield strains (right), strongly correlated with apparent density [17]

Schileo *et al.* [129] evaluated stress-based and strain-based failure criteria, by comparing patient-specific FE models from CT scans of 3 cadaver femurs with the experimental fractures in vitro under a clinically relevant single stance loading scenario. They found that the strain-based criterion acted as a better predictor of the failure, since the highly strained areas in the model agreed with those in the experimental fracture, and in fact, when the stress-based criterion was applied, the corresponding highly stressed areas did not match at all with the experimental ones.

Therefore, since the yield strain was demonstrated to be quite steady at approximately $0.78\% \pm 0.06$ strain across the entire range of densities (dotted line

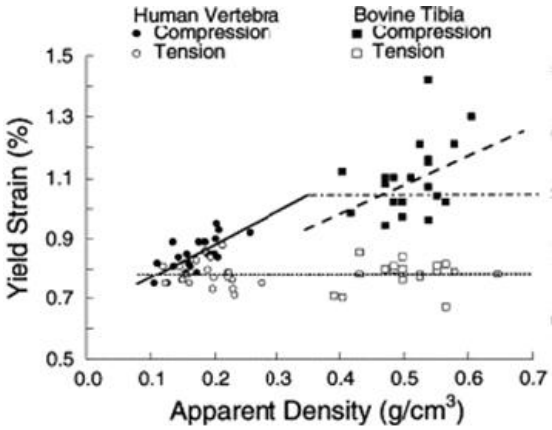

Figure 2.15: Compressive and tensile yield strains vs apparent density for both human vertebral and bovine proximal tibial trabecular bone specimens [17]

in Figure 2.15), a strain failure approach is considered to be a good performance indicator; note that there is also a correlation between low density values and the compressive yield strain [17]. Morgan and Keaveny [130], assessed the dependence of yield strain of human trabecular bone on anatomic site, and found it can differ across sites, but yield strain may be considered uniform within a given site despite substantial variation in elastic modulus and yield stress. In the case of the femoral neck, they found values for yield strains ranging from $0.85 \pm 0.10\%$.

Micromotion and Migration

These factors measure interface motion between bone and implant. Micromotion is defined as the 'elastic movement', since it is the relative motion that is recoverable on a single load cycle. Migration is also called 'plastic movement', and is the unrecoverable motion, the permanent displacement after a larger number of cycles. Migration is an important factor to look at when modelling friction interface between bone and implant. Clinical testing has shown that postoperative subsidence of the prostheses into the femurs take place. Some authors justify this subsidence as the effect of damaged bone resorption or heat generated through the polymerization of the cement [131, 132]. Excessive interface micromotions can promote fibrous connective tissue formation and may lead to aseptic loosening and failure of the implant. It has been observed that osseointegration takes place

in the presence of interface micromotions of up to $30\mu m$, while micromotions larger than $150\mu m$ have been reported to compromise or inhibit the biological integration of the implant [133].

Kassi *et al.* [133] investigated the influence of patient activity on the primary stability of cementless prostheses applying muscles forces from validated muskuloskeletal analyses. Normal walking and stair climbing were compared, implanting a CLS prosthesis in 18 composite femora and subjected to cyclical loading. The relative micromovements at the bone-prosthesis interface were measured with a linear encoder in the implant and six LVDTs. The measured micromovements appeared to be very sensitive to the specific patient activity. Stair climbing generated higher micromovements than normal walking. The largest migration averaged $177 \pm 68\mu m$ at the 75% load level, principally in the longitudinal direction. The largest micromotions averaged $50 \pm 5\mu m$.

The present work will look at the relative elastic motion recovered after as load is released during a single load cycle. This form of micromotion measurement has also been referred to as the 'inducible displacement' [134].

2.7 Statistical Methods: Data Analysis and Probabilistic Analysis

Most contemporary engineering problems involve a high degree of complexity and therefore responses can be difficult to predict. In particular, the response cannot often be defined as an explicit function of the input parameters. This problem is usually encountered when approaching a design or when optimizing the performance of a system. In Section 2.6 various parameters were used to define the contact pairs, such as contact elements, contact stiffness, convergence tolerance, or contact algorithm, and this is typical of the kind of problem that can make the FE model outcome uncertain.

The selection of the appropriate analysis method is important since it depends largely on the amount of available data and the nature of the system.

Statistical approaches are used to collect, analyse and interpret data, and try to

explain regular conditions in random phenomena. Data analysis and probabilistic analysis are different statistical tools, and both of them aim to describe the behaviour of a system. The former one uses a set of graphical and numerical tools to describe the system, for example scatter plots, histograms, variance and covariance. Probabilistic tools try to extract probabilistic information from data, by looking at a parameter that determines the failure of the system, without creating a model of the system. The probability of failure (pf or POF) is targeted, related to the frequency of values of a chosen output that are above a certain limit: probability functions, confidence intervals, simulation techniques, most probable point methods, are some examples of these tools.

The following sections describe different approaches and techniques used to describe systems and their uncertainties, from quantitative to graphical techniques, from pure modelling to probabilistic methods.

2.7.1 Techniques for Data Analysis

In the majority of scientific problems, the main goal is to find a way to characterize, predict or analyse the behaviour of the system. Different systems have different complexity, regardless of the number of random input factors. Features such as the number of factors and their interactions, the scatter of the output values, the statistics and values of the input factors, the presence of outlier values are inherent to the system and determine the kind of analysis that is more appropriate to describe or model its behaviour.

Three popular data analysis approaches are [19]: Classical, Exploratory Data Analysis (EDA) and Bayesian. These three approaches are similar in that they all start with a general problem and all yield conclusions. The difference is the sequence and focus of the intermediate steps.

For classical analysis, the sequence is:

$$Problem \Rightarrow Data \Rightarrow Model \Rightarrow Analysis \Rightarrow Conclusions$$

[19]

In this approach, after data collection a model is created and the analysis,

estimation and testing are focused on the parameters of that model. Classical techniques are generally quantitative in nature. These techniques have the characteristic of taking all of the data and mapping them into a few numbers ('estimates'). The advantage is that these few numbers focus on important characteristics (location, variation, etc.) of the population. The disadvantage is that concentrating on these few characteristics can filter out other characteristics (skewness, tail length, autocorrelation, etc.) of the same population. In this sense there is a loss of information due to this 'filtering' process [19].

For EDA, the sequence is:

$$Problem \Rightarrow Data \Rightarrow Analysis \Rightarrow Model \Rightarrow Conclusions$$

After data collection, an analysis is performed to decide what model would be appropriate. For exploratory data analysis, the focus is on the data: its structure, outliers, and models suggested by the data. The EDA approach allows the data to suggest admissible models that best fit the data. EDA techniques are generally graphical; they include scatter plots, character plots, box plots, histograms, bihistograms, probability plots, residual plots, and mean plots. The EDA approach often makes use of (and shows) all of the available data. In this sense there is no corresponding loss of information. This approach is applied in the present study.

For Bayesian, the sequence is:

$$Problem \Rightarrow Data \Rightarrow Model \Rightarrow PriorDistribution \Rightarrow Analysis \Rightarrow Conclusions$$

In this approach, the analyst attempts to incorporate engineering knowledge or expertise into the analysis by imposing a data-independent distribution on the parameters of the selected model; the analysis thus consists of formally combining both the prior distribution on the parameters and the collected data to jointly make inferences and/or test assumptions about the model parameters.

Nowadays, data analysts freely mix elements of all of the above three approaches (and other approaches).

Data analysis procedures can broadly be split into two categories: quantitative and graphical.

Quantitative techniques are the set of statistical procedures that yield numeric or tabular output. Examples of quantitative techniques include hypothesis testing, analysis of variance, points estimates and confidence intervals or least squares regression. These and similar techniques are all valuable and are the main techniques used in classical analysis.

Graphical techniques employ a large collection of statistical tools, such as scatter plots, histograms, probability plots, residual plots, box plots and block plots. The EDA approach relies heavily on these and similar graphical techniques.

2.7.2 Characterizing Variability of a System

The ultimate aim of this study is to quantify the uncertainties of the uncemented THR. Monte Carlo method has been selected so that a large enough datadase can be built and the statistical analysis can be performed.

This study uses mainly graphical tools for data analysis. However, to characterize the variability of the output, i.e., how spread the values of the output are, some quantitative factors are good indicators, namely:

Variance. The variance is roughly the arithmetic average of the squared distance from the mean (Equation 2.3). Squaring the distance from the mean has the effect of giving greater weight to values that are further from the mean. For example, a point 2 units from the mean adds 4 to the sum while a point 10 units from the mean adds 100 to the sum. Although the variance is intended to be an overall measure of spread, it can be greatly affected by the tail behaviour.

$$s^2 = \sum_{i=1}^{N} (Y_i - \bar{Y})^2/(N-1) \tag{2.3}$$

where $\bar{Y}$ is the mean of the data

Standard Deviation. This is the square root of the variance (Equation 2.4). It restores the units of the spread to the original data units (the variance squares

the units).

$$s = \sqrt{\sum_{i=1}^{N}(Y_i - \bar{Y})^2/(N-1)} \tag{2.4}$$

Average absolute deviation (AAD) is defined as:

$$AAD = \sum_{i=1}^{N}(\mid Y_i - \bar{Y} \mid)/(N-1) \tag{2.5}$$

where $\bar{Y}$ is the mean of the data and $\mid Y \mid$ is the absolute value of the data. This measure does not square the distance from the mean, so it is less affected by extreme observations than are the variance and standard deviation.

Interquartile range. This measure of variability is based on the concept of percentile: The pth percentile is a value such that at most $(100p)\%$ of the measurements are less than this value and at most 100(1- p)% are greater. The 50th percentile is called the median. The interquartile range is the value of the 75th percentile minus the value of the 25th percentile. This is a measure of the variability of points near the mean value [135].

2.7.3 Modelling

Data originated by either experimental measurements or by simulation techniques can be treated using the EDA process. Because there is a high number of observations, the use of graphical techniques may be sufficient to characterize the performance of the system. Posterior fitting of a model may be necessary for different targets: prediction, optimization or calibration. The basic steps of modelling are:

$$model\,selection \Rightarrow model\,fitting \Rightarrow model\,validation$$

Model fitting is the concise description of the total variation in one quantity, y, by partitioning it into a deterministic component given by a mathematical function of one or more other quantities, $x_1, x_2, \ldots$, plus a random component

that follows a particular probability distribution. The general form of the model is:

$$y = f(\vec{x}; \vec{\beta}) + \varepsilon, \tag{2.6}$$

where y denotes the response variable, $f(\vec{x}; \vec{\beta})$ is the mathematical function, and ε denotes the random errors.

The response variable is a quantity whose variability is analysed via the modelling process. Generally it is known that the variation of the response variable is systematically related to the values of one or more other variables before the modelling process is begun, although testing the existence and nature of this dependence is part of the modelling process itself.

The mathematical function consists of two parts. These parts are the *predictor variables*, $x_1, x_2, \ldots$, and the *parameters* or *estimators*, $\beta_0, \beta_1, \ldots$. The predictor variables are observed along with the response variable. They are inputs to the mathematical function, $f(\vec{x}; \vec{\beta})$. The collection of all of the predictor variables is denoted by $\vec{x}$.

$$\vec{x} \equiv (x_1, x_2, \ldots). \tag{2.7}$$

The parameters or estimators are the quantities that are estimated during the modelling process. Their true values are unknown and unknowable, except in simulation experiments. As for the predictor variables, the collection of all of the parameters is denoted by $\vec{\beta}$.

$$\vec{\beta} \equiv (\beta_0, \beta_1, \ldots). \tag{2.8}$$

Like the parameters in the mathematical function, the random errors are unknown. They are simply the difference between the data and the mathematical function. They are assumed to follow a particular probability distribution, which is used to describe their behaviour. The probability distribution that describes the errors has a mean of zero and an unknown standard deviation, denoted by σ.

Some of the most common methods for model fitting use the 'method of least

squares', developed in the late 1700's and the early 1800's by the mathematicians Karl Friedrich Gauss, Adrien Marie Legendre and Robert Adrain [136, 137, 138]. In the least squares method the unknown parameters are estimated by minimizing the sum of the squared deviations between the data and the model. The minimization process reduces the overdetermined system of equations formed by the data to a sensible system of p (where p is the number of parameters in the functional part of the model) equations in p unknowns. This new system of equations is then solved to obtain the parameter estimates. Some methods where least squares is applied are linear and nonlinear least squares regression, weighted least squares regression and locally weighted regression. The first is used in this study and is therefore detailed below:

Linear Least Squares Regression fits the data into a function which is linear in terms of the estimators, even if it is not linear with the observed variable/s. Examples of these functions have the following forms:

$$f(\vec{x};\vec{\beta}) = \beta_0 + \beta_1 x_1 + \beta_2 x_2$$

$$f(x;\vec{\beta}) = \beta_0 + \beta_1 x + \beta_{11} x^2$$

$$f(x;\vec{\beta}) = \beta_0 + \beta_1 ln(x)$$

$$f(x;\vec{\beta}) = \beta_0 + \beta_1 sin(x) + \beta_2 sin(2x) + \beta_3 sin(3x)$$

The stepwise regression procedures are another common regression family of methods, which allows the selection of probabilities (p-values) for adding or deleting model terms. This allows outliers in the data to be filtered. With 'stepwise forward regression', it is possible to build up from the simplest models by adding and testing higher-order terms. An iterative process of addition and deletion is run until no further changes to the model can be made. A p-value of 0.10 is usually selected, or the equivalent 0.90 confidence value. This method will be used to fit a response surface (see next Section 2.7.4.1) for the post-processing of the data in one of the models in Section 4.2 with a confidence of 95%.

2.7.3.1 Residuals

The residuals from a fitted model are the differences between the responses observed at each combination value of the explanatory variables and the corresponding prediction of the response computed using the regression function [139]. Mathematically, the definition of the residual for the i^{th} observation in the data set is written as:

$$e_i = y_i - f(\vec{x}_i; \vec{\beta}), \tag{2.9}$$

with y_i denoting the i^{th} response in the data set and $\vec{x}_i$ represents the list of explanatory variables, each set at the corresponding values found in the i^{th} observation in the data set. There are other methods that try to model the behaviour of the system performing a minimum number of simulations. Examples of this are the Design of experiments (DEX or DOE), and the Most Probable Point family of methods (MPP). However, when there is not enough data, methodology change does not solve the problem.

2.7.4 Design of experiments (DEX or DOE)

Design of experiments (DEX or DOE) aims to design the data collection strategy under a minimal expenditure of runs, time and expense. In the case of system modelling, the DOE aims at functionally modelling the process with the output being a good-fitting (or high predictive power) mathematical function, and to have good (or maximal accuracy) estimates of the parameters (estimators) in that function. For a desired model to fit, the DOE designs which values of the different predictor variables are needed to be run, minimizing the variance of the estimators.

A simple example for a line fitting is shown in the following equation:

$$y = \beta_0 + \beta_1 x, \tag{2.10}$$

where β_1 is the estimator.

The DOE will try to minimize the variance of the estimator given below:

$$Var(\beta_i) \propto \frac{1}{\sum_{i=1}^{N}(x_i - \bar{x})}. \tag{2.11}$$

2.7.4.1 Response Surface methods (RS)

An example of a DOE methods is the Response Surface method (RSM). The experiment is designed to allow us to estimate interaction and even quadratic effects, and therefore give us an idea of the (local) shape of the response surface we are investigating. For this reason, they are termed response surface method (RSM) designs. RSM designs are used to find improved or optimal process settings, troubleshoot process problems and weak points and to make a product or process more robust against external and non-controllable influences. 'Robust' means relatively insensitive to these influences. For most RSMs, the functions for the approximations are polynomials because of simplicity, though the functions are not limited to the polynomials. For the cases of quadratic polynomials, the response surface is described as follows:

$$y = \beta_0 + \sum_{j=1}^{k} \beta_j x_j + \sum_{j=1}^{k} \beta_{jj} x_j^2 + \sum_{i=1}^{k-1} \sum_{j=i+1}^{k} \beta_{ij} x_i x_j, \tag{2.12}$$

where k is the number of variables, x_i denotes the design variables and β_j, β_{jj}, β_{ij} are the regression coefficients of the regression model. Introduced during the 1950's, classical quadratic designs fall into two broad categories: Box-Wilson central composite (CCD) designs and Box-Behnken (BB) designs. For the CCD, each design consists of a factorial design (the corners of a cube) together with center and star points that allow for estimation of second-order effects (Figure 2.16). If the distance from the center of the design space to a factorial point is ± 1 unit for each factor, the distance from the center of the design space to a star point is $\pm\alpha$ with $\mid \alpha \mid > 1$. The precise value of α depends on certain properties desired for the design and on the number of factors involved.

In the BB method, design points are the midpoints of edges of the design space and at the centre (Figure 2.17). This design requires 3 levels of each factor. The geometry of this design suggests a sphere within the process space such that the

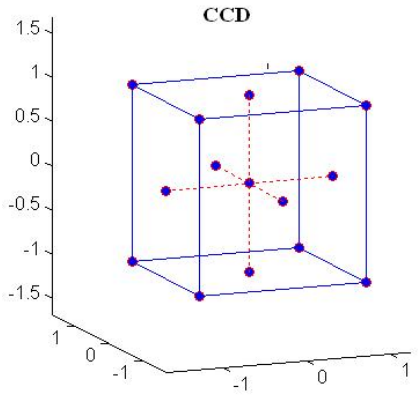

Figure 2.16: Central Composite Design representation

surface of the sphere protrudes through each face with the surface of the sphere tangential to the midpoint of each edge of the space.

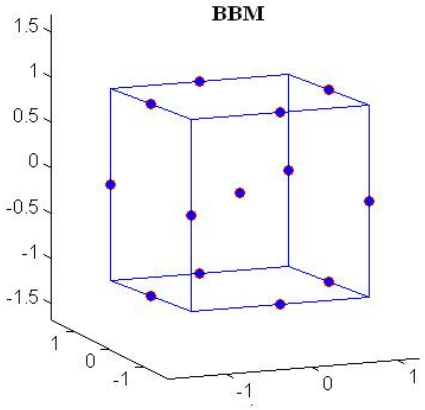

Figure 2.17: Box-Behnken Design representation

2.7.5 Probability Distributions

Probability distributions are a fundamental concept in statistics. Simulation studies often use random numbers generated from a specific probability distribution. This are meant to describe the values of a random variable. A detailed definition of these functions, together with some examples of typical distribution functions and cumulative distribution functions are presented in Appendix B.1.

2.7.6 Confidence Intervals

This section describes a set of probabilistic tools that use the probability of the values of the output as performance criteria to describe the model. Once a model has been fitted to a mathematical function as shown in Equation 2.6, an estimation of the model uncertainty, represented by ε in Equation 2.6 is needed. One way to get information about uncertainty prediction is by using intervals of plausible values that have a probabilistic interpretation. In particular, intervals that specify a range of values that will contain the value of the regression function with a pre-specified probability are often used. These intervals are called confidence intervals. The probability with which the interval will capture the true value of the regression function is called the confidence level, and is most often set to be 0.95, or 95%. The confidence level of an interval is usually denoted symbolically using the notation $1-\alpha$, with α denoting a user-specified probability, called the significance level, that the interval will not capture the true value of the regression function [135].

2.7.7 Most Probable Point methods (MPP)

These methods are based on the mapping of the original random variables $X = (x_1, x_2, ..., x_n)$ into independent standard normal variables $U = (u_1, u_2, ..., u_n)$ (i.e., having a mean of 0 and standard deviation of 1) and the determination of the MPP, which represents the points where the intersection of the standardized probability density function $f(U)$ along the curve $g(U) = 0$ is a maximum (Figure 2.18), and can be located because it has the highest frequency and is closest to the origin. Figure 2.18 demonstrates this change in the input variables.

The limit-state surface is $z(U) = g(U) - c$, with c the value that represents the change between the safe and failure states. β is the shortest distance from the origin to a point on the limit-state surface in U space. Mathematically, it is a minimization problem with an equality constraint:

$$\beta = \min_{U} \parallel U \parallel \tag{2.13}$$

subject to

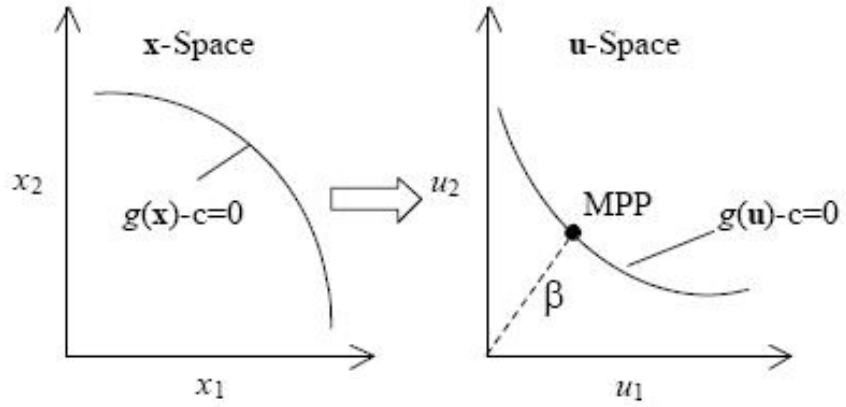

Figure 2.18: Transformation of the variables to the standardized normal u-space

$$g(U) - c = 0$$

The solution u_{MPP} is called the most probable point (MPP). β is also referred to as the safety index in reliability analysis and the MPP becomes the critical design point.

Methods such as First or Second Order Reliability methods (FORM and SORM) approximate the limit-state function by a first or second order polynomial at the MPP. The problem when these methods are used is that, when a performance function is implicitly defined and is highly nonlinear, it is difficult to assess the error introduced by the polynomial approximation. Also the optimization algorithms to search for the design point can cause difficulties, such as converging to a local MPP which is not real. The Mean Value family of methods (MV, AMV, AMV+) constructs a mean-based response function and computes the MPP for specified probability levels, i.e., specified values of probability of failure (pf). The Advanced Mean Value method with iterations (AMV+) requires more trials than the AMV but it has been shown to be very accurate even for non-linear problems.

2.7.8 Simulation Techniques

A simulation technique artificially simulates a large number of deterministic experiments whose results are used to evaluate the pf or any other output parameter, usually representative of the life or failure of the structure. Each RV is

assigned a number of values according to their distribution functions and the kind of simulation technique. These techniques are appropriate when available data is scarce, and usually the necessary time and resources to obtain the same amount of data experimentally are in some cases impossible to assume. One of the limitations of simulation techniques is that its accuracy depends on how the distribution functions of the input variables are close to the real ones. Previous data of the input variables can be used to fit them to a distribution function.

2.7.8.1 Monte Carlo Simulations

This is a relatively straightforward method that is applicable in cases where a system behaviour can be described by either an implicit equation or a model of interactions between the random variables (RVs).

The steps for a Monte Carlo simulation usually are [140]:

1. Describe the problem in terms of all random variables
2. Define the random variables by their statistics, i.e., means, standard deviations, etc.
3. Generate the samples of all random variables
4. Solve the deterministic structural problem for each set of realizations of all RVs.
5. Conclude the probabilistic information from the results.
6. Assess the accuracy and efficiency of the results.

In step 3, random samples ranging between 0 and 1 are created and then computed in step 4 to generate associated output values according to the distribution functions of the RVs. Then, the performance of the system is evaluated.

This technique is an exhaustive method that can produce accurate results and therefore can be used to benchmark complex or new techniques if enough samples are considered. However, it is computationally expensive and time consuming because of the large number of samples required for an accurate estimation of the output, especially for large-sized FE problems.

2.7.8.2 Sampling Methods

Pure Monte Carlo simulation samples the RVs randomly. This is performed by the so called 'random number generators', which is a computational or physical device designed to generate a sequence of numbers or symbols that lack any pattern, i.e. appear random. A fundamental feature of simulation techniques is the generation of random numbers with standard uniform distribution (Figure B.8, Appendix B.1). In computational methods, this sort of generator is called a 'pseudo-random number generator (PRNGs)', which is an algorithm that can automatically create long runs (for example, millions of numbers long) with good random properties. Eventually, the sequence will repeat exactly (or the memory usage grows without bound). One of the most common PRNGs is the linear congruential generator, which uses the recurrence (Equation 2.14) to generate numbers [141].

$$s_{n+1} = (a\, s_n + b)\, mod\, m, \tag{2.14}$$

where a, b, m = non negative integers, s_n = previous seed value of the recursion, and m = modulus, maximum number of numbers to produce.

A set of numbers with standard uniform distribution is obtained by normalizing the value calculated by 2.14 with the modulus m.

$p_n = \frac{s_n}{m}$

It is clear from 2.14 that an identical set of random numbers will be obtained if the same start value for the seed s_n is used. Therefore, the random numbers generated in this way are called 'pseudo numbers' [142].

Since the RVs are usually described by a probability function, as described in Section 2.7.5, the inverse transformation method is used to generate the random numbers. A set of random numbers for the random variable X having a cumulative distribution function $F_x(x)$ can be generated by using a set of standard uniformly distributed random numbers according to 2.14 and transforming them with the equation:

$$X_n = F_X^{-1}\,(p_n). \tag{2.15}$$

The way to calculate the inverse distribution function was explained in Section 2.7.5 (Appendix B.1)..

Other sampling methods can be used to manipulate the samples generation, fulfilling different criteria: enhancing the sampling around values that are more important, spreading the sampling all across the possible values of the input data, etc. Examples of these sampling methods are Importance Sampling [143], Stratified Sampling [144, 145] and Latin Hypercube Sampling [146]. The latter is detailed in the following section.

2.7.8.3 Latin Hypercube Sampling (LHS)

This is a variation of Monte Carlo simulation, which attempts to distribute the trials in such a way that a smaller number of trials is necessary. An even partition of the possible space is performed, so the trials are constrained to be spread in these partitions, and within them, the sample may be taken at a random point, or using the mean or median value. The partitions are done in such a way that the probability of each one is equal. A partition of a normal distribution function into 5 intervals is demonstrated in Figure 2.19.

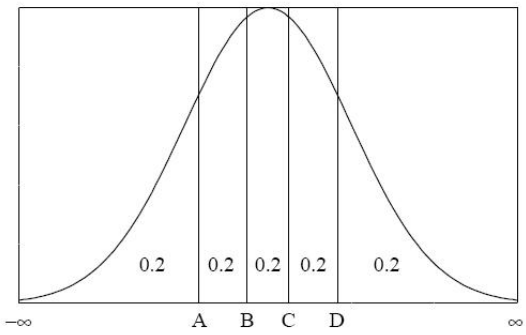

Figure 2.19: Partition of a normal distributed variable into 5 intervals

In multidimensional problems, the LHS method alone can still result in overlapping, and this increases with the number of trials, so the benefits of the use of LHS are greatest with a small number of trials (N), but when N tends to infinity, the pure Monte Carlo technique offers an excellent solution; however, the cost of computation of the models must be considered.

2.7.9 Sensitivity Factors

Probabilistic sensitivities are important in that they can be used to improve a design towards a more reliable and optimized design, or to save money while maintaining the reliability or quality of a product. A sensitivity factor evaluates how much the RVs or their variability affect the values or the variability of the *pf*. It is possible for a probabilistic analysis to evaluate the contribution of the RVs to the *pf*. In other words, the sensitivity to an input variable determines how important the influence of the input variables is on the performance of the system.

There is a difference between probabilistic sensitivities and deterministic sensitivities. Deterministic sensitivities are mostly only local gradient information. They are evaluated by varying the value of each RV at a time by low increments and checking the value of the output for these variations. Figure 2.20 illustrates two output lines Y_1 and Y_2, which are the values of the output parameter when varying two different input variables, namely X_1 and X_2. Under the same variation, the output is more sensitive to X_1 than to X_2, since $\Delta Y_1 > \Delta Y_2$.

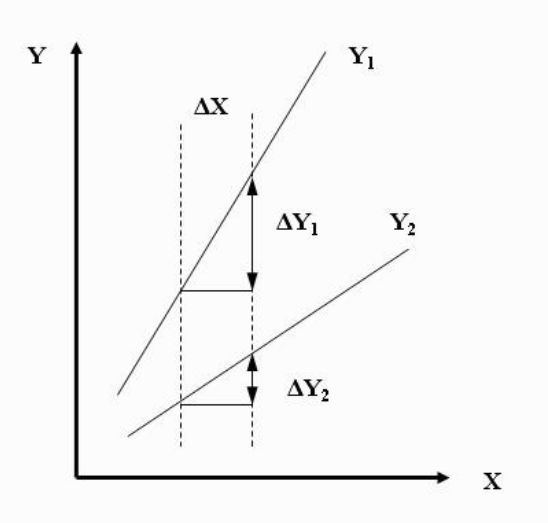

Figure 2.20: Deterministic sensitivity [18]

The main disadvantage of this deterministic sensitivity is that it neglects the effect of interactions between input parameters. An interaction between input parameters exists if the variation of a certain parameter has a greater or lesser effect if at the same time one or more other input parameters change their values as well. If interactions are important, then deterministic sensitivity analysis

can give incorrect results. However, using Monte Carlo simulations, all random variables are varied at the same time; thus if interactions exist then they will always be correctly reflected in the probabilistic sensitivities.

The method to calculate sensitivity depends on the method used to obtain and analyse the data and on the amount of available data. From the EDA perspective (Figure 2.21), after data collection and analysis using graphical techniques, a decision on the best fit of the data to a model, such as a polynomial, may be performed. This equation may be derivated with respect to the different parameters to get the sensitivities to each of them.

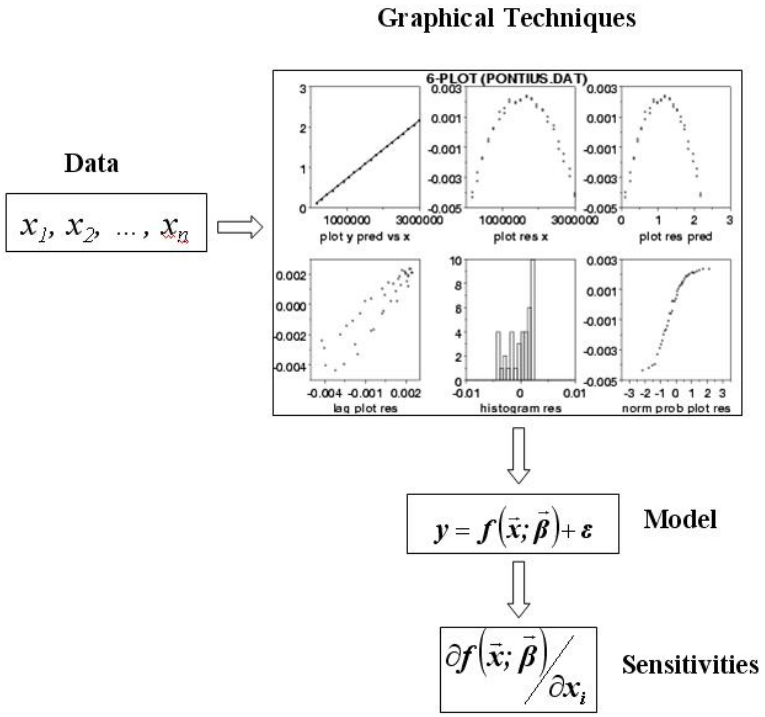

Figure 2.21: Exploratory Data Analysis process [19]

If a MPP method has been applied, a common sensitivity factor is the direction cosines (α) of the safety index vector (β) shown in Figure 2.18. Other common sensitivity factors when MV methods are applied are $\frac{\partial pf}{\partial \mu_i}$ or $\frac{\partial pf}{\partial \sigma_i}$, where i refers to the parameter with respect to which the sensitivity is being assessed.

2.7.10 Probabilistic Methods in Engineering

When designing a system, engineers have traditionally employed a deterministic approach, and applied a safety factor to account for any uncertainty in the system, for example, variability in expected loading or materials properties. There may, however, be significant uncertainty in the response of the system, caused by the inherent variability of the input factors. The degree of uncertainty is enhanced when an increased number of random design variables are considered. It would be extremely challenging to reproduce all possible random scenarios in a laboratory due to the time and resources that would be required. Thus, computational modelling approaches are required to address these types of problems. With advances in computational power and the development of software packages devoted to probabilistic analyses, the ability to solve increasingly complex models involving a large number of random variables becomes feasible.

The results obtained by applying different lifing methods to predict the life of the constructs differ, and there is no established procedure which is applicable to all load-bearing implants. In addition, lifing methodologies for load bearing implants vary with manufacturer; there is a potentially serious health risk if implants fail and for that reason implants tend to be over designed [147]. In many designs, the structural strength and the applied loads are given fixed values, and global safety factors are applied to cover any uncertainties in these quantities. A corresponding nominal safety factor can be applied to the resistance, so that allowable stress (or displacement) should not be violated, regardless of load. In a simple case, the nominal safety factor S_F can be calculated as [140]:

$$S_F = \frac{R_N}{S_N}, \tag{2.16}$$

where R_N and S_N are the deterministic values of the two design parameters (resistance and outcome). The structure is then declared either 'safe' or 'unsafe' depending on the outcome of the structural analysis [148]. The problem is that the deterministic safety factors do not take into account the underlying distributions of the parameters involved.

In the first structural studies, dependence of a design variation was predicted by analysing an initial design and then changing the design, re analysing the

structure, and calculating difference quotients to approximate derivatives. These are called parametric variation methods, and they were a very simple and general way to obtain stress dependence on design [149].

There is inherent uncertainty in the variables of a structure (material properties, component geometry and loading conditions, for example) that can dramatically affect component performance and the associated success and failure rates. For this reason, some authors developed a unified theory of structural design sensitivity analysis based on variational principles. The major advantage of this theory is that it provides a method for calculating the sensitivity of design to material property changes as well as shape changes. A second advantage is its potential for detecting errors in the finite element model [149].

To solve the problem of uncertainty and unify this with new concepts of sensitivity and failure analyses, probability and reliability models have been introduced to account for the impact of multiple random variables on a specific performance metric. There is a wide array of probability methods that differ in their efficiency to achieve a solution with a required accuracy. Some popular probability methods are Monte Carlo simulation, the Importance Sampling method, First-Order reliability methods, Advanced Mean Value methods, Second-Order reliability methods, Variance Reduction Techniques and Response Surface methods.

2.7.11 The Reliability Problem

The basic reliability problem can be considered as the simplest structural case and is usually defined using two parameters: the load effect represented by the displacement or the stress (S) and the resistance factor represented by the stiffness or the strength (R). The design of a structure is considered as safe if its strength is higher than the stress induced by the applied loads ($S < R$) and failed otherwise ($R < S$). In the deterministic Safety Factors and Risk-based designs, a safety factor is used to cover the structure uncertainty, within which an allowable stress (or displacement) should not be violated. However, these factors do not take into account the distributions of the parameters involved. Figure 2.22 illustrates the effect of uncertainty in stress and strength values - the overlapping area represents failure of the system.

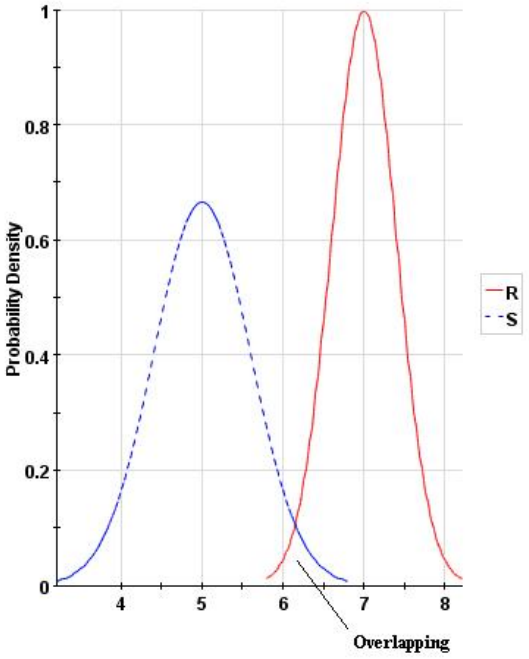

Figure 2.22: Probability distributions with overlapping values.

From the probabilistic approach, the probability of failure (pf) of the structure is defined by means of a performance function $Z = g(X) = g(x_1, x_2, ..., x_n)$, where x_i are the random variables (RVs) characterizing the uncertain design [140]. The system fails if $Z \leq 0$ and is safe otherwise, so the pf is defined as:

$$pf = P(z \leq 0) \tag{2.17}$$

and the general expression of pf is:

$$pf = \int \int ... \int_{g(x_i)<0} f_X(x_1, x_2, ..., x_n)\, dx_1\, dx_2\, dx_n, \tag{2.18}$$

where $f_X(x_1, x_2, ..., x_n)$ the probability density function (PDF), and $g(x_i) \leq 0$ is the region of failure. This equation is known as the fundamental equation of reliability analysis, and in practical problems, the evaluation of the integral becomes complex. For this reason, simulation methods and second moment methods have been performed to avoid the complex integration of Equation 2.18.

When the Monte Carlo method is applied, the reliability can be determined by

the number of passing trials divided by the total number of trials. In the same way, the pf can be determined as:

$$pf = \frac{N_f}{N}, \tag{2.19}$$

where N is the total number of trials and N_f is the number of failed trials.

In order to achieve high reliabilities a large number of trials is required and can result in excessive computation times. The accuracy of these kinds of estimates can be known by calculating the coefficient of variation (COV), for a given number of trials N and a probability of failure pf:

$$COV = \frac{\sqrt{\frac{(1-pf)pf}{N}}}{pf}. \tag{2.20}$$

Small values of COV mean that the simulation is more accurate. But this accuracy estimation must be applied with care; the results will be only accurate when a high number of trials (N) have been performed, and the input parameters of the RVs, as well as the physical model, are representative of the reality.

The main approach of the present study will involve probabilistic methods, with Monte Carlo simulations playing the principal role to create random samples of possible configurations of THRs, build the FE models for each configuration, simulate, and obtain the value of the desired output, for each random sample. In the present study, the data created by Monte Carlo simulations will be analysed mainly qualitatively, using both data analysis and probabilistic analysis tools, namely: scatter plots, means and standard deviations, cumulative distribution functions (CDFs), and sensitivity plots. The sensitivities will be calculated in different manner and will be detailed in the corresponding sections. The random variables will be modelled with typical probabilistic distribution functions, such as normal, lognormal or uniform. With the chosen tools, a qualitative description of the most probable values of the output (scatter plots, convergence of the mean value of the output), its variability (scatter plots, standard deviation), its randomness (cumulative distribution function), and its sensitivity to the input parameters will be plotted and calculated to characterize the system.

2.8 Probabilistic analyses in orthopaedic biomechanics

In structural mechanics, and in particular in biomechanics, the use of Finite Element analysis has enabled accurate multi-scenario modelling with ever decreasing run times [150, 151]. However, these analyses reproduce specific cases, and although many cases may be analysed, it is impractical to recreate the whole range of possible combinations. Therefore, to account for this randomness and variability, probability analyses have been introduced in biomechanics studies. Early work looked at the concept of sensitivity analysis as an alternative to parametric studies [149] in assessing an implant design with varying material properties and geometry. There have been a number of probabilistic investigations on cemented hip replacements, and response surface methods and sensitivity results have attempted to identify the most important parameters that may compromise the structural integrity of the implant [66, 69].

An important factor to take into consideration is the choice of probability method, which may change according to the model used, the accuracy required, and the available computational resources [68]. The most recent advances in this area have involved the development of Finite-Element based probabilistic tools that can build the geometry, create the finite element model and apply the probability methods as well as obtain sensitivity factors [122]. The following is a survey of the evolution of probabilistic approach in bioengineering, highlighting the methods, failure criteria and sensitivity results, since such elements are fundamental when designing and analysing a probability study.

Due to the wide ranging nature of the systems and methods employed in the academic literature, it is difficult to make direct comparisons between studies. The review therefore focuses on comparisons based mainly on the nature of the RVs rather than the methodology or the system.

Table 2.4 displays a number of probabilistic studies that have looked at the unimplanted and implanted femur. *G* means 'geometry' and *MP* means 'material properties'. The applied methods, the assessed systems and the RVs are noted and marked with an 'X' when they were considered in the investigation. It can be seen that load magnitude and bone material properties are most commonly

investigated. Almost all the investigations have focussed on the cemented hip replacement. Although the present work looks at the uncemented implant, a discussion of the previous studies is presented and compared to identify trends.

One of the earliest works where the integrity of a load bearing implant was investigated was by Browne *et al.* [147]. They applied the reliability theory to assess what factors most affect the fatigue performance of a tibial tray, using the ISO standard 14879 as a basis. A 1kN constant amplitude fatigue load was applied with a minimum variance of $\pm 2\%$. A pore was modelled at the position of a maximum bending stress, to adopt a conservative approach. The failure criterion was chosen as a maximum crack size within 5 million stress cycles. For each of the parameters, the mean and variance were identified.

The reliability analysis was applied to a confidence limit of six standard deviations of each parameter. The results showed that for the specified number of cycles, the reliability index was extremely high, i.e., the *pf* was too low for the pore sizes observed optically and the component would not fail. The size of the pore was varied until the *pf* was notably high, leading to a variation of the design point parameter. The tray turned out to be most sensitive to thickness variations and failure length variations at larger flaw sizes, while other parameters such as load and crack dimension had a lesser effect. Such a study highlighted the potential of the method to assist in design and development of new and existing implants

Thacker *et al.* [153] developed an experimentally validated three-dimensional finite-element model of the C4-C5-C6 spinal segment, to calculate the structural response of the lower cervical spine and to quantify the effect of uncertainties on the performance of the biological system. The Advanced Mean Value Method (AMV) was applied, and a sensitivity analysis was performed. The chosen random variables to account for the biological variability were the material properties and spinal segment loading. The failure criterion was chosen to be a particular value of the injury function, which depends on the injury tolerance, the spine response due to impact or inertial forces, and all the RVs. Cumulative probability distribution functions, probability density functions, and probabilistic sensitivity factors were determined. The results from the sensitivity factors showed that the variables contributing the most to failure probability were the loading as the dominant variable, followed by some bone material properties and geometric

			BONE		BONE CEMENT		IMPLANT			LOAD		OUTPUT			
	Method	System	Bone G	Bone MP	Bone Cement G	Bone Cement MP	Implant G	Implant MP	Implant Positioning	Load Magnitude	Load G	Failure Criteria	Failure Limit	Inter-Patient	Muscle Forces
Browne *et al.* [147]		Tibial Tray					X			X		X	X		
Bah and Browne [152]	RSM	Cemented THR	X		X	X				X	X				
Bah and Browne[66]	RSM	Cemented THR	X	X	X		X	X		X	X	X			
Nicolella *et al.* [67]	AMV+	Cemented THR		X		X				X	X	X	X		X
Mehrez *et al.* [68]	AMV, RSM	Cemented THR	X	X		X	X			X	X	X			
Pérez *et al.* [69]	MCS	Cemented THR				X (fatigue/ damage acum)		X (interface conditions)		X					X
Nicolella *et al.* [70]	MPP	Cemented THR		X		X				X			X		X
Laz *et al.* [71]	MCS, AMV	Femur		X											
Dopico González *et al.*	MCS	Uncemented THR	P	X			P	X	X	X		P		P	X

Table 2.4: Most representative probability studies performed to date. In columns, method, assessed system and the main RVs classified by its nature. The 'X' means that the study includes that parameter. P means that they are be compared parametrically. *G* means 'geometry' and *MP* means 'material properties'.

parameters.

Bah and Browne [66] developed a probabilistic analysis of a cemented hip implant to study the cement maximum von-Mises stress as a response variable, i.e., as the performance function $g(X)$. The Response Surface method was applied, approximating $g(X)$ by a second-order polynomial function with cross terms $g'(X)$. The probabilistic response was computed by NESSUS [154], coupled with the ANSYS FE program. From the sensitivity analysis it was shown that the most important parameters in descending order were the bone diameter, the axial load, the bone length, the transverse load, the cement thickness and Young's modulus. The work showed how geometric uncertainties affect the probability of failure of the cemented construct. In a second sensitivity analysis, the less important parameters were ignored, and it was found that bone diameter and length, cement thickness and axial joint loading were the most important parameters. This suggests that the consideration of different random variables may lead to different results in the sensitivity analysis, although at least in this case the most important variable was constant.

Bah and Browne [152] looked at the failure of the cement mantle in hip implants by applying the second order response surface method to find out which uncertain parameters were the most likely to influence the probability of failure. They considered the following parameters as RVs: bone diameter, length and Young's modulus; stem diameter, length and Young's modulus; transverse and axial joint loadings. They also considered four kinds of failure: compressive failure, tensile failure, shear failure and fatigue failure, and assessed the probability of each of them of leading to failure of the construct. The cumulative distribution functions revealed that tensile and fatigue failures were the most likely modes of failure . The bone parameters, cement thickness, loading and material strengths were found to be the parameters that were most likely to influence the cement stresses and therefore compromise the structural integrity of the implant. On average, the bone diameter had the largest contribution.

Nicolella *et al.* [67] looked at the risk of failure of a cemented hip implant, accounting for two different failure modes: failure of the bone cement-implant interface and failure of the bone cement mantle. The AMV+ method was applied and sensitivity factors were computed. For each mode of failure, different critical strength limits were considered. For the bulk cement failure mode, joint

loading was the dominant factor in compressive failure and shear failure while joint loading and the critical strength variable were dominant for the strain energy density failure criteria (SED). Variability in the joint loads had the greatest effect on the probability of failure. The dominant random variable for the fatigue failure mode was the fatigue limit stress; joint loading was also significant. In general, increasing the mean limit strength will result in a decrease in the probability of failure. For cement-implant interface failure, both joint loading and limit strengths significantly influenced the probability of failure for all interface failure mode criteria. Reductions in the mean values of the y- and z-component joint loads would result in a reduction in the probability of interface failure. Variations in the interface strengths also dominated the probability of failure. A reduction in the variability of interface strengths would result in a decrease in the probability of failure. These results suggest that the selection of the failure criteria is a factor that may influence in the sensitivity results, and therefore it must be considered in the design of the probabilistic model as a critical variable.

Laz *et al.* [155] looked at the effects of variability in the experimental setup of a knee wear simulation to assess its impact on predicted tibio-femoral mechanics. The potential envelope of joint kinematics and contact mechanics present during wear simulator loading was determined, and the sensitivity of the joint mechanics to the experimental parameters was evaluated. Using NESSUS, Advanced Mean Value (AMV) probabilistic design was conducted for 9 RVs: the anterior-posterior (AP) and inferior-superior (IS) position of the femoral flexion axis, the AP and medial-lateral (ML) position of the tibial internal-external (IE) rotation axis,the ML load split, the soft tissue spring constant, the coefficient of friction, the initial femoral flexion-extension angle, and the posterior slope of the insert. Over the gait cycle, the location of the rotational axes and coefficient of friction were most important, while the spring constant, posterior tilt and ML load split contributed negligibly. For AP translation, the IS location of the flexion axis and the coefficient of friction were most critical during the instances of maximum force, torque and flexion.

Mehrez *et al.* [156] applied probabilistic approaches to assess the structural integrity of a total hip replacement. A tapered 3D model of the femoral part of the THR construct was built to apply the FE method, which was completely parametrized so that the effects of material properties, geometry and loading

could be studied. The bone-cement interface was assumed to be fully bonded, while contact elements were used to simulate a debonded cement-stem interface condition. A limit relative displacement between the stem and the cement mantle was chosen as the failure criteria. The effects of 10 uncertain design, load and material parameters were examined: the axial load, the Young's moduli of the bone and the cement, the outer and inner radii of the bone at the proximal and distal ends, the distal and proximal radii of the stem, and the length of the femoral component. All the RVs were statistically independent, with lognormal distributions except Pz with normal distribution. The statistics and the FE models were computed using NESSUS [154] and ANSYS [18]. The Advanced Mean Value (AMV) method and a Response Surface (RS) method based on Monte Carlo simulation Technique (MCST) were applied, and sensitivity factors were computed at different probability levels (10%, 50%, 90%). The comparisons were done for a probability of failure (pf) of 50%. They obtained good efficiency with the AMV method, since only 12 FE analyses were needed to obtain results close to those from RS analysis, where 200 FE analyses were required. Standard MCST would have required at least 10,000 FE analyses. The sensitivity analysis for the 3 levels of pf showed that the Young's modulus of the cement, the proximal stem radius, the axial load and the bone geometry most contributed to the pf. It was concluded that variations in geometrical properties are important and need to be considered in probabilistic analyses.

Pérez *et al.* [69] developed a technique to determine the influence of the variability and uncertainty of the key mechanical factors on the performance of cemented implants, comparing the reliability of a cemented hip prostheses with differing surface finishes. To obtain the failure probability of the cement layer for a fixed number of cycles, a probabilistic methodology based on stochastic finite elements and cumulative damage approach was used. The applied loads, damage evolution and fatigue material properties were the model parameters considered as random variables. They concluded that the failure probability was highly dependent on the stem-cement interface condition and despite the need for several improvements to be added for a more accurate prediction of the reliability, they considered that this methodology could be useful for clinicians and implant designers.

Nicolella *et al.* [70] used MPP methods to assess the cemented THR and

the effect of three-dimensional prosthesis shape optimisation on the probabilistic response and failure probability of a cemented THR. They considered 9 input RVs in the model: cortical and cancellous bone and bone cement stiffnesses, joint load and muscle loads in X, Y and Z directions. They formulated several limit strength functions to assess the performance of both bulk cement mantle and the prosthesis-cement interface. They used the MPP method to model the performance function, and sensitivity results where obtained from the location of the MPP. The optimised implant was obtained by minimising the square of the von-Mises equivalent stress summed over all of the elements. They compared the probabilistic results for the intact and the optimised implant. The most likely mode of failure before implant optimisation was implant-bone cement interface tensile failure. The optimised implant reduced this *pf* for all of the performance functions. From the sensitivity results, they found that the load, cement strength and implant-cement interface strength most contributed to the *pf*.

Easley *et al.* [122] developed a finite element-based probabilistic tool for orthopaedic applications including dimensional variability in a complex geometry and incorporating more realistic modelling conditions while maintaining computational efficiency. The secondary objective was to demonstrate the tool for two applications, one investigating the effect of implant geometry and material property variability on the performance of a THR, the other the effect of component placement and experimental setup variability on the kinematics of a total knee replacement. The results of the first application are discussed here. This computational tool combines commercially available software with custom scripting to develop a flexible and robust model. The first application to a parametric design of a hip stem considered ten random variables for inputs to the probabilistic model: seven geometric parameters and three material properties (Young's modulus, Poisson's ratio and fatigue strength) of the implant.

The fatigue strength limit of the material was the determinant of the structural integrity performance function. A 1000-trial Monte Carlo simulation and the MPP (MV, AMV, AMV+) reliability methods were employed for the probabilistic analyses. With MV 10 FE analyses were required, although the nonlinearity of the model resulted in a notable inaccuracy of the MV method, while the results with AMV and AMV+ compared well with Monte Carlo results. The probabilistic model using AMV method needed 12 trials, while the AMV+ re-

quired 212 trials for convergence. From the sensitivity analysis, the uncertainty in the fatigue strength and the stem diameter contributed most to the variability in the predicted stress, and the implant neck angle variable contributed to a lesser extent. The uncertainties in the material properties did not contribute significantly.

In all the studies above, different probability methods were applied and the results from the sensitivity analyses gave an idea of which parameters were more important to have under control in the design processes. In hip replacement studies, the parameters whose variability have been found to play an important role in the variability of the probability of failure have been: bone geometry and material parameters, cement thickness, cement Young's modulus, the proximal stem radius, loading, and material strengths. Since the aim of this project is the performance of the uncemented hip replacement, the results above can be taken as indicative, but they may differ from the results obtained in the present study since the interface bone-implant will be modelled without bone cement.

The literature has shown a varied and increasing body of work on probabilistic techniques in the orthopaedic field. The selection of an appropriate failure criterion is very important in order to achieve accurate results. There are a wide variety of probability methods, failure criteria, random variables and associated distribution functions that could be considered. A compromise between accuracy and analysis time is also required in order to run the models in reasonable time with the available resources. Some work has been conducted assessing the suitability of probabilistic design methods in hip replacement design [68] and it was shown that there is not a universally applicable method; the best method depended on the characteristics of the model and the desired accuracy, although the FORM, SORM, and AMV methods were much more efficient than other methods. In addition, the sensitivity to a parameter changes according to the model, the boundary conditions and the statistics of the parameter.

A main necessity is now to create computational tools that enable implementation of the Probabilistic FE Model (PFEM) of real models so that all these unclear problems can be analysed realistically in minimum time. Some work has been done with cemented implants in this sense [69], showing that the results were very sensitive to model geometry and interface conditions. However, none of these studies looked at parameters related to bone-implant relative position,

and these are factors that would appear to influence the performance of a THR [84, 11, 89, 90]. A fundamental problem in modelling position related parameters is that the geometry of the finite element mesh must be changed automatically during the analysis process. In the present work, position-related parameters will be introduced, together with parameters analogous to those in the above studies, and the application of different probability methods, failure criteria and interface conditions to a database of real proximal femurs and implants will be carried out. A computational tool will be created that will make it possible to account for a significant number of variables involved in an THR. Although this will be applied to the THR it is hoped that the developed methodology will be extendable to other load bearing implants.

Chapter 3

Problem Description

3.1 Aims and Objectives

The primary aim of this work was to build a computational tool to assess the performance of the uncemented hip replacement using the tools described in the previous sections, i.e., Finite Element modelling for predicting the mechanical behaviour of the bone-implant system under prescribed loads and boundary conditions, and Statistical tools and Probability Analysis to assess the behaviour of the construct and the influence of the variability of specific parameters on the risk of failure.

This work has been developed assuming different priorities at every stage. At first, the focus centered on implementing a Probabilistic Finite Element Model (PFEM) of a THR. For this reason, a simplified deterministic model with a coarse mesh, homogeneous materials, one single hip contact load and fully bonded interface was used. In the probabilistic definitions, a reduced set of 4 variables not related to implant positioning was selected as random variables. The process was designed to be automatic so that it was as efficient as possible. The definitions of the FE model were refined to make it close to the natural THR. A mesh convergence study was performed to decide on the most suitable element size. Material properties were applied to every element using a computational resource described in the literature [79]. Fully bonded and frictional interfaces were modelled to simulate different phases of THR healing. Muscle forces were added

to make the performance more realistic. Two different sorts of constraints were applied for comparison. The definitions of the probabilistic model were refined to make it more robust and implant position related parameters were included as RVs. At all stages, the Monte Carlo Simulation Technique was performed, together with Latin Hypercube sampling where appropriate. Different statistics of the input variables were applied for comparison, and all possible combinations of three real bones and two implants were investigated. The effect of changes in the implant reference position was also investigated.

Finally, parametric comparisons between different bones and implants were performed to analyse the influence of inter-patient variability.

3.2 Materials and Methods

This section describes the simulated models and probabilistic techniques adopted in this project. The most representative definitions will be presented in this section. The specific definitions at each stage will be detailed in their corresponding chapter.

3.2.1 Finite Element Models

The geometries of three proximal femurs from patients with body mass index (BMI) of 19.8, 34.4 and 41.8 (Femur 1, Femur 2 and Femur 3) were generated by Radcliffe *et al.* [24] with Mimics software (Materialise NV, Leuven, Belgium) from slices obtained from computer tomography (CT) data (provided by DePuy International Ltd.). CT data was used to determine materials properties of the bones as well as geometry. Materials were assumed to be isotropic. Table 3.1 shows the characteristics of the patients whose femurs have been analysed in this work. Figure 3.1 shows the femur models used in the present study.

Reference geometry was determined for the femur using MATLAB modules. The longitudinal axis of the femur (intramedular canal), was calculated as the straight line that best fits the centres of mass of 5 parallel sections in the proximal end of the femur. The femoral neck axis was determined by finding the centre of

	Age	Sex	Weight (kg)	Height (m)	B.M.I.
Femur 1	18	m	69.9	1.88	19.8
Femur 2	35	m	115.2	1.83	34.4
Femur 3	57	m	136.1	1.80	41.8

Table 3.1: Patient data for the femurs analysed in this study [24]

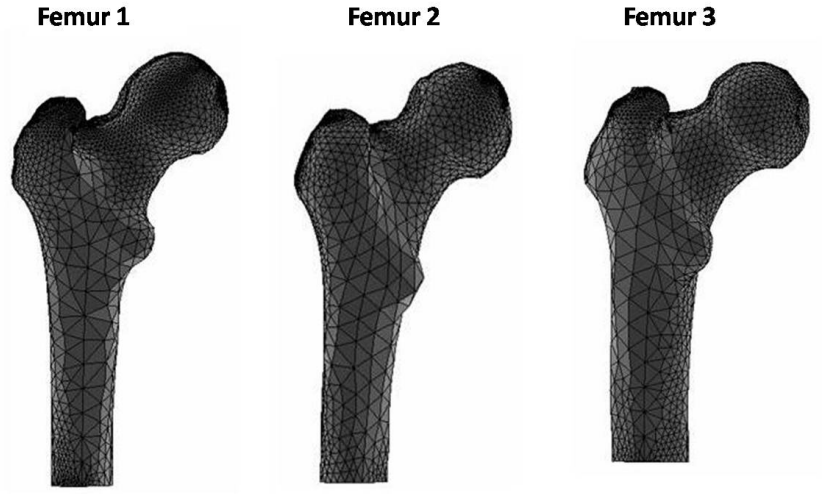

Figure 3.1: Femur models used in this study

the femoral head as the centre of the sphere that best fits a set of nodes selected on its surface [157], and then generating the line that contains this centre and cuts the longitudinal femoral axis at a 135° angle. The femoral head osteotomy was performed differently for the pilot models than for the final models, and details of these are presented in later sections. A reference co-ordinate system was used to define the implant position relative to the bone. This coordinate system was selected using the axes of the femur so that the z-axis corresponded to the femoral longitudinal axis and the x-z plane to the plane of both femoral axes.

The bones were virtually implanted with two implants, the short stem Proxima

(DePuy, Warsaw, USA) and the long stem IPS (DePuy, Leeds, United Kingdom) (Figures 3.2).

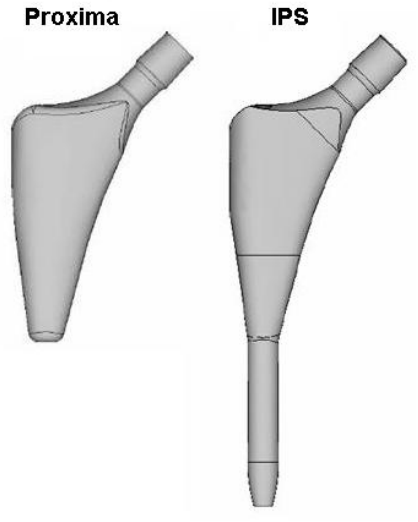

Figure 3.2: Implant models used in this study

The DePuy Immediate Postoperative Stability (IPS) femoral stem (DePuy, Leeds, United Kingdom) is a close proximal fit stem in the coronal and sagittal planes (see Figure 2.3) with a tapered distal stem, and was developed to minimize contact between the stem and femoral cortex and to keep the bone stock in the diaphyseal region [158]. This stem was designed to be an anatomic stem, using the proximal profile of the femur defined by an extensive study of femoral anthropometric data from Asian and white cadaver femora. There are two versions of IPS stem, the older version is manufactured in cobalt-chrome alloy, and the new version is manufactured in titanium alloy TiAlNb. Figure 3.3 shows both versions of the IPS femoral stem. In its horizontal section, the shape is rectangular, allowing a secure diaphyseal press-fit in the frontal plane of the femoral canal. This provides excellent rotational stability and increases primary mechanical fixation. The transition between a load bearing and non-load bearing stem section is short, avoiding metal-to-bone contact below the metaphysis. The short, narrow distal stem is centered in the femoral canal.

In a further effort to ensure the primary stability of an uncemented hip pros-

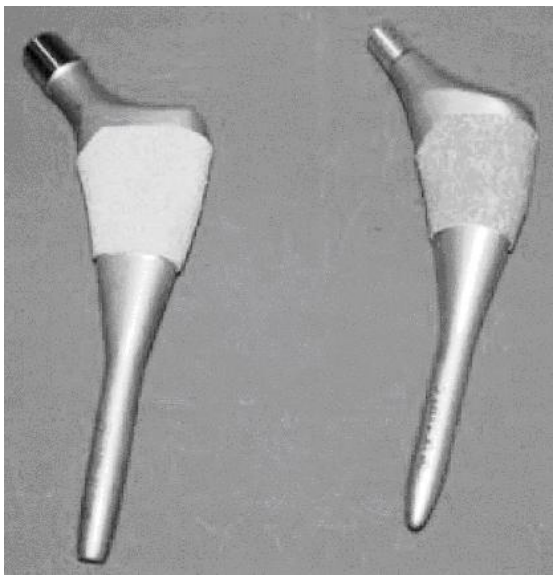

Figure 3.3: Frontal view of IPS stems with hydroxyapatite coating (left) and without hydroxyapatite (porous-coated, right) [9]

thesis, the proximal loading short stem (Proxima, DePuy, Warsaw, USA) was designed. There are two versions with either a ridged ('ZTT') surface or a 'porous coat' surface (Porocoat with hydroxyapatite-coating, see Figure 3.4). The shape of this implant is derived from the design of the proximal part of the IPS, but has no stem so is less invasive. Like the IPS, the Proxima is an anatomic implant, which means it was designed to follow the shape of the proximal femur in both the sagittal and the frontal plane. The shape of the prosthesis was designed based on measurements of key femoral dimensions from CT scans. As an anatomic stem, it comes in left and right-handed versions to fit the left and right femur.

Both implants are available in cobalt-chrome and titanium alloy form, and both will be investigated in this study.

3.2.2 Probabilistic Model

The Monte Carlo method was applied in the present study. The main steps involved in each Monte Carlo simulation were: the definition of the statistics of the RVs, sampling of these RVs, computation of the samples in the FE model

Figure 3.4: Proxima prosthesis with porous coated surface

and solution of the model. Pure random sampling was used in all the studies, and Latin Hypercube sampling was applied in the pilot studies.

Several performance indicators have been selected throughout the study; however, where fully bonded interface conditions were applied, the performance indicators were strain based. This criterion was selected as it has been found to be applicable for all patient types [17], as noted in Section 2.6.

Sensitivity analyses were performed in all cases, always based on linear correlation coefficients (see Section 2.7).

Different sets of RVs were selected within the study, the statistics of which can be seen in Tables 4.1, 4.2, C.2, C.3 and C.4 (Appendix C.2).

3.2.3 Computational Tools

Several tools and resources have been used. In the pilot simulations, ANSYS 11.0 [18] was used for FE modelling, which allowed the bone-implant geometry to be built, the mesh generated, the boundary conditions (loads and constraints) to be applied and the FE model solved. Additionally, Ansys incorporates a probabilistic package that enables Monte Carlo simulations to be performed, with random sampling and Latin Hypercube sampling, and sensitivity results to be obtained. The automation of the PFEM was possible using Ansys. However, several problems arose when trying to adopt different degrees of freedom in implant positioning. For this reason, a more robust tool was necessary that enabled the implant to be placed in any desired position. In the second stage, two further

software applications were included, to allow free manipulation of the implant position in the bone. Rhinoceros (McNeel, Seattle, USA) was used to build the geometry; this involved placing the implant in the desired position and cutting the bone. Ansys ICEM-CFD (Ansys Inc, Canonsburg, PA, USA) was used to mesh the resulting geometry, allowing the creation of a standard Ansys input file. This file was finally opened in Ansys, which was used to apply boundary conditions and run the simulations. All these softwares were controlled by a Visual Basic script. Figure C.2 (Appendix C.4) shows the flow diagram of the probabilistic loop performed in the main studies.

Chapter 4

Pilot Studies

4.1 Probabilistic Finite Element Analysis of an uncemented THR

The aim of this study was to conduct a probabilistic investigation of the uncemented hip replacement using Monte Carlo simulations. The output parameter for the limit state (performance indicator) was selected to be the maximum nodal von-Mises elastic strain in the bone (MAXSTR), since yield strain has been demonstrated as being quite constant across a wide range of bone densities [17]. Several variables have been analysed including, the applied joint load, the angle of the applied load with respect to the femoral longitudinal axis and the material properties of the bone and the implant. The probabilistic results have been complemented by a sensitivity analysis that shows the significance level of each parameter with regards to the integrity of the construct.

4.1.1 Materials and Methods

4.1.1.1 Finite Element Model

A deterministic model was initially used to assess the response of the uncemented THR system; the following elements were used: a 3-D model of a real proximal

femur obtained from CT scans, named 'Femur 1' in Section 3.2, and the proximal loading short stem (Proxima, DePuy, Warsaw, USA) with a porous coated surface (Section 3.2).

Reference geometry was determined using MATLAB modules for the femur as explained in Section 3.2. Two osteotomy planes were defined with an angle of 70° between the femoral neck axis and the first osteotomy plane and 100° between the first and second osteotomy planes. The intersection of the first osteotomy plane was chosen to be at 52 mm from the intersection of the femoral neck axis (**fn**) with the femoral head surface (**A**). Both osteotomy planes were chosen to be perpendicular to the plane formed by the femoral axes **fl** and **fn**. The second osteotomy plane was located at a distance of 15 mm from the intersection of the first osteotomy plane with the femoral neck axis. All these geometric parameters are shown in Figure 4.1.

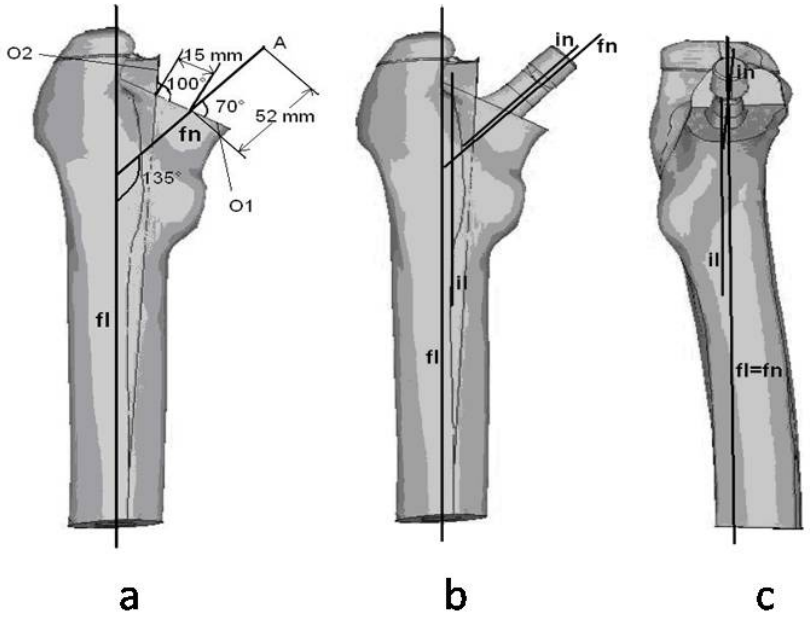

Figure 4.1: (a) Femur reference system. A: intersection of femoral neck axis (fn) with the femoral head surface; fl: longitudinal femoral axis; O1: first osteotomy plane; O2: second osteotomy plane. (b, c) Solid model of the implanted femur showing the relative position of femur and implant and the implant longitudinal axis (il) parallel to the femoral longitudinal axis (fl).

For the implant, (Figure 4.2) the longitudinal axis **il** was calculated as the

line that intersected the centres of gravity of two circular parallel sections in the implant base, and the neck axis **in** as the line that intersected the centres of gravity of two parallel sections through the head taper (where the head ball is placed). The relative position between bone and implant was constrained in the planes parallel and perpendicular to the femoral axes, being **fl** and **il** parallel in both cases, and it was located in a position such that the implant external surfaces did not intersect the bone external surfaces.

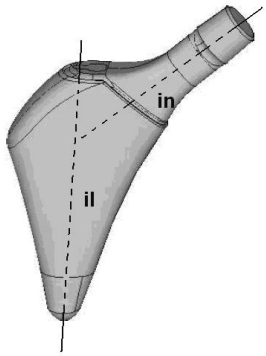

Figure 4.2: Model of Proxima Implant with axes: implant longitudinal axis (il) and implant neck axis (il).

Finite Element meshes of both bone and implant were built using Ansys [18], with 10-noded tetrahedral elements, resulting in 12,218 elements and 18,191 nodes.

The materials of both components were assumed to be elastic, linear and isotropic. The bone was considered completely homogeneous, no differentiation of cortical and cancellous bone was considered. A uniform average elastic modulus for bone [159] was adopted. The implant was cobalt-chrome alloy and both materials had a Poissons ratio of 0.3.

The bone was completely constrained at the inferior section, and the bone-prosthesis interface was assumed to be fully bonded. The load was applied at the centre of the proximal tip of the implant and the load case considered was for normal walking values as obtained by Bergmann *et al.* [23], for an individual weighting 75 kg. The FE model is shown in Figure 4.3.

4.1.1.2 Probabilistic Model

The variable parameters considered for the present study were (Figure 4.3): the magnitude of the applied load (**P**) and the angle between the load and the femoral longitudinal axis (**ANGZ**)) to account for different loading conditions, the Young's modulus of the bone (**EXB**) to represent inter-patient variability, and the Young's modulus of the prosthesis (**EXP**). All these parameters have been demonstrated to influence bone performance in previous probabilistic and parametric studies [67, 66, 156, 153, 70, 87, 83, 86].

The distributions of these parameters are shown in Table 4.1. The means and standard deviations of the load (P), the load angle (ANGZ) and the bone stiffness (EXB) were taken from previous studies [23, 25, 26]. The mean of the implant stiffness was the corresponding to a Cobalt-Chrome material with a standard deviation (SD) of approximately 15%. Both stiffenesses were modelled with lognormal distributions, to ensure that their values remained always positive. Different Monte Carlo based simulations were run, using direct sampling (DS) and Latin Hypercube Sampling (LHS) [146], with a maximum of 10,000 simulations.

The selection of the output or failure criterion plays an important role in the results [67, 152]. Bone strain to failure has been shown to be relatively independent of bone density [130] and strain-based criteria have been proposed as better predictors of failure than stress-based criteria [129]. The output parameter or failure criterion considered in this study was the maximum von-Mises elastic strain amongst all nodes in the bone (MAXSTR). Note that although the output in this case is not a failure as such, it can be referred to as a 'limit state'.

The convergence of the mean value of the output parameter was plotted, to assess the accuracy of the results. The evaluation of the sensitivities was performed with the probabilistic Ansys facility, which was based on the correlation coefficients between the input parameters and the output parameter MAXSTR. A Pearson linear correlation coefficient was calculated [160]. In Ansys the sensitivities can either have a significant influence on a particular random output parameter or not, based on a statistical significance test [18]. In the present work, the sensitivities are plotted for those significance levels for which all the random variables became significant.

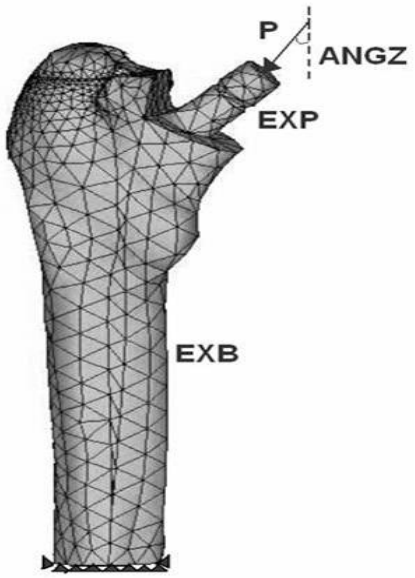

Figure 4.3: Variable parameters. ANGZ: angle between the applied load and the femoral longitudinal axis; EXB and EXP: Young's moduli of bone and implant, respectively; P: modulus of the applied load

Name	**Random Variable**	**Distribution**	**Mean**	**Standard Deviation**
EXB	Bone Young's modulus (MPa)	LogNormal	1,200	3,500
EXP	Implant Young's modulus (MPa)	LogNormal	210,000	38,000
ANGZ	Load angle-Z (°)	Normal	31.5	3.5
P	Load magnitude (N)	Normal	1,775	260

Table 4.1: Statistics of the RVs [23, 25, 26]

Ansys scripts were used to control the generation of geometry, mesh and run the simulations for each specific sample as well as to define the probabilistic analysis that controls the generation of the samples and the automatic simulations.

4.1.2 Results

In the following section, the term 'sensitivity' is used to describe how values of the RVs affect the values of the output parameters.

The results for 100 simulations were highly variable. The best matches between LHS and DS occurred at 1,000 simulations and above; therefore the following results focus mainly on comparing the outputs for 1,000 LHS and 10,000 DS simulations.

The maximum nodal strain was typically located in the compressed elements in the medial part of the bone, between the distal constrained section and the lesser trochanter. In Figure 4.4, the convergence of the mean of the output parameter is presented. It can be seen that the shape of the output improved gradually with increasing number of simulations. For 1,000 simulations with LHS (left), the curve has not completely converged, although the trend is clearly toward a value between 0.007-0.008 for the maximum strain. For 10,000 simulations with DS (right), the curve starts to stabilise at around 0.008 after approximately 1,500 simulations and is very stable after 5,000 simulations.

Figure 4.5 shows the empirical cumulative distribution functions (CDFs) of the output. For 100 LHS, the curve showed excellent agreement with those of 1,000 LHS and 10,000 DS. The maximum error between the CDFs of 100 LHS and 10,000 DS was about 5% for an output value of 0.0055. The probabilities of the output value were almost identical; for probabilities of 10%, 30% or 70%, maximum strain values were about 0.0013, 0.005 and 0.01.

The sensitivity results are presented in Figure 4.6. To confirm the trends observed at a lower number of simulations, the outputs from 10,000 LHS simulations are also presented.

At 1,000 LHS simulations (Figure 4.6), the bone maximum strain was most sensitive to bone stiffness, followed by the load, while it was much less sensitive to implant stiffness and load angle. Similar results were observed for 10,000 DS simulations and 10,000 LHS simulations (Figure 4.6).

It took 1 hour and 37 minutes to run 1,000 simulations using LHS. In contrast, it took approximately 3 days to run 10,000 LHS and 10,000 DS simulations; the estimated run time for 100,000 simulations would be 1 month, using the same

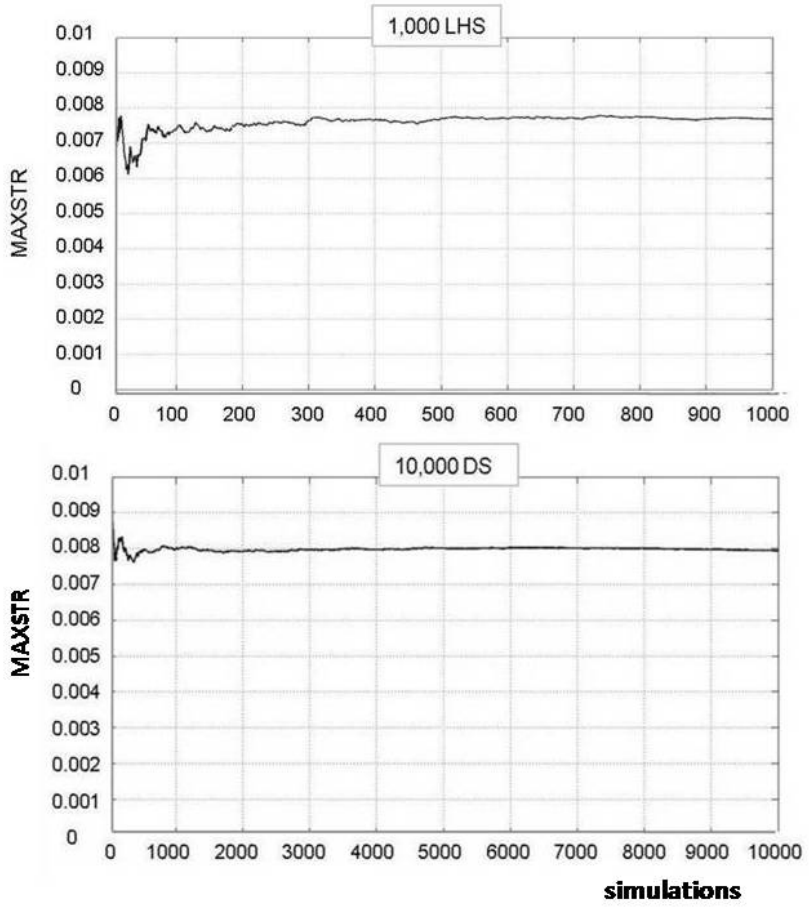

Figure 4.4: Mean value history of output parameter MAXSTR

computer.

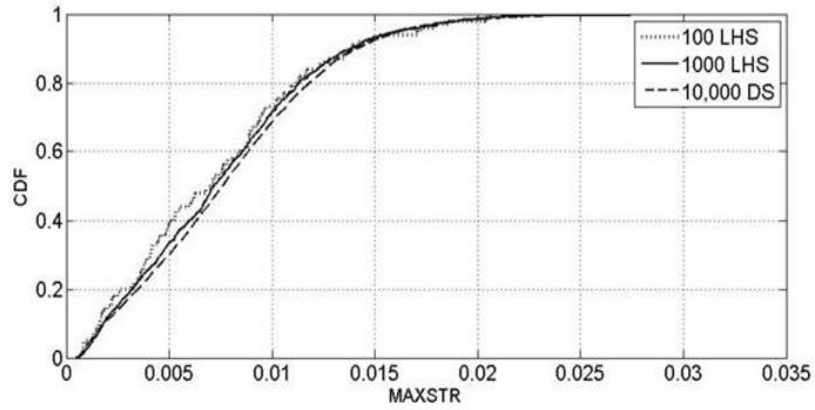

Figure 4.5: Cumulative Distribution Function of the output parameter MAXSTR for 100 LHS, 1,000 LHS and 10,000 DS simulations

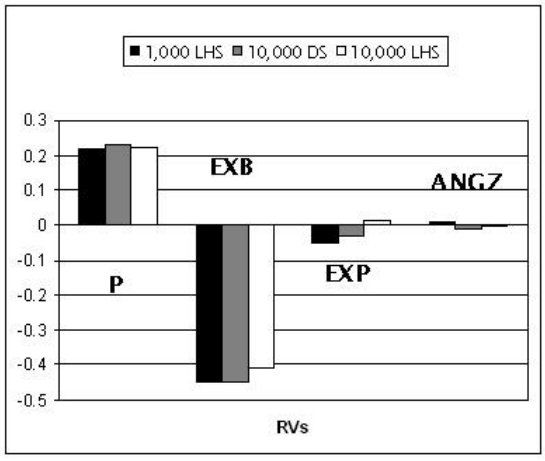

Figure 4.6: Sensitivity results for 1,000 LHS, 10,000 DS and 10,000 LHS simulations

4.1.3 Discussion

The primary objective of the present work was to consider variability in an implanted system by conducting a probabilistic finite element analysis of an uncemented implant. To make the problem more manageable, a number of simplifications were introduced, most notably, a fully bonded interface was assumed, and four random variables were selected. These random variables have been considered in previous studies and have been highlighted as playing a role in influencing the risk of failure [70, 153], and also parametric studies have shown how the implant stiffness and geometry play an important role in bone remodelling or stress levels [83, 86].

Monte Carlo simulation techniques were applied since, provided a sufficient number of simulations are performed, they are guaranteed to accurately assess the response of the system and they can therefore be used to benchmark results obtained by other methods. LHS has shown that equivalent results to DS can be achieved in a fraction of the time using a lower number of simulations. It took 1 hour and 37 minutes to run 1,000 simulations using LHS. In contrast, it took approximately 3 days to run 10,000 DS simulations. LHS attempts to run trials with parameter combinations distributed evenly across the entire sample space rather than at random intervals, thus reducing the number of trials necessary. However, when the problem becomes very complex, for example, it involves a high number of variables, the LHS method may become inefficient as it attempts to select trials from the whole of the sample space. In this case, 'clustering' can occur where many samples are taken from a particular region. Thus, as has been observed in the present work, at a very high number of trials, DS becomes more efficient and the advantages of LHS decrease. For a low number of trials, LHS is more suitable.

The results have highlighted the importance of the bone stiffness and load magnitude when considering the response of the implanted bone to loading (Figure 4.6). The direction of the sensitivity plots shows that the sensitivity to bone stiffness was negative, meaning that the smaller the bone stiffness the more likely was the maximum strain to be exceeded. The sensitivity to load was positive, that is, the larger the load the more likely was the maximum strain to be exceeded.

The high number of available probability methods, RVs, and systems makes it

very difficult to find a similar study for comparison. For this reason, comparisons are made based mainly on the nature of the RVs rather than the methodology or the system.

Table 2.4 shows a number of probabilistic studies where the unimplanted and implanted femur have been investigated. The applied methods, the assessed systems and the RVs are noted and marked with an 'X' when they were considered in the investigation. Columns corresponding to bone material properties are divided in 'uniform' and 'distributed'. Uniform material properties means that the whole femur was considered to have constant Youngs modulus within each model. Distributed material properties means that the bone properties were assigned with a more realistic approach, either differentiating between cortical and cancellous bone [67, 70], or assigning material properties to the bone elements according to density/Young's modulus relationship [161]. It can be seen that load magnitude and bone material properties are most commonly investigated. Almost all the investigations have focussed on the cemented hip replacement. Although the present work looks at the uncemented implant, a discussion of the previous studies is presented and compared with the present work to identify trends.

Bah *et al.* [66] used RSM to look at the cement maximum von-Mises stress in a cemented THR. By incorporating geometrical variability into the system, together with a cement layer, they found that the bone geometry was the most sensitive parameter, followed by cement thickness and load magnitude, in contrast to the present investigation.

Nicolella *et al.* [70] looked at the risk of failure of a cemented THR, and considered two failure modes: failure of the bone cement-implant interface and failure of the bone cement mantle. They applied AMV+ and found that the load magnitude and geometry were the most sensitive parameters. In both the above cases, bone cement was the fixation medium. This in itself introduces further uncertainty due to the increased number of interfaces and the associated boundary conditions.

Mehrez *et al.* [156] applied AMV and RS methods to a simplified model of a cemented THR, and looked at the relative displacement between the stem and the cement mantle or inducible displacement as the failure criteria. They found that the most sensitive parameters, in descending order, were the cement material

properties, implant geometry, load and bone geometry/material properties. This does not necessarily conflict with the findings of the present study since the most sensitive parameters were related to the inclusion of the bone cement and geometrical parameters, while loading and bone material properties remained moderately sensitive.

Perez *et al.* [69] looked at damage accumulation due to fatigue in a cemented THR using MCS. They considered various implant surface finishes, bone stiffness, load magnitude and muscle loads as RVs, and they found that the performance of the construct was highly dependent on the stem-cement interface conditions. However, no sensitivity analyses were performed.

Most recently, Nicolella *et al.* [70] used MPP methods to assess the cemented THR, formulating limit strength functions to assess the performance of both the bulk cement mantle and the prosthesis-cement interface. They found that the load, cement strength and implant-cement interface strength most contributed to the probability of failure (pf).

To the authors' knowledge, the only probabilistic study investigating the integrity of a cementless implanted hip system has been conducted by Viceconti *et al.* [162], who looked at the primary stability (micromotion) of a cementless implant using Monte Carlo simulations. Although sensitivity analyses were not performed, the authors quote 'the main risk factors' for insufficient primary stability to be the interface contact, the size of the host bone, and the body weight.

The most closely related studies to the present work have been deterministic in nature. In an experimental study by Gillies *et al.* [86] the loading conditions and implant geometry were varied, and it was found that the experimental strain distribution was highly dependent on the stem geometry, the loading orientation and muscle simulation.

Similar results were obtained experimentally by Decking *et al.* [88] when measuring the strain distribution of three different implant designs under similar loading conditions.

Weinans *et al.* [83] developed a finite element model and looked at a number of implants with different stiffnesses. They found that the strain-energy density was highly dependent on the implant material and the degree of bonding at the

interface.

Biegler *et al.* [87] developed finite element models of uncemented hips with two different implant geometries and surfaces, and under two loading conditions (one-legged and stair climbing). They looked at the amount of contact and the relative motion between bone and implant and found that torsional loads most contribute to implant micromotion, again highlighting the importance of the loading condition. In the present study, the average location of the maximum nodal strain was in the compressed elements in the medial part of the bone, between the inferior constrained section and the lesser trochanter.

In the above studies that looked at strain, the maximum strain was observed in the same location. It would be difficult to draw comparisons regarding the absolute strain values obtained from each of the studies since they used different metrics, loading conditions and measures of strain. In addition, a simplified model was necessary in the present case.

However, the simplifications employed in this work enabled probabilistic analyses to be conducted at a much reduced computational expense, thus allowing manageable runtimes. The FE model adopted a uniform bone stiffness (i.e. it did not differentiate between cancellous and cortical bone) with a fully bonded interface under static loading. This will have been a factor in the sensitivity analysis, which showed that bone stiffness played a major role in the response of the system. In future work, and with enough computational resources, this parameter could be investigated more thoroughly by, for example, focussing on the dynamic behaviour of the bone and the variability and uncertainty observed in the non linear experimental stress response of trabecular bone [163], and damage accumulation. Additionally, spatial variations in the bone material properties could be addressed using CT mechanical properties for the FE mesh. Material properties could be then assigned accordingly, and contact pairs used to define the interface [77]. Muscles forces should be considered in the future, since some authors have demonstrated their influence on the stresses and/or strains of the loaded bone [116, 117, 118, 119]. The selection of the constraints has been demonstrated to affect the output of the construct [89], so alternatives should be also considered in future probabilistic analyses.

It is important to clarify that the ultimate aim of probability sensitivity anal-

yses is to give a qualitative description of which parameters determine the risk of failure, and therefore the accuracy is heavily dependent on the selection of accurate values and distributions for the input parameters. With appropriate input parameters, a probabilistic study has the advantage over deterministic studies of being able to provide a more holistic description of the risk of failure of the system. In this way, designers can be made aware of the most important design parameters that influence implant performance at the design stage, and surgeons can be made aware of the influence of surgical factors (for example malpositioning) on the implant performance.

4.2 Probabilistic Finite Element Analysis of an Uncemented THR considering Implant Version

In the previous study (Section 4.1) a probabilistic investigation of an uncemented THR was carried out with a simplified model that enabled the automation of the probabilistic finite element loop. Four random variables were selected: bone and implant stiffnesses, load magnitude and geometry.

The aim of this work was to build a computational tool which would enable the probabilistic analysis of a finite element model of an uncemented hip replacement that considered variability in bone-implant version angle, since implant position parameters have been found to influence different performance indicators of the THR [84, 11, 89, 64]. For this purpose, using the same model as in Section 4.1, a probabilistic finite element model (PFEM) tool was developed, and a similar probabilistic analysis was performed, while considering variability in bone-implant version angle. The probabilistic results are again complemented by a sensitivity analysis that shows the significance level of each parameter on the integrity of the construct.

4.2.1 Materials and Methods

4.2.1.1 Finite Element Model

The deterministic model was identical to that used in Section 4.1, with the addition of an appropriate reference system to define the implant version angle, and the definition of interface contact pairs between bone and implant. The coordinate system was selected using the axes of the femur so that the z-axis corresponded to the femoral longitudinal axis and the x-z plane was in the plane of both femoral axes, as can be seen in Figure 4.7. The version angle was varied by turning the implant around the z-axis. The interface contact pairs were defined to enable future frictional interface simulations and to identify potential problems with this form of modelling.

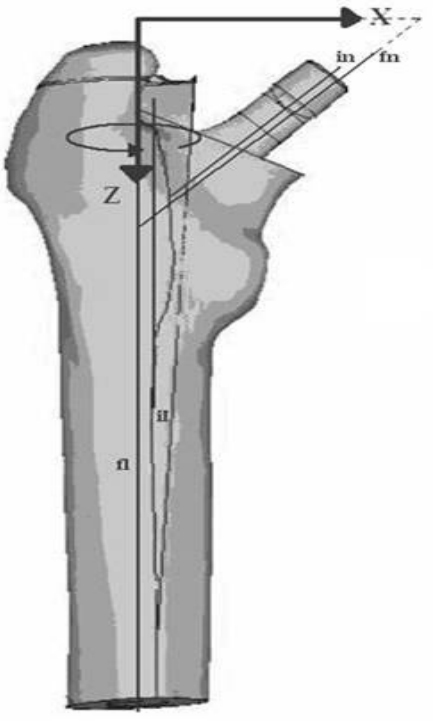

Figure 4.7: Relative position between femur and implant and local reference system for the bone-implant version angle. Implant longitudinal axis (il) parallel to femoral longitudinal axis (fl).

Finite element meshes of both bone and implant were generated using 10 noded

tetrahedral elements in the ANSYS finite element package. In the previous work (Section 4.1), the model possessed 12,218 elements and 18,191 nodes 12 . The present work employed a variable mesh when assessing implant version. This model had an average of 11,000 elements and 15,500 nodes.

The same simplifications as in previous model (Section 4.1) were adopted: the materials of both prosthesis and bone were assumed to be elastic, linear and isotropic and the bone was considered homogeneous, with a uniform average elastic modulus [159]. The implant was cobalt-chrome alloy and both materials had a Poisson's ratio of 0.3. The bone was completely constrained at the distal end, and the bone-prosthesis interface was assumed to be fully bonded. In the previous model (Section 4.1), the two meshes were merged at the interface, whereas in this study, fully bonded contact pairs were located at the interface. Although the fully bonded contact pairs approach leads to longer run times, the results are equivalent to the merged meshes approach and it has the advantage of enabling a frictional interface to be developed in future studies. As a result, it was necessary to use a reduced number of samples in order to avoid excessive run times (of the order of 2 months in a 3.20 GHz, 2.00 GB of RAM computer). The hip contact load was applied at the centre of the taper end face of the implant and the load magnitude was as measured for normal walking values by Bergmann *et al.* [23], for an individual weighting 75 kg. The FE model is shown in Figure 4.8.

4.2.1.2 Probabilistic Model

Four sources of uncertainty, or random variables, were considered in the previous model (Section 4.1) [164]: the magnitude of the applied load (P) and the angle between the load and the z-axis (ANGZ - to account for different loading geometries), the Young's modulus of the bone (EXB - to represent inter-patient variability) and the Young's modulus of the prosthesis (EXP) were considered. All these parameters have been demonstrated as influencing bone performance in previous probabilistic and parametric studies [67, 66, 156, 153, 70, 87, 83, 86]. In the present work, the implant version angle (ANTVR) was included as a RV. The associated distribution functions are presented in Table 4.2.

The mean and standard deviation of the implant version were selected arbi-

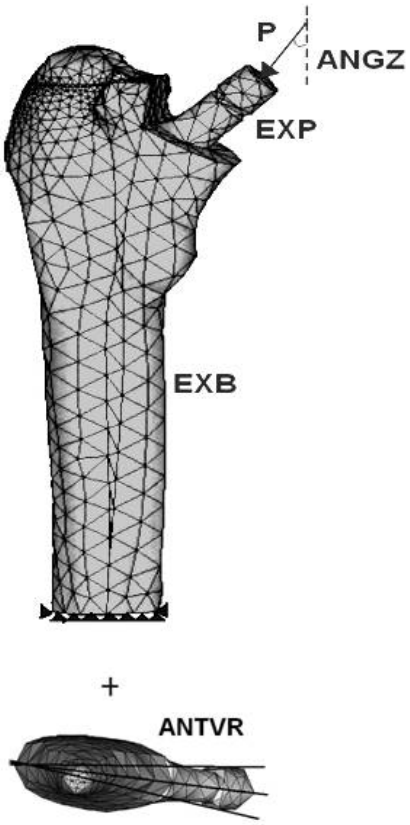

Figure 4.8: Variable parameters. ANGZ: angle between the applied load and the femoral longitudinal axis; EXB and EXP: Young's moduli of bone and implant, respectively; P: modulus of the applied load. ANTVR: bone-implant version angle

Name	Random Variable	Distribution	Mean	Standard Deviation
EXB	Bone Young's modulus (MPa)	LogNormal	1,200	3,500
EXP	Implant Young's modulus (MPa)	LogNormal	210,000	38,000
ANGZ	Load angle-Z (°)	Normal	31.5	3.5
P	Load modulus (N)	Normal	1,775	260
ANTVR	Implant Version (°)	Truncated Normal	0	2.5 (-2.5,5)

Table 4.2: Statistics of the RVs [23, 25, 26]

trarily, and truncation limits were adopted after several manual trials, to avoid the implant intersecting the inner surface of the bone ($-2.5°$, $5°$). The mean of the implant stiffness corresponded to a Cobalt-Chrome material with a standard

deviation (SD) of approximately 15%. Both stiffnesses were modelled with log-normal distributions, to ensure that their values were always positive. The values of the rest of the parameters were taken from several references [23, 25, 26], as in Section 4.1. The performance indicator adopted in the previous model (Section 4.1) was also used in the present study, the maximum von-Mises elastic strain amongst all nodes in the bone (MAXSTR).

Monte Carlo based simulations were run, applying either Direct Sampling or Latin Hypercube Sampling, for a maximum of 10,000 simulations.

In all the simulations, there were about 3.5% unconvergent simulations. The model code included commands to identify them, let the probabilistic loop to continue, and force the solution to equal zero. In this way, the unconvergent solutions were easily identified and were manually removed before post-processing. For 10,000 simulations, manual manipulation of the results file became time consuming and was not considered. Instead, the results from the Monte Carlo simulations were used to fit a quadratic response surface with cross-terms (see Section 2.7.4.1) that filtered the outliers using Forward Stepwise Regression, with a filtering confidence of 0.95 [18].

The convergence of the mean value of the output parameter was plotted, to assess the accuracy of the results. As in the previous Section 4.1, the evaluation of the sensitivities was performed with the probabilistic Ansys facility, which was based on the correlation coefficients between the input parameters and the output parameter MAXSTR [18]. In the present work, the sensitivities are plotted for those significance levels for which all the random variables became significant.

The inclusion of variability in bone-implant version angle led to a notable change in the computational flow, compared to the previous model (Section 4.1). The geometrical data base of the solids had to be updated to adopt the implant version values required for each sample, and thereafter a new mesh was computed each time. The computational flow is presented in Figure 4.9. The probabilistic script described the probabilistic method and created the samples. The geometric database was comprised of the unchangeable geometric definitions, where the implant was translated a known distance from the reference position that was adopted in previous study. A local coordinate system was defined in the implant parallel to the femur reference system described in Figure 4.7, and translated

with it. Each new sample was introduced into the FE model, varying first the implant orientation with respect to its local coordinate, and then translating it to its position within the bone. The Boolean operations and mesh were computed, and the simulation run to obtain the sought output parameter (MAXSTR).

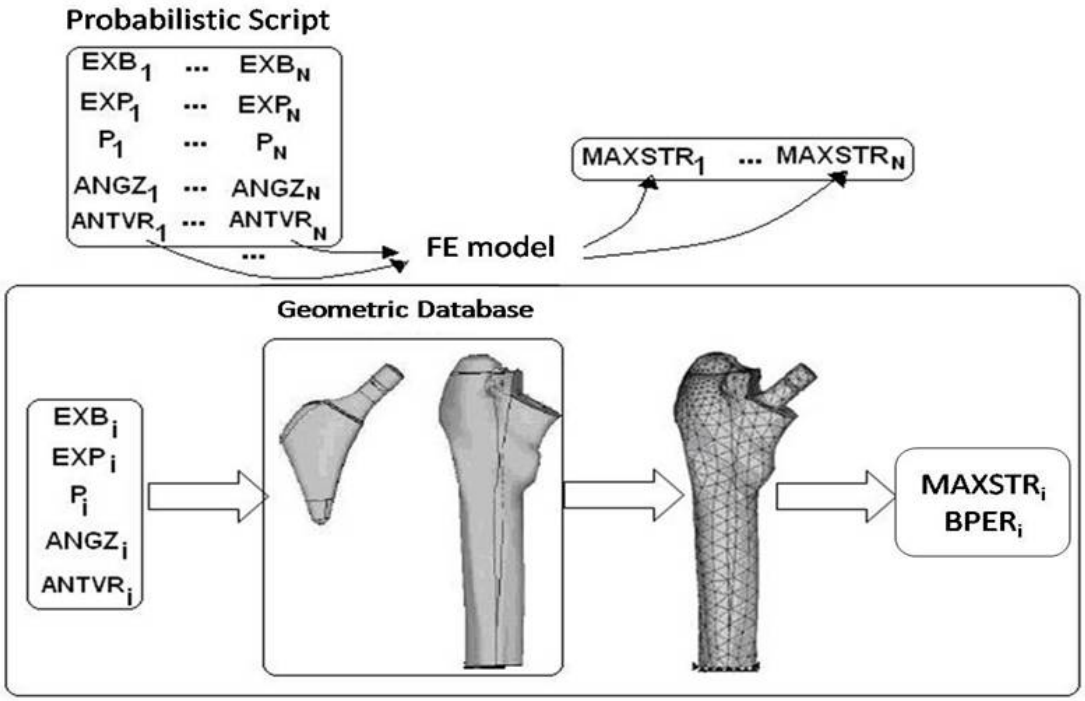

Figure 4.9: Computational flow including bone-implant version angle. 'Probabilistic Script' creates the input samples, and controls the Monte Carlo loops. The 'FE model' contains the constant geometric database, performs the geometric operations, and simulates the FE model. A value of the output (for 'BPERi', see next Section 4.3) results from each iteration.

4.2.2 Results

As in previous Section 4.1, the term 'sensitivity' is used to describe how changes in the RV values and their scatter effect the range of scatter of the output parameters [18].

Figure 4.10 shows the convergence of the mean value of the output parameter MAXSTR. It can be seen that the output starts to converge after 2,500

simulations approximately, to a value of almost 0.0065 (or 0.65%).

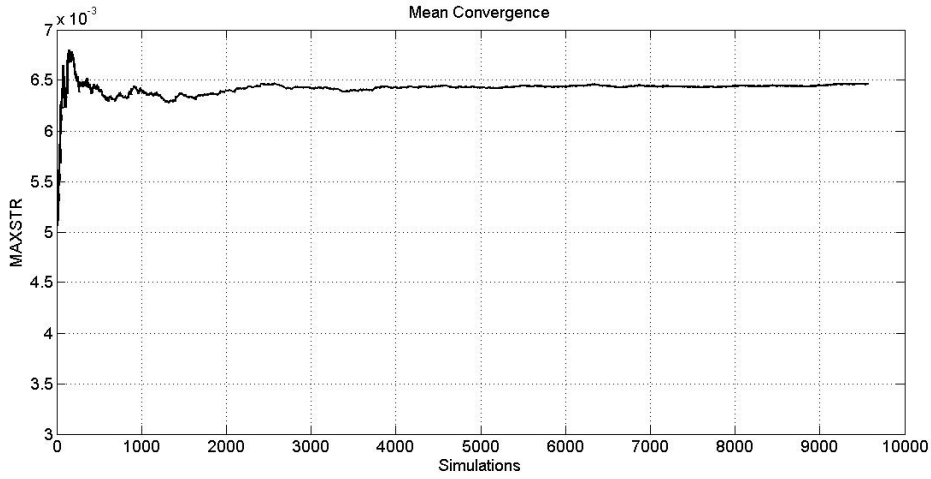

Figure 4.10: Mean value history of MAXSTR for 10,000 DS simulations

Figure 4.11 shows the empirical cumulative distribution function (CDF) of the output for the previous 10,000 DS four random variables model ('4RVs-10,000 DS') (Section 4.1) and the present five random variables with 1,000 DS, 1,000 LHS and 10,000 DS (5RVs-1,000 DS', '5RVs-1,000 LHS', '5RVs-10,000 DS'). An excellent agreement was found between the empirical CDFs of the present model, for 1,000 DS, 1,000 LHS and 10,000 DS simulations. Although in the first section of values of MAXSTR the present model converged faster than the 4 RVs model, from values around 0.015 of MAXSTR the present model converged slower for the 1,000 DS and 1,000 LHS simulation cases, as can be seen in Figure 4.11. The mean value of MAXSTR was about 0.65% corresponding to a probability of 0.5 in the empirical CDF, while for the previous 4RVs the mean value was 0.8% (Section 4.1).

The sensitivity results are shown in Figure 4.12. For this model, the application of LHS showed similar results compared to DS. For 1,000 simulations with DS and LHS, the most sensitive parameters were the implant version angle and the bone stiffness, but an inconsistent result was found for the load magnitude, which was minimally sensitive in both cases and negative for DS. When running 10,000 DS simulations, the load became highly sensitive and positive, in agreement with

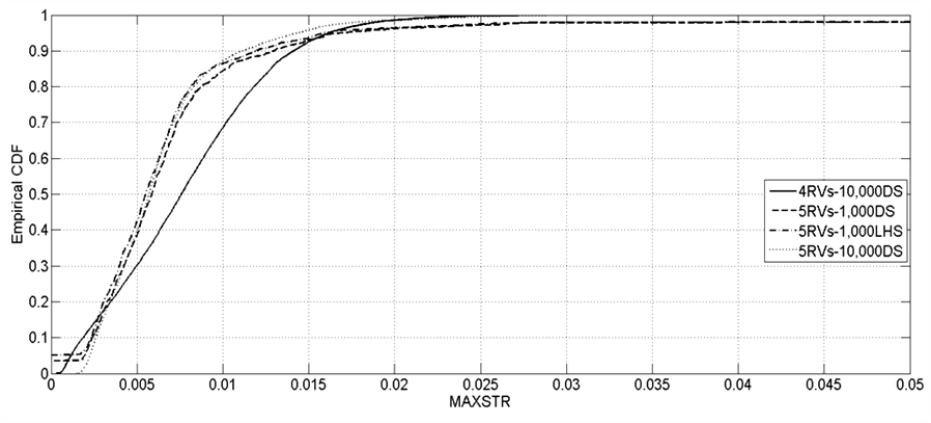

Figure 4.11: Empirical Cumulative Distribution Functions with 1,000 DS, 1,000 LHS and 10,000 DS simulations models.

the previous study (Section 4.1.2). This suggests that a large number of samples is needed to produce authentic results.

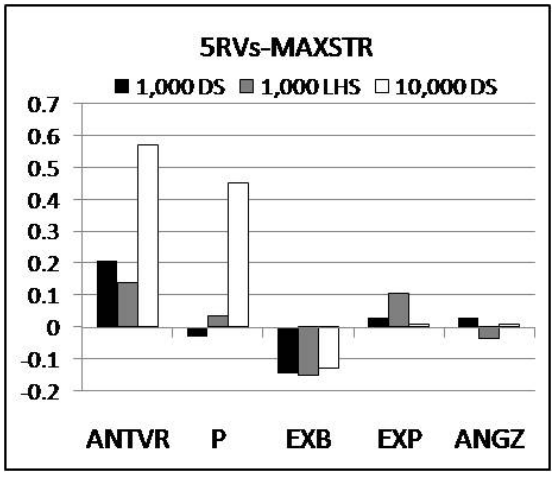

Figure 4.12: Sensitivity results for 1,000 DS, 1,000 LHS and 10,000 DS simulations.

4.2.3 Discussion

The aim of this work was to build a computational tool to enable probabilistic analyses of the uncemented hip replacement to be applied that could assess the effect of implant position related variability. In a previous study 4.1 [164] a preliminary model with 4 RVs was considered; these RVs were selected as they have been analysed in previous studies and highlighted as playing a role in influencing the risk of failure of the replaced hip [70, 153]. In this section implant version angle was included; several parametric studies have also highlighted its influence on the strain levels present in the bone and the occurrence of dislocation [11, 89, 64]. In order to minimize computational time, several simplifications were made, most notably: (i) the interface was fully bonded; (ii) the materials were linear, isotropic and homogeneous. The variability of bone-implant version angle was implemented in the probabilistic tool, which updated each simulation to the new implant position and re-meshed the model.

Monte Carlo simulation techniques were applied since, provided a sufficient number of simulations are applied, they represent an accurate method of assessing the response of the system and they can be used to benchmark results obtained by other methods.

As in the previous study (Section 4.1, [164]), the maximum nodal elastic strain in the bone was the output parameter. The most sensitive parameters were the bone stiffness and the load magnitude. The application of 1,000 LHS compared well with 10,000 DS simulations (Figure 4.6). However, when the implant version angle was included in the set of RVs in this study, there was little agreement between the results at 1,000 DS and LHS simulations and 10,000 DS simulations. This was probably due to the different approach adopted to post-process the results for 10,000 simulations, as explained in the methods section; however, it is thought that the output parameter behaved quite unstable when implant position was changed. Bone geometry is very irregular; it is therefore capable of experiencing different maximum strains when moving the implant in different directions. Some authors have looked at the changes in stress or strain distributions evident when varying the bone-implant interface definitions [165] and the fraction of bone supporting highly strained bone tissue has been measured in experimental studies [166] and hence, suggested as an appropriate failure indicator.

In line with this, the suggested improved performance indicator is the bone percentage of volume with strain higher than yield strain, which will be introduced in the next section.

This model took approximately 6 days to run 1,000 simulations compared to 1 hour and 37 minutes for the first model on the same computer. This difference was most probably due to the definition of contact pairs. This results in non-linearities that slow down the solution of the FE model, even if a fully bonded condition was defined. The application of LHS showed similar results to those of DS at 1,000, although it was noticeable that sensitivity to load magnitude was positive for LHS, as it was for 10,000 DS simulations. This suggests that LHS is more accurate for a lower number of simulations than DS, as might be expected. Further LHS analyses in the range of 1,000 to 10,000 simulations would be needed to confirm this.

The results have shown that the uncemented THR is highly sensitive to implant version angle, bone stiffness and load magnitude. The implant version is determined by the surgeon when positioning the implant during the surgery. The results of this study suggest that if implant version variability is not controlled, a too high strain may be developed in the bone, causing failure.

In the discussion for the previous model in Section 4.1 [164], results from relevant probabilistic and parametric studies were considered. Load magnitude was found to be one of the most significant parameters in determining the cement maximum von-Mises stress [66], failure of the bone-cement mantle [67], implant-cement inducible displacement [156] or the failure of the bone-cement interface or cement mantle [70]. Some parametric studies also varied the loading conditions and found that these variations affected the strain distributions [86, 88] or implant micromotion [87]. Bone stiffness has also been found to influence the inducible displacement of the stem-cement interface [156] or fatigue damage accumulation [69].

The most relevant studies to the model in this section have been deterministic in nature; it has been shown how implant geometry [86, 88, 87], loading [86, 87], implant stiffness [83] and implant positioning [89, 11] are parameters important in the performance of the construct.

Decking *et al.* [88] looked at the effect that 3 different hip stems had on the

in vitro strains in the proximal femur. They observed an effect of the implant geometry on the strain distribution of the implanted femur.

Nishii *et al.* [11], found out that the manipulation of the cup anteversion to compensate for high femoral neck anteversion may predispose the hip to postoperative dislocation.

Speirs *et al.* [89] considered 3 different set-ups after THR: implant located at the intact hip centre, implant placed in increased anteversion and implant with an offset, and they found that small changes in stem placement would be likely to have little influence on the internal loading of the femur after bone ingrowth has been achieved. However a reduction in strain energy density and therefore stress shielding was seen, which may have consequences for longer-term remodelling.

Aamodt *et al.* [90], found that the patterns of the principal strains in the proximal femur varied for anatomical and customised stems in human cadaver femurs.

As in the previous study (Section 4.1), the average location of the maximum nodal strain was in the compressed elements in the medial part of the bone. Some of the above studies looked at the strain patterns in the bone, but the metrics, loading conditions and measures of the strain were different to the present one. This makes it difficult to draw comparisons based on the absolute values of the strain. Nevertheless, the maximum strain was observed in a similar location.

The present model was built while prioritising the automation of the probabilistic tool. For this reason several simplifications regarding both the finite element model and the probabilistic model were adopted, thus allowing reduced runtimes. The FE model adopted a uniform bone stiffness, not differentiating between cortical and cancellous bone. In future development, this parameter could be investigated in depth, or any discontinuities in bone material could be assigned using the CT scans as the basis for the FE mesh [77], as has been performed in the main studies of the present work (Chapter 5). Once more, a fully bonded bone-implant interface was adopted. However, contact elements were applied in the bone-implant interface. The runtime consumed in this case was closer to that of a frictional interface model. In addition, muscle forces could be included, as many authors have demonstrated their influence on the stresses and/or strains of the loaded bone [116, 117, 118, 119].

An automatic probabilistic finite element model (PFEM) which can account for an implant position variability has been developed. The main limitation of this study compared to the model in Section 4.1 was the inconsistency of the sensitivity results. A new performance indicator was therefore applied, and this is discussed in the next section.

4.3 Determination of an improved performance indicator for the probabilistic analysis of implant version effects

In the previous studies (Sections 4.1 and 4.2) probabilistic analyses of an uncemented THR were carried out on a simplified finite element model to enable the implementation of the probabilistic finite element loops and the incorporation of an implant positioning parameter, namely the implant version angle. However, when the implant version angle was included in the set of RVs in this study, the sensitivity results were inconsistent. The exact reason for this is not clear, but it was thought that the irregularities or asymmetry of the geometry could have an effect on the value of the maximum nodal strain if the implant position was varied.

The aim of this study, therefore, was to determine an improved performance indicator for the probabilistic analysis of the model in Section 4.2. The new performance indicator was required to ensure the consistency of the sensitivity results, and therefore, the reliability of the probabilistic finite element model tool (PFEM). The same FE model used in Sections 4.1 and 4.2 was used in this study. Strain based output parameters have been found to be more indicative of the risk of failure of these kind of systems compared to stress based indicators [17, 129]. However, in the previous model (Section 4.2) the maximum nodal strain in the bone did not lead to convergence when implant version angle was included. It was suggested that, following the lines of other researchers [165, 166], a sensible performance indicator would be related to the amount of bone that is supporting high strain. The bone volume percentage exceeding certain limits of elastic von-Mises strain was adopted as the improved performance indicator. The

probabilistic results are again complemented by a sensitivity analysis that shows the significance level of each parameter on the integrity of the construct.

4.3.1 Materials and Methods

4.3.1.1 Finite Element Model

The FE model was identical to that used in Section 4.2.

4.3.1.2 Probabilistic Model

The input parameters were identical to those in the previous model in Section 4.2, and their statistics are shown in Table 4.2. A new performance indicator was selected for this model: the bone volume percentage exceeding von-Mises elastic strains of 0.8, 0.5 and 0.3% (BPER1, BPER2 and BPER3 respectively). Monte Carlo based simulations were run, with a maximum of 1,000 simulations using direct sampling (DS), and sensitivity analyses were performed with the probabilistic Ansys facility as in the previous Sections 4.1 and 4.2.

The computational flow was identical to that of Section 4.2, the same probabilistic script was used, and the calculation of the new performance indicator was adapted in post processing of the model.

4.3.2 Results

As in previous models (Sections 4.1, 4.2), the term 'sensitivity' is used to describe how changes in the RV values and their scatter affect the range of scatter of the output parameters [18].

Figure 4.13 shows the mean value of the output parameters BPER1, BPER2 and BPER3, for 1,000 simulations. It can be seen there is no convergence until approximately 700+ simulations, were mean values of 2.5%, 5.5% and 20% are noted, respectively.

Figure 4.14 shows the empirical cumulative distribution functions (CDFs) of the outputs. It can be seen that the probabilities of achieving the mean values

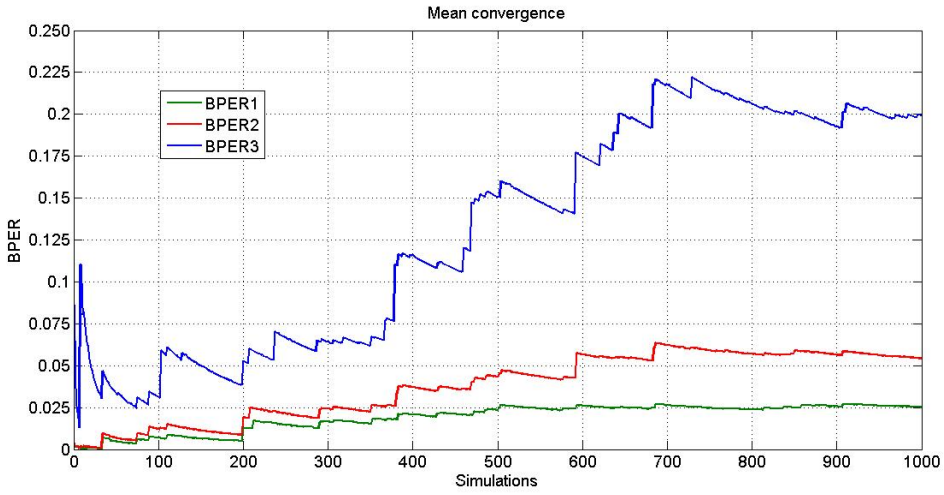

Figure 4.13: Mean value history of the outputs BPER1, BPER2 and BPER3, for 1,000 simulations.

were 0.95, 0.92 and 0.91 respectively.

The sensitivity results are shown in Figure 4.15. Results with 100 and 1,000 DS simulations matched well. This confirms the robustness of the new performance indicator. In both cases the most sensitive parameters were the bone stiffness, the load magnitude and the implant version, and for the most accurate results (1,000 simulations) and bone volume percentage under limit strain of 0.8% (black bars), the sensitivities of these three parameters were almost identical, the bone stiffness slightly higher than the others. When decreasing the limit strain to 0.5% and 0.3% (grey and white bars, respectively), all sensitivities increased, in particular bone stiffness.

4.3.3 Discussion

The aim of this study was to improve the model in Section 4.2 by implementing a new performance indicator. In the previous model, a large number of simulations was necessary in order to get convergent results. It was hypothesised that the performance indicator was not robust when implant anteversion was included, due to the non-linear behaviour of the bone for different implant positions; for exam-

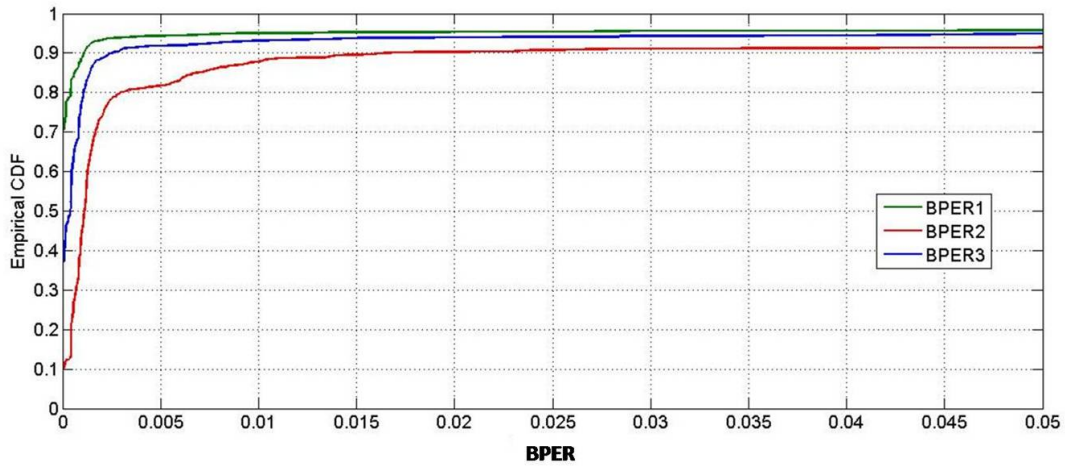

Figure 4.14: Cumulative Distribution Functions for Model 3 for strain limits of 0.8% (BPER1), 0.5% (BPER2) and 0.3% (BPER3) for 1,000 DS simulations

ple, the shape of the femur is not symmetric, thus moving the implant towards a certain angle would compress more or less elements than those compressed if the implant was angled towards the opposite direction. At the same time, it was thought that the single nodal maximum strain was not a good indicator of the risk of failure of the construct. The bone would break if a certain amount of its elements was suffering a high stress or strain level, and this type of indicator has been widely used in other studies [165, 166]. In order to minimize computational time, several simplifications were made, most notably: (i) the interface was fully bonded; (ii) the materials were linear, isotropic and homogeneous.

This study differs from the model in previous section in that a new performance indicator was chosen: the bone percentage of volume exceeding von-Mises elastic strains. When considering the nodal elastic strain in the previous model (Section 4.2), there was little agreement between the sensitivity results at 1,000 DS simulations and 10,000 DS simulations. The consistency and robustness of the results improved when the new indicator was selected, and it could be seen that for 100 DS simulations, the most sensitive parameters, bone stiffness, load magnitude and implant version, were the same as for 1,000 DS simulations. This model took approximately 6 days to run 1,000 simulations. The plot of the convergence of the mean values of the output suggests that it is necessary to run a

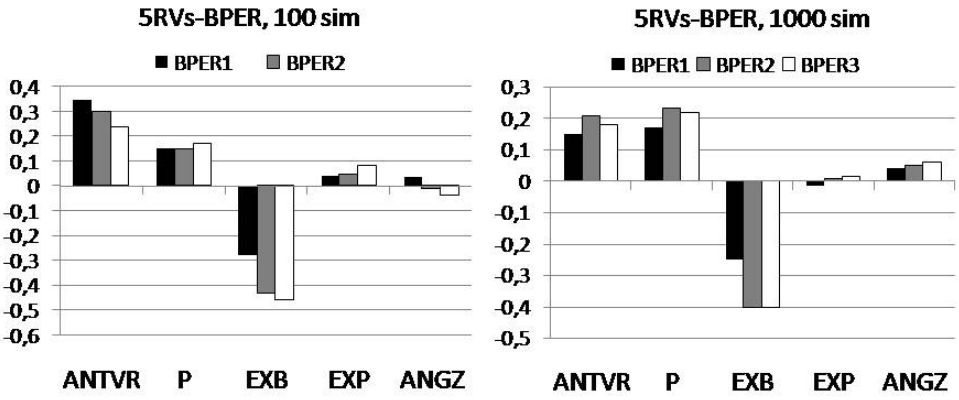

Figure 4.15: Sensitivity plots for 100 (left) and 1,000 simulations (right), for the three levels of the output: percentage of bone volume exceeding 0.8% (BPER1), 0.5% (BPER2) and 0.3% (BPER3) strain limits.

higher number of simulations in order to get convergence.

The results confirmed once more that implant positioning plays an important role in the performance of the THR. Bone stiffness and load magnitude were also significant. This has been observed in previous probabilistic and parametric studies. Probabilistic studies have looked at parameters such as bone or implant stiffness or load variability, see 2.4. Both parameters have been found to influence the cement maximum von-Mises stress [66], failure of the bone-cement mantle [67], implant-cement inducible displacement [156] or the failure of the bone-cement interface or cement mantle [70]. Some parametric studies also varied the loading conditions and found that this affected the strain distributions [86, 88] or implant micromotion [87]. To date, no probabilistic studies have included implant position related parameter as RVs. The most relevant studies have been deterministic; as was discussed in previous section, various studies have shown how implant geometry [86, 88, 87], implant stiffness [83] and implant positioning [64, 89, 11] are parameters important in the performance of the construct.

The mean value of the percentage of bone volume supporting von-Mises elastic strains higher than 0.8% is much lower than 1% (corresponding to a probability of 0.5 in the empirical CDF, see Figure 4.14), while it has been seen that the fraction of bone tissue supporting high tensile strains when loading the femur at the yield strain was about 6% [166]. This means that under these loading conditions, the present model would not fail. This is sensible since the mean and

standard deviation values of the load were those of normal gait, thus no risk of fracture should be present. If an accurate assessment of the probability of failure is sought, the loading conditions should be chosen with common values that lead to fracture [166]. In the present study, more importance is given to the influence of variability of the input parameters, thus the same hip contact force will be kept in the next studies.

This probabilistic study has provided a reliable description of the parameters that most influence the performance of the THR when implant position variability is considered. These highly sensitive parameters must be carefully refined and controlled. Future models should incorporate more exhaustive definition of their uncertainties, or at least they should be more realistically represented. Additional implant position parameters, assignment of material properties to the elements using CT scan data [77], and application of muscle forces are directly related to these three parameters, and therefore they represent a good action to be taken in the next models. Also it is important to consider other interface conditions, since fully bonded interface is representative of the long term state of the THR, while frictional interface represents states closer to the post operative conditions, when the possibility of implant malpositioning may have its greater effect on the stability of the THR [133, 167, 168]. The selection of different constraints should be also considered since some authors have demonstrated their effect on the output of the construct [89].

A factor that needs to be analysed is the influence of the type of distribution functions and the selection of their parameters. In the previous Sections 4.1, 4.2) and present studies, normal and lognormal distributions were assumed, and the means and SD were selected from single studies were a reduced number of samples were used. If uncertainty of a parameter has a great effect, a realistic description of this uncertainty is desirable to better quantify its sensitivity, and this will be considered in the next study (Section 5.1).

In practice, these results highlight that variability of implant positioning should be kept to a minimum. Research on highly precise surgical tools and/or computer-aided surgery to accurately place the implant to the desired position are some of the suggested actions in this line.

Chapter 5

Development of an automated probabilistic finite element analysis procedure for the uncemented hip replacement

5.1 Introduction

In previous models, the probabilistic finite element method (PFEM) was implemented using Ansys. This software was not flexible enough to deal with variations in implant position, which had to be revised manually. A new approach was adopted to deal with this issue, using different software. These are summarised in Section 3.2.3, and included Rhinoceros, Ansys ICEM-CFD and Ansys, together with a Visual Basic script that controls the execution loop. Using the model generated by this loop, a convergence study was performed to decide on the optimum maximum element size of the FE model.

Using the developed procedure, a PFEM could be applied to the uncemented THR, including 6 degrees of freedom in implant position. This PFEM was performed for all the possible combinations of the 3 femurs and 2 implants presented in Section 3.2. The FE models included several features to make them more real-

istic: muscle forces were applied, fully bonded and frictional interface conditions were modelled to simulate different stages after the THR, and two different kinds of constraints were incorporated parametrically to check their influence on the results. The effects of different statistics of the implant variables and of changes in the reference position of the implant were also investigated.

5.2 Materials and Methods

5.2.1 Finite Element Models

The geometries of three proximal femurs were considered in this work. These were presented in Section 3.2 and were generated by Radcliffe *et al.* [24], from patients with BMI of 19.8, 34.4 and 41.8 (Femur 1, Femur 2 and Femur 3), respectively. Table 3.1 shows the characteristics of the patients, and Figure 3.1 shows the three proximal femoral models. The femoral reference coordinate systems were also described in Section 3.2 and illustrated in Figure 4.1. The osteotomy or femoral head cut was performed using a single plane. The position of this plane was different for each femur due to limitations encountered performing boolean operations in Rhinoceros. A set of manual tests needed to be performed in order to find an orientation of the osteotomy plane that would successfully cut the femoral head while creating a suitable model. The positions were defined by the distance of the plane along the neck axis to the centre of the femoral coordinate system ($\mathbf{d}$), the angle of the plane with respect to the femoral neck axis in the XY plane ($\theta 1$), and the angle of the plane with respect to the Z axis in a plane that contains Z and is perpendicular to the osteotomy plane ($\theta 2$). Figure 5.2 illustrates these parameters, and Table 5.1 presents the values of the parameters for the three femurs. Variable lengths of the proximal femur were recorded by the CT-scan (Figure 5.1). The distance between the tip of the greater tronchanter and the inferior section were measured with the freeware DicomWorks (Philippe PUECH and Loic BOUSSEL), giving values of 126, 165 and 114 mm for Femur 1, 2 and 3, respectively. The thickness of the cortical bone in the slice where the tip of the lesser trochanter was located was also measured, giving values of 0.38, 0.44 and 0.39 cm, for Femur 1, 2 and 3, respectively.

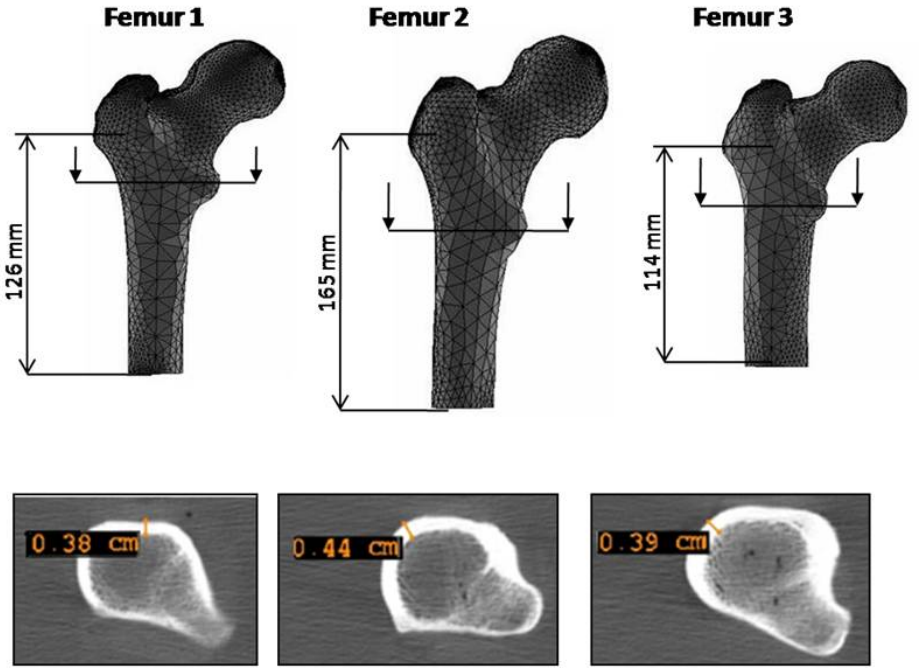

Figure 5.1: Finite element models of the three proximal femurs (top) and cortical thickness in section at lesser trochanter level (bottom).

	$\theta 1(^\circ)$	$\theta 2(^\circ)$	**d(mm)**
Femur 1	60	20	25
Femur 2	60	-20	25
Femur 3	60	0	60

Table 5.1: Values of the osteotomy position parameters for the three femurs

These bones were virtually implanted with the two implants described in Section 3.2, the short stem Proxima and the long stem IPS, both of titanium alloy, with a Young's modulus of 110 GPa and Poisson's ratio of 0.3 (Figure 3.2).

The implants were placed manually in reference positions such that the shaft axes of both femur and implant were almost parallel and the neck axes had an angle between $\pm 5^\circ$. The relative offsets were kept such that the approximated

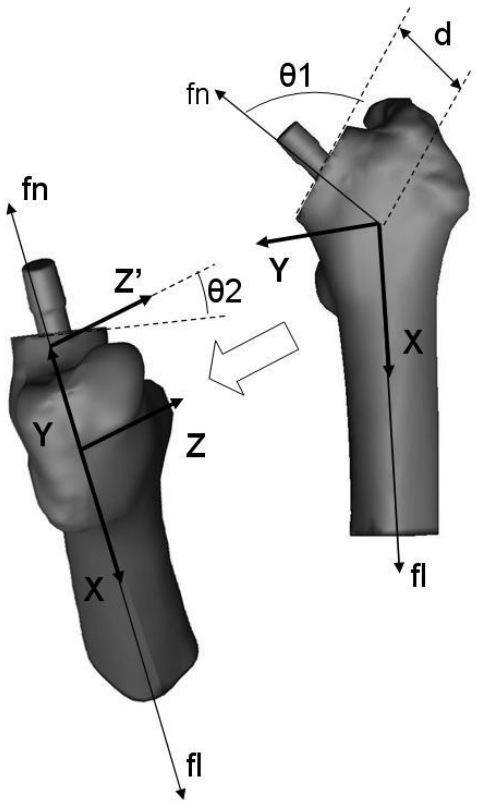

Figure 5.2: Femoral axes (fl, fn) and parameters that define the osteotomy plane ($\theta 1$, $\theta 2$)

femoral head centre and the centre of the implant tapered neck section had a distance of $\pm 2mm$ in the local X, Y and Z directions.

The combination of the three femurs and the two implants resulted in a total of six different FE models.

For the six models, the geometries were built using Rhinoceros software (McNeel, Seattle, USA), the finite element meshes were generated using 4-noded tetrahedral elements with a maximum element size determined by a convergence study (Section 5.2.4) of 6mm in the ANSYS-ICEMCFD package and the loads were applied and simulations run in Ansys (Ansys Inc, Canonsburg, PA, USA).

The material properties of the bones were applied to the bone elements using a modified version of the freeware program BoneMat (Zannoni et *al.* [77], Taddei

et *al.* [78]) (Rizzoli Institute, Bologna, Italy). The relationship between the pixel intensity (Hounsfield units, HU) and the apparent density (g/cm^3) was defined using calibration phantoms within the CT scans. These known values produced a linear relationship. The two points that describe this linear relationship were 0, 0.47 and 1500, 1.8. The apparent density of the voxels contained within each element was averaged; this value was used to calculate the Young's Modulus for each element (Section 2.5.1). The relationship between the apparent density and Young's Modulus was set according to Equation 2.2, and the values were chosen to lie within the ranges suggested by Keller [75]:

$$E = 10 + 2875\rho^3 \tag{5.1}$$

Figure 5.3 shows the contour plots of the elements stiffness for the three femurs assigned using Bonemat. It can be seen that femurs 1 and 2 had higher density of high stiffness elements than Femur 3. This data will be taken into account when discussing the results.

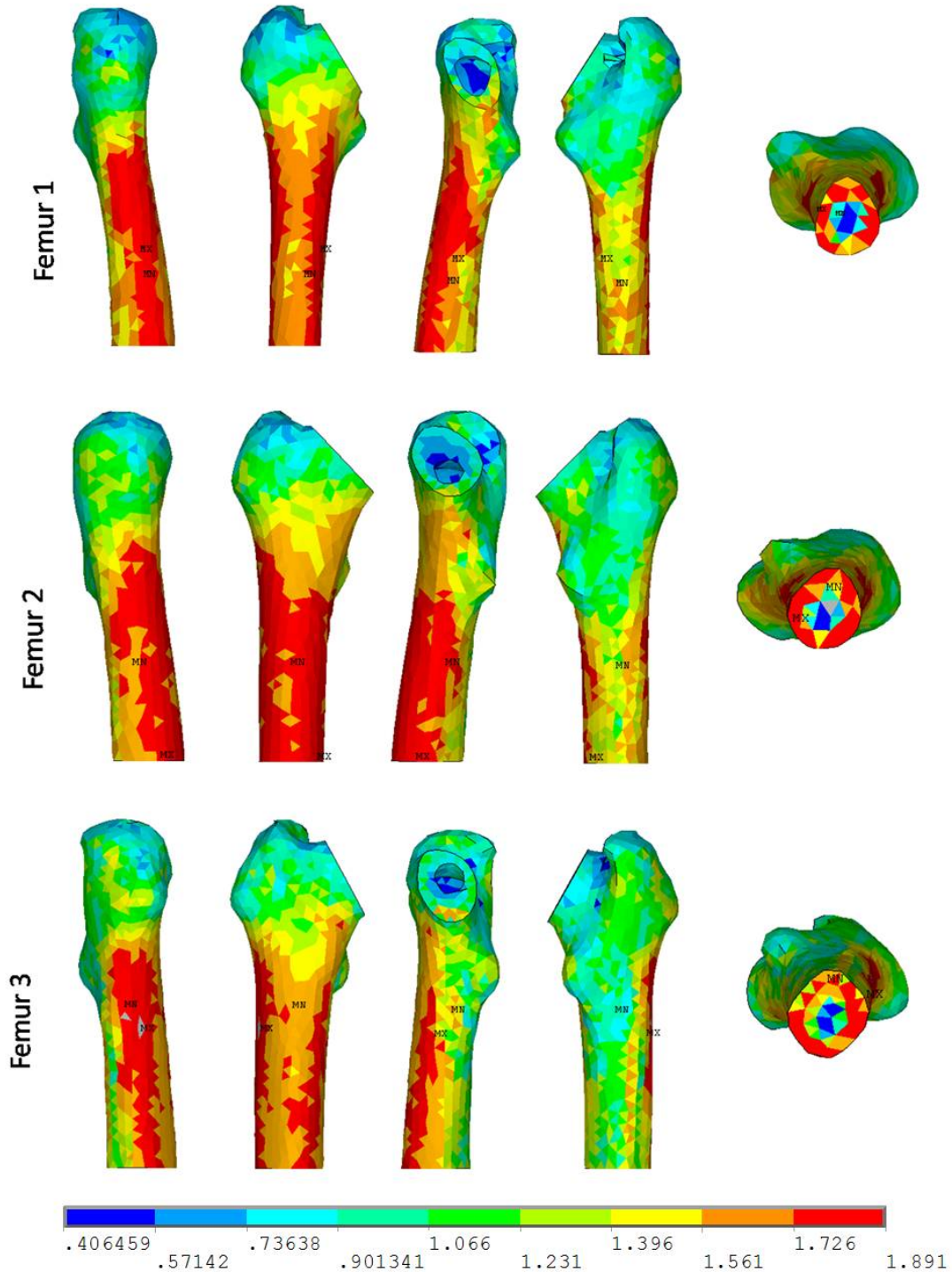

Figure 5.3: Contour plots of the stiffnesses in GPa assigned by Bonemat.

The muscle forces at the peak of the hip contact force measured during normal gait were applied. Some of the most important muscle forces in determining femoral bone strain during gait (gluteus minimus, gluteus medius, iliopsoas and vastus medialis) (Duda et *al.* [118]) were calculated with AnyBody software (AnyBody Tech, Aalborg, Denmark) using a model validated by Manders *et al.* [169] and applied to the FE models. The locations of the muscle attachment points were transferred from the AnyBody software, and the closest nodes to the location of these attachment points were selected for the application of the muscle forces. The values of these muscle forces are shown in Table C.1 (Appendix C.1).

The hip contact force (**L**) was applied at the implant node closest to the femoral head centre, the load magnitude and direction corresponded to the peak force measured for normal walking in an individual weighing 75 kg (Bergmann et *al.* [23]).

The bone-implant interface was defined with contact elements, in both fully bonded and frictional contact conditions. 4-node surface-to-surface contact elements were defined, to represent contact and sliding between the interface surfaces. The Augmented Lagrangian method was used as the contact algorithm, which is an iterative series of penalty methods [18]. The penalty method uses a 'spring' to establish a relationship between the two contact surfaces. The spring stiffness is called the contact stiffness. The Augmented Lagrangian method usually leads to better conditioning and is less sensitive to the magnitude of the contact stiffness. This method uses two factors: normal and tangent penalty stiffness (FKN and FKT respectively). The FKN determines the amount of penetration between contact and target surfaces. It is necessary to set a high enough stiffness that the penetration/slip is acceptably small, but a low enough sitffness to ensure the problem will converge. The usual factor range is between 0.01-1.0 [18] and a value of 0.5 was adopted in the present study. The FKT is proportional to the Poisson's ratio and the FKN. A default value of FKT=1 was adopted.

Two different constraints were compared, one that constrained all degrees of freedom in five nodes belonging to the distal section, named as '5NOD', and another that constrained all the nodes in a distal portion of 10mm thickness, named as 'DIST' (Figure 5.4).

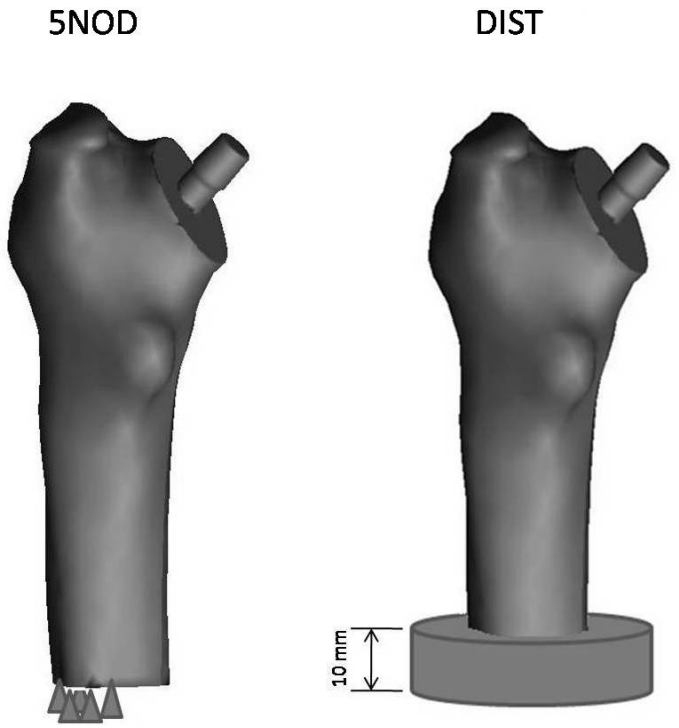

Figure 5.4: Five nodes constraint (left, '5NOD') and distal portion constraint (right, 'DIST').

5.2.2 Probabilistic Models

The random variables (RVs) considered in each model were (Figure 5.5): load magnitude and angles with respect to the local femoral axes Y and Z (L, ANGLY, ANGLZ), linear displacements of the prostheses with respect to the local femoral axes (OFFX, OFFY, OFFZ) and angular displacements of the prostheses with respect to the local femoral axes (ROTX, ROTY, ROTZ). Several statistical distributions were considered for the RVs to check their influence on the results. Truncated normal distributions were first adopted for the implant position parameters, with lower and upper bounds to ensure that the implant would not intersect the surface of the femur other than in the osteotomy section. However, due to the lack of data for these parameters, assumptions had to be made on means and standard deviations. It was decided that the mean value would correspond to the reference position at which each implant was located in each femur. Different cases for the standard deviation were analysed parametrically, referred to as high and low standard deviation cases. A uniform distribution case was also performed, where any value within the bounds had the same probability of occurrence. The statistics of the RVs for high and low standard deviation and uniform distribution cases are shown in Tables C.2, C.3 and C.4 respectively (Appendix C.1).

The mean, upper and lower limit values of the load corresponded to the peak values of the hip contact forces measured in normal walking for individuals weighing 75, 50 and 95 kg respectively (Bergmann et *al.* [23]). The load angle was varied to account for different loading conditions. 1,000 Monte Carlo simulations were performed for each model, and the performance indicators were the percentage of bone volume exceeding a von-Mises elastic strain of 0.8% and, in the frictional cases, the implant-bone maximum nodal micromotion. This was calculated as the vectorial sum of the sliding and the gap of the contact elements. Sensitivity analyses based on linear correlation coefficients between the random variables and the performance indicator were calculated using MATLAB R2008a (The MathWorks, Inc., Natick, MA, USA).

Figure C.1 (Appendix C.1) shows the plots of the empirical CDFs of the RVs for the different statistics cases: truncated normal with high and low standard deviation (TNH and TNL respectively) and uniform distributions (UN).

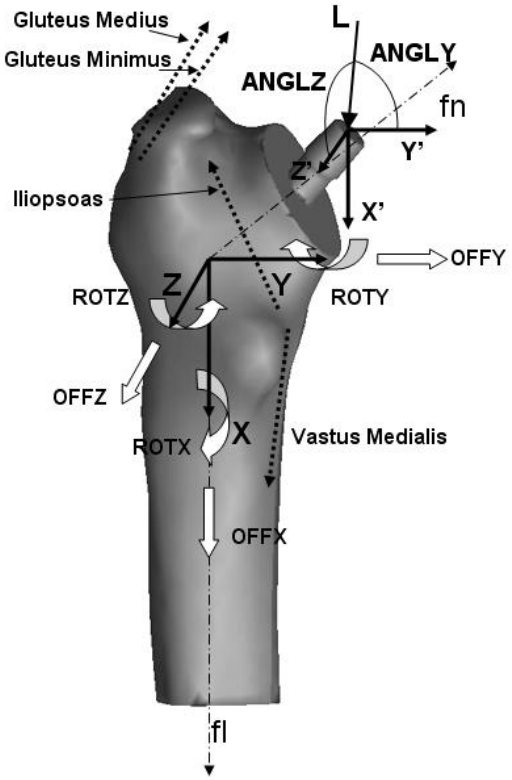

Figure 5.5: FE model with the random variables (ANGLY, ANGLZ, L, OFFX, OFFY, OFFZ, ROTX, ROTY, ROTZ), the constant muscle loads and the local reference coordinate system

5.2.3 Computational Process

As mentioned previously, the probabilistic finite element model was built using a set of software automatically interconnected using a Visual Basic algorithm:

- **Rhinoceros** was used to locate the implant at the desired position and to perform boolean operations to generate the osteotomy and the implant cavity.
- **Icem** was used to repair the geometry and mesh the construct.
- **Ansys** was used to apply all boundary conditions, define the bone-implant interface and solve the model.

Although the automation of the whole process was possible using a single Visual Basic script, the Ansys simulations were run in a set of cluster nodes available at the University of Southampton. This allowed a substantial time reduction since the FE simulation represents the most time consuming part of the model. The Visual Basic script represents what is referred to as 'Hip Implanter'. A flow chart of the process of creation of the PFEM is shown in Figure C.2 (Appendix C.1).

5.2.4 Convergence Study

Before performing the probabilistic analysis, a convergence study was carried out in order to decide on the element size that would give results with enough accuracy while minimising solution time. Several representative THR models comprising Femur 1 and the Proxima implant (previously described) were generated using the Hip Implanter script described in the previous subsection. Two different interface conditions were analysed: fully bonded and frictional interface with coefficient of friction of 0.3. In both situations, maximum element sizes ranging from 2 to 8 mm were used. The mean values of the parameters shown in Table C.2 (Appendix C.1) were adopted. Only the hip contact force was applied and the model was constrained at 5 nodes in the distal section. The bone volume percentage exceeding von-Mises elastic strains of 0.8, 0.5 and 0.3% (BPER1, BPER2, BPER3) were used as the outputs.

5.2.4.1 Results from the Convergence Study

Figures 5.6 and 5.7 show plots of the values of the bone percentage of volume exceeding 0.8, 0.5 and 0.3 von-Mises elastic strain (BPER1, BPER2 and BPER3 respectively) (left), and the times to solve this models (right), for maximum element sizes ranging from 2 to 8 mm.

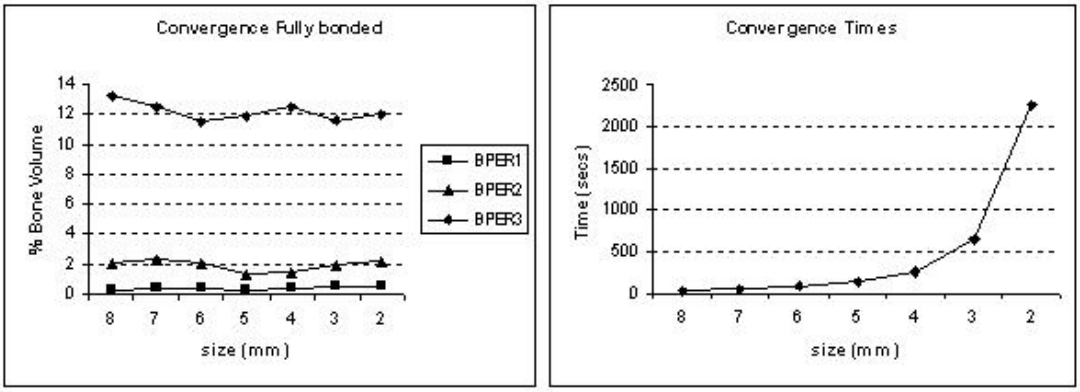

Figure 5.6: Convergence plots for fully bonded interface

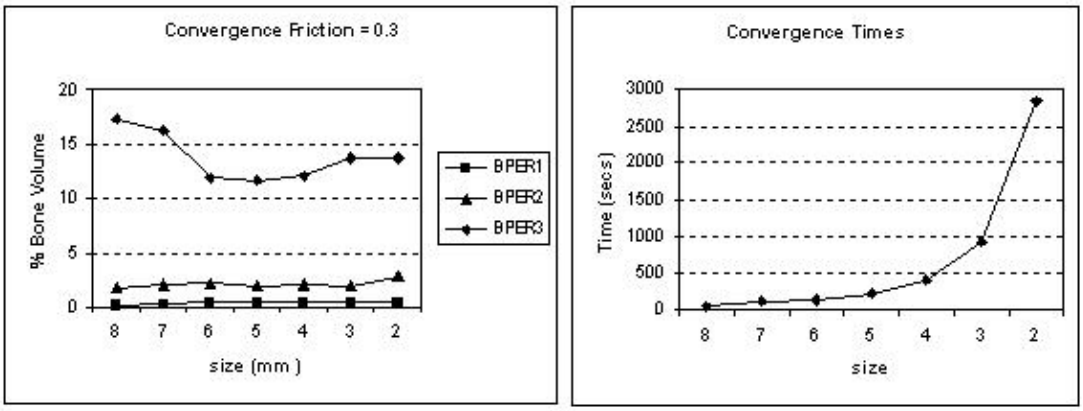

Figure 5.7: Convergence plots for frictional interface

It can be seen from Figure 5.6 for fully bonded interface that the values of BPER1, BPER2 and BPER3 do not differ substantially for any maximum element

size, but the run times grow exponentially. Similar results were found for the frictional interface (Figure 5.7), although in this case BPER3 varied more than in the fully bonded case. A maximum element size of 6 mm was adopted as optimum since results were in all cases close to those for a maximum element size of 2 mm but the run time was still low.

5.2.5 Bad model Filtering

The statistics of the implant positioning input variables were truncated to avoid the implant intersecting the inside surface of the bone. However, this method did not always prevent this from happening for several reasons:

- The values of the limits were estimated from the reference position of the Proxima implant in Femur 1. They were kept the same for all the models in order to make reliable comparisons. Nevertheless, different bones and implants may need different limits.
- Each limit value was a good estimation providing that the others remained in the reference position. However, combinations of certain values of the six degrees of freedom may cause the implant to break through the bone.

For these reasons, three 'filters' were applied to the created models to detect bad models. The first one was defined by the truncation limits on the input statistics themselves. This meant that those possible models 'out' of the truncation limits were not created and hence the cost of running them was avoided. As has been mentioned throughout the thesis, minimizing running times is essential, hence totally or partially avoiding creation of bad models was highly beneficial to the process. The second filter was applied during the geometry creation process in Rhinoceros; once the implant was positioned in the desired location, the intersection between the surfaces of the two bodies was checked, and if this was true, the creation of that model stopped and restarted with the following model of the sample. In this way, half of the time that Rhinoceros needed to create the models, plus the Ansys ICEM-CFD execution were avoided for bad models. This filter was automated in the Visual Basic script detailed in subsection 5.2.3. Since Rhinoceros is not totally consistent when working out boolean operations

between meshes, some bad models remained in the samples, and as such a third filter was needed. The third filter consisted of a Visual Basic module that reads the ansys input text files of each model and checks if the definitions of the model are correct. The third filter was applied independently after the creation of the samples by Hip Implanter, although it would be simple to include it during the automation process.

Figure C.3 (Appendix C.1) shows the location of the three filters in the model creation process.

5.2.6 Parametric studies

The present work presents multiple parametric studies of different probabilistic analyses, i.e., different conditions have been considered either in the finite element model or in the probabilistic model, and for each parametric situation a probabilistic analysis was performed. A classification of the parametric variations may be made as follows:

1. **Femurs**: Three different femurs.
2. **Implants**: Two different implants.
3. **Bone-Implant Interface**: Fully bonded and frictional bone-implant interface
4. **Constraints**: Five distal nodes constraint and distal portion constraint
5. **Statistics of the RVs**: Truncated Normal distributions with high and low standard deviation and uniform distribution of the RVs.
6. **Implant reference position**: Two different reference positions (mean value of implant position).

In each of these studies, the different parametric variations resulted in a set of models that were then run in the PFEM tool. Table 5.2 shows an outline of the different parametric studies. The terms 'TN HSD' and 'TN LSD' correspond to the Truncated Normal distributions with high and low standard deviations

respectively. The '5NOD' constraint refers to the 5 constrained nodes at the distal section case, and the 'DIST' refers to the constrained 10 mm distal portion case. There is an 'X' where the case was run in the PFEM, and the X' in the Femur 2-IPS row corresponds to the modified reference position (or modified mean valued of the implant position). A total of 35 models were run in the PFEM, with the specifications detailed in Section 5.2.2.

Interface		**FULLY BONDED**						**FRICTION**
Statistics		**TN HSD**		**TN LSD**		**Uniform**		**Uniform**
Constraints		5NOD	DIST	5NOD	DIST	5NOD	DIST	DIST
Femur 1	Proxima	X		X		X	X	X
	IPS	X		X		X	X	X
Femur 2	Proxima	X		X		X	X	X
	IPS	X/X'		X/X'		X/X'	X/X'	X/X'
Femur 3	Proxima	X		X		X	X	X
	IPS	X		X		X	X	X

Table 5.2: Parametric studies run in the PFEM.

5.3 Results

Two different outputs were examined for all models: bone volume percentage exceeding von-Mises strain of 0.8%, referred to as BPER, and the maximum nodal micromotion, occasionally referred to as micromotion. Throughout the results and discussion sections, the term 'outliers' will be used to refer to values that are numerically distant from the rest of the data [170].

Due to the large number of models run, the main results plots have been placed at the end of the section: plots of mean and standard deviation in Section 5.3.6 (Figures 5.18, 5.19, 5.20, 5.21, and 5.22), the empirical cumulative distribution functions (CDF) in Section 5.3.7 (Figures 5.23, 5.24, 5.25, 5.26, and 5.27), and sensitivities in Section 5.3.8 (Figures 5.28, 5.29, 5.30, 5.31, 5.32, 5.33, 5.34, 5.35, 5.36, 5.37, 5.38) are presented. The last sensitivity plots (Figures 5.34, 5.35, 5.36, 5.37, and5.38) show the absolute values of the sensitivities.

The results are presented in the following subsections:

- **Variation of input Statistics, Femurs and Implants**: For each of the three femurs, combined with the two implants, with fully bonded interface and 5 distal nodes constraint, the results for the different RVs statistics are compared.
- **Variation of Constraints**: All femur-implant combinations with uniform distributions, the 5 nodes and distal portion constraint cases are compared.
- **Variation of Interface Conditions**: For all femur-implant combinations with distal portion constraint, fully bonded and frictional interfaces cases are compared.
- **Variation of Reference Position**: For Femur 2 and IPS, the reference position of the implant was varied, all the parametric runs were repeated and their results are compared.

There were a number of failed simulations due mainly to undesired positions of the implant within the bone, which were rejected by the filters described in Section 5.2.5. These can be classified as follows:

- Filter 1: models rejected during boolean geometric operations in Rhinoceros.
- Filter 2: models rejected after meshing with Ansys ICEM-CFD.
- Unconvergent: unconvergent models rejected at the end of the simulations.

Figure 5.8 shows the histograms of the different failed models, for all combinations of femurs and implants, all statistics of the inputs, distal portion constraint and friction interface case. The highest number of failed models for combinations with Proxima occurred for Femur 1, the bone and implant intersected in about 50% of the models. The remaining combinations had a very low failure rate, the maximum corresponding to Femur 3 for TNH case with about 14% of failed models. The minimum number of failed models (between 0.1 and 2%) corresponded to Proxima combined with Femur 2. In general, most of the failed models were detected by Filter 2. For combinations with IPS, again Femur 1 had the highest number of failed models (70% in the TNH case), whereas for TNL and UN cases the failure rate decreased substantially to values between 9.4 and 12.6%. Femur

2 had a failure rate of about 23% for the uniform distribution case. Femur 3 had a very low failure rate, with a maximum of 13.6% for the TNH case, and the remainder between 0.7 and 1.5%.

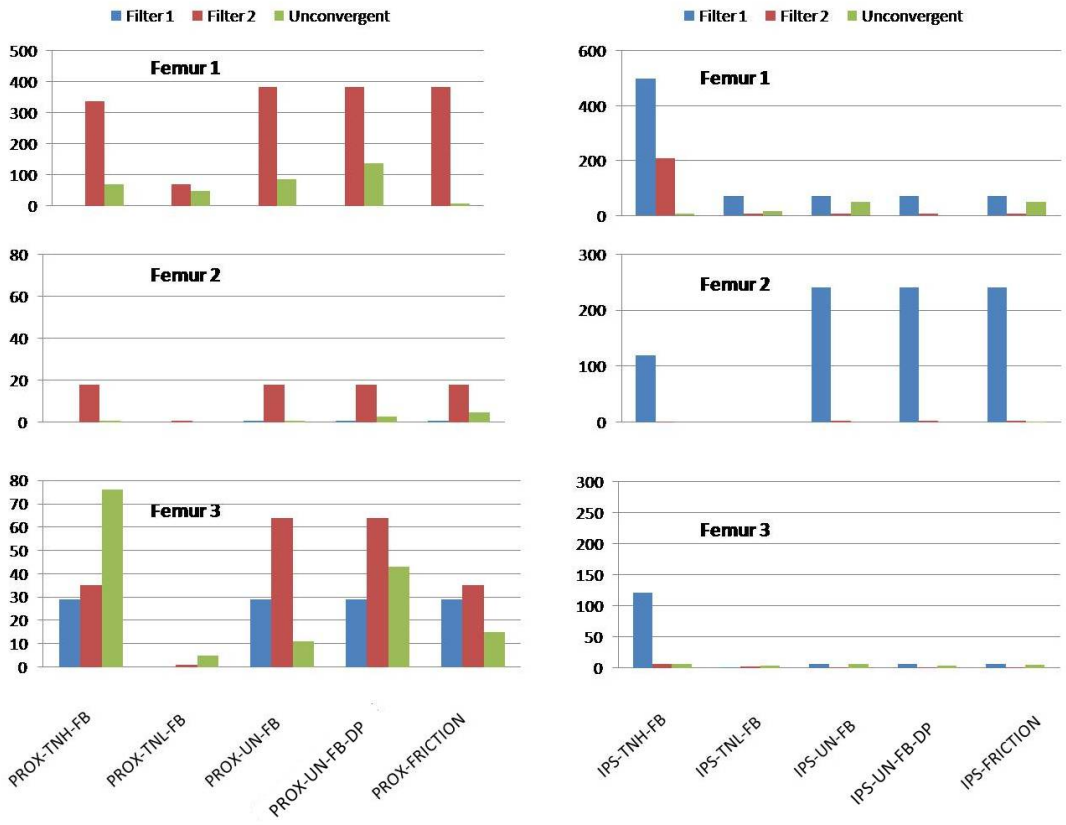

Figure 5.8: Failed models, for all combinations of femurs (Femur1, 2 and 3) and implants (PROX and IPS), all statistics of the inputs (TNH, TNL and UN), distal portion constraint (DP) and friction interface case.

Figures 5.9 and 5.10 show the empirical cumulative distribution functions (CDF) of the original statistics of the input variables against the statistics of the successful and the failed samples, for two particular cases (Femur 1 combined with the Proxima and the IPS prostheses, for the TNH case). A good agreement is observed for all the RVs, except for OFFX and OFFY in the case of Femur 1 with the Proxima implant (Figure 5.9, centre row). The good agreement in all the other RVs means that the results were not biased by removing the rejected samples. Figure 5.11 shows the histograms with a fitted normal distribution of the RVs OFFX (top) and OFFY (bottom), for the original (left), the successful (centre) and the failed (right) samples. Table 5.3 shows the interquartile ranges of the RVs OFFX and OFFY, for the successful, original and failed samples. This

is a measure of the dispersion of the data.

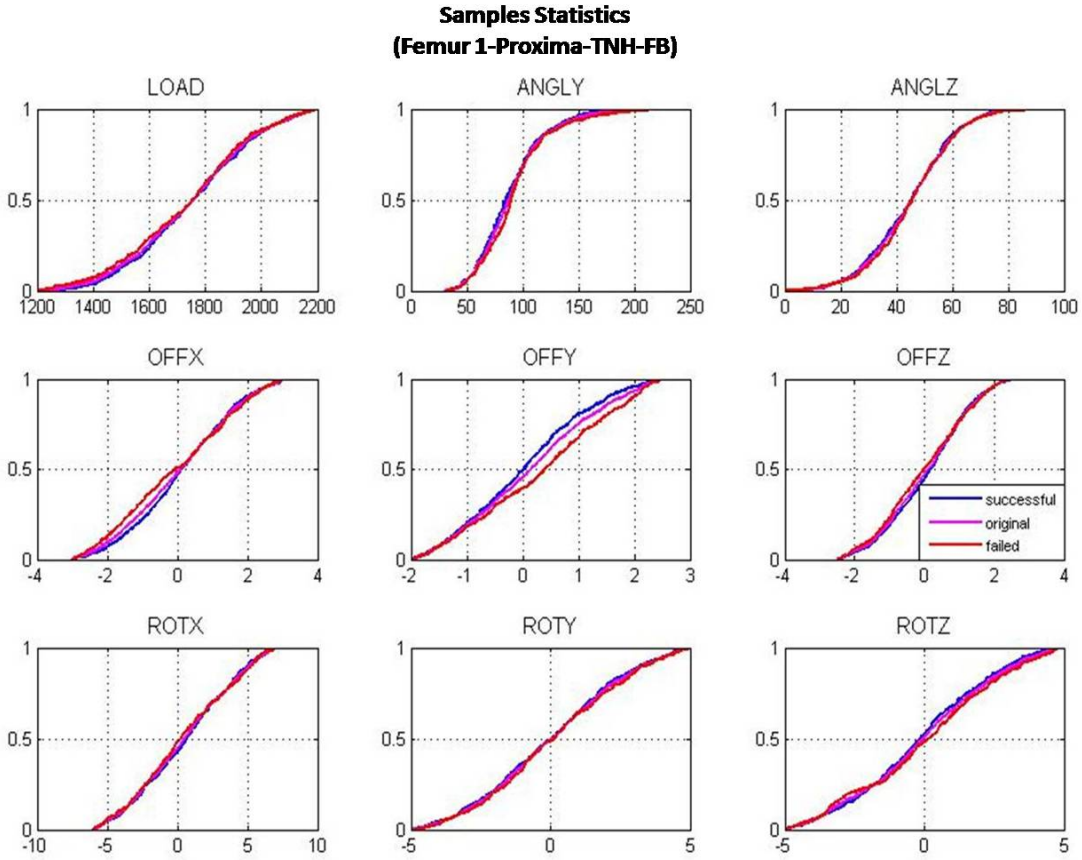

Figure 5.9: Empirical CDFs of the inputs for combinations with Proxima, for the original, successful and failed samples.

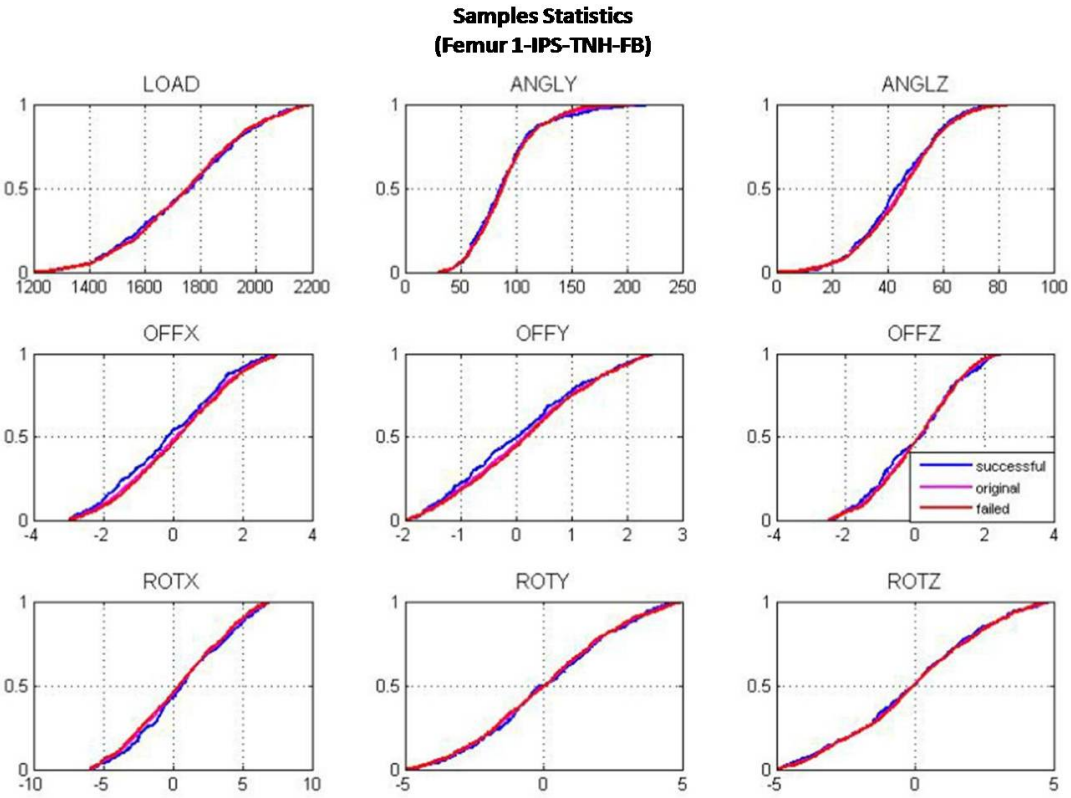

Figure 5.10: Empirical CDFs of the inputs for combinations with IPS, for the original, successful and failed samples.

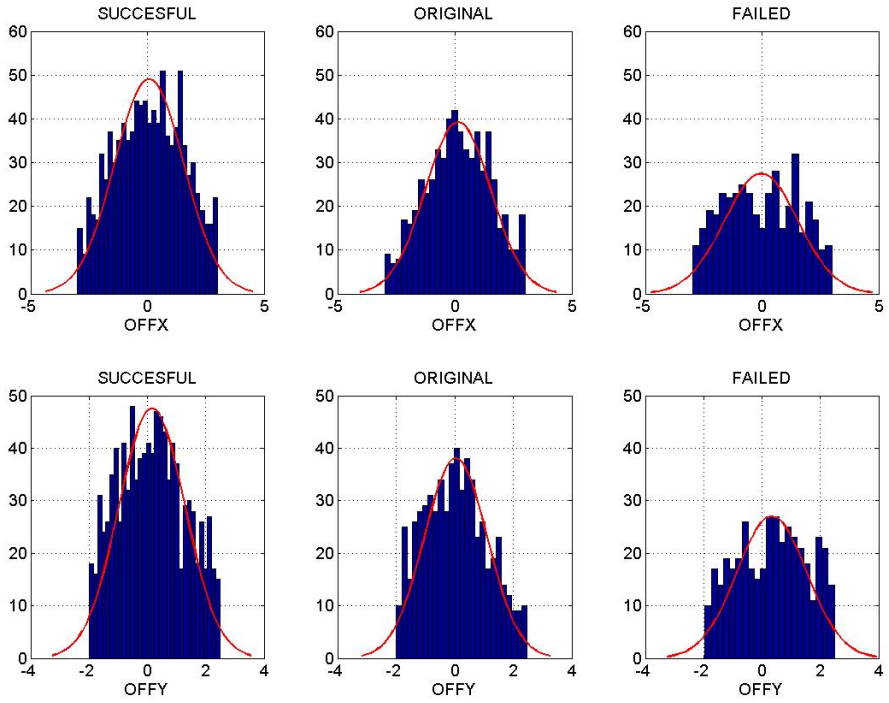

Figure 5.11: Histograms with fitted normal distributions for the RVs OFFX (top) and OFFY (bottom), for the original (left), the successful (centre) and the failed (right) samples.

	Successful	**Original**	**Failed**
OFFX	2.3479	2.0755	2.6805
OFFY	1.7459	1.5858	1.9314

Table 5.3: Interquartile ranges of OFFX and OFFY, for the successful, original and failed samples.

Figure 5.12 presents some scatter plots of the bone volume fraction exceeding 0.8% of strain (BPER) for the fully bonded interface (top) and micromotion for the frictional interface (bottom) cases. It can be seen that most of the points are below 3% BPER and below 40μm respectively.

Figures 5.13 and 5.14 show some of the plots of the convergence of the mean value of BPER (top) and micromotion (bottom). Mean values of BPER and micromotion started to converge at about 200 simulations. The mean value of BPER (Figure 5.13) with the Proxima implant converged to values of about 0.9% with Femurs 2 and 3, and 1.80% with Femur 1. For the IPS implant, the mean value of BPER converged to values of about 1.80% for Femurs 1 and 3 and 0.60% for Femur 2. Mean values of micromotion (Figure 5.14), for the Proxima implant, converged to values of about 20μm for femur 2, and 50μm for Femurs 1 and 3. For the IPS implant, micromotion converged to values between 30 and 38μm for the three femurs. Table 5.4 shows the outlier values of the maximum micromotions found for all the models. It can be seen that all the values remain stable around values between 277 and 299μm.

	Femur 1	**Femur 2**	**Femur 3**
Proxima	295	297	299
IPS	294	277	279

Table 5.4: Outliers of maximum nodal micromotion in micrometres.

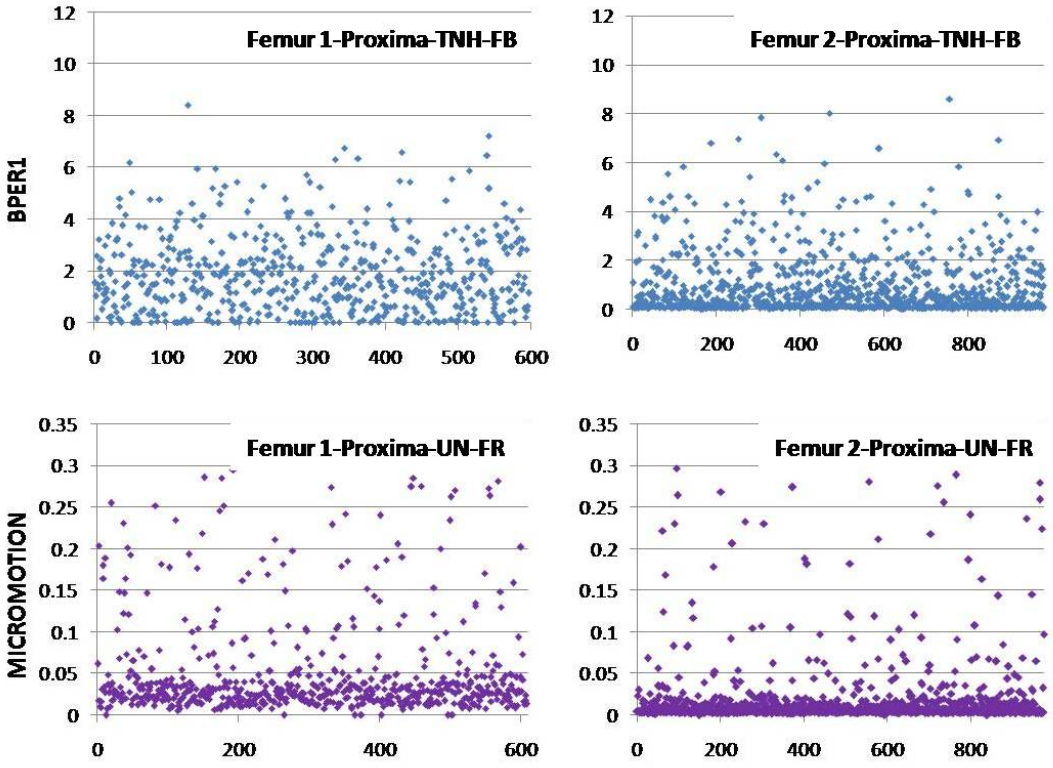

Figure 5.12: Some scatter plots of BPER (top), i.e. bone volume percentage exceeding 0.8% von-Mises elastic strain, and micromotion (bottom).

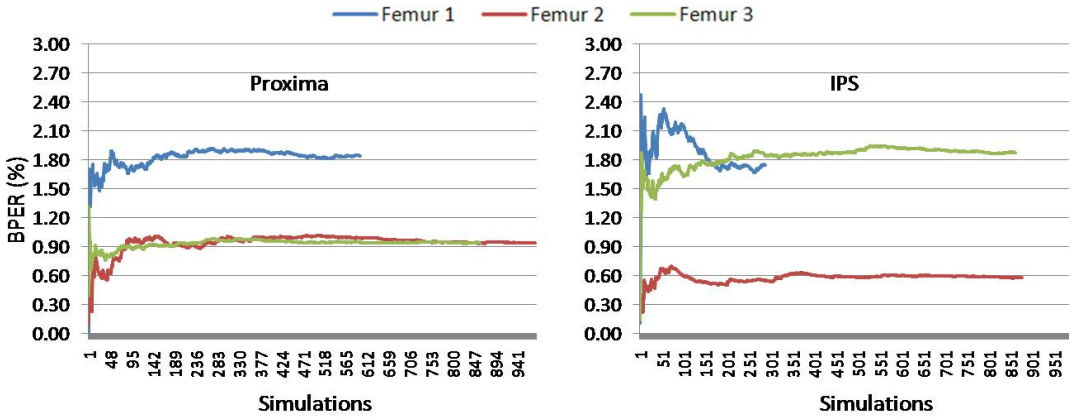

Figure 5.13: Convergence of the mean value of BPER, i.e. bone volume percentage exceeding 0.8% von-Mises elastic strain, for the three femurs combined with Proxima (left) and combined with IPS (right) for the TNH case.

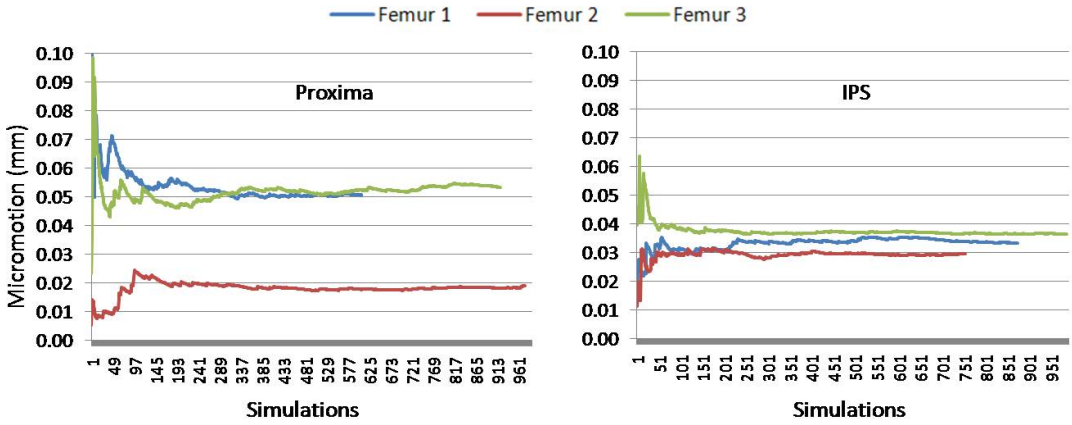

Figure 5.14: Convergence of the mean value of the micromotion in millimetres for the three femurs combined with Proxima (left) and combined with IPS (right).

5.3.1 Strains and Micromotions plots

Figure 5.15 shows deformed shape and contour plots of the von-Mises elastic strain for a model of combination of Femur 3 with Proxima, when the output BPER was higher than 4.5%, i.e., for outlier values. The 5 distal nodes constraint and fully bonded interface were considered.

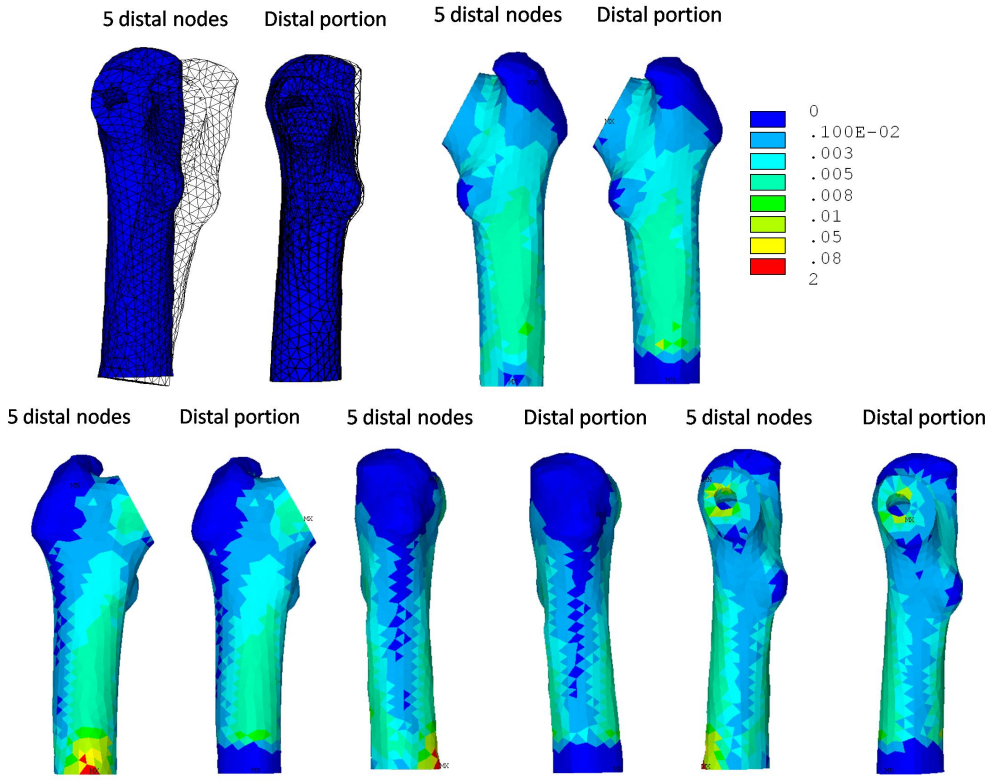

Figure 5.15: Deformed shape (top left), and von-Mises elastic strain contours of Femur 3 with Proxima, 5 distal nodes constraint and distal portion constraint, fully bonded interface, for BPER1 $>$ 4.5%.

Figures 5.16 and 5.17 show contour plots of the nodal sliding of the contact elements between Femur 3 with the Proxima implant and the IPS implant, respectively, for values of micromotion around the mean (50 and 35μm for the Proxima and the IPS implants, respectively).

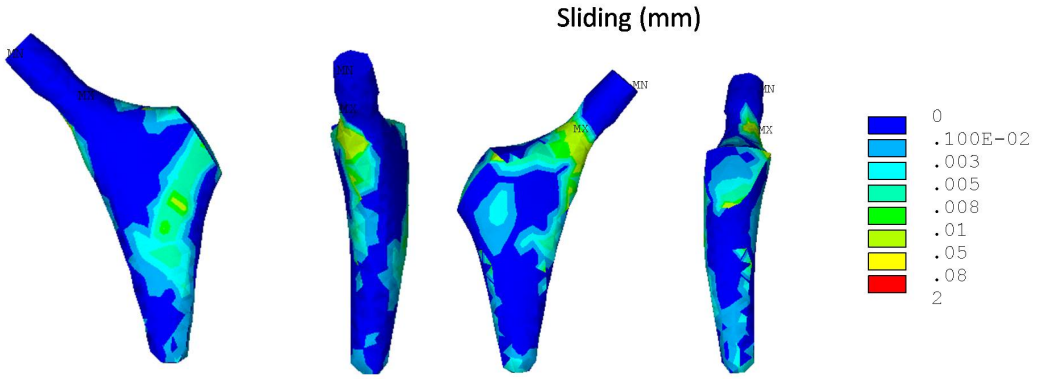

Figure 5.16: Example of nodal sliding of contact between Femur 3 and the Proxima implant in millimetres

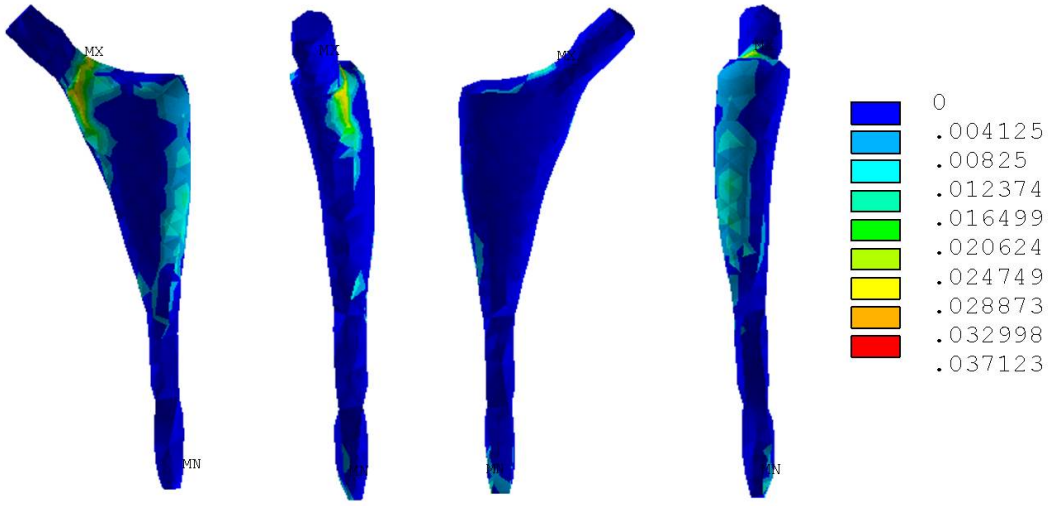

Figure 5.17: Example of nodal sliding of contact between Femur 3 and the IPS implant in millimetres

5.3.2 Effect of Statistics

Mean values and standard deviations (SD) of the outputs for each femur and the statistics of the input variables explained above are shown in Figures 5.18 and 5.19.

For the Proxima prosthesis (Figure 5.18), the mean value of BPER varied between 1.2 and 1.8% approximately, and was at a maximum for Femur 1 with high SD (TNH) and a minimum for both Femur 2 and Femur 3 in the TNH cases. There was an inconsistent trend in the variation of the value of BPER between bones, with respect to the statistics of the RVs. For the IPS prosthesis (Figure 5.19), the mean value of BPER varied between 0.65 and 1.85, the maximum value occurring in combination with Femur 3 in the TNH and UN cases, and minimum value in combination with Femur 2 in the TNH and TNL cases. These values were quite constant within Femurs 1 and 2, although in Femur 1, values of BPER were near the maximum, whereas in Femur 2, these values were near the minimum. Mean values of BPER in Femur 3 varied substantially, with values near the maximum in the TNH and UN cases and near the minimum in the TNL case. Again, the mean value of BPER was inconsistent for the IPS implant with respect to the statistics of the RVs.

The standard deviations (SD) of BPER (Figure 5.18, cross markers), were highly variable, particularly for the IPS. Femurs combined with the Proxima prosthesis gave varying values of the SD of BPER, between 0.60 when combined with Femur 3 in the TNH case, and 1.50 when combined with Femur 1 in the TNH case. The IPS prosthesis gave values of the SD of BPER which varied between 0.55 with Femur 3 in the TNL case, and 2.30 with Femur 1 in the TNL and UN cases.

In all cases, the mean value and SD of BPER were much higher for the TNH, TNL and UN cases, than with a varied constraint (distal portion) and a frictional interface.

Empirical CDFs for the three femurs with the Proxima prosthesis are shown in Figure 5.23, for the statistics of the inputs cases; the corresponding CDFs for the IPS are shown in Figure 5.24.

The empirical CDFs for the Proxima prosthesis (Figure 5.23) were highly

smooth and close to a normal distribution. The shape of the curves varied slightly, the steepest ones corresponding to those for Femur 3 and the least steep for Femur 2. The CDFs for Femur 1 were quite steep in most of its domain, but they became smoother when close to 1. Values are quite constant within the same femur, with respect to the statistics of the RVs. The value of BPER with a 50% of probability varied between 3 and 3.5% for Femur 1, 0.8 and 1% for Femur 2, and 1.5 and 1.8% for Femur 3. Convergence to 100% was reached quicker for Femur 3, for the TNH case.

The empirical CDFs for the three femurs with the IPS prosthesis (Figure 5.24) were noisy for Femurs 1 and 2 (top and centre, respectively). The curve for Femur 2 in the TNL and UN cases, had a zero slope for values of BPER between 1.5 and 3.5%. The curve for Femur 2 in the TNL case had an inflexion point in the same range of BPER. The rest of the curves fit a normal distribution quite well. The values of BPER with a probability of 50% varied between 0.5 and 1% for Femur 1, were quite constant around 1.7% for Femur 2, and varied between 0.5 and 2% for Femur 3. Curves corresponding to Femur 3 were the steepest ones, whereas those for Femur 2 were the least steep.

Sensitivity results are shown in Figure 5.28. In all cases the sensitivities to implant positioning related parameters were higher than to load magnitude and geometry. Results for TNH and UN cases were similar. For Femur 1 the Proxima prosthesis, the maximum sensitivities were to ROTY in the TNH and UN cases. Femur 1 combined with the IPS prosthesis had maximum sensitivities to OFFY in the TNH and UN cases, whereas OFFX was most sensitive for the TNL case. For Femur 2 with the Proxima prosthesis, higher sensitivities were evident for the UN case compared to the TNH case, mainly to ROTX, ROTY and ROTZ. All the implant position parameters were most sensitive in the TNL case. Femur 1 with IPS had higher sensitivities for the UN case compared to the TNH case, mainly to ROTY and ROTZ. In the TNL case, the maximum sensitivities were those to OFFX ROTY and ROTZ.

5.3.3 Effect of Constraints

Figures 5.20 and 5.21 show the mean values and standard deviations (SD) for all femur-implant combinations, with uniform distribution statistics, for the 5 distal

nodes constraint (5NOD) case against the distal portion constraint cases (DIST) (fully bonded and frictional interfaces cases, 'FB' and 'FRI' respectively). It can be seen that in all cases, the mean value of BPER decreased when the distal portion constraint was applied. The minimum reduction occurred for Femur 2, from 0.85 to 0.15% with the Proxima implant, and from 0.75 to 0.15% with the IPS implant. The maximum reduction occurred with Femur 3, from 1.40 to 0.07% for the Proxima implant, and from 1.85 to 0.08% for the IPS implant. The standard deviation had a similar reduction in all cases, except for Femur 1, where in both cases it had a slight increase of less than 0.10%.

The empirical CDFs are presented in Figures 5.25 and 5.26. All the results for the three femurs (Femur 1, top; Femur 2, centre; Femur 3, bottom) and the two implants (Proxima, Figure 5.25; IPS, Figure 5.26) are shown.

The effect of the different constraints (with uniform distribution in the inputs in all cases) is shown with the green (5 distal nodes constraint, 'UN-5NOD-FB') and red (distal portion constraint, 'UN-DIST-FB') curves (Figures 5.25 and 5.26). In all cases, the curves converged towards 1 much faster with the distal portion constraint. The CDF of Femur 1/IPS prosthesis (5.26, top) with the 5 nodes constraint had an anomalous shape, no values of BPER were evident between 1 and 3.4%. There were two ranges of values of BPER, most of them occurring between 0 and 1%, and the second range between 3.5 and 5%. On the other hand, this model was the most rapidly convergent when the new constraint was applied. For the 5 nodes constraint, the value of BPER with a 60% of probability was between 0.5 and 1.85%. For the distal portion constraint, values of BPER higher than 0.025% had a probability of approximately 100% in all cases. Most of the values of BPER were concentrated in the low range between 0 and 0.05%.

Figure 5.29 shows the sensitivity results for the 5 distal nodes constraint cases against the distal portion constraint cases. It can be seen that the sensitivities were much lower with the distal portion constraint. The relative sensitivities were very similar, although the absolute values were reduced to values less than $\mid 0.03 \mid$. Again the implant position related parameters were the most significant parameters, compared to load magnitude and geometry.

5.3.4 Effect of Interface Condition

Figures 5.20, 5.21, and 5.22 show the mean values and standard deviations (SD) of both output parameters: bone volume percentage exceeding von-Mises elastic strain of 0.8% (BPER) and maximum nodal micromotion. For all the combinations of the three femurs and the two implants, both interface conditions are compared for the uniform distribution case. The distal portion constraint was adopted in all cases. Mean values of BPER (Figures 5.20 and 5.21) were almost identical in most of the cases for fully bonded and frictional interface cases. For Femur 2 combined with the Proxima implant, the mean value of BPER decreased from 0.10 to 0.025%, while for Femur 1 combined with the IPS implant it increased slightly from 0.005 to 0.025%. In addition, the standard deviations were almost identical. Mean values of maximum nodal micromotion (Figure 5.22) were very similar for combinations with both implants, varying between 20 and $50\mu m$ for combinations with the Proxima implant, and between 25 and $30\mu m$ for combinations with the IPS implant. The standard deviations were very high for Femur 1 combined with the Proxima implant, about $370\mu m$, while for all the other cases these values were between 70 and $180\mu m$.

The effect of the different interface conditions (uniform distribution in the inputs and distal portion constraint in all cases) on the empirical CDFs of BPER is shown in Figures 5.25 and 5.26 with the red (fully bonded, 'UN-5NOD-FB') and cyan (frictional interface, 'UN-DIST-FRI') curves. Femur 1 with the IPS implant (Figure 5.26, top) and Femur 2 with the Proxima implant (Figure 5.25, centre) present slightly different behaviour to their counterparts. In the former, the fully bonded case was more rapidly convergent than the frictional case, while for the latter the situation was the opposite. In both interface cases, most of the values of BPER ranged between 0 and 0.05%.

Figure 5.27 shows the empirical CDFs of the micromotion, for combinations with the Proxima implant (continuous lines) and the IPS implant (dashed lines), for the three femurs (Femur 1, blue; Femur 2, green; Femur 3, red). The empirical CDFs of maximum nodal micromotion show excellent agreement for the three femurs. The best match occurred between Femurs 1 and 3 combined with the Proxima implant, with identical CDFs. For combinations with the Proxima implant (left), the probabilities of values of micromotion $\leq 50\mu m$ were identical

for the three femurs, and for combinations with the IPS implant they were quite close. It can be seen that for a 50% probability, the value of the maximum nodal micromotion was about $25\mu m$ for all the models.

Figures 5.30 and 5.31 show the sensitivity results for all combinations of femurs and implants. Sensitivities of BPER are shown for the fully bonded case against the frictional interface case in Figure 5.30. It can be seen that the sensitivity trend of each combination of femur and implant was quite consistent for most of the models, except for Femur 1; when combined with the IPS prosthesis, the absolute values of the sensitivities of BPER were much lower than for the rest of the models, with a maximum of the order of $\mid 0.002 \mid$ for the sensitivity to OFFX. Also in this case the sensitivities to load variability (ANGLY and ANGLZ) were higher than to implant positioning. Femur 1 combined with the Proxima prosthesis had a more consistent trend for both interface conditions, although the sensitivities to OFFY and to OFFZ were substantially decreased and increased, respectively. The rest of the models presented similar sensitivities in both interface cases. Sensitivity to OFFY was one of the highest in all cases. Sensitivity to ROTZ was also relatively high in all cases. Sensitivities of the maximum nodal micromotion are shown in Figure 5.31, for combinations with the Proxima prosthesis (left) and the IPS prosthesis (right). Combinations with the Proxima prosthesis had much higher sensitivities than combinations with the IPS prosthesis. In models with the Proxima implant, micromotion was most sensitive to OFFZ, followed by OFFY, ROTY and ROTZ, in order of significance, with Femurs 1 and 3 the most sensitive in the majority of the cases. In combinations with the IPS prosthesis, Femur 2 had the highest sensitivities to ROTZ, ROTY, ROTX and OFFZ, in order of significance. Femur 1 had relatively high sensitivities, to OFFZ, OFFY, ROTX, ROTY and ROTZ, in order of significance. Femur 3 presented the minimum sensitivities, except to OFFY, to which it showed the highest value. In all cases, sensitivities of the maximum micromotion to implant positioning parameters were much higher than to load magnitude and geometry.

5.3.5 Effects of Change in Reference Position

Figures 5.19, 5.21 and 5.22 show the mean values and standard deviations (SD) of BPER and the maximum nodal micromotion, for Femur 2 combined with the

IPS prosthesis for reference position 1 (blue) and 2 (red lines and markers). Mean values of BPER are shown for the fully bonded interface with TNH, TNL and UN statistics, and the frictional interface case. In all cases, the mean value of BPER increased substantially. Maximum values increased from 0.70% to 2.60% in the fully bonded UN case, and minimum values increased from 0.55% to 2.50% in the fully bonded TNH and TNL cases. For the frictional interface, the mean value of BPER had a lower relative increase, from 0.15 to 0.20% approximately. The relative increase of the standard deviations were very similar, with a maximum increase from 0.80 to 3.10% in the fully bonded TNH case. The mean value of the maximum nodal micromotion (Figure 5.22) increased, although the relative increase was lower than for BPER, from 29 to 37.5μm approximately. The standard deviation increased from 36 to 39μm approximately.

The effect of changes in the reference position of Femur 2/IPS on the empirical CDFs of BPER and micromotion are shown in Figures 5.26 (centre, dashed lines for reference position 2, 'REF 2') and 5.27 (dashed black lines for 'REF 2'), respectively.

For the CDFs of BPER (Figure 5.26, centre), reference position 1 ('REF 1') had faster convergence than reference position 2 ('REF 2'). For REF 1, the three curves corresponding to TNH (continuous, blue), TNL (continuous, magenta) and UN (continuous, green) were almost identical, having a value of about 0.60% BPER for an 80% probability. For the reference position 2, the curves corresponding to TNH (dashed, blue) and UN (dashed, green) cases were almost identical, but with very low convergence for values higher than 0.60% of BPER, which had about 40% probability. For the reference position 2 and TNL case (dashed, magenta), the curve presents an irregularity similar to that of Femur 1 combined with the IPS prosthesis in the UN case (Figure 5.26, top). There was little increase in the CDF from 0.6 to 3.8% BPER.

The empirical CDFs of the maximum nodal micromotion (Figure 5.27), showed a good agreement between the CDFs for the two reference positions (dashed green lines for 'REF 1' and dashed black line for 'REF 2'). Values of micromotion with 10%, 50% and 80% probabilities were about 12μm, between 12 and 30μm, and between 45 and 60μm, respectively.

Figures 5.32 and 5.33 show the sensitivity results for Femur 2 combined with

the IPS prosthesis, for fully bonded with 5 distal nodes constraint and friction interface with distal portion constraint cases respectively. In the fully bonded case (Figure 5.32), sensitivities of BPER were much lower for the TNH case. Sensitivities to ROTX, ROTY and ROTZ decreased substantially for reference position 2, while sensitivities to OFFY and OFFZ increased. For TNL case, sensitivities to ROTX, ROTY and ROTZ were almost the same for both reference positions, while those to OFFX and OFFZ increased. For the UN case, all the sensitivities increased for the reference position 2, with the highest value for ROTY, followed by ROTZ, ROTX, OFFY and OFFZ, in order of significance. For TNL and UN, sensitivity trends were to increase when reference position 2 was adopted. In the frictional interface case (Figure 5.33), sensitivities of BPER (left) were almost identical in both reference positions, except for those to OFFX and OFFY, which increased substantially . Maximum sensitivity was found to ROTZ, ROTY, OFFY, ROTX and OFFX. Sensitivities of maximum nodal micromotion (right) were very similar to ROTX, ROTY, ROTZ and OFFZ, while it decreased substantially to OFFY for reference position 2. Maximum sensitivity was found to ROTZ, followed by ROTY, OFFY (in reference position 1 only), ROTX and OFFZ. In general, micromotion was less sensitive to any of the parameters than BPER.

5.3.6 Means and Standard Deviations

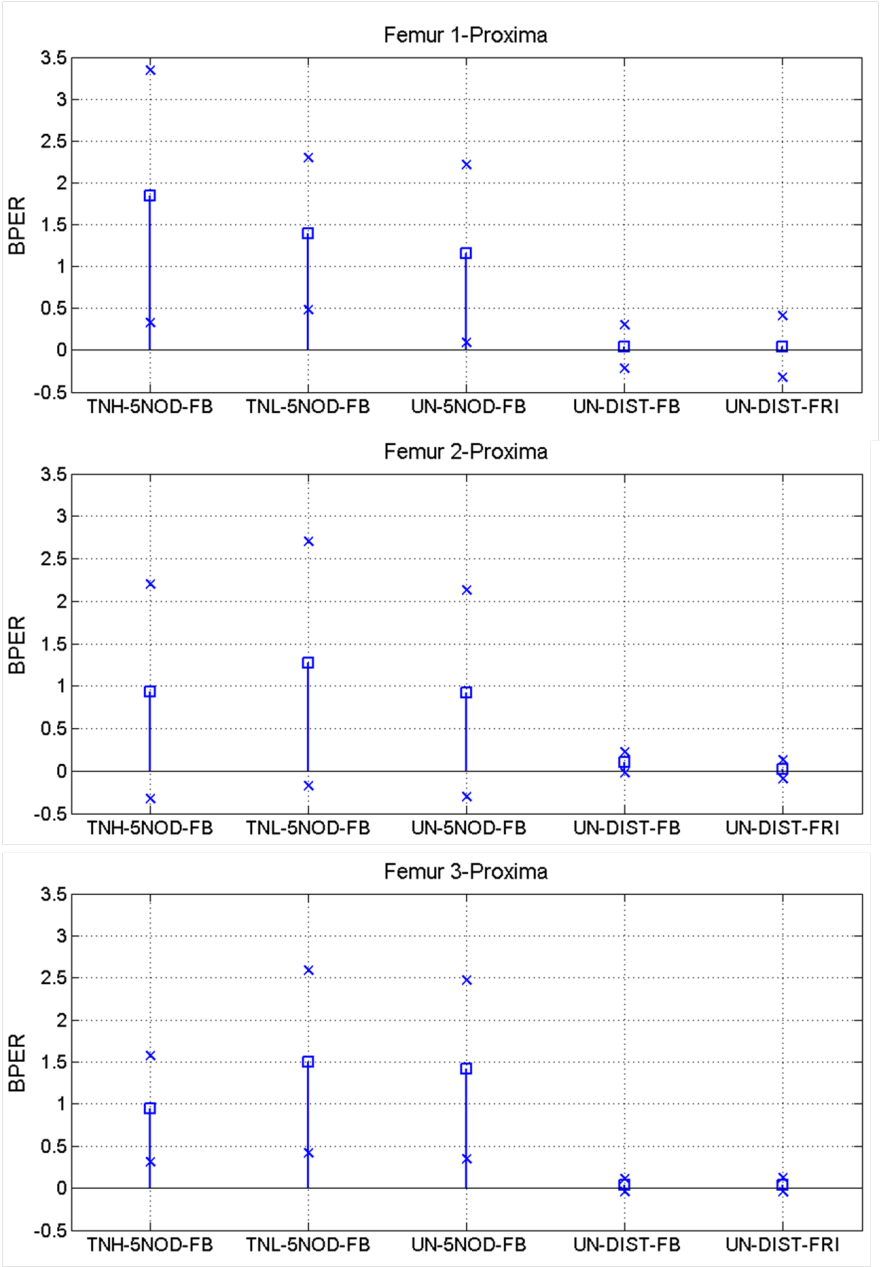

Figure 5.18: Mean value (square markers) and standard deviation (cross markers) of the output of Femur 1, 2 and 3 combined with Proxima implant, for normal distribution with high and low SD and uniform ('TNH', 'TNL' and 'UN' respectively) with the 5 distal nodes constraint ('5NOD'), together with the value for the distal portion constraint ('DIST') for fully bonded ('FB') and frictional interface cases ('FRI').

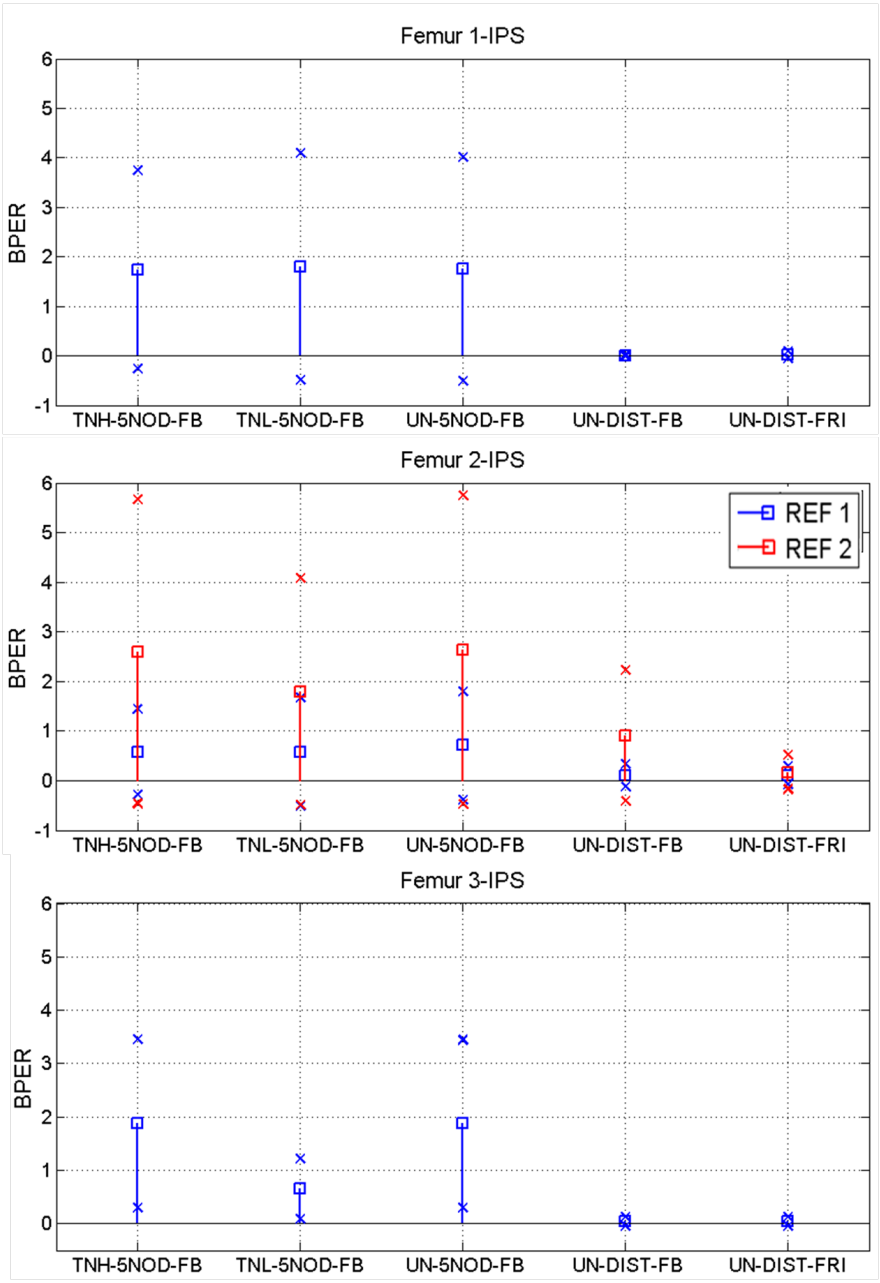

Figure 5.19: Mean value (square markers) and standard deviation (cross markers) of the output of Femur 1, 2 and 3 combined with IPS implant, for normal distribution with high and low SD and uniform ('TNH', 'TNL' and 'UN' respectively) with the 5 distal nodes constraint ('5NOD'), together with the value for the distal portion constraint ('DIST') for fully bonded ('FB') and frictional interface cases ('FRI'). Also the corresponding values for the second reference position of Femur 2/IPS is shown in the centre figure (red).

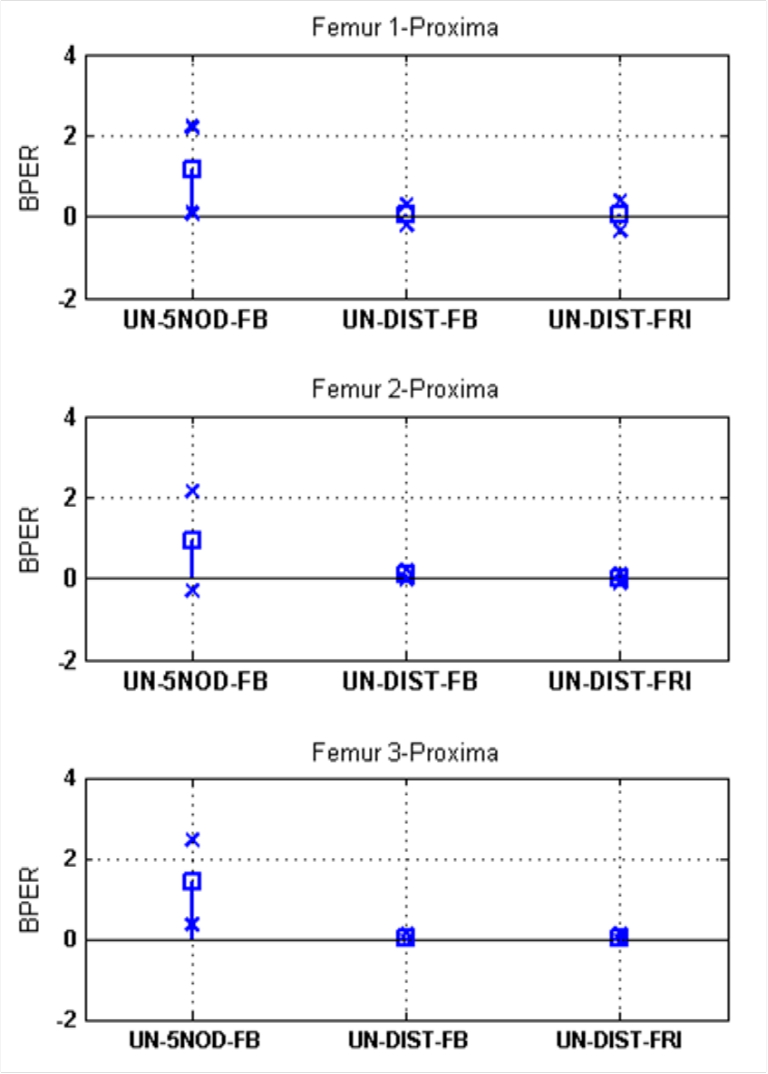

Figure 5.20: Mean value (square markers) and SD (cross markers) of the Proxima implant, for the uniform distribution case ('UN'), with 5 distal nodes constraint ('5NOD') and distal portion constraint ('DIST'), for fully bonded ('FB') and frictional interface cases ('FRI').

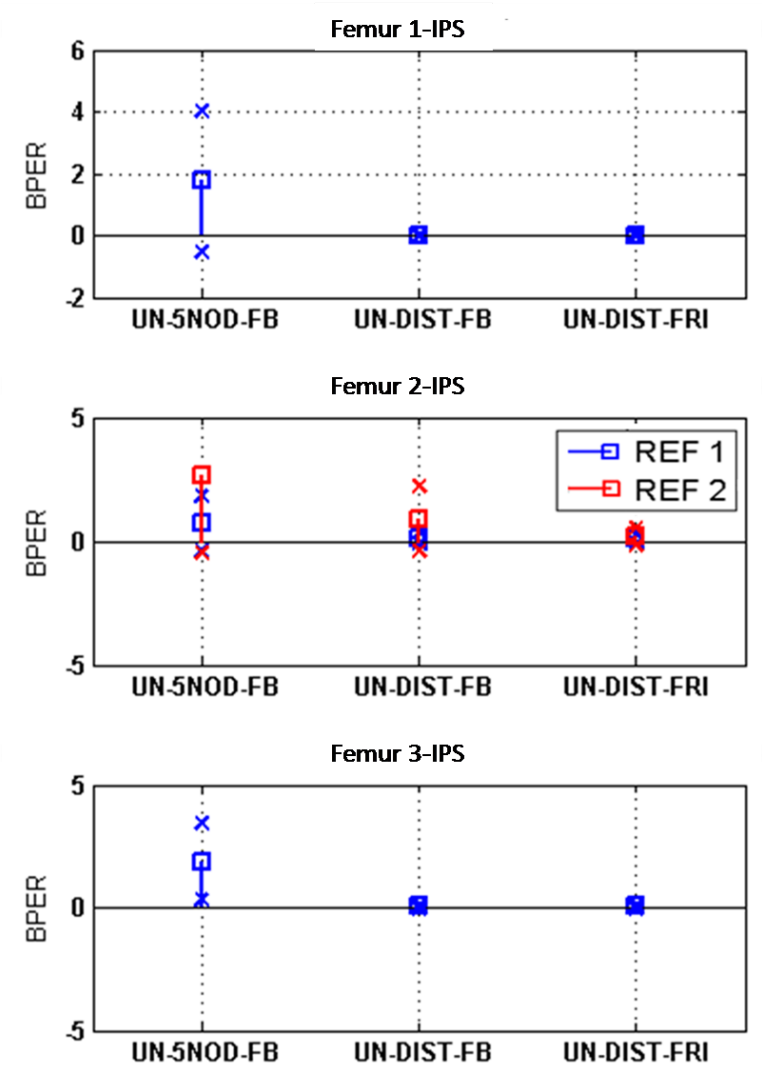

Figure 5.21: Mean value (square markers) and SD (cross markers), of the IPS implant, for the uniform distribution case ('UN'), with 5 distal nodes constraint ('5NOD') and distal portion constraint ('DIST'), for fully bonded ('FB') and frictional interface cases ('FRI'). Also the corresponding values for the case of change in reference position of Femur 2/IPS is presented in the centre figure (red).

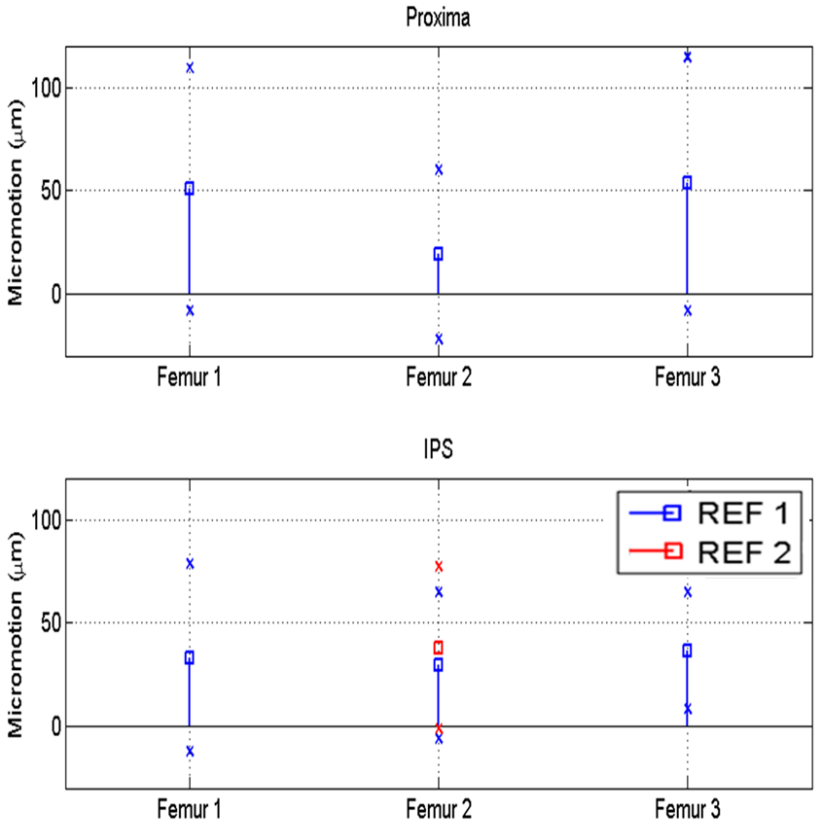

Figure 5.22: Mean value (square markers) and standard deviation (cross markers) of the micromotion for combinations of the three femurs with the Proxima implant (top) and the IPS implant (bottom). Also the corresponding values for the case of change in reference position of Femur 2/IPS is presented in the bottom figure (red).

5.3.7 Empirical Cumulative Distribution Functions (CDFs)

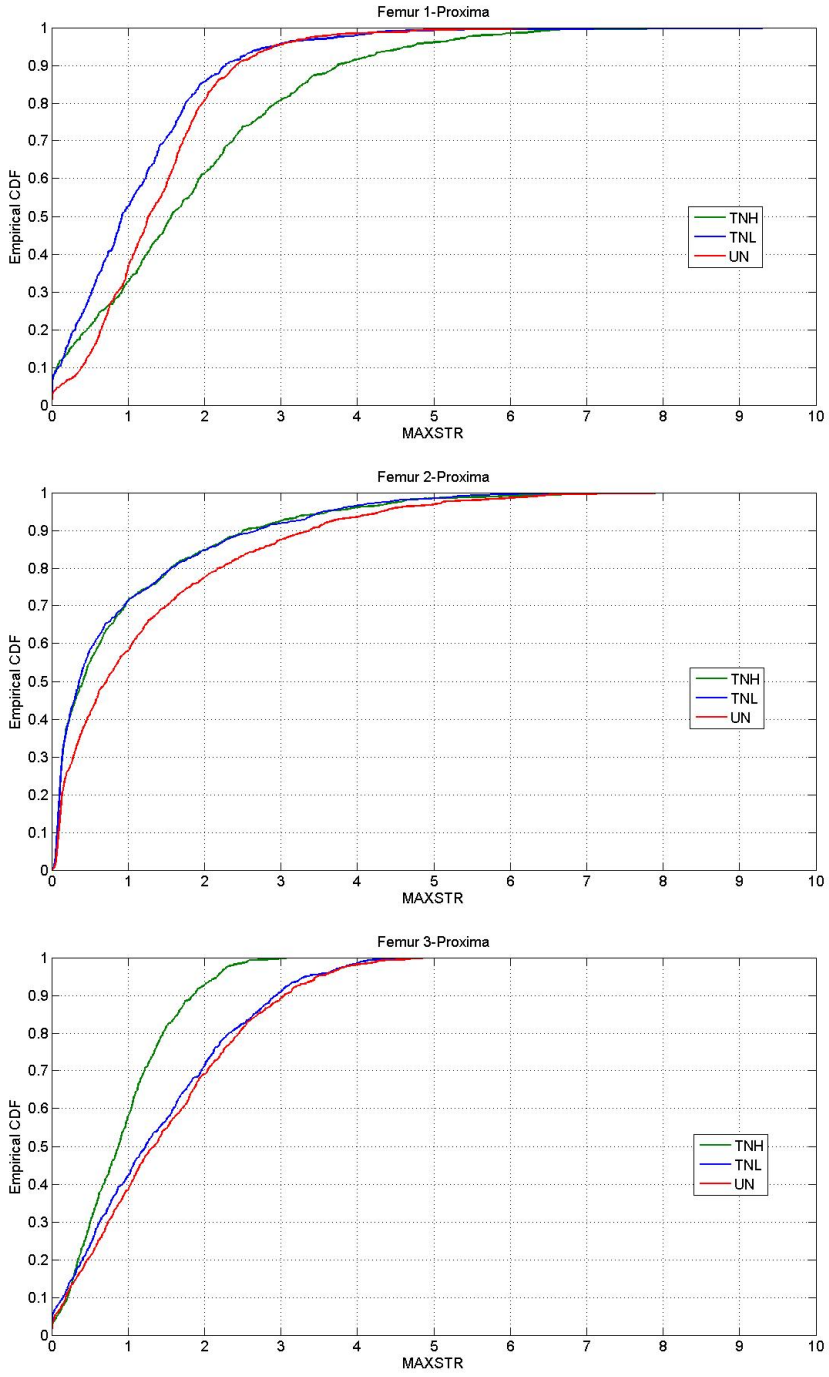

Figure 5.23: Empirical CDFs of Femur 1 (top), Femur 2 (centre) and Femur 3 (bottom) combined with Proxima, for normal distribution with high and low SD and uniform (TNH, TNL and UN respectively)

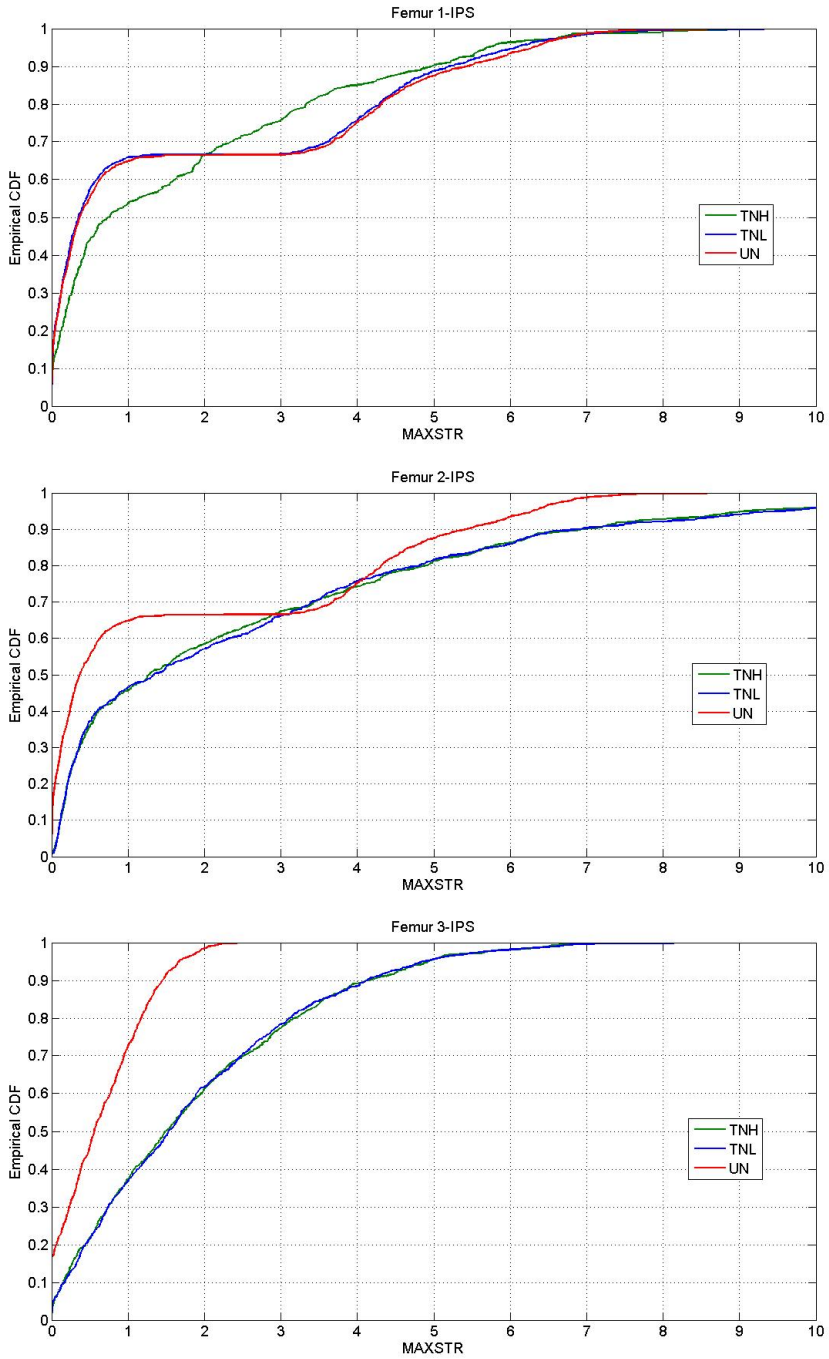

Figure 5.24: Empirical CDFs of Femur 1 (top), Femur 2 (centre) and Femur 3 (bottom) combined with IPS, for normal distribution with high and low SD and uniform (TNH, TNL and UN respectively)

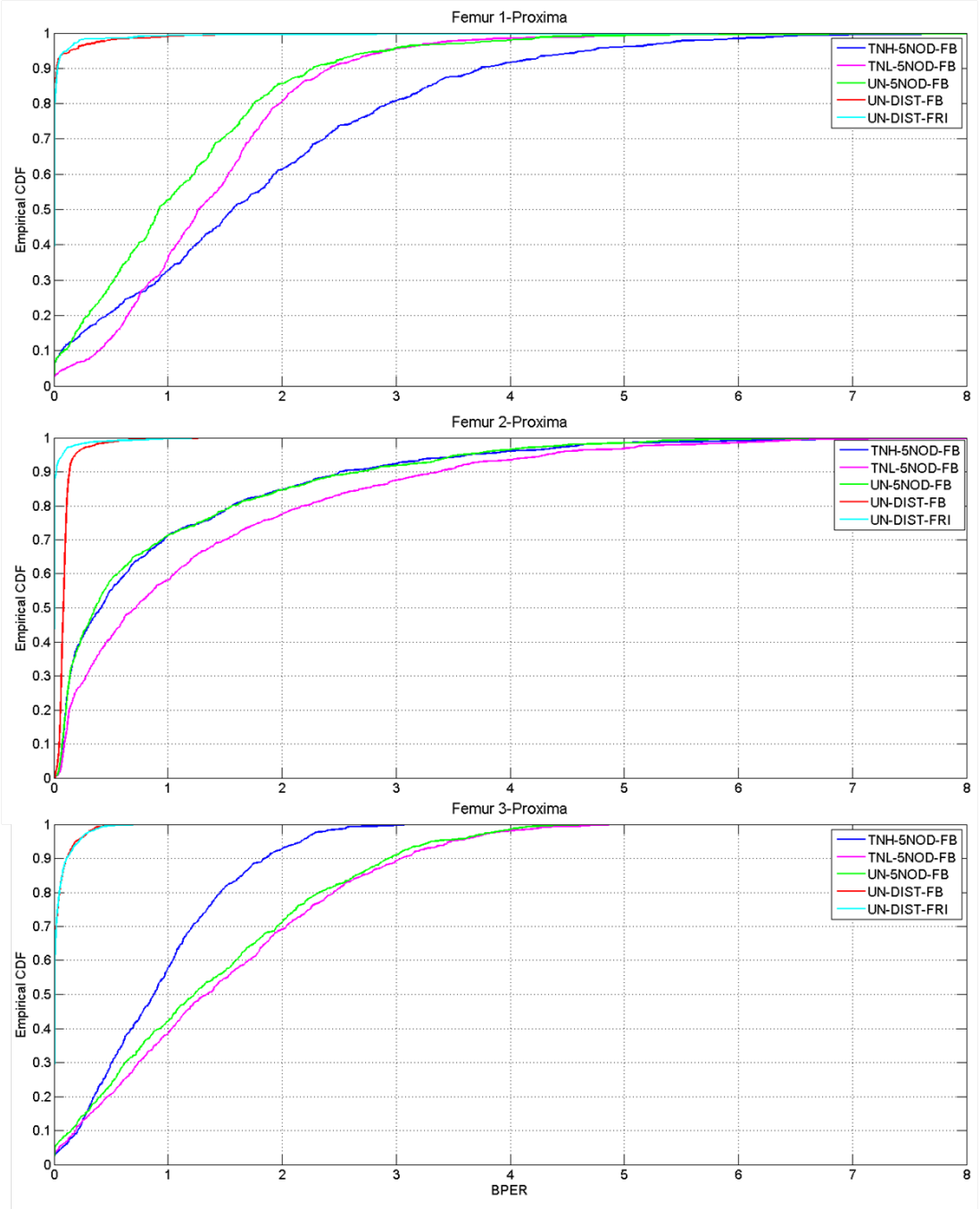

Figure 5.25: Empirical CDFs of BPER for the Proxima implant, with Femur 1 (top), Femur 2 (centre) and Femur 3 (bottom), for all the studies.

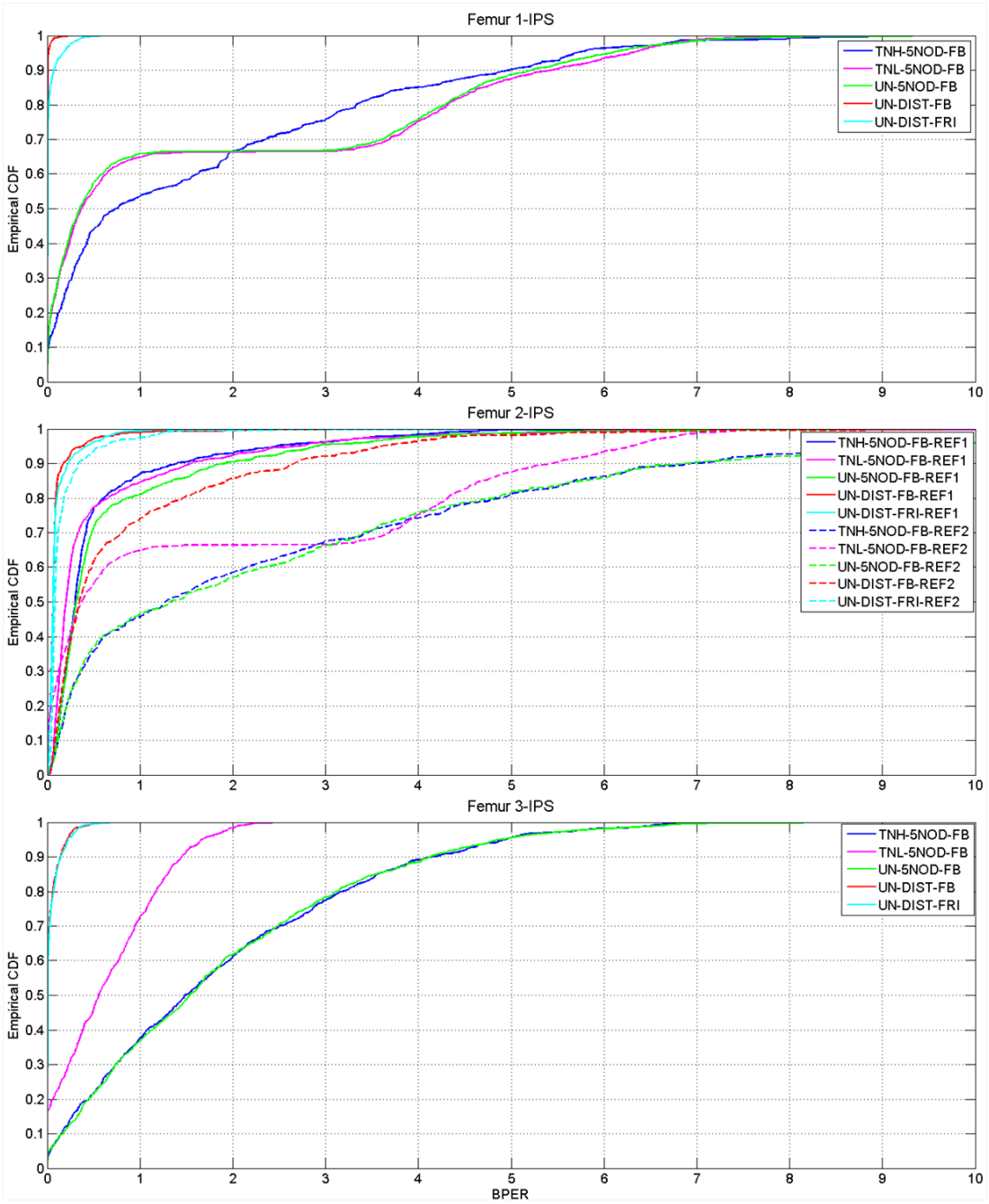

Figure 5.26: Empirical CDFs of BPER for the IPS implant, with Femur 1 (top), Femur 2 (centre) and Femur 3 (bottom), for all the studies.

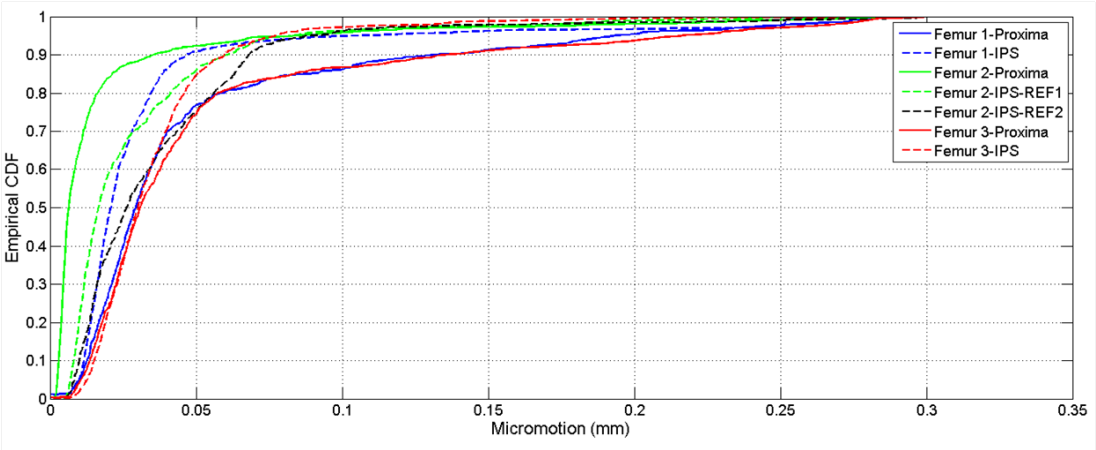

Figure 5.27: Empirical CDFs of Micromotion for all the studies.

5.3.8 Sensitivities

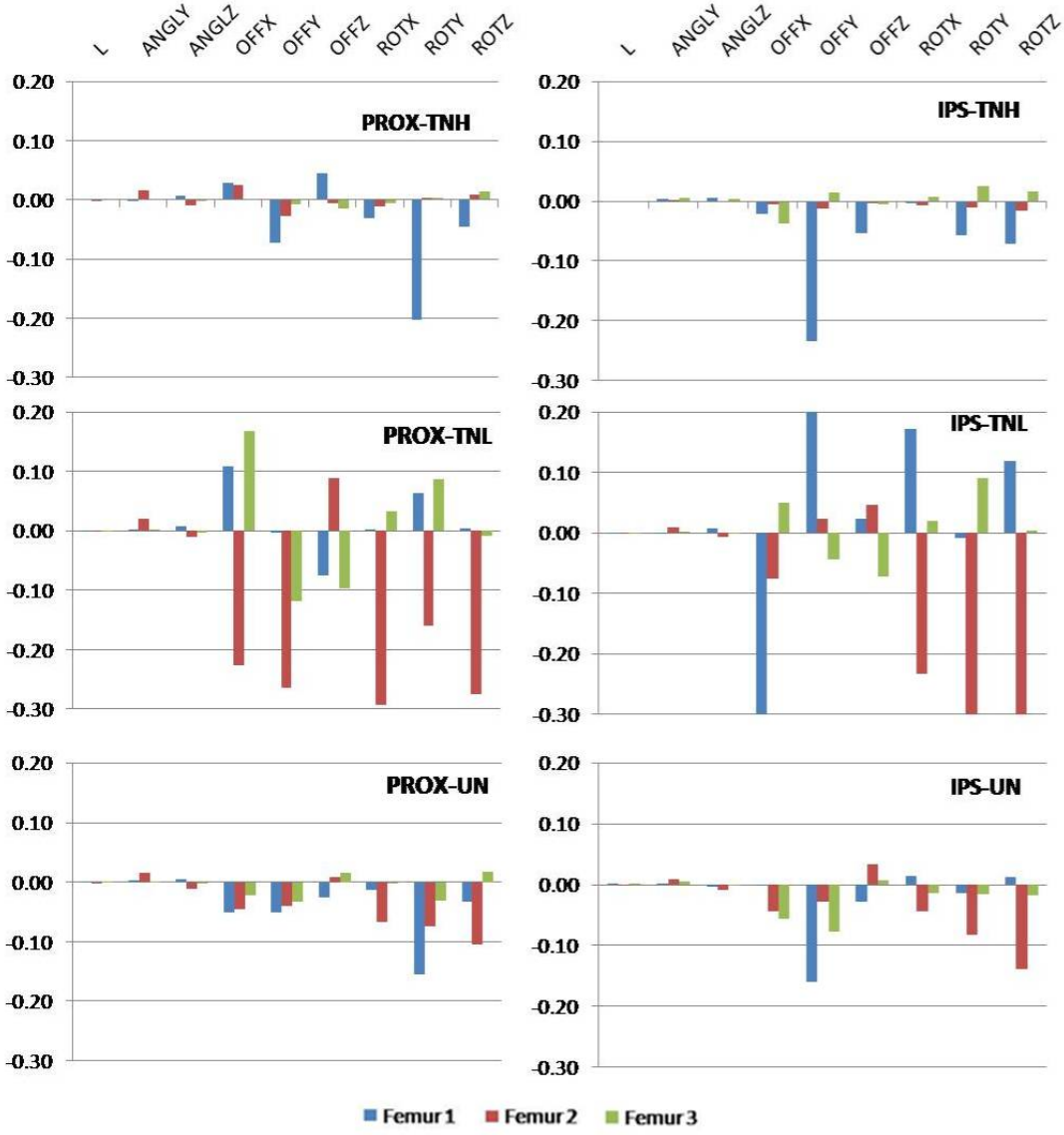

Figure 5.28: Sensitivities for combinations with Proxima (left) and with IPS (right), for the three statistics of the input variable cases (TNH, TNL and UN; top, centre and bottom figures, respectively.

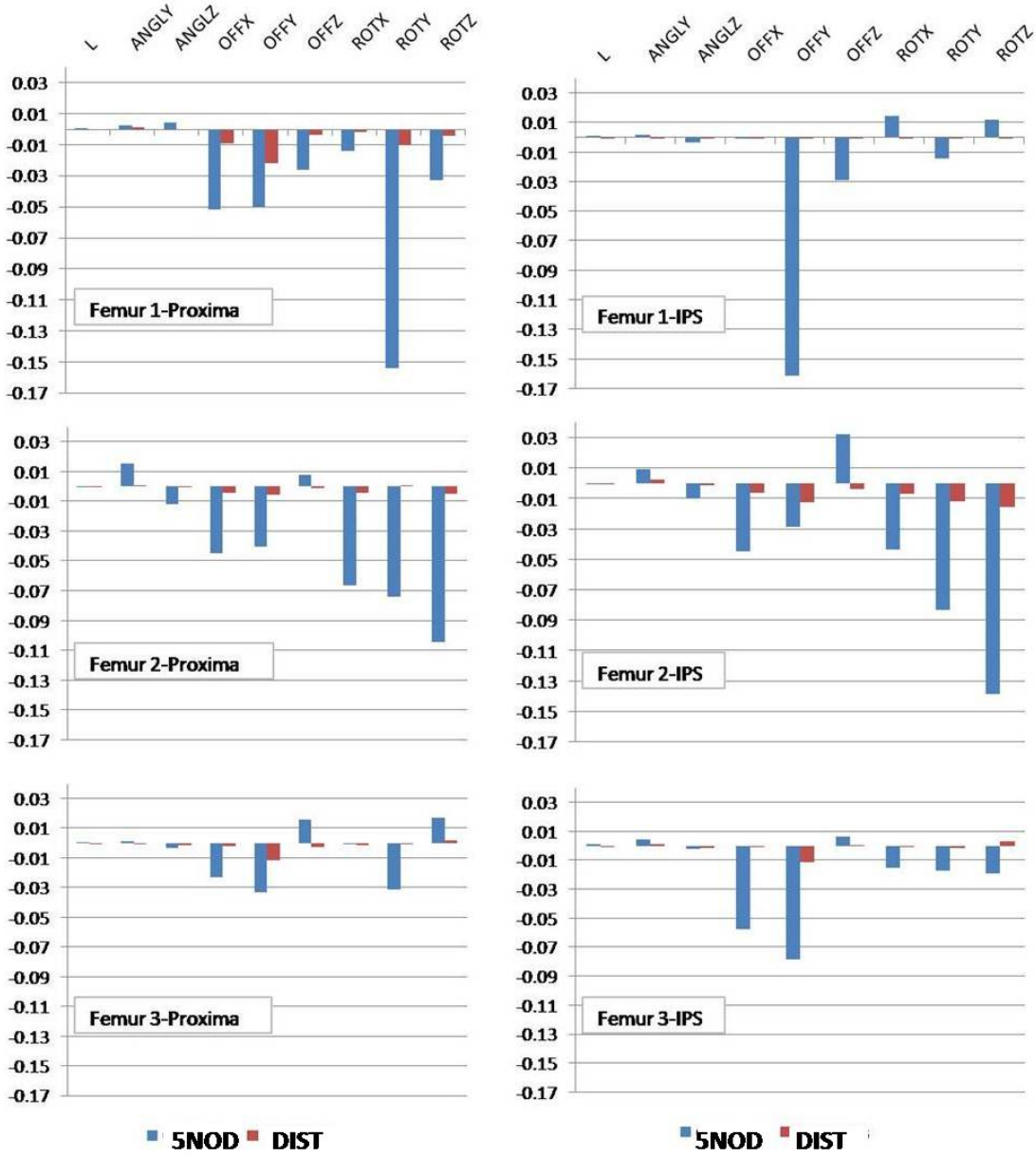

Figure 5.29: Sensitivity results for combinations of the three femurs with the Proxima implant (left) and the IPS implant (right), for the UN case, with 5 distal nodes constraint (OLD BCs) against the distal portion constraint (NEW BCs)

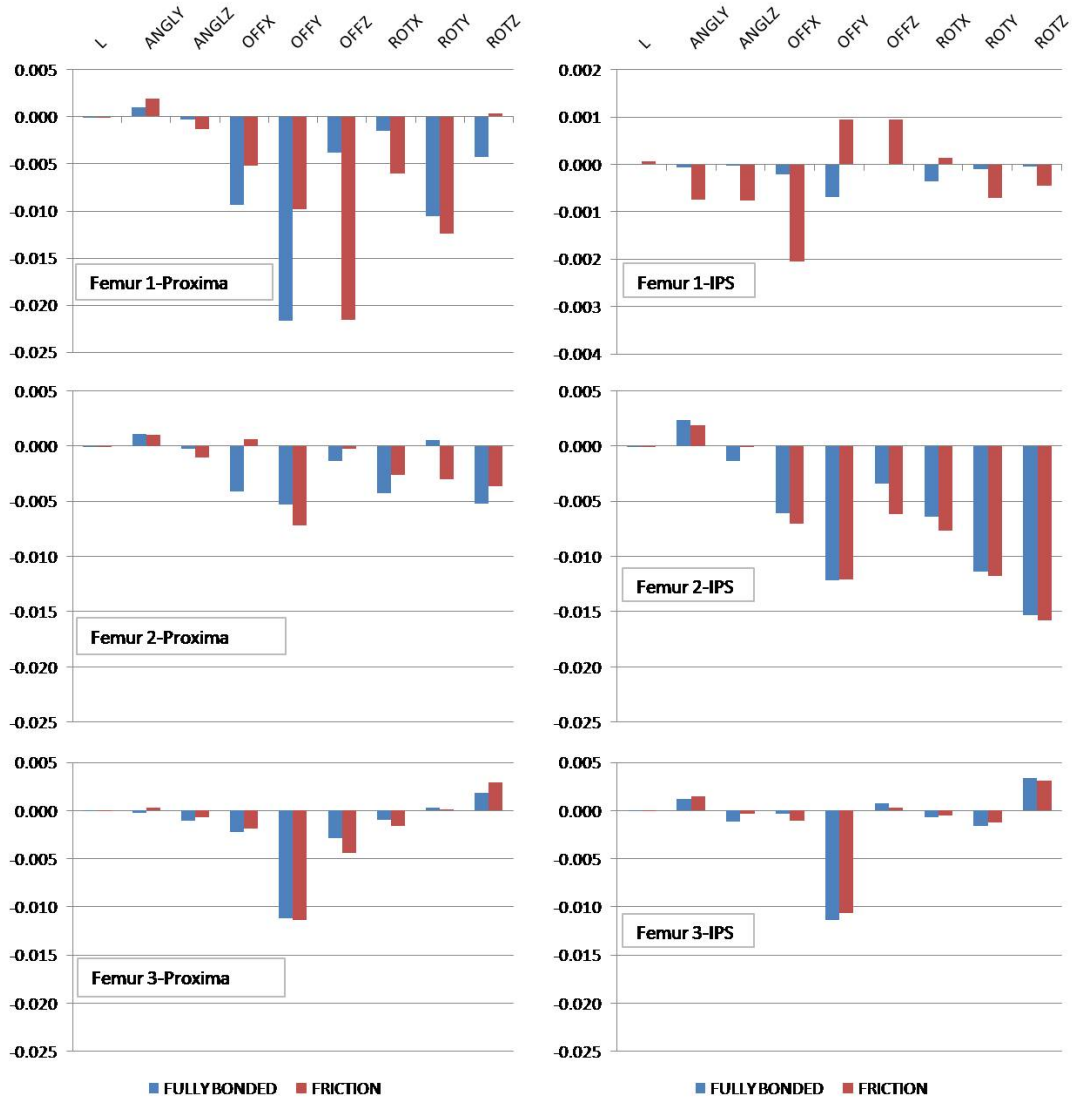

Figure 5.30: Sensitivity of BPER for the three femurs combined with the Proxima prosthesis (left) and the IPS prosthesis (right), for the uniform distribution case with distal portion constraint, with fully bonded against frictional interface cases.

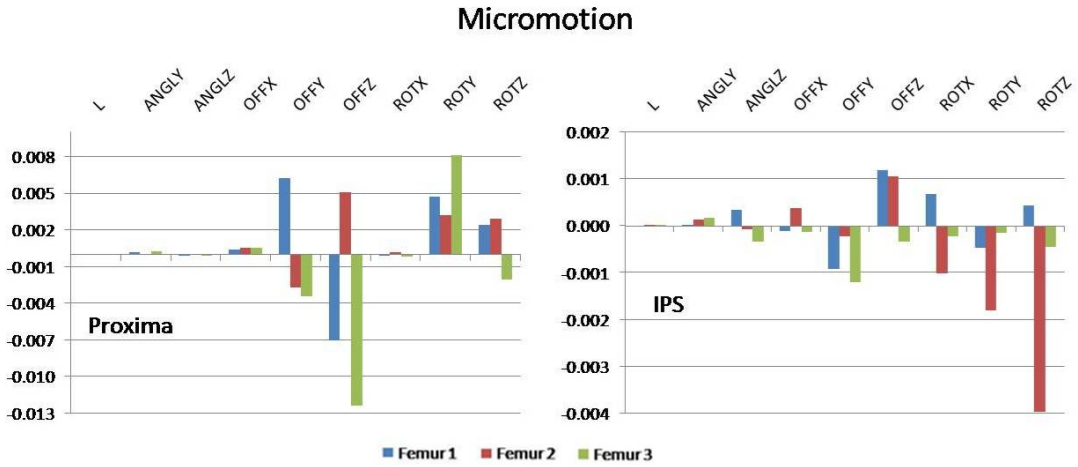

Figure 5.31: Sensitivity of the micromotion for the three femurs combined with the Proxima prosthesis (left) and the IPS prosthesis (right), for the uniform distribution case with distal portion constraint, with fully bonded against frictional interface cases.

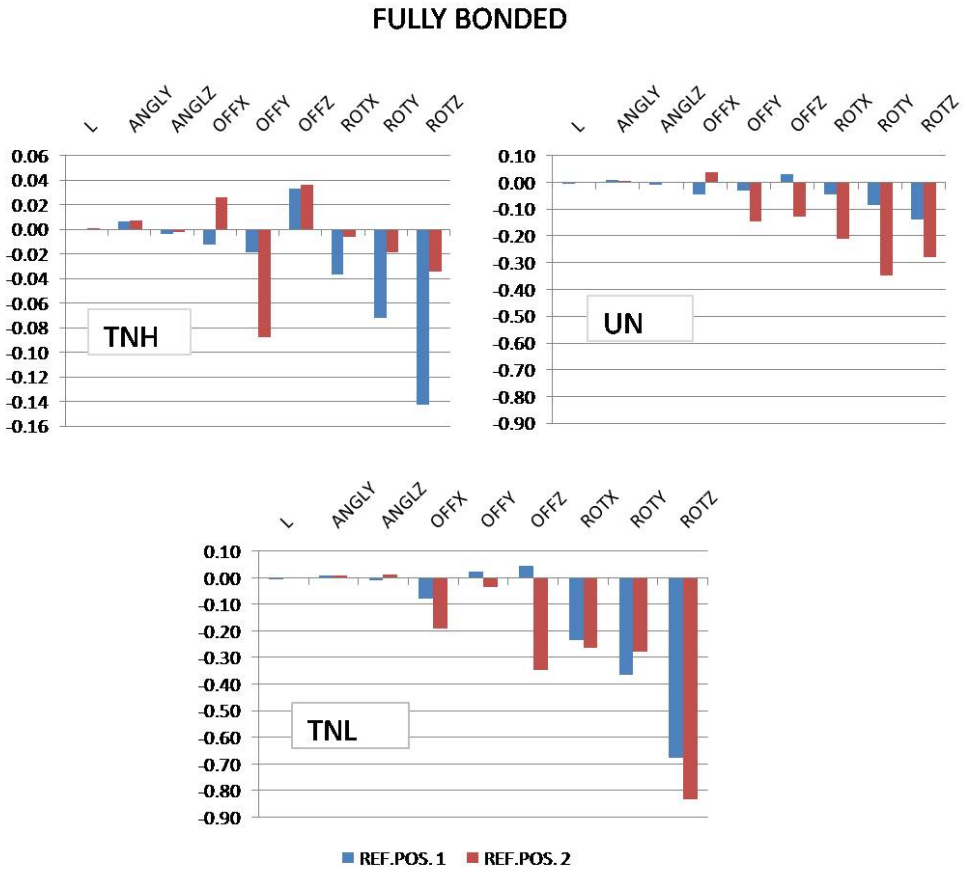

Figure 5.32: Sensitivity of BPER for fully bonded cases, for Femur 2 combined with the IPS prosthesis and UN case, with two different reference positions (REF.POS 1 and REF.POS.2 respectively).

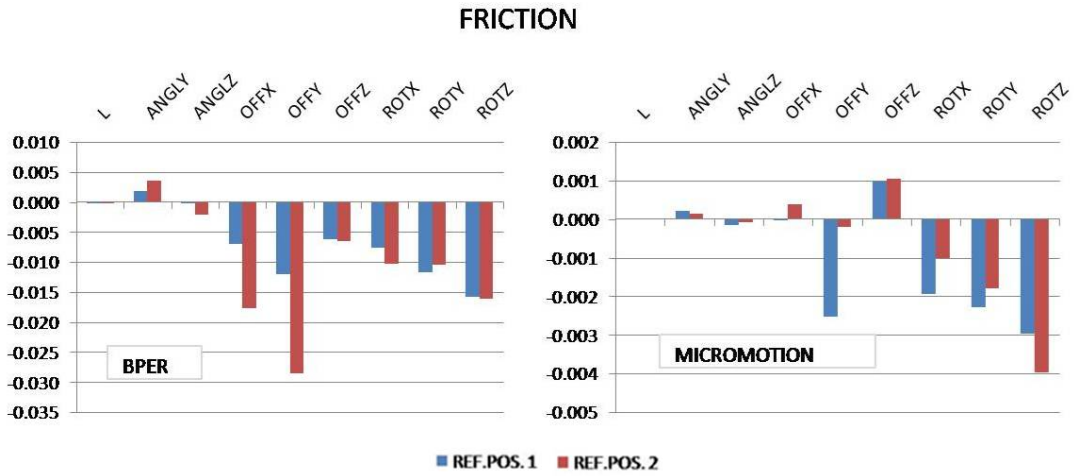

Figure 5.33: Sensitivity of BPER (left) and micromotion (right) for friction interface case, for Femur 2 combined with the IPS prosthesis and UN case, with two different reference positions (REF.POS 1 and REF.POS.2 respectively).

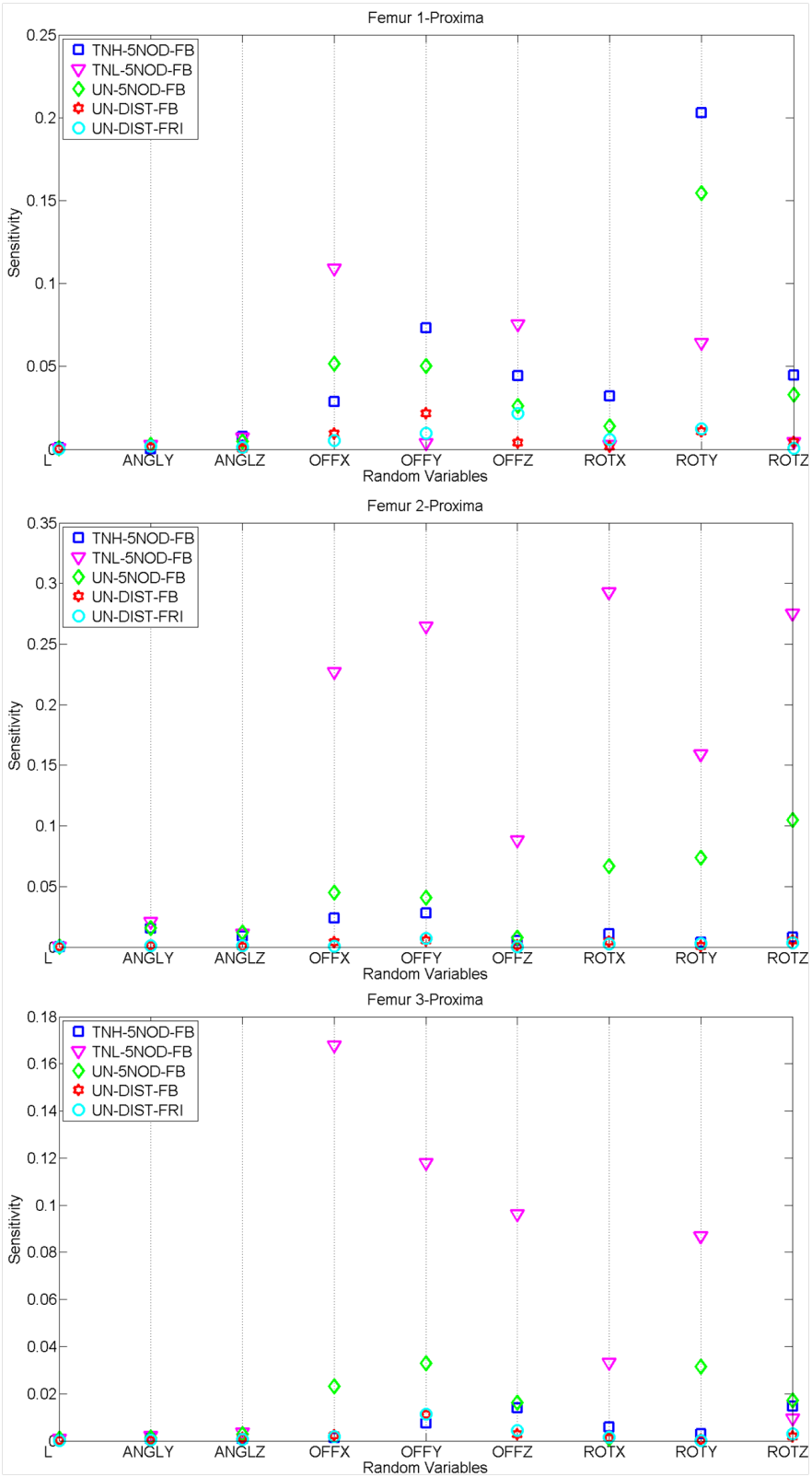

Figure 5.34: Absolute values of sensitivity of BPER for the Proxima implant, with Femur 1 (top), Femur 2 (centre) and Femur 3 (bottom), for all the studies.

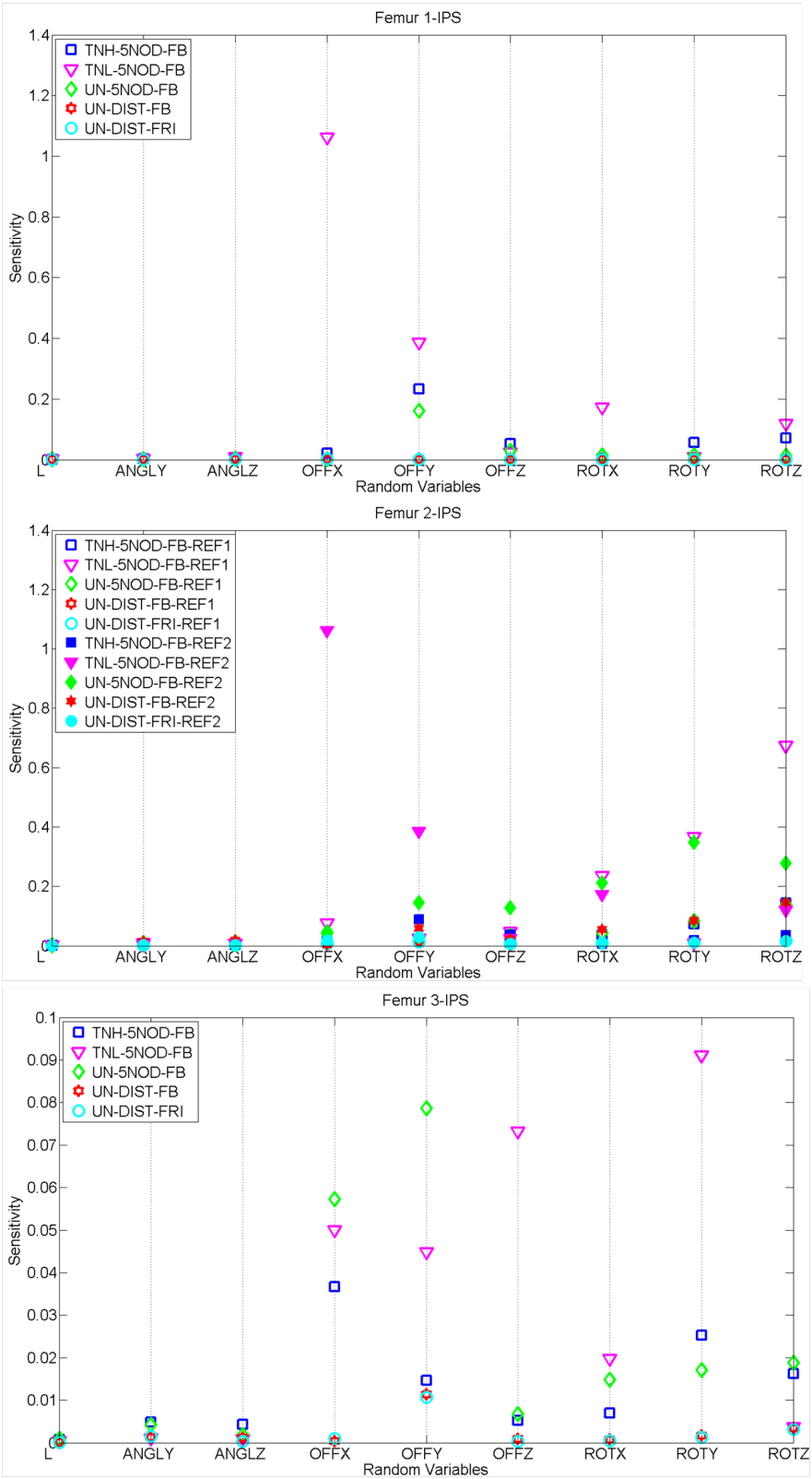

Figure 5.35: Absolute values of sensitivity of BPER for the IPS implant, with Femur 1 (top), Femur 2 (centre) and Femur 3 (bottom), for all the studies.

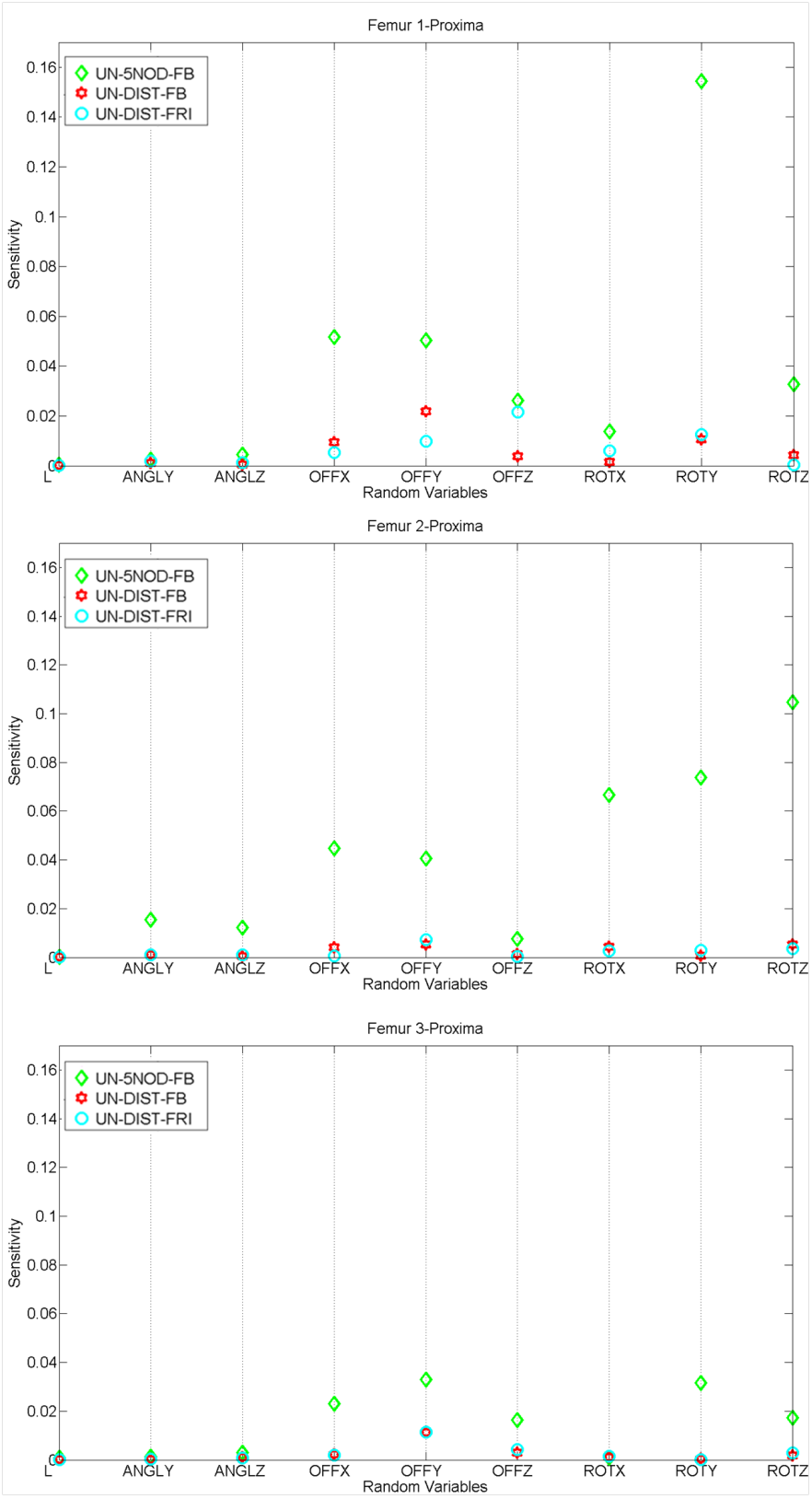

Figure 5.36: Absolute values of sensitivity of BPER for the Proxima implant, with Femur 1 (top), Femur 2 (centre) and Femur 3 (bottom), for the uniform distribution studies.

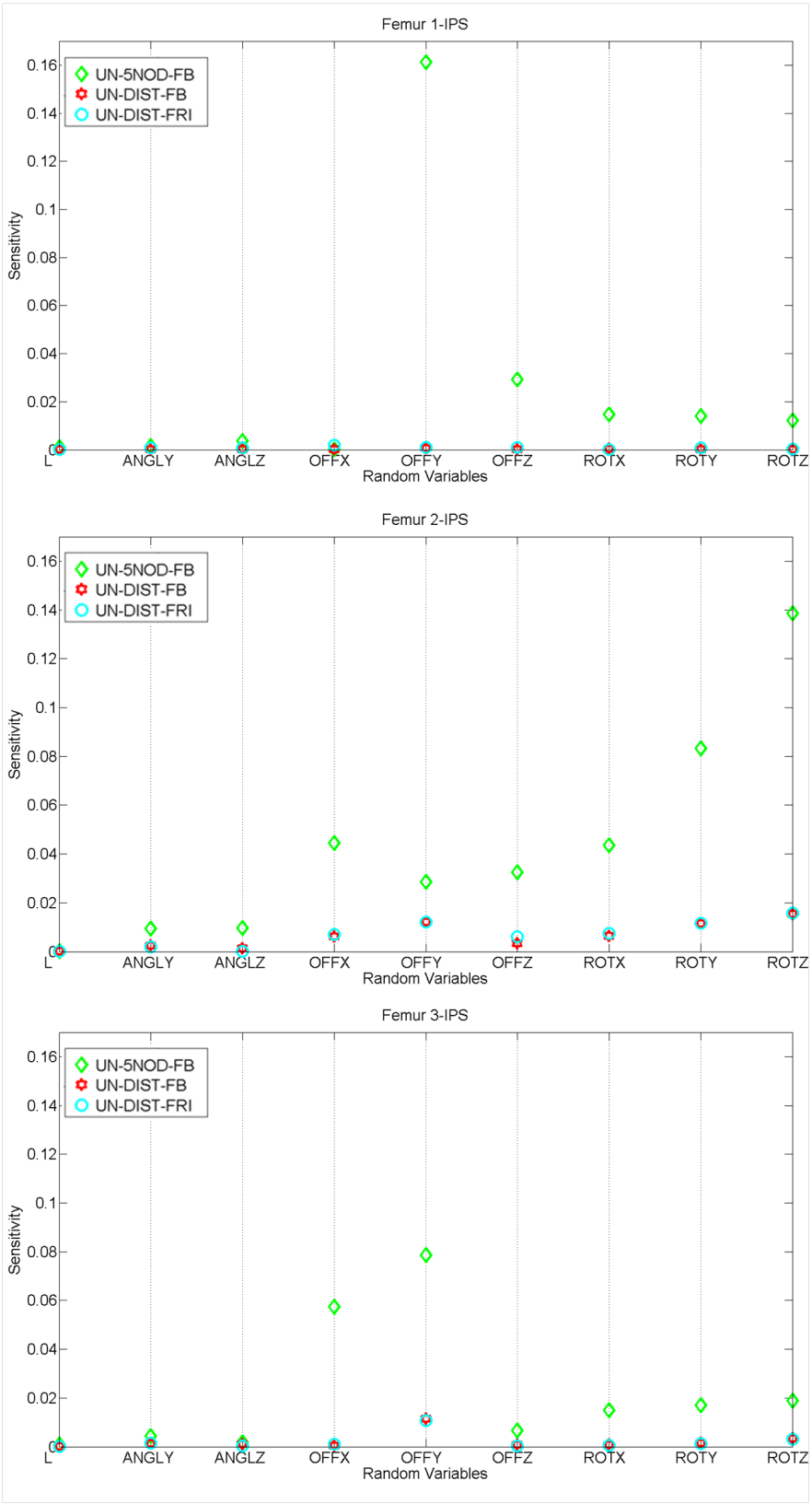

Figure 5.37: Absolute values of sensitivity of BPER for the IPS implant, with Femur 1 (top), Femur 2 (centre) and Femur 3 (bottom), for the uniform distribution studies.

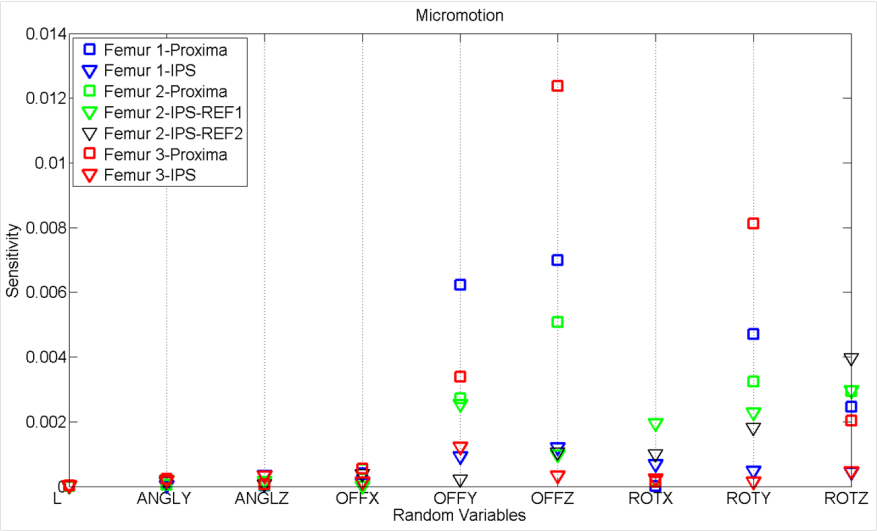

Figure 5.38: Absolute values of sensitivity of Micromotion for all the studies.

5.4 Discussion

The aim of this study was to build a probabilistic finite element model of the uncemented THR which considered implant position variability among the RVs. In order to benchmark the robustness of the implemented methodology, a series of parametric studies were performed. Several models were analysed, combining three different real femurs and two implants, the Proxima and the IPS (see Section 3.2): the effects of different constraints, bone-implant interface condition, statistics of the input random variables, and changes in the implant reference position were assessed.

Together with load magnitude and geometry, the six degrees of freedom of the implant position were considered as RVs.

The percentage of bone volume exceeding a elastic von-Mises strain of 0.8% and the maximum nodal micromotion in the frictional interface case were the performance indicators.

A maximum element size of 6 mm was adopted, according to the results from a convergence study.

Monte Carlo simulations were applied for a total of 35 models, and initially, 1,000 samples with combinations of values of the 9 RVs were randomly created. However, some of the samples had to be rejected since the implant intersected the inner surface of the bone. The 'bad samples' were detected at two stages, one during the geometrical operations and another after meshing. A small number of unconvergent samples were rejected at the end of the simulations. The worst cases occurred with Femur 1, with 50% rejections when combined with the Proxima implant, and a up to 70% when combined with the IPS implant. The statistics of the original, successful and failed samples were plotted for the 9 RVs, for these worst cases, in Figures 5.9 and 5.10. With the exception of OFFX and OFFY, the rest of the RVs showed an excellent agreement between the three sets of samples, even for such a high rate of rejection. This proves that removing the failed samples did not bias the statistics of the successful samples with respect to the original ones. The histograms with fitted normal distributions for OFFX and OFFY (Figures 5.11) showed that the successful and the original samples were more similar than the failed samples. A good indicator is that a higher

concentration of samples around the mean value was found in the successful set, for both RVs. The failed samples were more spread towards the tails of the intervals. This was also shown by the interquartile ranges presented in Table 5.3, which showed the highest values in the failed samples cases, for both RVs. This means that the failed samples had higher variability, they were more spread away from the mean value. This result indicates that, although the distributions of the successful samples were close to the original ones, a better reference position of the implant would be preferable, based on the CDFs of OFFX and OFFY (Figure 5.9). It could be seen that the values of OFFX between -2.5 and 0 mm and values of OFFY between -0.5 and 2 mm were more frequent in the successful samples. Thus moving the reference position towards the middle of these ranges may result in a higher rate of successful samples. This represents the first instance in which the effect of the reference position is evident. In subsequent studies, this factor will be discussed as being one of the most determinant in the results.

One of the limitations of this work was the difficulty in finding a reference position that was the same for all the models. Ideally, the models should have the same reference position so that accurate comparisons can be made between them. However, it was complicated to find a common value of the 6 degrees of freedom of the implant position that would locate the implant in a reasonable position in all the femurs, and with an acceptable rate of successful samples. One of the reasons may be the weak selection of the femoral neck axis. This was the line that contained the approximate centre of the sphere of the femoral head and cut the femoral shaft axis at a 135° angle. A more robust criteria should be selected in the future to determine this axis. A possible solution is to find the axis of the cylinder that best approximates the femoral neck surface, and take this and the approximated centre of the femoral head as points to approximate the femoral neck axis. In this study, the implants were first located with all values of implant position parameters equal to zero, and they were manually altered to find the most reasonable solution for each case.

GENERAL RESULTS

As seen in Figures 5.1 and 5.3, Femurs 1 and 2 had similar stiffness distributions, whereas femurs 1 and 3 had similar length. The thickness of the cortical bone was lowest for Femur 1, followed by Femur 3 and Femur 2, in ascending order. Femur 1 had the thinnest shaft, followed by Femur 2 and Femur 3. These

factors could potentially affect the results, and this will be highlighted throughout the discussion.

The mean value of BPER converged mainly towards values below 2% and the mean value of micromotion was more convergent towards values below $50\mu m$ when combined with the Proxima implant, and below $30\mu m$ for combinations with the IPS prosthesis (Figures 5.12 and 5.13). The values of BPER can not be compared with previous publications since different criteria were chosen to calculate the strain. The fact that the average locations of the maximum strains were more frequently found in the medial section of the femur, between the lesser trochanter and the constrained nodes, as observed in previous studies [86, 88, 83, 87] (Figure 5.15) increases the confidence in the results. For the purposes of discussion, the results are compared with those in the pilot studies (Section 4.3), the mean value of BPER (corresponding to BPER1 in Figure 4.13) converged towards 2.5%, i.e. a 25% higher than the one in the present study. This difference may be justified by the effect of including muscle forces in the model, which may compensate the deformation produced by the hip contact force alone. This outcome confirms the findings of previous publications, which demonstrated the importance of including the main muscle forces in computational and *in vitro* studies of the THR [116, 117, 118, 119].

The values of the maximum nodal micromotion corresponded well with those of previous studies [133, 167, 168]. The average value of the maximum nodal micromotion for the IPS implant was around $30\mu m$ (Figure 5.14), which is the maximum value that has been observed for osseointegration to take place [133].

Kassi *et al.* [133] experimentally simulated several human activities in composite femora implanted with the uncemented CLS prosthesis. They measured the relative micromovements at the bone-prosthesis interface. They found that the largest micromotions averaged $50 \pm 5\mu m$, and were recorded at the approximated centre of mass of the implant in agreement with the present study, in particular for the Proxima prosthesis (Figure 5.16).

Callaghan *et al.* [167] compared the bone-implant micromotions for two different femoral stems, a curved (anatomic) and a straight (Harris-Galante) stem. They applied single-leg and torsional loading to seven pairs of frozen cadaveric femora. The micromotions were measured with extensometers in the proximal

area and at the distal tip of the stem. For axial loading, they measured average values of micromotion of less than $25\mu m$. This agrees with the present results for the IPS stem, which has a similar geometry to the curved stem used in Callaghan's study. For torsional loading, higher micromotions were measured by Callaghan, even closer to the values found in the present study. They also found that the micromotion was lower for the curved stem than for the straight stem, further highlighting the effects of geometry. In the present study, higher micromotions were found with the Proxima implant than with the IPS implant, indicating that higher post-operative stability may be found with long stems than with short stems.

A similar study was developed by Burke *et al.* [168], who evaluated the initial stability of cemented and uncemented femoral components in cadaveric femurs, during single leg standing and stair climbing. They also found higher micromotions under torsional loading during stair climbing simulations, in particular, for the uncemented components. For single-leg standing, values of maximum micromotion of $42\mu m$ were found for the cemented components, and $30\mu m$ for the uncemented implants, close to those observed in the present study. They also found that the uncemented components were less stable than cemented stems under torsional loading, with a maximum value of $280\mu m$ (outlier). This value also corresponds with the outliers of maximum micromotion found in this study. For the Proxima implant, the outliers were around $295\mu m$, and for the IPS they ranged between 277 and $294\mu m$. These findings provides evidence for the robustness of the methodology implemented in this project. They also highlight the importance of initial stability of uncemented implants, particularly in the case of short stem implants.

The strain-based performance indicator used in this study is thought to be a good indicator of the risk of failure of the femur, as some studies have suggested the use of strain-based failure criteria as fracture predictors [171, 129, 130, 17]. It is assumed that the femur will break when a certain amount of bone suffers strains over a limit close to the yield strain, believed to be approximately $0.78\% \pm 0.06$ [17]. Some studies have looked at the changes in stress or strain distributions under varying conditions [165]; the fraction of bone supporting highly strained bone tissue loaded to the apparent yield strain has been measured in experimental studies [166], and hence, suggested as a failure indicator.

One limitation in the implementation of this performance indicator was that all the elements of the bone were considered when computing the von-Mises elastic strains exceeding 0.8%. It is desirable that the percentage of bone volume exceeding this value corresponded to elements that are in the same region. Ideally, those elements exceeding 0.8% of elastic von-Mises strain that are located 'out' of the main region of maximum strains should be rejected. Nevertheless, the values obtained in this study are more conservative than the ideal values, and therefore they represent a good indicator of the risk of failure. In the future, and with the use of a finer mesh, the most likely regions of risk of failure can be defined to check the strains using the same performance indicator.

MEAN VALUES

The effect of different statistics on the mean value of BPER depended mainly on the femur. However, it was seen that different statistics did not lead to substantial changes on the values of BPER within each bone. Femur 1 had the maximum mean values of BPER for both implants (Figure 5.18 and 5.19, top). This had the thinnest shaft and cortical bone, and hence these factors may determine the mean value of BPER. Again, bone geometry seems to highly affect the results. Femur 3 presented more significant variability between different statistics of the RVs than Femur 1 and Femur 2. Similar trends were found for the standard deviations in all cases. Femur 3 had the lowest density of high stiffness elements, therefore this may be the factor that determines the higher variability of BPER. Stiffness distribution uncertainty should be considered in future probabilistic studies. As previously stated, bone material properties and geometry have been shown to affect the output in similar probabilistic studies [66, 67, 68, 69, 70, 71, 164], as it was also evident in the pilot studies (Sections 4.1, 4.2 and 4.3).

The effect that the two different implants had on the mean value of BPER also depended on the femur in which they were implanted. This suggests that the responses of different implant geometries depend on the femur in which it is implanted.

The effect of changes in the constraints on the mean value of BPER was also analysed. With the distal portion constraint (DIST, Figure 5.20), the mean value of BPER was considerably reduced in all cases. In addition, the standard deviations decreased substantially for most of the femurs. As with the empirical

CDFs, the selection of the constraints had a considerable effect on the mean value of BPER.

The effect of bone-implant interface condition (fully bonded versus frictional interface) on the mean values of BPER was also analysed, together with the values of maximum nodal micromotion for the frictional interface cases. In general, the mean value of BPER did not change significantly for both interfaces (Figure 5.20). The same was true with the standard deviations, which were quite similar in both cases. This suggests that fully bonded and frictional interface conditions present similar amounts of bone with von-Mises elastic strains close to the yield strain. The mean value of the maximum nodal micromotion was very similar for all combinations of the three femurs and the two implants, although Femur 1 combined with the Proxima implant presented very high variability (Figure 5.22). Thus, for Femur 1, micromotions were more stable with the IPS than with the Proxima implant, and hence, this behaviour could be repeated with femurs with thin shafts and/or cortical bone. This again highlights the need of including bone related factors in probabilistic analyses.

The effect of changes in the reference position on both the mean value of BPER and micromotion was also analysed (Figures 5.18 and 5.19, red lines and markers for the second reference position, 'REF 2'). For REF 2, the mean value of BPER notably increased, in some cases more than three-fold, for all the fully bonded cases, and slightly increased for the frictional case. These values were almost identical, around 2.50%. Similar trends occurred for the standard deviations. This confirms the influence of the reference position, i.e., the mean value of the implant position parameters, on the values of BPER. However, the mean value of the maximum nodal micromotion did not experience a proportionally high increase, rising from almost $30\mu m$ to about $37.5\mu m$. This may be due to a more consistent behaviour of the maximum micromotion with changes in the reference position, and also to the use of the distal portion constraint for the frictional interface; results with the first implant position were more convergent and stable with lower values.

EMPIRICAL CDFs

The empirical CDFs of the output BPER for the 6 femur/implant combinations are presented in Figures 5.25 and 5.26 to better understand the difference

and/or similarities between cases. The curves were generally smoother and more rapidly convergent for the Proxima implant than for the IPS implant. The lines corresponding to the three different statistics cases for the Proxima implant (blue, magenta and green, Figure 5.25) had a maximum error of 23% at a value of BPER of 2% for Femur 1, and similar for Femur 3. The same lines for the IPS implant (Figure 5.26) presented a maximum error of 80% at a value of BPER of 1.5% for Femur 3. However, the plots for Femur 2 (Figure 5.26) show how the reference position (dashed lines) radically changed the shape, encountering sections with zero slope, as it happened also with Femur 1 for the TNL and UN cases (magenta and green, Figure 5.26, top). Implant reference position had a large effect on the results, therefore it should be carefully selected.

The most representative finding from the empirical CDFs of both implants is that the distal portion constraint significantly changed the curves (cyan and red lines, Figures 5.25 and 5.26); they were much more rapidly convergent, and little difference was present between the fully bonded and frictional contact interface cases, being coincident in most cases. The flat region of the curve for the Femur 1/IPS implant combination also disappeared (magenta and green, Figure 5.26, top). This suggests that the selection of different constraints has a high impact on the amount of bone predicted to suffer high strains. This is directly related to the risk of failure of the construct. Clearly, an accurate representation of the real constraints should be adopted for a reliable quantification of the risk of failure. This has also been suggested by Speirs *et al.* [89], who simulated an FE model of a femur, with nodes constrained in the diaphysis and nodes constrained on the distal condyles, more representative of the physiological constraints. They found that the latter represented most accurately the physiological deflections of the femoral head. The diaphysis constraint models generally produced the lowest strain levels, as in the present case. It is thought that, although the distal portion constraint gives lower and more convergent values of BPER, and it limits the displacement of the whole femur (Figure 5.15), a solution close to the 5 distal nodes constraint may be more representative of the physiological constraints, as it allows more deflection of the femoral shaft.

It can also be seen that, within the same bone, and for the same constraint, the curvature of the lines is very similar, i.e., they present the inflexion points around the same value of BPER, and the slopes after these points are very similar. This

is especially evident for the Proxima implant (Figure 5.25). This is a reflection of the influence of bone features in the results, since they are quite consistent within the same bone, but very different between them.

The influence of bone geometry and material properties has been demonstrated in several probabilistic studies [66, 67, 68, 69, 70, 71, 164]. In addition, the pilot studies (Sections 4.1, 4.2 and 4.3) showed that the bone stiffness was one of the parameters to which the output (maximum nodal micromotions and the same BPER) had the highest sensitivity.

Bah *et al.* [66] looked at the cement maximum von-Misses stress in a cemented THR. They found that the bone geometry was the most sensitive parameter, followed by cement thickness and load magnitude. Mehrez *et al.* [156] applied AMV and RSM methods to a simplified model of a cemented THR, and looked at the relative displacement between the stem and the cement mantle. They found that the most sensitive parameters were the cement material properties, implant geometry, load and bone geometry/material properties. Perez *et al.* [69] performed a MCS on a cemented THR, and looked at the damage accumulation due to fatigue. They considered various implant surface finishes, bone stiffness, load magnitude and muscle loads as RVs, and they found that the performance of the construct was highly dependent on the stem-cement interface conditions. Nicolella *et al.* [70] assessed a cemented THR, and they found that the load, cement strength and implant-cement interface strength most contributed to the POF. Viceconti *et al.* [162], looked at the primary stability (micromotion) of a cementless implant using Monte Carlo simulations. The authors found that the main risk factors for insufficient primary stability were the interface contact, the size of the host bone, and the body weight. In the pilot studies (Section 4.1), the maximum nodal strain in the bone was examined, while considering bone and implant stiffnesses, load magnitude and geometry as random variables. MCS method was performed; bone stiffness and load magnitude were found to be the parameters to which the maximum nodal strain was most sensitive. There is clear evidence in the literature therefore, that the incorporation of bone geometry and material properties variability is necessary in future probabilistic studies.

The effect of implant geometry and surface finishes has been analysed by some authors [88, 86, 87]. Decking *et al.* [88] analysed 3 different hip stems and evaluated their influence on the in vitro strains in the proximal femur. They

found that the implant geometry had an effect on the strain distribution of the implanted femur. Tanner *et al.* [85] found out that interface contact stress levels were lower under the proximal neck with a full length implant stem, compared to those of a similar implant with a short stem [85]. Studies have also found different values of bone-impant micromotion for different implant designs [167]. The above findings suggest that implant design has an effect on the stress and strains found in the bone, but this in turn depends significantly on the bone. If bone variability is considered in the future, the influence of implant design will be more accurately described, and therefore decisions on the best implant in patient specific scenarios can be reliably taken.

The empirical CDFs of the maximum nodal micromotion for all femur/implant combinations were presented in Figure 5.27. A good convergence was achieved for all the models. For combinations with the Proxima implant, the CDF of Femur 1 and 3 were almost identical (blue and red continuous lines), and Femur 2 converged more rapidly (green continuous line). The average maximum micromotion, corresponding to the value with a 50% probability of occurring, was always below $50\mu m$. In summary, the three femurs behaved similarly with the Proxima implant when maximum nodal micromotion was assessed, i.e., with little dependence on the different bones. In addition, the values of micromotion found here highly agree with those in the literature, as previously stated. The robustness of micromotion as a performance indicator may also hold true for similar short stem implant designs.

The empirical CDFs of the IPS also showed a good agreement (dashed lines), with the three femurs highly convergent for values between 0 and $50\mu m$, although in this case there was more variation between the curves. Thus, for this output, the IPS performance was slightly less stable than the Proxima. The change in reference position did not affect the CDF significantly (black dashed line). The agreement with published values and the high convergence for the three femurs highlights the suitability of the maximum nodal micromotion as a performance indicator.

SENSITIVITIES

The absolute values of the sensitivities of the output BPER for the 6 femur/implant combinations are presented in Figures 5.34 and 5.35. Magnitudes

of the sensitivities were highest for the TNL case, regardless of the femur and implant (magenta triangle). The TNH and UN cases presented similar values and relative sensitivities. However, the relative sensitivities were similar within each femur in combination with the Proxima implant (Figure 5.34), regardless of the statistics of the inputs, the interface condition or the constraint. The same did not happen with the IPS (Figure 5.35), which presented more variability of the relative sensitivities with different statistics of the inputs, while for the distal portion constraint they were almost constant.

For the Proxima implant in the TNH and UN cases, the sensitivities were highest to ROTY, i.e. closest to a rotation around the neck axis or 'torsion'. The next most sensitive parameter was ROTZ, i.e., around an axis perpendicular to the plane that contains both the femoral shaft and the neck axes or 'inclination'. Following this, the sensitivities to ROTX (or 'version'), OFFY, OFFX, and OFFZ were also relatively high. Similar results were obtained for the IPS implant, where Femur 1 presented the highest sensitivities, in particular in the TNH and UN cases. However, in this case sensitivities were highest to OFFY, i.e., moving the implant towards or away from the centre of the femoral head had the highest impact on the value of BPER compared to the other parameters. Following this, sensitivities to ROTZ (inclination) and ROTY (torsion) were significantly high, and to ROTX (version), OFFX and OFFZ were relatively high. For both implants, sensitivities to implant position parameters were higher than to load magnitude and geometry in all cases. This highlights the importance of including these parameters in probabilistic analyses of implanted bones.

A change in the reference position of Femur 2/IPS implant (Figure 5.35, filled markers, centre) had a great effect on the magnitude of the sensitivities of BPER, and also some effect on the relative values. The selection of the reference position seems to be very important for this performance indicator.

Figures 5.36 and 5.37 show the sensitivities of the cases where the uniform distribution of the input variables was adopted, i.e., changes in constraints, interface conditions and reference position. The distal portion constraint cases, both fully bonded (UN-DIST-FB) and frictional interface cases (UN-DIST-FRI) showed lower magnitudes of sensitivity for all femur/implant combinations. Each femur presented almost identical sensitivities in both fully bonded and frictional interface cases when distal portion constraint was applied (blue and red markers),

regardless of the implant. This suggests that, when a distal portion constraint is adopted, the percentage of strained bone volume is similar within each femur/implant combination, with no effect of interface contact. A small difference between both interface cases was found for Femur 1, suggesting a possible influence of femur shaft thickness. However, the main effect was produced by the change in the constraints. These results suggest that the model should represent accurately the real constraints in order to get reliable results. If, as has been noted earlier, the physiological constraints were closer to the 5 distal nodes constraint, then the sensitivities to implant position related parameters were more significant.

Both implants presented similar sensitivities to all the implant position parameters within each femur, with the highest difference in Femur 1. This is especially noted in the UN-5NOD-FB case (green markers), were a similar profile is evident for the same femur with the two implants. Therefore, implant geometry may only have a mild effect on the relative sensitivities compared to femur variability. Femur 2 showed a slightly higher sensitivity to load orientation (ANGLY, ANGLZ, Figures 5.34 and 5.35, middle plots). These results suggest that femur geometry has an impact on the magnitude of the sensitivities, and implant geometry has a mild effect on the relative sensitivities. In any case, implant positioning has a higher impact than load magnitude and orientation on the amount of bone suffering high strains, and this impact is more important than implant geometry. However, the noted sensitivities to load orientation for Femur 2 suggests that further investigation should account for femur variability features together with load orientation to benchmark a possible relation between both sources of uncertainty. In addition, the importance of implant orientation suggests that future effort should concentrate on improving its primary stability, rather than on its design. This involves investigations to improve the techniques, tools and resources that can help to reduce the variability in the placement of the implant in the bone during the surgery.

As mentioned in the pilot studies (Sections 4.1, 4.2 and 4.3), the influence of implant positioning has been considered by some researchers, and some studies have looked at parametric variations of implant version angle (equivalent to ROTX) and some offsets [11, 89].

Nishii *et al.* [11] found that the manipulation of the cup version angle to

compensate for high femoral neck anteversion was related to postoperative dislocation. Speirs *et al.* [89] looked at the effect of an increased anteversion and an offset on the stress and strains of the femur with a short stem implant. They found that a reduction in strain energy density and therefore stress shielding was seen when implant position was varied from the neutral position, which may have consequences for longer-term remodelling.

Aamodt *et al.* [90], found that the patterns of the principal strains in the proximal femur varied for anatomical and customized stems in human cadaver femurs, which could be related to any differences in neck version angle. The implants analysed in the present study had similar proximal shape, i.e., similar angles between the implant axes. This resulted in the sensitivities to implant version being equivalent for both implants. It should be noted that the maximum variability in implant version adopted in this study was between -6 and 7°, i.e., an amplitude of 13°. This amplitude is similar to those found in clinical studies, where variability around the neutral position of the implant was found to be between ±6.2 and ±6.5° [92, 11, 12]. This suggests that the sensitivity results for ROTX are realistic. This study showed that sensitivities to ROTY or to OFFY may be more important than to implant version, and future work should be focused on reproducing the real variability of these parameters in order to get more accurate results.

The absolute values of the sensitivities of the maximum nodal micromotion are presented in Figure 5.38. Sensitivities for the Proxima implant were generally much higher than for the IPS implant in all cases (square markers). Although the magnitude of the sensitivities varied between femurs, it was noted that the relative sensitivities were very similar. Maximum sensitivities to (in this order) OFFZ , ROTY (torsion), OFFY and ROTZ (inclination) were common for both implants. Furthermore, the change of reference position for Femur 2/IPS implant did not have much influence on the sensitivities (black and green triangles). For the IPS implant, the highest sensitivities occurred for Femur 2, which presented the longest shaft, while femurs 1 and 3 had almost identical sensitivities, and also had similar cortical bone thickness. Again, femur variability seems to affect the magnitude of the sensitivities to maximum nodal micromotion. In summary, implant geometry has the highest effect on the sensitivities of maximum nodal micromotion, while femur variability also had a significant effect. However, a

change in implant reference position, i.e., mean value of implant position parameters, did not have a significant effect on the sensitivities, in contrast to the sensitivities of BPER.

As previously stated, the values of maximum nodal micromotion were very similar to those found in previous studies [133, 167, 168]. There are no probabilistic studies that have looked at micromotion as the output parameter; however parametric studies indicate an implant geometry effect [167]. Callaghan *et al.* [29] showed that a curved stem, similar to the IPS implant, produced less micromotions than a straight stem, with values less than $25\mu m$, similar to those obtained in the present study.

In summary, the sensitivities of BPER were greatly affected in magnitude and relative values by the selection of different statistics of the input variables, especially for the TNL case. The femur had a significant effect on the magnitude and relative values of the sensitivities, while the implant variability had only a mild effect on some of the magnitudes. The distal portion constraint greatly decreased the magnitudes, as did the changes in implant reference position. The interface condition did not seem to affect the sensitivities substantially; however, the frictional interface cases were modelled with the distal portion constraint, which has been seen to highly decrease the sensitivities of BPER. This could be the reason for its stability with changes in reference position and femur variability.

In all cases, and for both performance indicators, sensitivities to implant position parameters were much higher than to load magnitude and orientation. A most important finding of the present research therefore, is that efforts should be focussed on improving surgical approaches and techniques to decrease the variability of bone-implant relative position parameters, in order to predict the behaviour of the UTHR with more confidence.

Chapter 6

General Conclusions and Future Development

6.1 Conclusions

The combination of Finite Element modelling with probability methods enables the simulation of multiple scenarios in much reduced times compared to those of experimental or parametric studies. It allows a large number of data to cover the full domain of values of a system with no need for experimental realizations. In the case of implant design, it has the potential to identify the key factors that have a major effect on the performance of the construct. Consequent actions can be taken to control their uncertainties and improve the predictions of the behaviour of the system, such as investigation of surgical approach and implant design. Some authors have applied probability methods to orthopedic systems, and they found that parameters such as bone, implant or cement material properties and geometry had an influence on the chosen output. However, none of them included uncertainty in the bone-implant positioning, due to the challenge of its computational implementation. This work achieved this challenge, and several parametric applications confirmed the reliability of the computational tool.

The aim of the present work was to build a computational tool to perform probabilistic finite element analyses of the uncemented hip replacement using

Monte Carlo simulation (MCS) techniques. This process was automated to enable the analyses to be conducted as efficiently as possible. A set of priorities were established in two different stages:

- In the first stage, the priority was to implement a simple probabilistic model of a simplified finite element model of the uncemented hip replacement. Bone and implant stiffness and load magnitude and geometry were the selected random variables. The efficiency of latin hypercube sampling (LHS) method was analysed. Once the PFEM was achieved, an important implant position parameter, the implant version, was introduced as a random variable. The model was refined by introducing a more robust performance indicator. The bone percentage of volume exceeding von-Mises elastic strains of 0.8% was chosen as the output parameter for these and the main studies.
- In the second stage, the priority was to ijmplement a probabilistic model that enabled variability in implant positioning in the six degrees of freedom on a more realistic finite element model of the uncemented THR. Muscle forces were applied, bone properties were assigned from the CT scans, and fully bonded and frictional bone-implant interface conditions were modelled on combinations of three different proximal femurs with two different implants. The probabilistic finite element model (PFEM) was implemented and its reliability was analysed through several parametric studies: the effects of statistics of the input variables, interface conditions, constraints and implant reference position were analysed. Together with the bone percentage of volume exceeding von-Mises strain of 0.8%, the maximum nodal micromotion was adopted as an output parameter in the frictional interface cases.

The main conclusions from all the above studies, are presented below:

- In the pilot studies, the parameters that most affected the value of the performance indicator depended on the considered set of RVs.
- For the first model (Section 4.1), the bone stiffness, followed by the load magnitude and the prosthesis stiffness were the most sensitive parameters. The load angle did not seem to affect the results significantly. The results

suggested that the number of simulations run is important in order to obtain reliable sensitivity analyses. Indeed, the probability of obtaining a certain output value changed with the number of simulations.

The most significant parameters were the same for 1,000 and 10,000 LHS simulations as for 10,000 DS simulations. This suggested that it is possible to determine the most important parameters with 1,000 simulations using LHS at significantly reduced computational expense, although a last larger trial of for example 100,000 simulations would be necessary to confirm the convergence of these results.

- For the second model (Section 4.2), the parameters that most affected the value of the maximum strain depended on the number of simulations. The implant version angle became one of the most sensitive parameters, together with the bone stiffness and load magnitude. A last trial of a higher number of simulations would be necessary to confirm the convergence of these results.

  The application of Latin Hypercube sampling for 1,000 simulations presented similar results to DS. However, the change in results for 10,000 simulations suggests that the efficiency of LHS should be demonstrated with a number of simulations between 1,000 and 10,000.

- For the third model (Section 4.3) the refinement of the failure criteria produced consistent results for 100 and 1,000 simulations and results were in agreement with the previous model. These findings suggest that:

  1. The addition of new random variables may change the sensitivity results.
  2. Including the implant version angle showed the maximum nodal strain in the bone was a weak performance indicator highlighted by the inconsistency of the sensitivity to load magnitude.
  3. The application of LHS was suitable (accurate and efficient) for the first model but its efficiency was not completely demonstrated when the implant version angle was considered. However, it was noted that the sign of the sensitivities were closer to those of a higher number of simulations.

4. The system was highly sensitive to the implant version angle, together with bone stiffness and load magnitude.
5. The bone volume percentage under limit strains was seen to be a robust performance indicator.

In practice, these findings suggest that further investigation should focus on improving tools and resources to control the variability of implant positioning. In addition, heterogeneity in the bone should be considered in further work. The pilot studies used a simplified model to reduce computational cost. With additional computational resources, the inclusion of parameters such as muscle forces or interface friction, together with bone heterogeneity, would make the model more clinically representative. Some of these improvements were considered in the models investigated in Chapter 5.

- The main limitation of the pilot studies was the inability to account for variability in all degrees of freedom of the implant position due to software limitations. In fact, the amplitude of the implant version had to be kept very low. For this reason, more suitable software was adopted to perform different operations on the models in the main studies.

- In the main studies (Chapter 5), the implementation of the PFEM was successfully fulfilled with a Visual Basic module that linked three programs: Rhinoceros, to perform the boolean operations; Ansys ICEM-CFD to mesh the models; and Ansys, to perform the FE simulations.

- Values of micromotion found in previous studies highly agree with the ones obtained in this study, especially for the IPS stem. This confirmed the robustness of the methodology implemented in this thesis. These results suggests that initial stability of uncemented implants should be improved to enhance bone ingrowth, especially for the short stem implants.

- Similarities were shown between the results with truncated normal distribution with high standard deviation and with uniform distribution in the statistics of the input variables. This suggests that a uniform distribution may be adopted to get results with enough reliability.

- Implant geometry affected the sensitivity results of the maximum nodal micromotion more than those of BPER: Both implants presented similar

sensitivities of BPER to all the implant position parameters, although for BPER, the Proxima implant was more sensitive to torsion than the IPS implant, and the IPS implant was more sensitive to OFFY than the Proxima implant. However, the implant geometry did have an effect on the sensitivities of the maximum nodal micromotion. The magnitudes of the sensitivities were in all cases higher for the Proxima implant than for the IPS. Nevertheless, the effect of implant geometry on the sensitivity results of both performance indicators was less important than the effect of implant positioning variability.

- Influence of implant geometry was equally important on the empirical CDFs of both performance indicators. The Proxima implant was in general more rapidly convergent than the IPS implant. The CDFs of the Proxima implant was also less influenced by bone variability than the IPS implant. Therefore, variability of the values of the performance indicators with the IPS implant is more significant than with the Proxima implant.

- Sensitivities of BPER to ROTY or to OFFY were in most cases more important than to implant version, and ROTZ in some cases. More effort should be focussed on describing the variability of these implant position parameters, particularly since torsion and inclination seem to be angles less controllable by the surgeon than the anteversion. The findings in this sense represent a considerable change on the importance given to implant version over the other parameters. It is crucial to address ways to control inclination and torsion, together with anteversion, and offset in the mediolateral direction. Due to the difficulties that the surgeon has to deal with during the intervention, where most of the accuracy of the positioning is due to manual manipulation, the engineering community should focus its research on improving methods, such as more precise tools (hardware) and the potential accuracy of computer aided navigation (software).

- The distal portion constraint gave more consistent results, higher convergence and lower sensitivities than the 5 distal nodes constraint. This highlights the need to represent the real physiological constraints, since they have a great influence on the probabilistic values of BPER. It has been hypothesized that, although the distal portion constraint gave more con-

vergent results, a solution close to the 5 distal nodes constrain may be more representative of the physiological constraints, presenting more deflection of the femoral shaft.

- Fully bonded and frictional interface conditions showed similar values of BPER when the distal portion constraint was modelled. This demonstrates the robustness of the implemented model.

- Results of the maximum nodal micromotion were mainly affected by the femur in terms of both convergence for the CDFs, and magnitude of the sensitivities. It is important to note that these models adopted the distal portion constraint; this made the models much more convergent and less sensitive to any parametric variation. More realistic constraints should be considered to benchmark these results.

- Sensitivities of Femur 1 were more variable than for the other femurs, highlighting the effect of femoral shaft size. However, in practical scenarios different implant sizes are selected for different bone sizes. Therefore, variability in implant size should be included to benchmark the influence of femoral shaft size.

- Changes in implant reference position, i.e., the mean value of the implant position parameters, had a great effect on the values of BPER but almost no effect on the results for the maximum nodal micromotion. The latter may be influenced by the distal portion constraint. Further investigation on more realistic constraints should be carried out to benchmark the low dependence of the maximum nodal micromotion on changes of implant reference position.

- The sensitivities to hip load magnitude and direction were minimal, i.e. they did not have a great effect on the probabilistic results. However, a slightly higher effect for Femur 2 was noted, suggesting further investigation of the effect of femur variability is necessary. In any case, the low sensitivity to load variability is advantageous, as the efforts to replicate the same loading conditions in computational and experimental studies can be reduced. A similar configuration may be adopted in both types of studies if validation is sought, as it does not have a great effect on the strain distribution and the maximum nodal micromotion.

- There were a few simplifications regarding the finite element models, namely: 4 noded tetrahedral elements, materials were linear, elastic and isotropic, and a 6 mm maximum element size was chosen after performing the convergence study. The accuracy of the values of maximum nodal micromotion found in this work suggests that these simplifications do not distort the real values, and therefore the values obtained with a finer mesh and non linear elements would not differ significantly from the simplified models presented in this study.
- The inclusion of muscle forces resulted in a reduction of the sensitivity to load magnitude, compared to the results obtained in the pilot studies. This is an evidence of the importance of including muscle forces in these models, particularly in probabilistic analyses. A better understanding of the correlations of the muscle forces between them and with the hip contact force should be accomplished for an accurate modelling of inter-patient and intra-patient uncertainties.

6.2 Future Development

Although the study has been successful in achieving its aim, a number of limitations were noted that should be considered in future developments of this work:

- Bone variability, for example in geometry and material properties, should be considered, since this work highlighted inconsistencies in the probabilistic results that need further analysis. This would be necessary to allow a more accurate characterisation of the influence of implant design. This is crucial in pre-operative planning, when a decision about the implant to use may need to be made.
- A more robust reference system can be defined identifying different landmarks on the bones, which may also help to describe their geometric variability. This may enable the repetition of the reference position of the implants in different bones, ensuring better comparisons between them.
- The strain-based failure criteria used in the main studies could be refined, and nodes in areas most likely to failure could be used to investigate the

strained volume. This approach would be more representative to find the risk of failure of the bone.

- Constraints have been found to markedly influence the magnitude of the outputs and relative sensitivities, hence accurate physiological constraints should be applied for reliable probability results. However, it does not seem to highly affect the relative sensitivities, hence a trade off between convergence and accuracy must determine their selection.

- It was shown that sensitivities to ROTY or to OFFY can be more important than to implant version. Hence, future work should be focused on reproducing the real variability of these parameters.

- As more computational power becomes available, and with accurate data from clinical studies, more appropriate representations of muscle forces, their variability and their correlations with the hip contact force should be investigated.

- The osteotomy differed for the three bones. Further investigation on the influence of this variability should be carried out.

- As with any computational study, experimental validation would be desired to verify the results. Selected implant positions need to be verified experimentally and compared with the computational predictions. This could incorporate some variability to account for worst case positions. However, this would only be qualitative because not all variables would be able to be considered.

- Further work should be addressed to investigate the efficiency of Latin Hypercube sampling for implant positioning variability, since it has the potential to get accurate results with a reduced number of simulations.

- The number of simulations needed to produce consistent results was variable, and varied according to the simulation method used. It would be important to assess the number that is necessary to run in order to get accurate and reliable results, while achieving manageable runtimes.

Appendix A

Publications

A.1 Publications

Three conference papers have been published from this body of work to date, these being:

- Carolina Dopico-González, Andrew M New and Martin Browne (2007) *Probabilistic Analysis of an Uncemented Total Hip Replacement*, Oral presentation in European Society of Biomechanics Workshop 2007: Finite Element Modelling in Biomechanics and Mechanobiology. Dublin, Ireland.
- Carolina Dopico-González, Andrew M New and Martin Browne (2008) *Probabilistic Analysis of an Uncemented Hip Replacement Considering Implant Version*, Oral presentation in Computational Modelling in Biomechanics and Biomedical Engineering Conference. Porto, Portugal
- Carolina Dopico-González, Andrew M New and Martin Browne (2008) *Probabilistic Analysis of an Uncemented Hip Replacement Considering Implant Version*, Poster presentation in European Society of Biomechanics Congress. Lucerne, Switzerland. Published in Journal of Biomechanics.

Three journal papers have been written based on work in this thesis, one of them has been published, and two of them are under peer review process:

- Carolina Dopico-González, Andrew M New and Martin Browne (2009) *Probabilistic Analysis of an Uncemented Hip Replacement.* Medical Engineering Physics, 15-January-2009. Journal impact index: 1.471.

- Carolina Dopico-González, Andrew M New and Martin Browne (2008) *A Computational Tool for the Probabilistic Analysis of an Uncemented Hip Replacement Considering Implant Version.* Computational Methods in Biomechanics and Biomedical Engineering. Accepted for publication. Journal impact index: 0.779.

- Carolina Dopico-González, Andrew M New and Martin Browne (2009) *Probabilistic finite element analysis of the uncemented hip replacement effect of femur characteristics and implant geometry.* Journal of Biomechanics. Submitted for revision. Journal impact index: 2.897.

Appendix B

Probability Functions

B.1 Probability Functions

The mathematical definition of a discrete probability function, $p(x)$, is a function that satisfies the following properties:

1. The probability that x can take a specific value is $p(x)$. That is

$$P[X = x] = p(x) = p_x \tag{B.1}$$

2. $p(x)$ is non-negative for all real x.

3. The sum of $p(x)$ over all possible values of x is 1, that is

$$\sum_j p_j = 1 \tag{B.2}$$

where j represents all possible values that x can have and p_j is the probability at x_j. One consequence of properties 2 and 3 is that $0 \leq p(x) \leq 1$.

The mathematical definition of a continuous probability function, f(x), is a function that satisfies the following properties:

1. The probability that x is between two points a and b is

$$p[a \leq x \leq b] = \int_a^b f(x)dx \tag{B.3}$$

2. It is non-negative for all real x.

3. The integral of the probability function is one, that is:

$$\int_{-\infty}^{+\infty} f(x)dx = 1 \tag{B.4}$$

Since continuous probability functions are defined for an infinite number of points over a continuous interval, the probability at a single point is always zero. Probabilities are measured over intervals, not single points. That is, the area under the curve between two distinct points defines the probability for that interval. This means that the height of the probability function can in fact be greater than one. The property that the integral must equal one is equivalent to the property for discrete distributions that the sum of all the probabilities must equal one. Continuous probability functions are referred to as probability density functions (*pdf*). For a continuous function, the *pdf* is the probability that the variate has the value x. Since for continuous distributions the probability at a single point is zero, this is often expressed in terms of an integral between two points (Equation B.5).

$$\int_{-\infty}^{+\infty} f(x)dx = Pr[a \leq X \leq b] \tag{B.5}$$

Figure B.1 shows the plot of a normal pdf.

The cumulative distribution function (cdf) is the probability that the variable takes a value less than or equal to x. That is:

$$F(x) = Pr[X \leq x] = \alpha \tag{B.6}$$

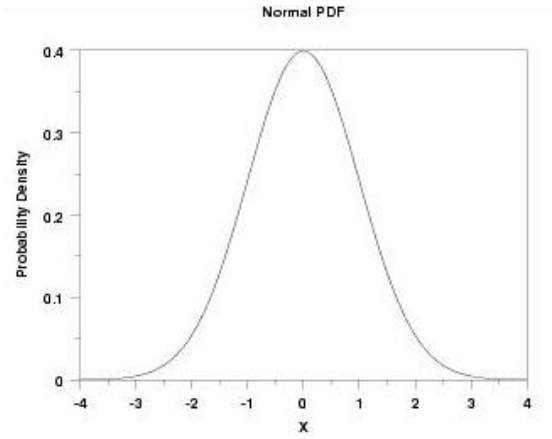

Figure B.1: Normal probability distribution function

For a continuous distribution, this can be expressed mathematically as:

$$F(x) = \int_{-\infty}^{x} f(u)du \tag{B.7}$$

Figure B.2 shows the plot of the normal cdf.

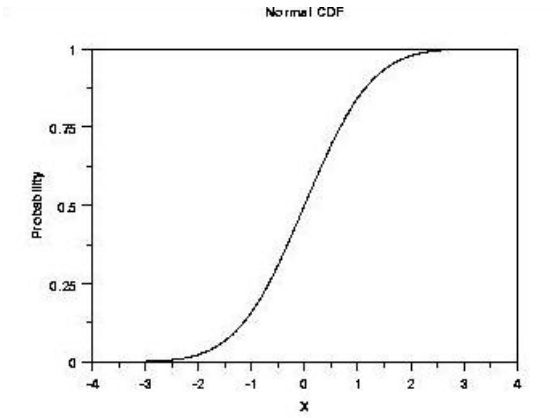

Figure B.2: Normal cumulative distribution function

The horizontal axis is the allowable domain for the given probability function. Since the vertical axis is a probability, it must fall between zero and one. It increases from zero to one as we go from left to right on the horizontal axis.

The inverse of the cumulative distribution function is also called the percent point function (ppf). For a distribution function the probability that the variable is less than or equal to x for a given x is calculated. For the inverse of the cumulative distribution function, we start with the probability and compute the

corresponding x for the cumulative distribution. Mathematically, this can be expressed as:

$$Pr[X \leq G(\alpha)] = \alpha \tag{B.8}$$

or alternatively:

$$x = G(\alpha) = G(F(x)) \tag{B.9}$$

Figure B.3 shows the plot of the normal inverse distribution function.

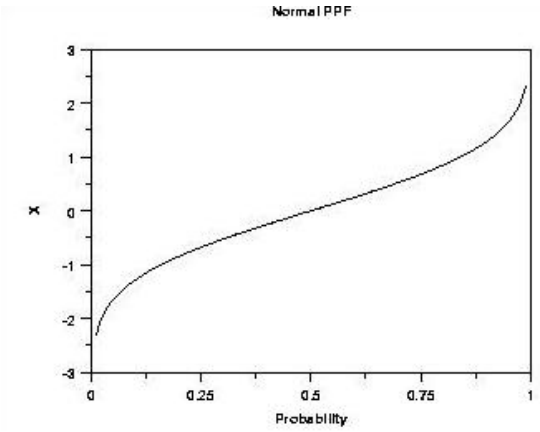

Figure B.3: Inverse normal cumulative distribution function

Since the horizontal axis is a probability, it goes from zero to one. The vertical axis goes from the smallest to the largest value of the cumulative distribution function.

Survival functions are most often used in reliability. The survival function is the probability that the variate takes a value greater than x.

$$S(x) = Pr[X > x] = 1 - F(x) \tag{B.10}$$

Figure B.4 show the plot of the normal survival function.

For a survival function, the y value on the graph starts at 1 and monotonically decreases to zero. The survival function is the inverse of the cumulative distribution function.

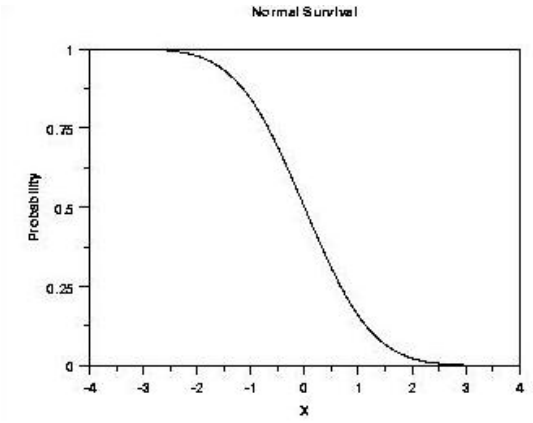

Figure B.4: Survival normal function

The hazard function is the ratio of the probability density function to the survival function, $S(x)$.

$$h(x) = \frac{f(x)}{S(x)} = \frac{f(x)}{1 - F(x)} \tag{B.11}$$

Figure B.5 shows the plot of the normal distribution hazard function.

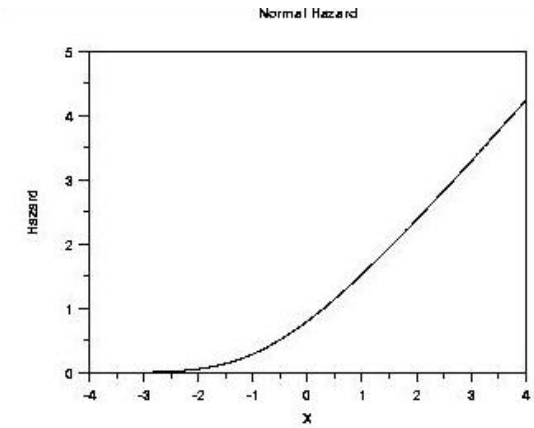

Figure B.5: Normal distribution hazard function

Hazard plots are most commonly used in reliability applications.

The aim of probability distributions is to model the data. This involves the determination of the best-fitting distribution and the estimation of the parameters for that distribution. There are various methods, both numerical and graphical, for estimating the parameters of a probability distribution, such as maximum likelihood or least squares [19].

B.2 Typical Distribution Functions

Detailed information on a few of the most common distributions can be found in the literature [172]. Some of the most common distribution functions are the normal, lognormal and uniform density distribution functions, whose plots and equations are:

Normal distribution:

$$f(x) = \frac{e^{\frac{-(x-\mu)^2}{2\sigma^2}}}{\sigma\sqrt{2\pi}} \tag{B.12}$$

where μ is the location parameter and σ is the scale parameter [19].

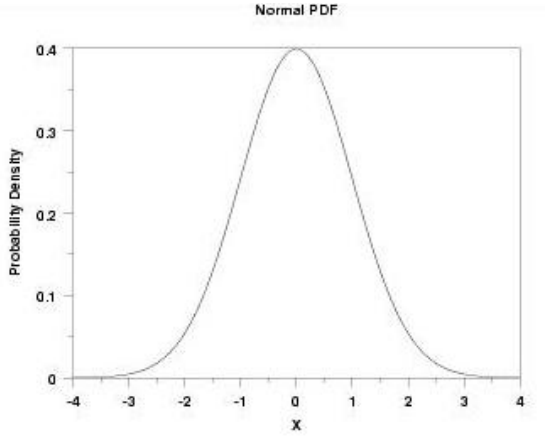

Figure B.6: Normal distribution function

The normal distribution is probably the most important distribution in statistics. Many classical statistical tests are based on the assumption that the data follow a normal distribution. In modelling applications, such as linear and nonlinear regression, the error term is often assumed to follow a normal distribution with fixed location and scale. The normal distribution is used to find significance levels in many hypothesis tests and confidence intervals [19]. The central limit theorem provides a theoretical basis for its wide applicability. The central limit theorem basically states that as the sample size becomes large, the sampling distribution of the mean becomes approximately normal regardless of the distribution of the original variable and the sampling distribution of the mean is centered at the population mean, μ, of the original variable. In addition, the

standard deviation of the sampling distribution of the mean approaches $\sigma/\sqrt{N}$.

Lognormal distribution:

$$f(x) = \frac{e^{-((ln((x-\theta)/m))^2/(2\sigma^2))}}{(x-\theta)\sigma\sqrt{(2\pi)}} \tag{B.13}$$

for

$$x \geq \theta; \quad m, \sigma > 0$$

where σ is the shape parameter, θ is the location parameter and m is the scale parameter [19]

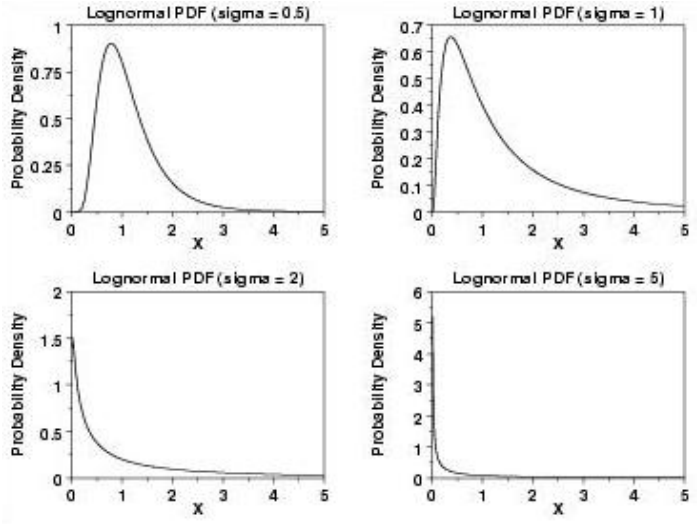

Figure B.7: Lognormal distribution function

The lognormal distribution is used extensively in reliability applications to model failure times.

Uniform distribution:

$$f(x) = \frac{1}{B-A} \tag{B.14}$$

for

$$A \leq x \leq B$$

where A is the location parameter and $(B-A)$ is the scale parameter [19].

The uniform distribution defines equal probability over a given range for a continuous distribution. For this reason, it is important as a reference distribu-

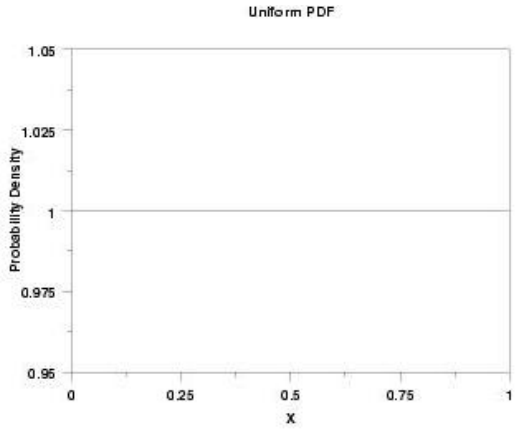

Figure B.8: Uniform distribution function

tion. One of the most important applications of the uniform distribution is in the generation of random numbers. That is, almost all random number generators generate random numbers on the (0,1) interval. For other distributions, some transformation is applied to the uniform random numbers.

Appendix C

Main Studies Data

C.1 Muscle Forces

	Femur 1	**Femur 2**	**Femur 3**	
Gluteus Minimus 1	-93.41	-86.1770	-94.4750	X
	-11.0738	-44.2855	-9.4440	Y
	-23.0719	-2.4923	-19.0338	Z
Gluteus Minimus 2	-92.2757	-94.8074	-93.3627	X
	6.5574	-27.3093	7.3517	Y
	-37.0373	-14.5135	-33.9954	Z
Gluteus Minimus 3	-86.6447	-102.2642	-87.8705	X
	28.2256	-4.8615	27.7124	Y
	-56.9386	-32.8921	-55.2688	Z
Gluteus Medius 1	-221.1824	-168.3625	-225.4163	X
	-112.3301	-185.2311	-107.1347	Y
	-33.6103	5.8166	-19.2420	Z
Gluteus Medius 2	-177.4105	-166.6315	-178.8517	X
	-8.1806	-72.2454	-4.7682	Y
	-37.7347	2.4474	-30.7728	Z
Gluteus Medius 3	-170.9275	-193.2293	-172.3090	X
	52.7976	-12.6400	53.4527	Y
	-82.1828	-35.9681	-78.7677	Z
Iliopsoas	-481.8674	-392.1126	-486.2308	X
	-138.9206	-305.7086	-125.1379	Y
	-24.6667	70.3514	0.6435	Z
Vastus Medialis	-0.2293	-0.2867	-0.2222	X
	-0.2536	-0.2917	-0.2739	Y
	-0.3266	-0.2833	-0.3311	Z

Table C.1: Values of the muscle forces applied to the models in Newtons (N).

C.2 Statistics of the Random Variables

	Distribution	**Mean (SD) [limit1,limit2]**
L (N)	Truncated Normal	1775 (260) [1200,2200]
ANGLY (°)	LogNormal	90 (30)
ANGLZ (°)	Truncated Normal	45 (15) [0,90]
OFFX (mm)	Truncated Normal	0 (2) [-3,3]
OFFY (mm)	Truncated Normal	0 (1.5) [-2,2.5]
OFFZ (mm)	Truncated Normal	0 (1.5) [-2.5,2.5]
ROTX (°)	Truncated Normal	0 (5) [-6,7]
ROTY (°)	Truncated Normal	0 (3) [-5,5]
ROTZ (°)	Truncated Normal	0 (3) [-5,5]

Table C.2: Statistics of the random variables for high standard deviation (SD).

	Distribution	**Mean (SD) [limit1,limit2]**
L (N)	Truncated Normal	1775 (260) [1200,2200]
ANGLY (°)	LogNormal	90 (30)
ANGLZ (°)	Truncated Normal	45 (15) [0,90]
OFFX (mm)	Truncated Normal	0 (0.5) [-3,3]
OFFY (mm)	Truncated Normal	0 (0.25) [-2,2.5]
OFFZ (mm)	Truncated Normal	0 (0.25) [-2.5,2.5]
ROTX (°)	Truncated Normal	0 (1) [-6,7]
ROTY (°)	Truncated Normal	0 (0.5) [-5,5]
ROTZ (°)	Truncated Normal	0 (0.5) [-5,5]

Table C.3: Statistics of the random variables for low standard deviation (SD).

	Distribution	**Mean (SD) [limit1,limit2]**
L (N)	Truncated Normal	1775 (260) [1200,2200]
ANGLY (°)	LogNormal	90 (30)
ANGLZ (°)	Truncated Normal	45 (15) [0,90]
OFFX (mm)	Uniform	[-3,3]
OFFY (mm)	Uniform	[-2,2.5]
OFFZ (mm)	Uniform	[-2.5,2.5]
ROTX (°)	Uniform	[-6,7]
ROTY (°)	Uniform	[-5,5]
ROTZ (°)	Uniform	[-5,5]

Table C.4: Statistics of the random variables for Uniform Distributions.

C.3 Empirical Cumulative Distribution Functions of the Input Random Variables

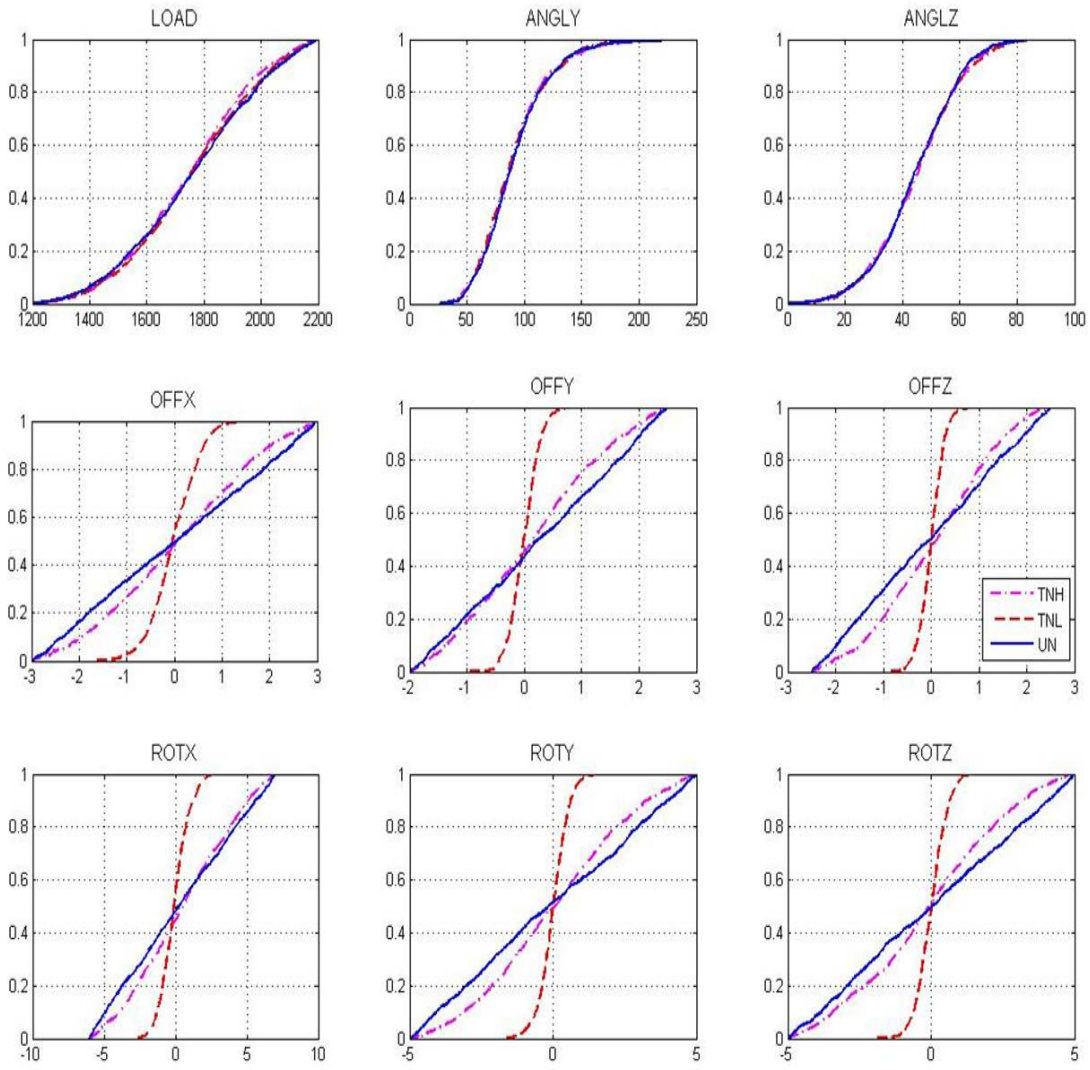

Figure C.1: Empirical CDFs of the input RVs (TNH, TNL and UN distribution cases)

C.4 Computational Flow

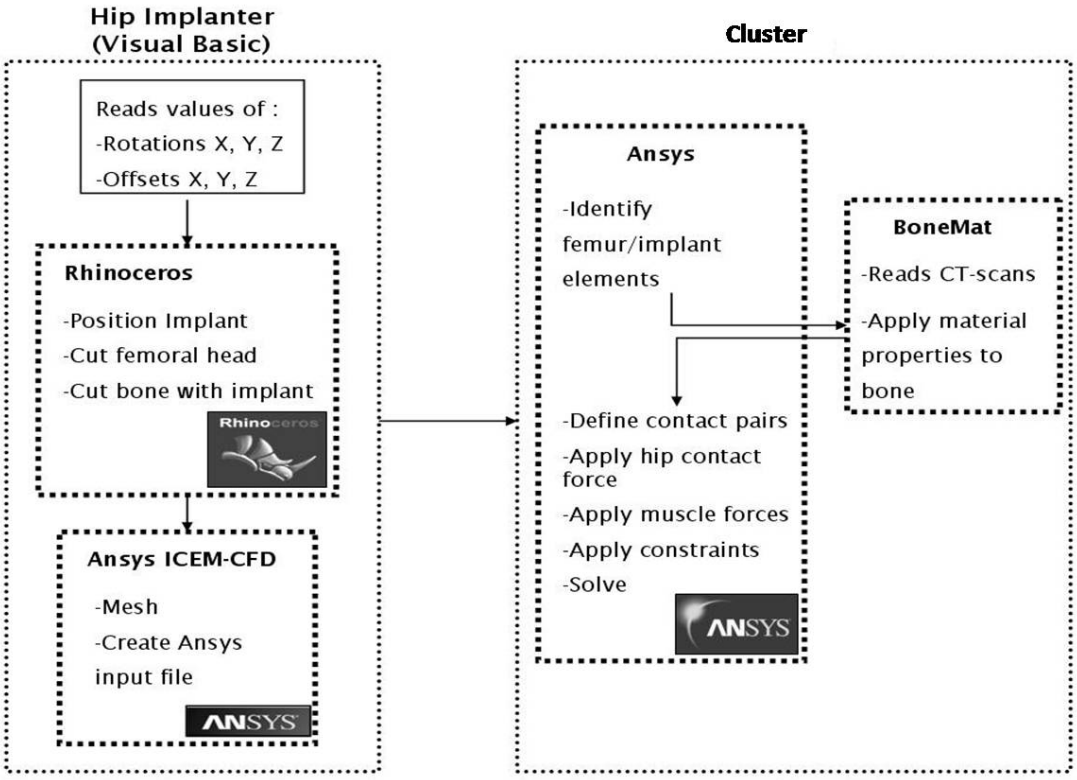

Figure C.2: Computational flow

C.5 Bad Models Filters

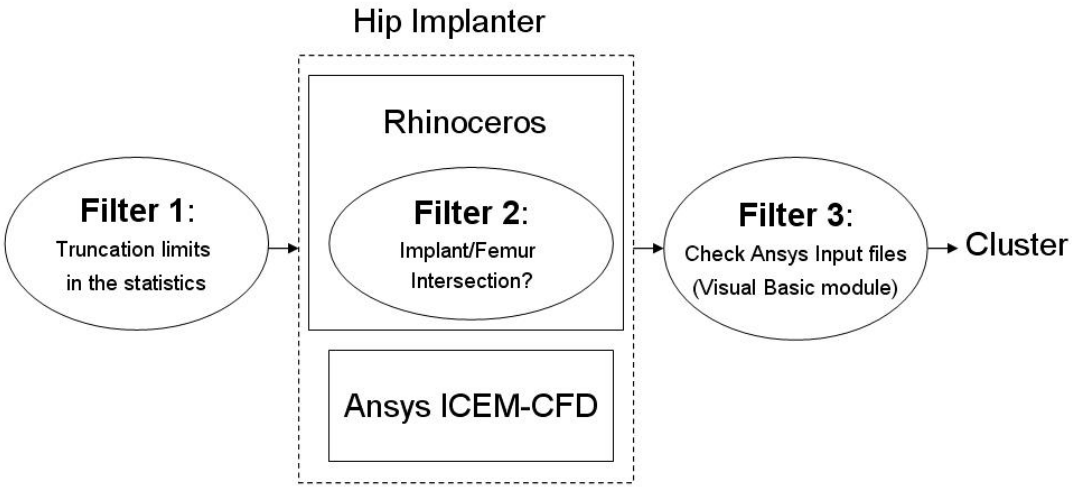

Figure C.3: Position of the three bad models filters in the computational flow

Appendix D

Glossary

Acetabulum	Concave surface of the pelvis where the head of the femur meets with the pelvis, forming the hip joint.
Ankylosing spondylitis	It is a chronic, painful degenerative inflammatory arthritis primarily affecting spine and sacroiliac joints, causing eventual fusion of the spine.
Anterio	Towards the front (of the body or body part)
Arthritis	An inflammatory condition that affect joints, causing pain when moved.
Aseptic loosening	Loosening of an implant where infection is not present.
Avascular necrosis	A disease resulting from the temporary or permanent loss of the blood supply to the bones. Without blood, the bone tissue dies and causes the bone to collapse. If the process involves the bones near a joint, it often leads to collapse of the joint surface. This disease also is known as osteonecrosis, aseptic necrosis, and ischemic bone necrosis.
Bone ingrowth	Process of bonding of the implant components to the bone by cell proliferation into areas of porous coated prosthesis, resulting in cell allocation inside the porous layer.

Bone modelling	An adaptive response to an increase in loading and results in the deposition of new bone, increasing the thickness of the cortex in long bones and increasing the apparent density of cancellous bone.
Bone ongrowth	Process of bonding of the implant components to the bone by cell proliferation on the areas of an implant, not necessarily porous coated.
Bone remodeling	Process of removal and redeposition of bone, responsible for maintaining the equilibrium state of bone, bone repair and bone resorption.
Bone resorption	Process by which osteoclasts break down bone and release the minerals, resulting in a transfer of calcium from bone fluid to the blood.
Bursae	A bursa is a small fluid-filled sac located at the point where a muscle or tendon slides across bone. It serves to reduce friction between the two moving surfaces.
Calcar femorale	A bony spur springing from the underside of the neck of the femur above and anterior to the lesser trochanter, adding to the strength of this part of the bone.
Cancellous bone	A porous form of bone found at the ends of the long bones. This kind of bone only represents 20% of the skeletal mass, but 80% of the bone surface. Also called trabecular bone, it is less dense, more elastic and has a higher remodeling rate than cortical bone.
Cartilage	The material covering the joint surfaces which in the normal joint provides a low-friction bearing surface.
Cementless/ Uncemented	Without bone cement.
Condyle	A smooth round articular projection of the surface of the bone. It can refer to lateral condyle and medial condyle (for the femur).

Cortical bone	Cortical bone represents nearly 80% of the skeletal mass. It is also called compact bone, because it forms a protective outer shell around every bone in the body. Cortical bone has a slow remodeling rate and a high resistance to bending and torsion. It provides strength where bending would be undesirable as in the middle of long bones.
Diaphysis	Main or mid section (shaft) of a long bone. It is usually filled with yellow marrow, which is made mostly of adipose (fat). Distal Away from an attached base.
Epiphysis	Rounded end of a long bone. It is filled with red marrow, which produces arythrocytes, or red blood cells.
Hoop Strain	Change in the length of a fiber of material around the circumference of the solid.
In vitro	A process taking place outside a living body, in scientific apparatus.
In vivo	A process taking place in a living body.
Lateral	Away from the bodys longitudinal axis.
Medial	Towards the bodys longitudinal axis.
Metaphysis	Portion of a long bone between the epiphyses and the diaphysis.
Microporous	A material containing pores with diameters less than 2 nm.
Migration	Movement of the implant within the bone or the cement with time.
Osteoarthrosis	A condition where the joints are affected by degeneration.
Osteoarthritis	It is characterised by the breakdown (wear out) of the joints cartilage. Cartilage breakdown causes bone to rub against each other, causing pain and loss of movement.
Osseointegration	It is the direct structural and functional connection between living bone and the surface of a load-bearing artificial implant, typically made of titanium.
Osteolysis	The destruction of bone, especially by bone resorption through removal or loss of calcium.
Osteopenia	Decreased calcification or density of bone.

Osteoporosis	A problem in which bones are less dense and more fragile and thus at greater risk of fracture, even with a small amount of trauma.
Osteotomy	The surgical cutting of a bone.
Posterior	Towards the back (of the body or body part).
Press-fit	Also called interference fit, it is a fastening between two parts which is achieved by friction after the parts are pushed together.
Proximal	Closer to an attached base, usually the body. For example, the knee is proximal to the ankle.
p-value	In statistical hypothesis testing, the p-value is the probability of obtaining a result at least as extreme as a given data point, assuming the data point was the result of a chance alone.
Significance level	In a sensitivity analysis, it is the probability that a variable is not significant.
Significant	In a sensitivity analysis, a variable is significant if the output parameter depends on it, for a given significance level.
Strain Energy Density	A quantity describing the energy stored in a material as a result of deformation. For a linear elastic material it is equal to $\frac{1}{2}$ x stress x strain.
Stress Shielding	Osteopenia occurring in bone as a result of removal of normal stress from the bone by an implant.
Synovial fluid	It is produced by the synovial membrane to provide lubrication that reduces the friction between the moving surfaces.
Synovium/synovial membrane	It lines the joint cavity and produces a viscous synovial fluid that separates cartilage covering the ends of bones.
Trabeculae/Trabecular bone	Another term for cancellous bone.
Trochanter	Part of the thigh bone. It can refer to greater trochanter and lesser trochanter.
Yield Strain	The amount of strain at which a permanent (plastic) deformation in a component becomes measurable.

References

[1] H Rodrigues. A mixed variational formulation for shape optimization of solids with contact conditions. *Structural Optimization*, 6:19–28, 1993.

[2] http://adam.about.com/encyclopedia/diseased-hip.htm, October 2006.

[3] www.bioeng.umfiasi.ro. Basic anatomy of the hip, October 2006.

[4] http://www.spineuniverse.com/displayarticle.php/article1023.html, October 2008.

[5] J DeLisa. *Gait analysis in the science of rehabilitation.* Rehabilitation research and development service.

[6] http://www.surgeryencyclopedia.com/images/gesu-02-img0110.jpg, October 2006.

[7] http://www.jnjgateway.com, December 2007.

[8] J A Epinette, C Nourissat, R Petit, and J P Vidalain. Resultats a 10 ans des protheses totales sans ciment. Etude multi-centrique. *Journee de Chirurgie Orthopedique de la Martinique*, 2001.

[9] Y Kim, S H Oh, and J S Kim. Primary total hip arthroplasty with a second-generation cementless total hip prosthesis in patients younger than fifty years of age. *The Journal of Bone & Joint Surgery*, 85(A):1, 2003.

[10] J W Harkess. Arthroplasty of the hip. In Canale ST, editor, *Campbell's operative orthopaedics, 9th edn.*, pages 296–471. Mosby, St. Louis, 1998.

[11] T Nishii, N Sugano, H Miki, T Koyama, M Takao, and H Yoshikawa. Influence of component positions on dislocation. Computed tomographic

evaluations in a consecutive series of total hip arthroplasty. *Journal of Arthroplasty*, 19(2), 2004.

[12] K T Suh, L H Kang, H L Roh, K P Moon, and H J Kim. True femoral anteversion during primary total hip arthroplasty. Use of postoperative computed tomography-based sections. *The Journal of Arthroplasty*, 21(4):599–605, 2004.

[13] S Choi. Technical tips for surface-to-surface contact analysis in MES, October 2008.

[14] http://commons.wikimedia.org/wiki/image:posterior-hip-muscles-1.heb.png, October 2008.

[15] http://commons.wikimedia.org/wiki/image:anterior-hip-muscles-2.heb.png, October 2008.

[16] http://commons.wikimedia.org/wiki/image:posterior-hip-muscles-3.heb.png, October 2008.

[17] D L Kopperdahl and T M Keaveny. Yield strain behaviour of trabecular bone. *Journal of Biomechanics*, 31(7):601–8, 1999.

[18] ANSYS. Release 10.1 documentation.

[19] http://www.itl.nist.gov/div898/handbook/eda, October 2008.

[20] E R Bohm, M Lavigne, R Bourne, B Lewis, K L Brown, B Ling, D Dickinson, and J MacKenzie. Total hip and total knee replacements in Canada. *Canadian Joint Replacement Registry (CJRR)*, 2005.

[21] National joint registry. Annual report 2005-2006. *National Joint Registry*, 2006.

[22] A Faulkner, L G Kennedy, K Baxter, J Donovan, M Wilkinson, and G Bevan. Effectiveness of hip prostheses in primary total hip replacement: a critical review of evidence and an economic model. *The NHS Health Technology Assessment Programme*, 2(6):134, 1998.

[23] G Bergmann, G Deuretzbacher, M Heller, F Graichen, A Rohlmann, J Strauss, and G N Duda. Hip contact forces and gait patterns from routine activities. *Journal of Biomechanics*, 34:859–871, 2001.

[24] I Radcliffe, P Prescott, H S Man, and M Taylor. Determination of suitable sample sizes for multi-patient based finite element studies. *Medical Engineering & Physics*, 29:1065–1072, 2007.

[25] E Genda, N Iwasaki, G Li, B A MacWilliams, P J Barrance, and E Y S Chao. Normal hip joint contact pressure distribution in single-leg standing, effect of gender and anatomic parameters. *Journal of Biomechanics*, 34:895–905, 2001.

[26] John D Currey. *Bones: Structure and Mechanics*. Princeton, New Jersey, 2002.

[27] D S Hungerford. Anatomy and biomechanics of the hip relevant to arthroplasty.

[28] D Fender, W Harper, and P Gregg. Outcome of the charnley total hip replacement across a single health region in England. *J Bone Joint Surgery*, 81(B):577–581, 1999.

[29] T J Puolakka, K J Pajamaki, Halonen P J, Pulkkinen P O, P Paavolainen, and J K Nevalainen. The finnish arthroplasty register. *Acta Orthopedica Scandinavian*, 72(5):433–441, 2001.

[30] www.orthopaedics.about.com, October 2006.

[31] T Gruen, G McNeice, and H Amstutz. Modes of failure of cemented stem-type femoral components: A radiographic analysis of loosening. *Clinical Orthopedics*, 141:17–27., 1979.

[32] D B Burr, R B Martin, M B Schaffer, and E L Radin. Bone remodeling in response to in vivo fatigue microdamage. *Journal of Biomechanics*, 18(3):189–200, 1985.

[33] S Glynn-Jones, H S Gill, P McLardy-Smith, and D W Murray. Roentgen stereophotogrammetric analysis of the Birmingham hip resurfacing arthsoplasty. A two year study. *Journal of Bone Joint Surgery*, 86(2):172–6, 2004.

[34] A Laupacis, R Bourne, C Rorabeck, D Feeny, P Tugwell, and C Wong. Comparison of total hip arthroplasty performed with and without cement: A randomized trial. *The Journal of Bone & Joint Surgery*, 84-A(10):1823–1828, 2002.

[35] A Dambreville. Uncemented hip prostheses with more than 10 years follow-up. *European Journal of Orthopaedic Surgery & Traumatology*, 13:212–229, 2003.

[36] W H Harris, A L Schiller, J M Scholler, R A Freiberg, and R Scott. Extensive localized bone resorption in the femur following total hip replacement. *Journal of Bone Joint Surgery (Am)*, 58(A):612–8, 1976.

[37] J Galante, W Rostoker, R Lueck, and R D Ray. Sintered fibre metal composites as a basis for attachment of implants to bone. *Journal of Bone Joint Surgery (Am)*, 53(1):101–114, 1971.

[38] R G T Geesink, K Groot, and C P A T Klein. Chemical implant fixation using hydroxyl-apatite coatings - the development of a human total hip prosthesis for chemical fixation to bone using hydroxyl-apatite coatings on titanium substrates. *Clinical Orthopaedics and Related Research*, 225:147–170, 1987.

[39] K Soballe, S Toksvig-Larsen, J Gelineck, S Fruensgaard, E S Hansen, L Ryd, U Lucht, and C Bunger. Migration of hydroxyapatite coated femoral prostheses. *Journal of Bone Joint Surgery (Br)*, 75(B):681–7, 1993.

[40] L Ahnfelt, P Herberts, H Malchau, and G B Andersson. Prognosis of total hip replacement. A swedish multicenter study of 4,664 revisions. *Acta Orthopedic Scandinavian Supply*, 238:1–26, 1990.

[41] K Knutson, A Lindstrand, and L Lidgren. Survival of knee arthorplasties. A nation-wide multicentre investigation of 8000 cases. *British Editorial Society of Bone and Joint Surgery*, 1986.

[42] P Paavolainen, M Hamalainen, H Mustonen, and P Slatis. Registration of arthroplasties in Finland. A nationwide prospective project. *Acta Orthopaedic Scandinavian Supply*, 241:27–30, 1991.

[43] L I Havelin, B Espehaug, S E Vollset, and L B Engesaeter. Early failures among 14,009 cemented and 1,326 uncemented prostheses for primary coxarthrosis. The Norwegian Arthroplasty Register, 1987-1992. *Acta Orthopaedic Scandinavian*, 65(1):1–6, 1994.

[44] L I Havelin, L B Engesaeter, B Espehaug, Ove Furnes, Stein A Lie, and Stein E Vollset. The Norwegian Arthroplasty Register. *Acta Orthopedic Scandinavian*, 71(4):337–353, 1993.

[45] J Duparc and P Massin. Results of 203 total hip replacements using a smooth, cementless femoral component. *Journal of Bone Joint Surgery (Br)*, 74(B):251–6, 1992.

[46] L I Havelin, B Espehaug, S E Vollset, and L B Engesaeter. Early aseptic loosening of uncemented femoral components in primary total hip replacement. *British Editorial Society of Bone and Joint Surgery*, 77(B), 1995.

[47] M Schramm, F Keck, D Hohmann, and R P Pitto. Total hip arthroplasty using an uncemented femoral component with taper design: outcome at 10-year follow-up. *Architecture Orthopaedic and Traumatologic Surgery*, 120:407–412, 2000.

[48] L Spotorno, S Romagnoli, N Ivaldo, G Grappiolo, E Bibianni, D J Blaha, and T A Gruen. Das CLS-System. Theoretisches Konzept und Ergebnisse. *Acta Orthopaedic Belg*, 59(Suppl 1):144–148, 1993.

[49] M J Archibeck, R A Berger, J J Jacobs, L R Quigley, S Gitelis, A G Rosenberg, and J O Galante. Second-generation cementless total hip arthroplasty. *The Journal of Bone & Joint Surgery*, 83(A):11, 2001.

[50] J A Bojescul, J S Xenos, J J Callaghan, and C G Savory. Results of porous-coated anatomic total hip arthroplasty without cement at fifteen years. *The Journal of Bone & Joint Surgery*, 85(A):6, 2003.

[51] E Garcia-Cimbrelo, A Cruz-Pardos, R Madero, and M Ortega-Andreu. Total hip arthorplasty with use of the cementless Zweymuller alloclassic system. *The Journal of Bone & Joint Surgery*, 85(A):2, 2003.

[52] R K Sinha, D S Dungy, and H B Yeon. Primary total hip arthroplasty with a proximally porous-coated femoral stem. *The Journal of Bone & Joint Surgery*, 86(A):6, 2004.

[53] J Dumbleton and M T Manley. Hydroxyapatite-coated prostheses in total hip and knee arthroplasty. *The Journal of Bone & Joint Surgery*, 86(A):11, 2004.

[54] P O Kroon and M A Freeman. Hydroxyapatite coating of hip prostheses. Effect on migration into the femur. *Journal of Bone Joint Surgery (Br)*, 74(B):518–22, 1992.

[55] J A D'Antonio, W N Capello, and M T Manley. Remodelling of bone around hydroxyapatite-coated femoral stems. *The Journal of Bone & Joint Surgery (Am)*, 78:1226–34, 1996.

[56] W N Capello, J A D'Antonio, M T Manley, and J R Feinberg. Hydroxyapatite in total hip arthroplasty: Clinical results and critical issues. *Clinical Orthopaedics & Related Research*, 355:200–211, 1998.

[57] M J Coathup, G W Blunn, N Flynn, C Williams, and N P Thomas. A comparison of bone remodelling around hydroxyapatite-coated, porous-coated and grit-blasted hip replacements retrieved at post-mortem. *Journal of Bone Joint Surgery (Br)*, 82(B):118–123, 2000.

[58] S A McNally, J A N Shepperd, C V Mann, and J P Walczak. The results at nine to twelve years of the use of a hydroxyapatite-coated femoral stem. *Journal of Bone Joint Surgery (Br)*, 82(B):378–82, 2000.

[59] J A D'Antonio, W N Capello, M T Manley, and R G T Geesink. Hydroxyapatite femoral stems for total hip arthroplasty: 10- to 13-year follow-up. *Clinical Orthopaedics & Related Research*, 393:101–111, 2001.

[60] R E Kennon, J M Keggi, R S Wetmore, L E Zatorski, M H Huo, and K J Keggi. Total hip arthroplasty through a minimally invasive anterior surgical approach. *Journal of Bone and Joint Surgery Am*, 85:39–48, 2003.

[61] R Meneghini, M W Pagnano, Rt T Trousdale, and W J Hozack. Muscle damage during MIS total hip arthroplasty. Smith-peterson versus posterior approach. *Clinical Orthopaedics and Related Research*, 2006.

[62] A A Halpern, J Tanner, and L Rinsky. Does persistent fetal femoral anteversion contribute to osteoarthritis?: a preliminary report. *Clinical Orthopaedics Related Research*, Nov-Dec(145):213–216, 1979.

[63] O Reikeras, I Bjerkreim, and A Kolbenstvedt. Anteversion of the acetabulum in patients with idiopathic increased anteversion of the femoral neck. *Acta Orthopedica*, 53(6):847–852, 1982.

[64] K Herrlin, H Pettersson, G Selvik, and L Lidgren. Femoral anteversion and restricted range of motion in total hip prostheses. *Acta Radiologica*, 29(5):551–3, 1988.

[65] M O Heller, G Bergmann, G Deuretzbacher, L Claes, N P Haas, and G N Duda. Influence of femoral anteversion on proximal femoral loading: measurement and simulation in four patients. *Clinical Biomechanics*, 16:644–649, 2001.

[66] M T Bah and M Browne. Probabilistic analysis of a cemented hip implant. In *International Congress on Computational Bioengineering*, Zaragoza, 2003.

[67] D P Nicolella, B H Thacker, H Katoozian, and D T Davy. Probabilistic risk analysis of a cemented hip implant, 2001.

[68] L Mehrez. *The application of probabilistic methods for the assessment of hip implant performance*. PhD thesis, University of Southampton, 2007.

[69] M Perez, J Grasa, J Garcia-Aznar, J Bea, and M Doblare. Probabilistic analysis of the influence of the bonding degree of the stem-cement interface in the performance of cemented hip prostheses. *Journal of Biomechanics*, 39(10):1859–1872, 2006.

[70] D P Nicolella, B H Thacker, H Katoozian, and D T Davy. The effect of three-dimensional shape optimization on the probabilistic response of a cemented femoral hip prosthesis. *Journal of Biomechanics*, 39:1265–1278, 2006.

[71] P J Laz, S Pal, J P Halloran, M A Baldwin, J E Langenderfer, and P J Rullkoetter. Probabilistic finite element analysis in orthopaedic biomechanics.

In Y. Gonzalez Cerrolaza and M., editors, *Bioengineering Modelling and Computer Simulation*, pages 70–92, Barcelona, Spain, 2007. CIMNE.

[72] C M Les, J H Keyak, S M Stover, K T Taylor, and A J Kaneps. Estimation of material properties in the equine metacarpus with use of quantitative computed tomography. *Journal of Orthopaedic Research*, 12:822–833, 1993.

[73] L Peng, J Bai, X Zeng, and Y Zhou. Comparison of isotropic and orthotropic material property assignments on femoral finite element models under two loading conditions. *Medical Engineering and Physics*, 28:227–233, 2005.

[74] D R Carter and W C Hayes. The compressive behavior of bone as a two-phase porous structure. *Journal of Bone and Joint Surgery Am*, 59:954–962, 1977.

[75] T S Keller. Predicting the compressive mechanical behaviour of bone. *Journal of Biomechanics*, 27(9):1159–68, 1994.

[76] E F Morgan, H H Bayraktar, and T M Keaveny. Trabecular bone modulus-density relationships depend on anatomic site. *Journal of Biomechanics*, 36:897–904, 2003.

[77] C Zannoni, R Mantovani, and M Viceconti. Material properties assignment to finite element models of bone structures: a new method. *Medical Engineering & Physics*, 20:735–740, 1998.

[78] F Taddei, A Pancanti, and M Viceconti. An improved method for the automatic mapping of computed tomography numbers onto finite element models. *Medical Engineering and Physics*, 26:61–69, 2004.

[79] F Taddei, E Schileo, B Helgason, L Cristofolini, and M Viceconti. The material mapping strategy influences the accuracy of CT-based finite element models of bones: An evaluation against experimental measurements. *Medical Engineering and Physics*, 29:973–979, 2007.

[80] E Schileo, F Taddei, A Malandrino, L Cristofolini, and M Viceconti. Subject-specific finite element models can accurately predict strain levels in long bones. *Journal of Biomechanics*, 40:2982–2989, 2007.

[81] E Schileo, E Dall'Ara, F Taddei, A Malandrino, T Schotkamp, M Baleani, and M Viceconti. An accurate estimation of bone density improves the accuracy of subject-specific finite element models. *Journal of Biomechanics*, 41:2483–2491, 2008.

[82] A Sarmiento and T A Gruen. Radiographic analysis of a low-modulus titanium-alloy femoral total hip component. Two to six-year follow-up. *Journal of Bone and Joint Surgery Am*, 67(48-56), 1985.

[83] H Weinans, R Huiskes, and H J Grootenboer. Effects of material properties of femoral hip components on bone remodelling. *Journal of Orthopedic Research*, 10:845–853, 1992.

[84] R L Barrack. Dislocation after total hip arthroplasty: Implant design and orientation. *Journal of American Academy of Orthopaedic Surgery*, 11:89–99, 2003.

[85] K E Tanner, A L Yettram, M Loeffler, W D Goodier, M A R Freeman, and W Bonfield. Is stem length important in uncemented endoprostheses? *Medical Engineering and Physics*, 17(4):291–296, 1995.

[86] R M Gillies, P H Morberg, W J M Bruce, A Turnbull, and W R Walsh. The influence of design parameters on cortical strain distribution of a cementless titanium femoral stem. *Medical Engineering and Physics*, 24(109-114), 2001.

[87] F B Biegler, J D Reuben, T P Harrigan, F J Hou, and J E Akin. Effect of porous coating and loading conditions on total hip femoral stem stability. *The Journal of Arthroplasty*, 10(6), 1995.

[88] R Decking, W Puhl, U Simon, and L E Claes. Changes in strain distribution of loaded proximal femora caused by different types of cementless femoral stems. *Clinical Biomechanics*, 21:495–501, 2006.

[89] A D Speirs, M O Heller, W R Taylor, G N Duda, and C Perka. Influence of changes in stem positioning on femoral loading after THR using a short-stemmed hip implant. *Journal of Clinical Biomechanics*, 22:431–439, 2007.

[90] A Aamodt, J Lund-Larsen, J Eine, E Andersen, P Benum, and O S Husby. Changes in proximal femoral strain after insertion of uncemented standard

and customised femoral stems. An experimental study in human femora. *The Journal of Bone & Joint Surgery (Br)*, 83-B(6), 2001.

[91] I A Karnezis. A technique for accurate reproduction of the femoral anteversion during primary total hip arthroplasty. *Architecture Orthopaedic and Traumatologic Surgery*, 121:343–345, 2001.

[92] C Schidlo, C Becker, V Jansson, and J Refior. Anderung des CCD-Winkels sowie des femoralen Antetorsionswinkels durch Hatprothesenimplantation. *Zeitschrift fur Orthopedie*, 137:259–264, 1999.

[93] F Mazoochian, C Pellengahr, A Huber, J Kircher, H J Refior, and V Jansson. Low accuracy of stem implantation in THR using the CASPAR-system. *Acta Orthopedic Scandinavian*, 75(3):261–264, 2004.

[94] W A Brekelmans, H W Poort, and T J Slooff. A new method to analyse the mechanical behaviour of skeletal parts. *Acta Orthopaedic Scandinavian*, 43(5):301–17, 1972.

[95] P B Chang, B J Williams, K S B Bhalla, T W Belknap, T J Santner, W I Notz, and D L Bartel. Design and analysis of robust total joint replacements: Finite element model experiments with environmental variables. *Journal of Biomechanical Engineering*, 123:239–246, 2001.

[96] C Tai, S Chun-Hsiung, C Weng-Pin, L Shiuann-Sheng, L Yu-Liang, H Pang-Hsin, and C Wen-Jer. Finite element analysis of the cervico-trochanteric stemless femoral prosthesis. *Clinical Biomechanics*, 18:53–58, 2003.

[97] A Ramos and J A Simoes. Tetrahedral versus hexahedral finite elements in numerical modelling of the proximal femur. *Medical Engineering & Physics*, 28(9):916–924, 2006.

[98] J Stolk, N Versdonschot, and R Huiskes. Sensitivity of failure criteria of cemented total hip replacements to finite element density. In *European Society of Biomechanics, July 8-11*, Toulouse, France, 1998.

[99] P R Fernandes, J Folgado, C Jacobs, and V Pellegrini. A contact model with ingrowth control for bone remodelling around cementless stems. *Journal of Biomechanics*, 35:167–176, 2002.

[100] S B Goodman. The effects of micromotion and particulae materials on tissue differentiation. Bone chamber studies in rabbits. *Acta Orthopaedic Scandinavian Supply*, 258:1–43, 1994.

[101] D P Pioletti, H Takei, S Y Kwon, D Wood, and K L P Sung. The cytotoxic effect of titanium particles phagocytosed by osteoblasts. *Journal of Biomedicine & and Material Research*, 46:399–407, 1999.

[102] P Aspenberg and P Herbertsson. Periprosthetic bone resorption: particles versus movement. *Journal of Bone Joint Surgery (Br)*, 78:641–666, 1996.

[103] R Skripitz and P Aspenberg. Pressure-induced periprosthetic osteolysis: a rat model. *Journal of Orthopaedic Research*, 18:481–484, 2000.

[104] H M van-der Vis, P Aspenberg, R K Marti, W Tigchelaar, and C van Noorden. Mechanical compression of a fibrous membrane surrounding bone causes bone resorption. *Acta Histochemistry*, 101:203–212, 1999.

[105] H van-der Vis, P Aspenberg, R de Kleine, W Tigchelaar, and C J van Noorden. Short periods of oscillating fluid pressure directed at a titanium-bone interface in rabbits lead to bone osteolysis. *Acta Orthopaedic Scandinavian*, 69:5–10, 1998a.

[106] H van-der Vis, P Aspenberg, R K Marti, W Tigchelaar, and C J van Noorden. Fluid pressure causes bone resorption in a rabbit model of prosthetic loosening. *Clinical Orthopaedics*, 350:201–208, 1998b.

[107] P J Prendergast, R Huiskes, and K Soballe. Biophysical stimuli on cells during tissue differentiation at implant interfaces. *Journal of Biomechanics*, 30:539–548, 1997.

[108] X Yuan and R Huiskes. Wear particle diffusion and tissue differentiation in TKA implant fibrous interfaces. *Journal of Biomechanics*, 33:1279–1286, 2000.

[109] N Nuño and M Amabili. Modelling debonded stem-cement interface for hip implants: effect of residual stresses. *Clinical Biomechanics*, 17:41–48, 2002.

[110] T M Keaveny and D L Bartel. Mechanical consequences of bone ingrowth in a hip prosthesis inserted without cement. *The Journal of Bone & Joint Surgery*, 77:911–923, 1995.

[111] M A Stulpner, B D Reddy, G R Starke, and A Spirakis. A three-dimensional finite analysis of adaptive remodelling in the proximal femur. *Journal of Biomechanics*, 30(10):1063–1066, 1997.

[112] P Büchler, D P Pioletti, and L R Rakotomanana. Biphasic constitutive laws for biological interface evolution. *Biomechanical Modelling & Mechanobiology*, 1(239-249), 2002.

[113] M Viceconti, R Muccini, M Bernakiewicz, M Baleani, and L Cristofolini. Large-sliding contact elements accurately predict levels of bone-implant micromotion relevant to osseointegration. *Journal of Biomechanics*, 33:1611–1618, 2000.

[114] K A Mann, D L Bartel, T M Wright, and A H Burstein. Coulomb frictional interfaces in modelling cemented total hip replacements, a more realistic model. *Journal of Biomechanics*, 28(9):1067–1078, 1995.

[115] M Bernakiewicz and M Viceconti. The role of parameter identification in finite element contact analyses with reference to orthopaedic biomechanics applications. *Journal of Biomechanics*, 35:61–67, 2001.

[116] L Cristofolini, M Viceconti, A Toni, and A Giunti. Influence of thigh muscles on the axial strains in a proximal femur during early stance in gait. *Journal of Biomechanics*, 28(5):617–624, 1995.

[117] G N Duda, E Schneider, and E Y S Chao. Internal forces and moments in the femur during walking. *Journal of Biomechanics*, 30(9):933–941, 1997.

[118] G N Duda, M Heller, J Albinger, O Schulz, E Schneider, and L Claes. Influence of muscle forces on femoral strain distribution. *Journal of Biomechanics*, 31:841–846, 1998.

[119] J Stolk, N Verdonschot, and R Huiskes. Hip-joint and abductor-muscle forces adequately represent in vivo loading of a cemented total hip reconstruction. *Journal of Biomechanics*, 34:917–926, 2001.

[120] D R Carter, R Vasu, D M Spengler, and R T Dueland. Stress fields in the unplated and plated canine femur calculated from in vivo strain measurements. *Journal of Biomechanics*, 14:63–70, 1981.

[121] H Weinans, P van Loon, B Roszek, and R Huiskes. Measurement of the load components on the tibia of the goat using in vivo strain gage techniques. In *ORS*, page 538, Washington (USA), 1992.

[122] S Easley, S Pal, P Tomaszewski, A Petrella, P Rullkoetter, and P Laz. Finite element-based probabilistic analysis tool for orthopaedic applications. *Computer Methods and Programs in Biomedicine*, 85(1):32–40, 2007.

[123] K Polgar, H S Gill, M Viceconti, D W Murray, and J J O'Connor. Strain distribution within the human femur due to physiological and simplified loading, finite element analysis using the muscle standardised femur model. In *Institute of Mechanical Engineers*, volume H 217, pages 173–189, 2003.

[124] M E Taylor, K E Tanner, M A R Freeman, and A L Yettram. Stress and strain distribution within the intact femur: compression or bending? *Medical Engineering and Physics*, 18(2):122–131, 1995.

[125] C H Turner, V Anne, and R Pidaparti. A uniform criterion for trabecular bone adaptation. Do continuum-level strain gradients drive adaptation? *Journal of Biomechanics*, 30:555–563, 1997.

[126] N Cabtree, M Lunt, G Holt, H Kroger, H Burger, S Grazio, K T Khaw, R S Lorenc, J Nijs, J Stepan, J A Falch, T Miazgowski, P Raptou, H A Pols, J Dequeker, S Havelka, K Hoszowski, I Jajic, S Czekalski, G Lyritis, A J Silman, and J Reeve. Hip geometry, bone mineral distribution, and bone strength in European men and women: The EPOS study. *Bone*, 27(1):151–159, 2000.

[127] J C Lotz, E J Cheal, and C Hayes. Stress distributions within the proximal femur in gait and falls: Implications for osteoporotic fracture. *Osteoporosis International*, 5(4):252–261, 2005.

[128] X G Cheng, G Lowet, S Boonen, P H F Nicholson, P Brys, J Nijs, and J Dequeker. Assessment of the strength of proximal femur in vitro: Relationship to femoral bone mineral density and femoral geometry. *Bone*, 20(3):213–218, 1997.

[129] E Schileo, F Taddei, L Cristofolini, and M Viceconti. Application of a maximum principal strain failure criterion in subject-specific finite element

models of bones. In M. Doblare J. Ambrosio M. Viceconti M. Cerrolaza, H. Rodrigues, editor, *III International Congress on Computational Bioengineering*, pages 143–148, Caracas, Venezuela, 2007. INABIO.

[130] E F Morgan and T M Keaveny. Dependence of yield strain of human trabecular bone on anatomic site. *Journal of Biomechanics*, 34:569–577, 2001.

[131] J Kiss, D W Murray, A R Turner-Smith, J Bithell, and C J Bulstrode. Migration of cemented femoral components after THR - roentgen stereophoetogrametric analysis. *Journal of Bone and Joint Surgery (Br)*, 78B(5):796–801, 1996.

[132] B Mjoberg. Fixation and loosening of hip prostheses - a review. *Acta Orthopedica*, 62(5):500–508, 1991.

[133] J Kassi, M O Heller, U Stoeckle, C Perka, and G N Duda. Stair climbing is more critical than walking in pre-clinical assessment of primary stability in cementless tha in vitro. *Journal of Biomechanics*, 38:1143–1154, 2004.

[134] J Britton and P J Prendergast. Preclinical testing of femoral hip components: an experimental investigation with four prostheses. *Journal of Biomechanical Engineering*, 127, 2005.

[135] P Dienes. *The Taylor Series. An Introduction to the Theory of Functions of a Complex Variable.* The Clarendon Press, Oxford, 1931.

[136] S M Stigler. Mathematical statistics in the early states. *The Annals of Statistics*, 6:239–265, 1978.

[137] H L Harter. *Least Squares.* Encyclopedia of Statistical Sciences, Kotz, S. and Johnson, N.L., eds., John Wiley & Sons, New York, pp. 593-598, 1983.

[138] S M Stigler. The history of statistics: The measurement of uncertainty before 1900. *The Belknap Press of Harvard University Press, Cambridge, Massachusetts.*

[139] R D Cook. *Residuals and Influence in Regression.* Chapman and Hall, New York, 1982.

[140] A Haldar and S Mahadevan. *Probability, Reliability and Statistical Methods in Engineering Design.* John Willey & Sons, New York, USA, 2000.

[141] http://en.wikipedia.org/wiki/random_ number_ generator# computational_ methods, December 2008.

[142] J M Hammersley and D C Handscomb. *Monte Carlo Methods.* John Willey & Sons, New York, USA, 1964.

[143] R E Melchers. Improved importance sampling method for structural system reliability calculation. In *5th International Conference on Structural Safety and Reliability (ICOSSAR)*, San Francisco, 1989.

[144] R Y Rubinstein. *Simulation and the Montecarlo Method.* John Wiley & Sons, 1981.

[145] M D McKay, R J Beckman, and W J Conover. A comparison of three methods for selecting values of input variables in the analysis of output from a computer code. *Technometrics*, 42(1):55–61, 1979.

[146] M Stein. Large sample properties of simulations using latin hypercube sampling. *Technometrics*, 29(2):143–151, 1987.

[147] M Browne, R S Langley, and P J Gregson. Reliability theory for load bearing biomedical implants. *Biomaterials*, 20:1285–1292, 1999.

[148] R S Langley and C S Ribas. The application of level II reliability theory. *Proceedings of the Institution of Mechanical Engineers. Pt. G. Journal of Aerospace Engineering*, 209(G4):291–8, 1995.

[149] R J Yang, K K Choi, R D Crowninshield, and R A Brand. Design sensitivity analysis: a new method for implant design and comparison with parametric finite element analysis. *Journal of Biomechanics*, 17(11):849–854, 1984.

[150] P J Prendergast. Finite element models in tissue mechanics and orthopaedic implant design. *Clinical Biomechanics*, 12:343–366, 1997.

[151] R Huiskes and B Rietbergen. Preclinical testing of total hip stems, the effects of coating placement. *Clinical Orthopaedics & Related Research*, 319:64–76, 1995.

[152] M T Bah and M Browne. Failure of the cement mantle in hip implants: a probabilistic approach. In *50th Annual Meeting of the Orthopaedic Research Society*, San Francisco, USA, 2004.

[153] B H Thacker and D P Nicolella. Probabilistic finite element analysis of the human lower cervical spine. *Journal of Mathematical Modelling and Scientific Computing*, 1998.

[154] NESSUS. Version 8.30 theoretical manual, 1998.

[155] P Laz, S Pal, J Halloran, A Petrella, and P Rullkoetter. Probabilistic finite element prediction of knee wear simulation mechanics, 2005.

[156] L Mehrez, M T Bah, and M Browne. Assessment of variability and uncertainty in total hip replacements: probabilistic analysis of a 3d finite element contact model. In *51st Annual Meeting of the Orthopaedic Research Society*, 2005.

[157] G Calafiore. Approximation of n-dimensional data using spherical and ellipsoidal primitives. 32(1083-4427(02)06006-X):267–278, 2002.

[158] Y Kim. Cementless total hip arthroplasty with a close proximal fit and short tapered distal stem (third-generation) prosthesis. *The Journal of Arthroplasty*, 17(7):841–850, 2002.

[159] R Ashman and J Rho. Elastic modulus of trabecular bone material. *Journal of Biomechanics*, 21(3):177–81, 1988.

[160] J Cohen, P Cohen, S G West, and L S Aiken. *Applied multiple regression/correlation analysis for the behavioural sciences. (3rd ed.)*. Lawrence Erlbaum Associates, Hillsdale, New Jersey, 2003.

[161] P J Laz, J Q Stowe, M A Baldwin, A Petrella, and P J Rullkoetter. Incorporating uncertainty in mechanical properties for finite element-based evaluation of bone mechanics. *Journal of Biomechanics*, 40:281–2836, 2007.

[162] M Viceconti, G Brusi, A Pancanti, and L Cristofolini. Primary stability of an anatomical cementless hip stem: A statistical analysis. *Journal of Biomechanics*, 39:1169–1179, 2005.

[163] T L Bredbenner, D P Nicolella, and D T Davy. Modelling variability and uncertainty in the experimental response of vertebral trabecular bone, 2008.

[164] C Dopico-Gonzalez, A M New, and M Browne. Probabilistic analysis of un uncemented hip replacement. *Medical Engineering and Physics. Accepted for publication*, 2009.

[165] A S Wong, M Taylor, A M New, and A Ritchie. Influence of an interference fit on the strain distribution in the implanted proximal femur. International Society of Biomechanics XVIIIth Congress. Zurich, Switzerland, July 12th 2001.

[166] J Homminga, B R McCreadie, T E Ciarelli, H Weinans, S A Goldstein, and R Huiskes. Cancellous bone mechanical properties from normals and patients with hip fractures differ on the structure level, not on the bone hard tissue level. *Bone*, 30(5):759–764, 2002.

[167] J J Callaghan, C S Fulghum, R R Glisson, and S K Stranne. The effect of femoral stem geometry on interface motion in uncemented porous-coated total hip prostheses. Comparison of straight-stem and curved-stem designs. *Journal of Bone and Joint Surgery Am*, 74:839–848, 1992.

[168] D W Burke, D O O'Connor, E B Zalenski, M Jasty, and W H Harris. Micromotion of cemented and uncemented femoral components. *Journal of Bone and Joint Surgery (Br)*, 73(B):33–37, 1991.

[169] C Manders, A New, and J Rasmussen. Validation of musculoskeletal gait simulation for use in investigation of total hip replacement. European Society of Biomechanics Conference, Luzerne (Switzerland), July 6th-9th 2008.

[170] http://en.wikipedia.org/wiki/extreme_ outlier, February 2009.

[171] H H Bayraktar, E F Morgan, G L Niebur, G E Morris, E K Wong, and T M Keaveny. Comparison of the elastic and yield properties of human femoral trabecular and cortical bone tissue. *Journal of Biomechanics*, 37:27–35, 2004.

[172] N L Johnson, S Kotz, and N Balakrishnan. *Continuous Univariate Distributions, Volumes I and II, 2nd.* John Wiley & Sons, 1994.